University of Calabria

PhD Course in Chemical and Materials Engineering

Thesis

PREPARATION AND CHARACTERIZATION OF MESOSTRUCTURED FUNCTIONAL MATERIALS WITH DIFFERENT MORPHOLOGIES

Settore Scientifico Disciplinare ING-IND/22 Scienza e tecnologia dei materiali

Supervisors

Prof. Rosario Aiello

Prof. Flaviano Testa

PhD Student

Daniela Aiello

Ciclo XXI

PhD Coordinator

Prof. Raffaele MOLINARI

A.A. 2007-2008

TABLE OF CONTENTS

CHAPTER IV: Mesoporous Thin Film

Abstract

PREPARATION AND CHARACTERIZATION OF MESOSTRUCTURED FUNCTIONAL MATERIALS WITH DIFFERENT MORPHOLOGIES

Mesoporous materials with their good surface and structural properties and versatility can be synthesized in different morphologies (thin films, fibers, membranes, etc.) and represent excellent host matrices, highly functional and with great potentials for advanced applications. In this research work, mesoporous powders and thin films have been successfully achieved and then functionalized with special guest molecules such as organic molecules, organometallic complexes, fluorescent dyes, all having specific and interesting properties. Mesoporous matrices have been prepared by sol-gel chemistry with different mesostructures and high order degree. Chemical modifications approaches (post-synthesis grafting and one-pot synthesis) applied to porous supports highly organized have allowed to product a new class of functional materials, particularly interesting for various applications (opto-electronic, photovoltaic materials, etc.). Surface and structural characterization techniques (FTIR, UV-Vis, fluorescence, ellipsometry spectroscopies, electron transmission microscopy, XRD diffraction and porosimetry analysis) have allowed to investigate the effects of the introduction of guest species inside mesoporous matrices and to identify noteworthy changes about organization and mesostructures. Results show that mesoporous materials, both as powders and thin films, do not suffer significant reductions of surface (surface area, pore volume and diameter) and structural properties (order degree, mesostructure organization, stability) after functionalization process, representing confined environment well adapted to various guest species, with the advantage to increase their activity and physic-chemical properties. In particular, guest species are well trapped into rigid porous matrices with an increase of their functional properties and inorganic network stability. All results have demonstrated that the high structural homogeneity, the control over surface and morphological properties and also the possibility to host different molecules permit to project and engineer high potential technological materials for applications in optic and electro-optic fields.

Riassunto

PREPARAZIONE E CARATTERIZZAZIONE DI MATERIALI MESOSTRUTTURATI FUNZIONALI CON DIFFERENTI MORFOLOGIE

I materiali mesoporosi, per le eccellenti proprietà superficiali e strutturali e soprattutto per la versatilità di sintesi sotto forma di diverse morfologie (film, polveri, fibre, membrane, etc.), rappresentano ottime matrici ospitanti altamente funzionalizzabili e con grandi potenzialità per applicazioni avanzate. In questo lavoro di tesi sono stati sintetizzati polveri e film sottili mesoporosi, successivamente funzionalizzati con speciali molecole ospiti (molecole organiche, complessi organometallici, dye fluorescenti), ognuna caratterizzata da interessanti proprietà specifiche. Le matrici mesoporose, preparate mediante chimica sol-gel, sono state ottenute con differenti mesostrutture, tutte ad elevato grado di ordine. Le procedure di modifica chimica (grafting post-sintesi e co-condensazione) applicate ai supporti porosi altamente organizzati hanno permesso di ottenere una nuova classe di materiali funzionali, particolarmente interessanti per molteplici applicazioni (materiali opto-elettronici, fotovoltaici, etc.). Le tecniche di caratterizzazione superficiali e strutturali (spettroscopia FTIR, UV-Vis, di fluorescenza, ellissometrica, microscopia elettronica a trasmissione, XRD e porosimetria) hanno permesso di investigare gli effetti provocati dall'introduzione delle specie ospiti all'interno delle matrici mesoporose e sui cambiamenti nell'organizzazione delle mesostrutture. I risultati ottenuti mostrano che tutti i materiali mesoporosi non subiscono significative variazioni delle proprietà superficiali (area specifica, volume e diametro dei pori) e strutturali (grado d'ordine, organizzazione della mesostruttura, stabilità) a seguito delle procedure di funzionalizzazione, rappresentando dunque ambienti confinanti ben adattabili alle diverse molecole ospiti, con il vantaggio di incrementarne l'attività e le proprietà chimico-fisiche. In particolare, le specie ospiti risultano ben intrappolate all'interno delle matrici porose rigide con un incremento delle loro proprietà funzionali e della stabilità del "network" inorganico. L'insieme dei risultati ottenuti ha dimostrato che l'alta omogeneità strutturale, il controllo delle proprietà superficiali e morfologiche e la possibilità di ospitare in maniera efficace differenti molecole permette di progettare ed ingegnerizzare materiali ad alto potenziale tecnologico per applicazioni soprattutto nei campi dell'ottica e dell'elettro-ottica.

PREFACE

The research work developed during the Ph.D. Course in Chemical and Materials Engineering was devoted to the synthesis and characterization of nanomaterials with controlled porosity, in particular of mesoporous materials, obtained as powders (pore diameter ≈ 30 Å) and thin films (thickness ≈ 200÷400 nm). Topological design of mesoporous materials, pore architecture, pore size and morphology are currently major issues in areas such as catalytic conversion of bulky molecules, adsorption, host-guest chemistry, etc.

Morphological control confers them versatility when employed whether as bulk powders, monoliths, thin films, or embedded in coatings. In recent years mesoporous powders, especially those exhibiting ordered pore systems and uniform pore diameters, have shown great potential for many applications, including separation technology (chromatography), catalysis, nanoelectronics, sensors and spatially defined host materials for substances or reactions.

Mesoporous films are a fine example of a self-assembled nanosystem, containing ordered porosity in the 2–50 nm range. A great number of properties, including framework nature (composition, crystallinity), surface area, pore dimension, shape, accessibility and pore array symmetry and interconnection can be tuned using chemistry synthesis techniques. These materials present potentials in all those fields where a large functional interfacial area contained in a strong framework is required.

The chemical modifications of surface (i.e. addition of organic or biological functions) and pore interior (inclusion of nanoparticles, clusters or biomolecules) of mesoporous powders and thin films leads to more complex materials with tailored features. Mesoporous hybrid inorganic-organic materials are very promising multifunctional materials with high surface areas, controlled pore size and tailored organic functions dangling from the walls or embedded into the framework.

In this work mesoporous solids have been functionalized on specific sites with special guest molecules exhibiting improved activity, selectivity and stability in, for example, optical and electronic fields. The experimental work was developed following two research lines: within the first line, the synthesis and the characterization of mesoporous silica-based functional powders

with different structural symmetries was studied; within the second, silica- and titania-based mesoporous thin films were obtained and characterized. In both cases, the materials have been modified to evaluate their properties for technologically innovative applications.

In particular, in the first chapter, a brief overview of the mesoporous materials and their main related problems will be mentioned and considered. Attention will be then focused on synthesis methods and characterization of ordered mesoporous silica powders.

In the second chapter mesoporous hybrid organic-inorganic materials and functionalization processes will be examined and described, with particular reference to the differences between various chemical modification approachs. Moreover, the interesting properties and applications of these host-guest systems will be described.

In the third chapter, the functionalization of mesoporous materials powders by using a Schiff base zinc(II) complex in order to prepare a luminescent solid will be repeated. Modification with model molecules to understand their interaction with matrix and produced changes will be discussed. The solids have been characterized by XRD diffraction, transmission electron microscopy (TEM) and N_2 sorption analysis to obtain structural informations, by Fourier Transform Infrared Spectroscopy (FTIR) and elemental analysis to obtain compositional informations.

In the fourth and fifth chapter, an overview of mesoporous thin films silica- and other oxides-based, their synthesis and formation mechanisms will be showed, together with the structural and textural characterizations and most important applications.

In the sixth chapter, an extensive discussion on the major advances in the field of hybrid thin films for future applications, including micro-optics and photonic devices will be present.

In the seventh chapter, block-copolymer template mesoporous thin films will be prepared and functionalized with a luminescent zinc(II) complex and a laser dye, Rhodamine 6G, to obtain electroluminescent materials. The characterization in function of the functionalization time and dye concentration, respectively, by FT-IR, ellipsometry, fluorescence and UV-Vis spectroscopies, and emission quantum yield measurement to understand the effects of the incorporation process and the important implications for future developments will be presented and discussed.

CHAPTER I

MESOPOROUS MATERIALS

1.1 INTRODUCTION

Mesoporous materials are of great research interest for their potential application as catalysts, absorbents, chemical sensors and optical/electronic nanodevices, due their high surface area and pore volume. According to the IUPAC definition, porous materials are divided into three classes: microporous (< 2 nm), mesoporous (2–50 nm) and macroporous (>50 nm). Well-known members of the microporous class are the zeolites, which provide excellent catalytic properties by virtue of their crystalline aluminosilicate network. However, their applications are limited by the relatively small pore openings; therefore, pore enlargement was one of the main aspects in zeolite chemistry. Larger pores are present in porous glasses and porous gels, which were known as mesoporous materials at the time of the discovery of MCM-41, in 1992 by scientist at *Mobil Oil Research Development Corporation*, using ionic surfactants [1].

However, these materials showed disordered pore systems with broad pore-size distributions. In the last years many efforts have been carried out to make these materials stable, to expand the range of reachable pore size, to extend the framework composition and finally to examine new supramolecular templates [2]. MCM-41 (*Mobil Composition of Matter*) material was the first mesoporous solid synthesized that showed a regularly ordered pore arrangement and a very narrow pore-size distribution (2÷50 nm).

After the discovery of MCM-41, the research interest was focused on the following main subjects: (1) characterization; (2) mechanism of formation; (3) synthesis of new materials based on the MCM-41 synthesis concept; (4) morphology control and (5) applications technological of MCM-41 and related mesoporous materials. Moreover, different chemical compositions of the final material are achievable: transition metal oxides [3], metal sulphides, hybrid silica/organic compounds and materials with different structure symmetry. Depending on the initial precursor and synthetic conditions such as chemical composition and surfactant molecular structures, we can distinguish these groups: 1) MCM-41 and SBA-15 both with unidirectional pores and sometimes with a secondary micropore system that interconnects the hexagonal channels; 2)

MCM-48 which exhibits a three-dimensional pore system, formed by intersected longitudinal pores along the three directions in space.

Because of the large pore dimensions, high surface area (near to 1000 m^2/g) and thermal stability, there is interest either in using these materials as catalysts and supports or in developing their electronic, optical or sensing applications.

1.2 SYNTHESIS TOOLS FOR MESOSTRUCTURE PRODUCTION

Soft chemistry is an interesting starting point for the development of a "biomimetic approach" for the preparation of mesostructured materials, in view of the typical synthesis conditions: low temperatures; coexistence of inorganic, organic, and even biologically moieties; widespread choice of precursors (monomers or condensed species); possibilities of controlled shaping (i.e., powders, gels, films). Exploration in this field is persistently growing and a number of biomimetic synthesis strategies have been recently developed [4,5].

The large set of smart materials, ranging from nanostructured materials to more complex materials having hierarchical architectures, reported during the past 10 years, is testified by to the scientific success of this field. **Fig.1** presents a depiction of the main general synthesis strategies used to construct these materials, in which the chemical, spatial, and structural properties of the texturing agent, or the "reaction pockets", must be thoroughly adjusted by controlling the rates of chemical reactions, the nature of the interfaces and the encapsulation of the growing inorganic phase. These synthesis strategies can be categorized following two principal approaches:

1) The molecular/supramolecular templates are present in the synthesis media from the beginning; the self-assembly process of the templates is followed by (or synchronized with) the formation of the mineral network, deposited around the "self-assembled substrate". "Inorganic replication" occurs at accessible interfaces built by pre-organized or self-assembled molecular or supramolecular templates, which create the mesostructure in the material. These templates can be organic compounds (surfactant molecules, amphiphilic block copolymers, dendrimers, etc.) or biomolecules, forming micellar assemblies and/or liquid crystal mesophases or even mesoporous silica frameworks that can be used as a template (nano- or microcasting) to embed any other component or material (r*oute A*).

In many cases, a "cooperative self-assembly" can take place in situ between the templates and the mineral network precursors yielding the organized architectures (*route B*).
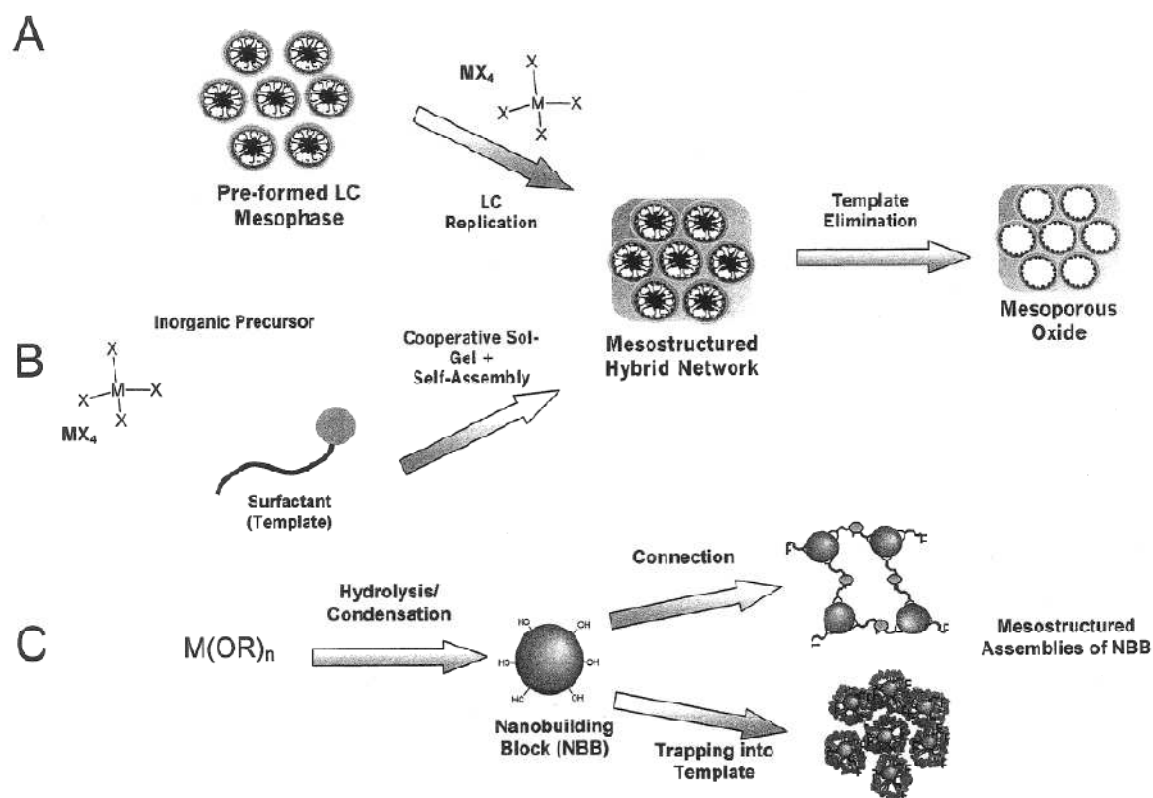
Fig.1: Main synthetic approaches for mesostructured materials. The mesostructure can be previously formed (*route A*) or a cooperative process (*route B*) can take place. *Route C* makes use of preformed nanobuiding blocks (NNB).

2) In the second approach, a nanometric inorganic component is formed (by inorganic polymerization or precipitation reactions). Nanoparticle formation can take place not only in solution but also in micelle interiors, emulsions, or vesicles, leading to complex shaped materials. The control of the dynamics of precipitation of this Nanometric Building Block (NBB) is a key point when syntheses are performed under these conditions. These NBB can be subsequently assembled and linked by organic connectors or by taking advantage of organic functions dangling on the particle surface (*route C*) [6].

The synthetic strategies and routes using NBB leading to ordered or disordered hybrid networks, have been recently reviewed.

All of these strategies based on transcription, synergic assembly, and morphosynthesis can also be simultaneously combined (integrative synthesis) to give rise to hierarchical materials [4]. The key feature in the synthesis of mesostructured materials is to achieve a well-defined segregation of organic (generally hydrophobic) and inorganic (hydrophilic) domains at the nanometric scale; here, the nature of the hybrid interface plays a fundamental role.

The most relevant thermodynamic factors affecting the formation of a hybrid interface have been first proposed by Monnier *et al.* [7] and discussed in depth by Huo *et al.* [8] in their description of the "charge matching" model. The free energy of mesostructure formation ($\mathbf{\Delta G_{ms}}$) is composed of four main terms, which represent, respectively, the contributions of the inorganic-organic interface ($\mathbf{\Delta G_{inter}}$), the inorganic framework ($\mathbf{\Delta G_{inorg}}$), the self-assembly of the organic molecules ($\mathbf{\Delta G_{org}}$), and the contribution of the solution ($\mathbf{\Delta G_{sol}}$).

$$\Delta G_{ms} = \Delta G_{inter} + \Delta G_{inorg} + \Delta G_{org} + \Delta G_{sol}$$

In the classical liquid crystal templating (*route A*), the contribution due to the organization of the amphiphilic molecules prevails over the other interactions. In the cooperative assembly route (B), template concentrations may be well below those necessary for obtaining liquid crystalline assemblies or even micelles. Thus, the creation of a well-defined and compatible hybrid interface between the inorganic walls and the organic templates (i.e., ΔG_{inter}) is central to the generation of a well-ordered hybrid structure with adequate curvature.

This has been demonstrated for silica systems in strongly alkaline media (pH 13) at ambient temperature, where extended silica polymerization is not possible (i.e., $|\Delta G_{inorg}| \rightarrow 0$). In these conditions, hydrolysis and inorganic condensation are separate events [9]. From the kinetic point of view, the formation of an organized hybrid mesostructure is the result of the delicate balance of two competitive processes: phase separation/organization of the template and inorganic polymerization. This issue, well-known in microscale phase segregation [10,11] is essential when one is working with systems where inorganic condensation is fast. In conditions where

condensation is slow (i.e., pH near the pH_{iep} isoelectric point of silica), the kinetic constants (k_i) of the different processes should be ordered as follows:

$$k_{inter} > k_{org} > k_{inorg}$$

Thus, the formation of ordered phases is controlled by the self-assembly involving the hybrid interface. Hence, two aspects are essential to fine-tune the self-assembly and the construction of the inorganic framework: the reactivity of the inorganic precursors (polymerization rate, isoelectric point, etc.) and the interactions to generate a well-defined hybrid interface. These central points are not only relevant for mesostructured silica but can also be translated into the domain of the more reactive non-silica systems.

1.2.1 LIQUID CRYSTAL TEMPLATING (LCT) APPROACH

The obtained mesostructure for M41S materials depends in principle on the surfactant concentration and hydrophobic chain length and on the presence of organic swelling agents, dissolved in the hydrophobic spaces. This analogy with liquid crystal mesophases led Beck [19] and co-workers to initially propose mechanisms in which the texturing effect was provided by a liquid crystalline phase. Two LCT pathways for MCM-41 formation were proposed (**Fig.2**):

(i) Silicate precursors fill the water-rich spaces of the hydrophilic domains of a preformed lyotropic LC hexagonal phase and settle on the polar heads, located at the external surface of the micelles.

(ii) The inorganic species direct the self-assembly process of the surfactant, forming hybrid hexagonal co-arrangements. In both cases, the negatively charged mineral moieties interact preferentially with the ammonium polar heads of the surfactant, which are positively charged. Subsequent condensation leads to a continuous inorganic phase. The formation of MCM-41 begins with the deposition of a silicate layer (consisting of two or three monolayers) on the surface of isolated rodlike micelles. These "rods" are randomly ordered, eventually surrounded by a hexagonal silica mesostructure. Heating and aging of this material complete silicate condensation, leading to the MCM-41 structure.
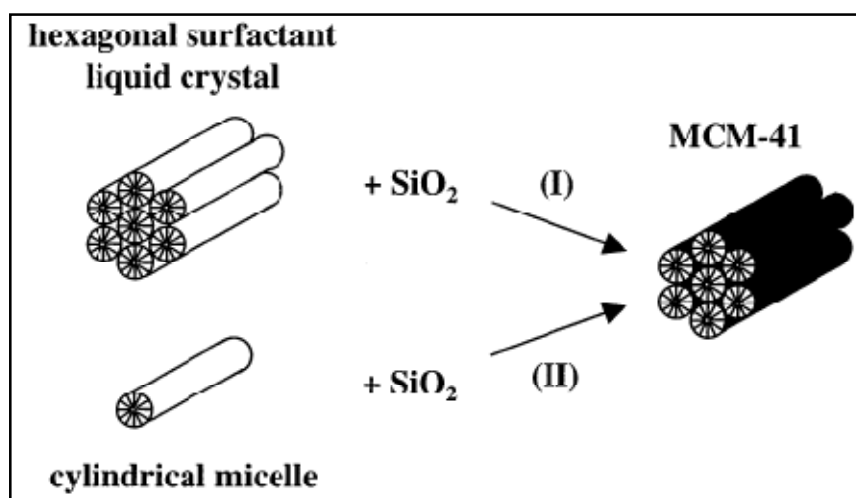
Fig.2: Schematic pathways proposed by Beck *et al.* for MCM-41 formation.

1.2.2 COOPERATIVE ASSEMBLY APPROACH

The use of silica-organic interface interactions that are weak compared to other competing assembly forces, together with kinetic control of the silica polymerization makes it possible to simultaneously control the periodic mesostructure and particle shape. Electrostatic or hydrogen bonding interactions between the surfactant and the growing inorganic species usually leads to a phase separation into a surfactant-rich gel phase and a dilute isotropic solution in which polymerization to the final product occurs [12,13]. The structure of the resulting inorganic solid depends sensitively on the reaction conditions such as concentration, temperature and pH.

During synthesis and processing and before the extensive silica polymerization, the inorganic/organic structures may readily undergo structural changes or transformation to relieve stress trough rotational displacements of the surface (disciplination defects): the use of weaker interaction at the silica/surfactant interface, like hydrogen-bonds, enhances precursor fluidity and synthesis processing. The early synthesis of mesoporous materials was carried out in basic media with anionic silica species and cationic surfactant. In this case the surfactant is positively charged and is balanced by a negative charge of the silica walls. The formation of the inorganic-organic composites is based on electrostatic interaction between the positively charged surfactants and the negatively charged silicate species. First, the oligomeric silicate polyanions act as

8

multidentate ligands for the cationic surfactant head groups, leading to a strongly interacting surfactant/silica interface with lamellar phase. In second step the charge density matching (S^+I^- where S^+ = cationic surfactants and I^- = inorganic species), can directly lead to a phase transformation to, for example, hexagonal or cubic phase [14,15].

Until now, calcination is the more used method to remove organic templating agents, but often it leads to decrease long-range ordering of mesostructure or to partial collapse of mesoporous channels producing a great deal of CO_2 gases and organic compounds. Solvent extraction is a good alternative, not only because it is environmental friendly and the surfactant could be recycled, also because the mesostructure could be easily maintained after this treatment [16]. The preferred shape of self-assembled surfactant molecules in the final material depends on the effective mean molecular parameters that establish the value of the packing parameter *g*. This parameter is defined as:

$$g = \frac{V}{a_0 l_c}$$

where *V* is the effective volume of the hydrophobic chain, a_0 is the mean aggregate surface area per hydrophilic head group and l_c is the critical hydrophobic chain length.

The parameter *g* depends on the molecular geometry of the surfactant molecules, such as the number of carbon atoms in the hydrophobic chain, the degree of chain saturation and the size and charge of the polar head group.

g	**Expected structure**
⅓	Cubic (*Pm3n*)
½	Hexagonal (*p6*)
½ - ⅔	Cubic (*Ia3d*)
1	Lamellar

Tab.1: Parameter *g* of different micellar structures.

In addition, the effects of solution conditions, including ionic strength, pH, co-surfactant concentration, temperature, are implicitly in *V*, a_0 and l_c . In classical micelle chemistry, mesophase transition occurs when the *g* value is increased above critical values: the phase

transitions also reflect a decrease in surface curvature from the cubic over the hexagonal to the lamellar phase (**Tab.1**). Moreover, spherical aggregates are preferentially formed by surfactants possessing large polar head groups: if the head groups are small and packed tightly, the aggregation number increases, resulting in rod-like or lamellar aggregates (**Fig.3**).
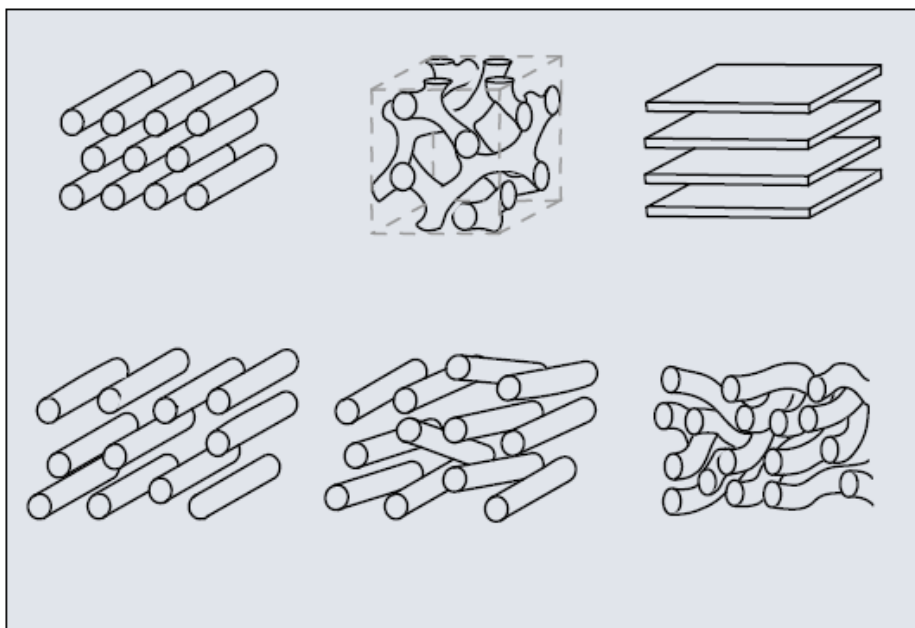
Fig.3: Examples of possible mesophase structure by self-assembly processes.

Ionic surfactant template. According to Mobil's technology, long-chain quaternary ammonium surfactants minimize their energy in solution by assembling into micelles. Under certain conditions these micelles can adopt a rod-like shape and even organize into long-range hexagonal arrays with the charged head groups pointing toward the solution and the long hydrocarbon chains (hydrophobic) pointing toward the center of the micelles.The formation of the micellar rods and their organization into hexagonal arrays is strongly dependent on the surfactants' alkyl chain length, concentration, the nature of the halide counter-ion, and temperature of the solution. Ionic surfactant templating pathways to ordered mesostructures use assemblies of charges surfactant ions (S^+ or S^-) as templates to organize an inorganic framework from charged inorganic oxide precursors (I^- or I^+). These charged templates are usually expensive, strongly bonded to the charged inorganic framework and difficult to recover. In

general, the electrostatically bonded templates are removed by either a calcination process or by an ion-exchange reaction with an ion donor solution. Also, electrostatic templating affords as-synthesized MCM-41 materials with a relatively low degree of framework cross-linking and small framework wall thickness influencing the thermal and hydrothermal stability.

Neutral surfactant templates. Mesoporous materials prepared in the presence of neutral surfactants as the templates usually have improved stability. In case of primary amine, the pore size of the final mesoporous silicas (designed as HMS) may be adjusted by changing the hydrophobic tail length of amines. It is proposed that hydrogen bonding interactions and self-assembly between neutral primary amine micelles (S^o) and neutral inorganic precursors (I^o) directs the formation of mesophases. The mesoporous materials have greater wall thickness due to the absence of electrostatic or charge-matching effects and thus higher thermal stability than M41S materials. However, the materials exhibit only short range hexagonal ordering and disordered channel structure. The high cost and toxicity of amines also limit their use in large-scale production. Polyethylene oxide (PEO) surfactants are a convenient alternative to primary amines and has demonstrated advantageous in solving the problems of ionic surfactant, since the PEO surfactants are neutral, nontoxic, and biodegradable. This approach allows for the preparation of mesoporous molecular sieves with large framework wall thickness, small particle sizes, and complementary framework confined and textural mesoporosity.

In addition, $S^o I^o$ approach allows for cost reduction by employing less expensive reagents and mild reaction conditions while providing for the effective and environmentally benign recovery and recyclability of the templates. It can classify them as:

1) Di-block copolymers with one hydrophobic and one hydrophilic part;

2) Tri-block copolymers with two hydrophilic terminal groups and a central hydrophobic chain;

3) Star copolymers with more hydrophilic and one hydrophobic terminations: Brij (two-block linear), Pluronic (tree block linear) and Tween (star copolymer) are represented in **Fig.4**.

Fig.4: Molecular structures of Brij (a), Pluronic (b) e Tween (c).

In polar environment, because they have amphiphilic properties, the non-ionic block-copolymers reorganize to form macro-molecular structures (micelles) where the non-polar groups of each molecule are closed inside by the polar ones (**Fig.5**). Moreover, these self-assembled structures can give rise to different mesophases (i.e. phase separation with dimension of the order of ten nanometers) according to the effective concentration of copolymer in solution and the particular types of used copolymer: via control of the concentration cubic, hexagonal or lamellar mesophases can be obtained [17-18] while dimension of pore can be controlled using different types of copolymers.

Fig.5: Micellar section in polar environment: different self-assembled structures for BriJ (a), Pluronic (b) and Tween (c). Black lines represent polar groups and grey lines apolar ones of copolymer.

1.3 CHARACTERIZATION OF MESOPOROUS MATERIALS

To dispose of effective methodologies for mesoporous materials characterization is need to understand synthetic mechanisms and determine the connections between synthetic parameters (composition, temperature, pH, etc.) and the properties of obtained materials, with precise techniques to verify the process and the produced materials having desired structural and chemical-physical characteristics. The procedure involves, first, the use of X-Ray powder Diffraction (XRD) which should be carried out at wide and low angles.

The XRD powder *d* spacings of well-prepared MCM-41 and MCM-48 (**Fig.6**) can be indexed on a hexagonal and cubic lattice, respectively. XRD combined with other techniques, such as HRTEM, electron diffraction, and lattice images, are key methods for the characterization of these materials and identification of the phase obtained, i.e. cubic (MCM-48), hexagonal (MCM-41), and lamellar (MCM-50).
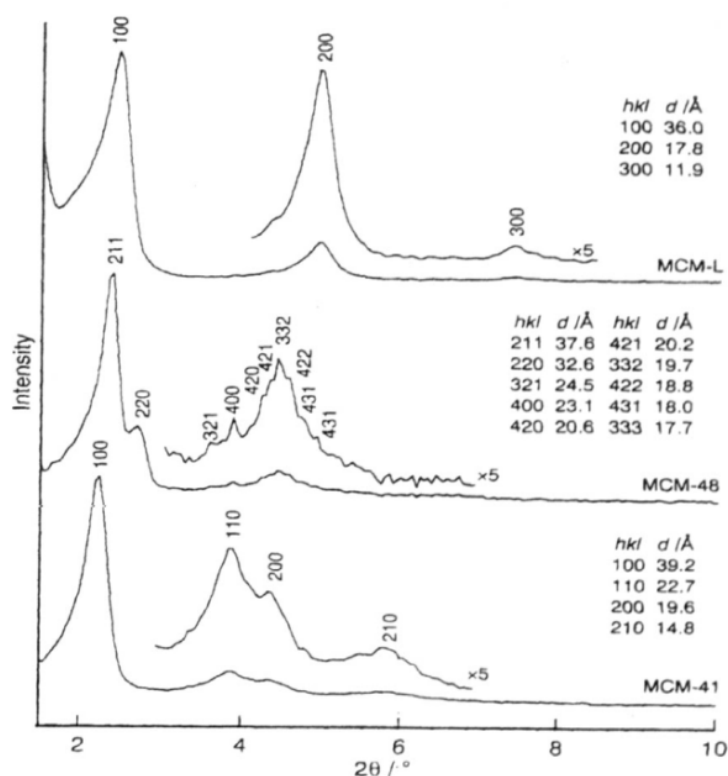
Fig.6: Diffraction Patterns (Cu Kα) of MCM41, MCM48, MCM50 mesophases.

From a combination of these techniques, two structural models with amorphous walls have been constructed for MCM-41 as shown in **Fig.7**.
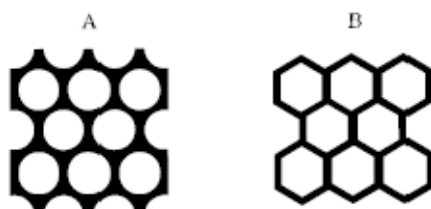
Fig.7: Structural model of MCM-41 with cylindrical pore (A) and hexagonal pore (B).

Adsorption of molecules has been widely used to map the pore size distribution of mesoporous solids. In this sense, the physisorption of gases such as N_2, O_2, and Ar have been used to characterize the porosity of M41S samples and more specifically MCM-41. When adsorption was carried out on a MCM-41 sample (**Fig.8**), it was found that the isotherm for N_2 is type IV in the IUPAC classification, and no adsorption-desorption hysteresis was found at the boiling temperature of N_2 (77.4 K). In the case of Ar and O_2 the isotherm is also of type IV, but they exhibit well-defined hysteresis loops of the VI type. These results can be attributed to capillary condensation taking place within a narrow range of tubular pores confirming the high degree of pore uniformity. Owing to the success of N_2 and Ar adsorption in terms of the determination of the pore diameter, one can combine the XRD results together with the pore size determined from gas adsorption experiments to find the thickness of the wall. Adsorption studies, besides their convenience for measuring the textural properties of these materials, can also be used to study the interaction of molecules with the walls of the pores, a feature of particular importance from the point of view of the diffusion and catalytic properties of the material. In this sense, adsorption studies of polar and no polar molecules can be quite useful for measuring the hydrophobic and hydrophilic properties of M41S mesoporous materials. Another powerful technique for the characterization of M41S mesoporous materials is NMR spectroscopy. Its benefits include the determination of the pore size and the mechanism of formation of the material, to the study of the diffusion of molecules in the pores, and finally, to the organization of the walls in the pure silica and in the isomorphous substituted materials, before and after calcinations pretreatments. It has to be noted that most of the NMR work has been performed to determine the state of Si and Al in the walls of the M41S materials, with some incursion into the mechanism of formation.
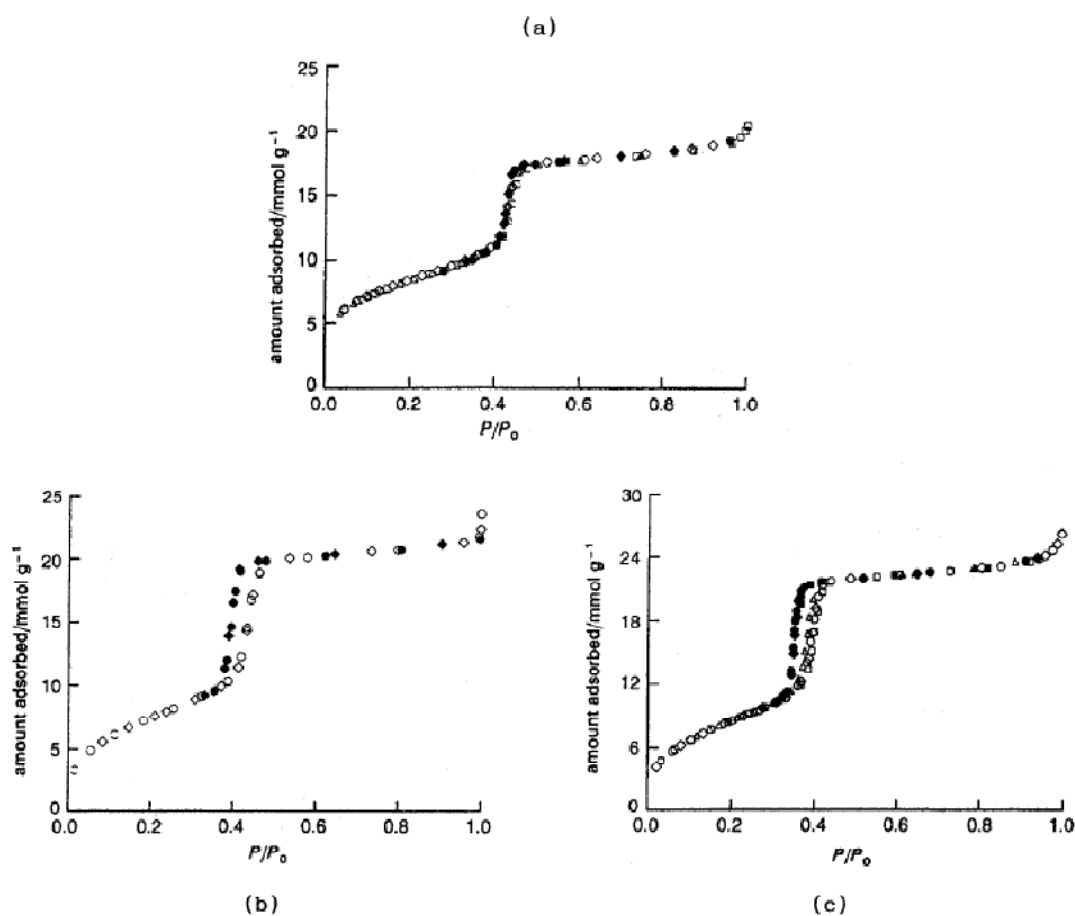
Fig.8: Adsorption isotherms of N_2 (a), argon (b) and oxigen (c) on MCM-41 at 77K.

An other technique is differential scanning calorimetry (DSC) in which the difference in the amount of heat required to increase the temperature of a sample and reference are measured as a function of temperature. The main application of DSC is in studying phase transitions, such as melting, glass transitions, or exothermic decompositions. These transitions involve energy changes or heat capacity changes that can be detected by DSC with great sensitivity. This curve can be used to calculate enthalpies of transitions. This is done by integrating the peak corresponding to a given transition.

Thermogravimetric Analysis (TGA) is a type of testing that is performed on samples to determine changes in weight in relation to change in temperature. Such analysis relies on a high degree of precision in three measurements: weight, temperature, and temperature change. TGA is commonly employed in research and testing to determine characteristics of materials such as

polymers, to determine degradation temperatures, absorbed moisture content of materials, the level of inorganic and organic components in materials, decomposition points of explosives, and solvent residues. For mesoporous materials, TGA allows to know the amount of surfactant or other organic species, present into the structure and water absorbed from the sample.

FTIR spectroscopy is most useful for identifying chemicals that are either organic or inorganic. The term Fourier Transform Infrared Spectroscopy (FTIR) refers to a fairly recent development in the manner in which the data is collected and converted from an interference pattern to a spectrum. FTIR is the most powerful tool for identifying types of chemical bonds (functional groups). The wavelength of light absorbed is characteristic of the chemical bond as can be seen in this annotated spectrum.

To identify less common materials, IR will need to be combined with nuclear magnetic resonance, mass spectrometry, emission spectroscopy, X-ray diffraction, and/or other techniques. Because the strength of the absorption is proportional to the concentration, FTIR can be used for some quantitative analyses.

REFERENCES

1. C.T. Kresge, M.E. Leonowicz, W.J. Roth, J.C. Vartuli, J.S. Beck, *Nature*, **1992**, 359, 710;

2. B.J. Scott, G. Wirnsberger, G. Stucky, *Chem. Mater.*, **2001**, 13, 3140;

3. P.D. Yang, D. Y. Zhao, D.I. Margolese, B.F. Chmelka, G.D. Stucky, *Nature*, **1998**, 396, 152;

4. S. Mann; S.L Burkett, S.A. Davis, C.E. Fowler, N.H. Mendelson, S.D. Sims, D.Walsh, N. T. Whilton, *Chem. Mater*, **1997**, 9, 2300;

5. E. Dujardin, S. Mann, *Adv. Mater.,* **2002**, 14, 775;

6. C. Sanchez, G.J.A.A. Soler-Illia, F. Ribot, C. Mayer, V. Cabuil, T. Lalot, *Chem. Mater.,* **2001**, 13, 3061;

7. A. Monnier, F. Schuth, Q. Huo, D. Kumar, D. Margolese, R.S. Maxwell, G.D. Stucky, M. Krishnamurty, P. Petroff, A. Firouzi, M. Janicke, B.F. Chmelka, *Science,* **1993**, 261, 1299;

8. Q. Huo, D.I. Margolese, U. Ciesla, D.K. Demuth, P. Feng, T. E. Gier, P. Sieger, A. Firouzi, B. F. Chmelka, F.Schuth, G.D. Stucky, *Chem. Mater.*, **1994**, 6, 1176;

9. A.Firouzi, F.Atef, A.G. Oertli, G.D. Stucky, B.F. Chmelka, *J. Am. Chem. Soc.* **1997**, 119, 3596;

10. K.Nakanishi, *J. Porous Mater.*, **1997**, 4, 67.

11. J.Y. Ying, C.P. Mehnert, M.S. Wong, *Angew. Chem., Int. Ed.,* **1999**, *38*, 57;

12. Q. Huo, D.I. Margolese, U. Ciesla, P. Feng, T.E. Gier, P. Sieger, R. Leon, P.M.Petroff,; F. Schuth, G.D. Stucky, *Nature,* **1994**, *368*, 317;

13. C.J. Brinker, G.W. Scherer, *Sol Gel Science*, Academic Press, Orlando, **1990;**

14. U. Ciesla, F. Schuth, *Micropor. Mesopor. Materials*. **1999**, 27, 131;

15. D. Zhao, P. Yang , Q. Huo, B.F. Chmelka, G.D. Stucky, *Curr. Op. Sol. St. and Mat. Sc.,* **1998**, 3, 111;

16. Z.L. Hua, J.L. Shi, L. Wang, W.H. Zhang, *J. Non-Cryst. Sol.*, **2001**, 292, 177;

17. C.T. Kresge, M.E. Leonowicz, W.J. Roth, J.C. Vartuli, J.S. Beck, *Nature*, **1992**, 359, 710;

18. P.C.A. Alberius, K.L. Frindell, R.C. Hayward, E.J. Kramer, G.D. Stucky and B.F. Chmelka, *Chem. Mater*., **2002,** 14, 3284;

19. J. S. Beck, J.C.Vartuli, W.J. Roth, M.E. Leonowicz, C.T. Kresge, K.D. Schmitt, C.T.W.Chu, D.H. Olson, E.W. Sheppard, S.B. McCullen, J.B. Higgins, J.L. Schlenker, *J. Am. Chem. Soc*. **1992**, *114*, 10834.

CHAPTER II

MESOPOROUS ORGANIC-INORGANIC HYBRID MATERIALS

2.1 INTRODUCTION

The possibility to graft organic functional groups on the walls pore of mesoporous material allows to product a new class at high performances materials: *organic-inorganic hybrid materials* [1,2]. Organic functionalization of mesoporous silica matrix allows a precise control of surface properties, modifying hydrophilic-hydrophobic and bulk properties of materials and protecting the surface from chemical attacks. It uses the term hybrid material indicating a covalent bond between the organic and inorganic components within the material. In contrast, the term composite materials is used to describe systems composed of two or more distinctively different components that exhibit an interface; in this case, the interactions between organic and inorganic components are provided by hydrogen bonds, Van der Waals forces and p interactions, or are electrostatic in nature. The control over density, distribution and incorporated organic composites placement is a key factor to shape and control properties and function of hybrid materials. Three pathways are available for the synthesis of porous hybrid materials based on organosilica units: 1) the subsequent modification of the pore surface of a purely inorganic silica material ("grafting"), 2) the simultaneous condensation of corresponding silica and organosilica precursors ("co-condensation") and 3) the incorporation of organic groups as bridging components directly and specifically into the pore walls by the use of bis-silylated single-source organosilica precursors (Periodic Mesoporous Organosilicas (PMO)) (**Fig.1**).

2.2 GRAFTING

Grafting refers to the subsequent modification of the inner surfaces of mesostructured silica phases with organic groups usually after surfactant removal. Mesoporous silicates possess surface silanol (Si-OH) groups that can be present in high concentration and like in amorphous silica, act as convenient anchoring points for organic functionalization. This process is carried out primarily by reaction of organosilanes of the type $(R'O)_3SiR$, or less frequently chlorosilanes $ClSiR_3$ or silazanes $HN(SiR_3)_3$, with the free silanol groups of the pore surfaces (**Fig.2**).

Reagent	Formula	R	R'
CPS	$Si(OCH_3)_3(CH_2)_3Cl$	$(CH_2)_3Cl$	CH_3
PTS	$Si(OCH_3)_3(C_6H_5)$	C_6H_5	CH_3
APS	$Si(OCH_3)_3(CH_2)_3NH_2$	$(CH_2)_3NH_2$	CH_3
MPS	$Si(OCH_3)_3(CH_2)_3SH$	$(CH_2)_3SH$	CH_3
TFTS	$Si(OC_2H_5)_3(CH_2)_2(CF_2)_5CF_3$	$(CH_2)_2(CF_2)_5CF_3$	C_2H_5
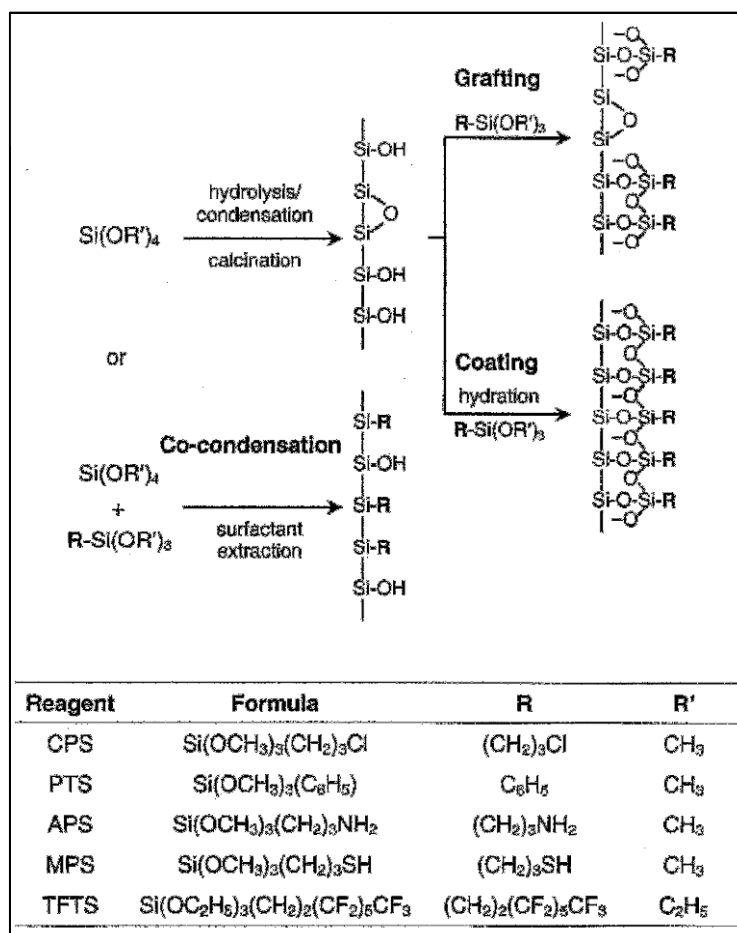
Fig.1: Surface functionalization of mesoporous silica materials.

The functionalization with a variety of organic groups can be realized in this way by variation of the organic residue R. This method of modification has the advantage that the mesostructure of the starting silica phase is usually retained, whereas the lining of the walls is accompanied by a reduction in the porosity of the hybrid material (**Fig.3**). If the organosilanes react preferentially at the pore openings during the initial stages of the synthetic process, the diffusion of further molecules into the center of the pores can be impaired, in turn leading to a no homogeneous distribution of the organic groups within the pores and a lower degree of occupation.
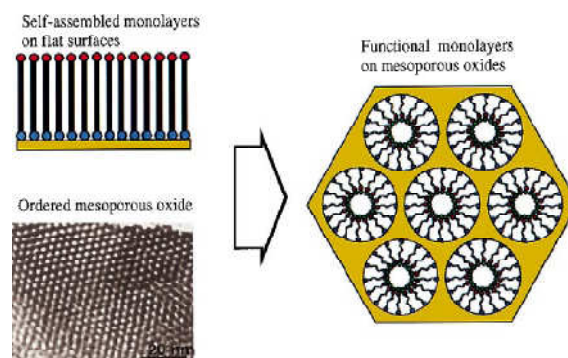
Fig.2: Schematic representation of hybrid mesoporous material by grafting.

In extreme cases (e.g., with very bulky grafting species), this can lead to complete closure of the pores (pore blocking). The process of grafting is frequently erroneously called immobilization, which is a term that we believe should be reserved for adsorptive methods (e.g., the removal of toxic or environmentally relevant contaminants by adsorbent materials).
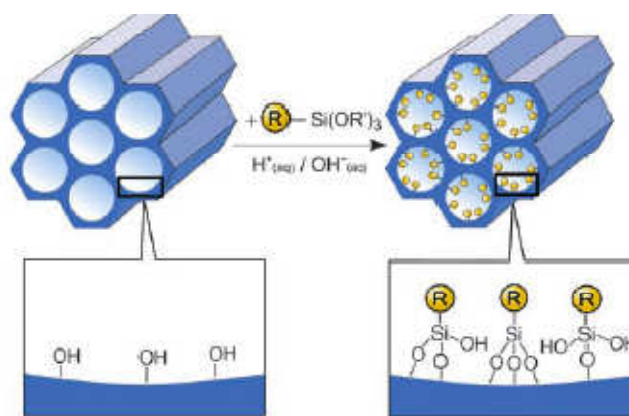
Fig 3: Grafting to organic modification of pure mesoporous silica with terminal organosilanes type (R'O)$_3$SiR.

One of the most spectacular works in the area of subsequent organic functionalization of silica phases was done by Mal et *al.* [3], who successfully constructed a photo-chemically controlled system for compound uptake and release by anchoring coumarin to the pore openings of MCM-41 silica phases. Tournè-Peteilh *et al.* [4] constructed another potential active-compound transport system by chemically anchoring ibuprofen to the inner surface of MCM-41 materials [5]. Rodman *et al.* [6] developed an optical sensor based on mesoporous silica monoliths for the quantitative analysis of Cu(II) ions in aqueous solutions. The post synthetic functionalization of

mesoporous silica phases is also used for the development of adsorbents. Thus, MCM-41, MCM-48 and SBA-15 silica materials have been functionalized with, for example, amino or aminopropyl groups, diamino, triamino, ethylenediamine, malonamide, carboxy, thiol and imidazole groups as well as saccharides. Multiple grafting has also been realized. For example, if uncovered areas remain after silylation (e.g., leaving hydrophilic sites) they can be passivated by trimethylsilylation [7,8], changing the hydrophobicity of the surface and thereby controls adsorption of polar/non-polar molecules. In grafting reactions, the external surface is more easily accessible and is functionalized predominantly over the internal mesopore surface [9]. The functional groups on the external surface are again more accessible in subsequent reactions, leading to reduced selectivities in processes that benefit from pore confinement. Controlled dual functionalization has been achieved by two different methods (**Fig.4**).
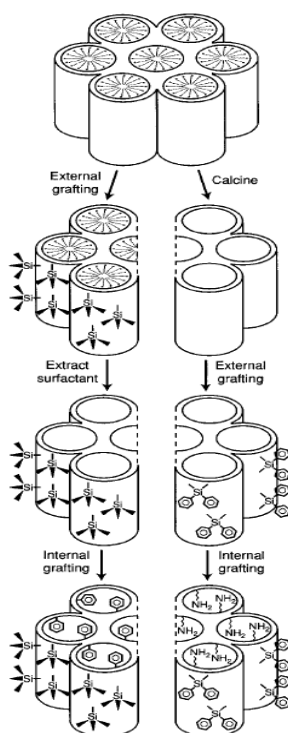
Fig.4: Selective grafting method on the internal and external surfaces of mesoporous silica.

Shephard *et al.* [10] assumed that silanol groups on the external surface of a calcined MCM-41 sample are kinetically more accessible for functionalization. Calcined MCM-41 was modified

first with Ph$_2$SiCl$_2$ to passivate the external surface and then with (MeO)$_3$SiCH$_2$CH$_2$CH$_2$NH$_2$ as an anchor for a redox-active ruthenium cluster acting as a stain in high-resolution transmission electron microscopy. De Juan and Ruiz-Hitzky employed an alternate approach for selective functionalization of external and internal MCM-41 surfaces [11]. The first external grafting step was carried out with the as-synthesized mesoporous sieve whose pores were still filled with the surfactant template. Exposure of this support to a solution of trimethylsilyl chloride resulted in functionalization mainly of the external surface due to steric restrictions in the surfactant-filled mesochannels. The template was then extracted and the internal pore surfaces were functionalized with phenylpropyldimethylchlorosilane.

2.3 CO-CONDENSATION (ONE-POT SYNTHESIS)

An alternative method to synthesize organically functionalized mesoporous silica phases is the co-condensation (one-pot synthesis). It is possible to prepare mesostructured silica phases by the co-condensation of tetraalkoxysilanes [(RO)$_4$Si (TEOS or TMOS)] with terminal trialkoxyorganosilanes of the type (R'O)$_3$SiR in the presence of structure-directing agents leading to materials with organic residues anchored covalently to the pore walls (**Fig.5**).
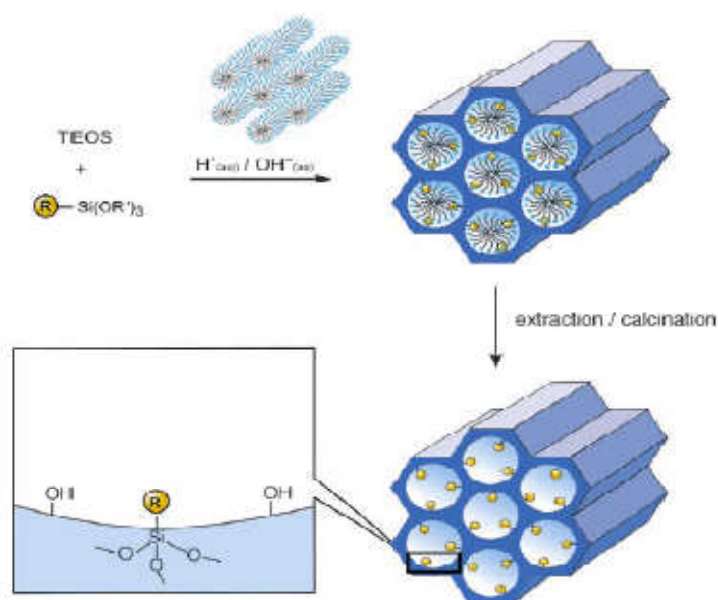
Fig.5: One-pot functionalization method.

Since the organic functionalities are direct components of the silica matrix, pore blocking is not a problem in the co-condensation method. Furthermore, the organic units are generally more homogeneously distributed than in materials synthesized with the grafting process (**Fig.6**).

= functional organosilane
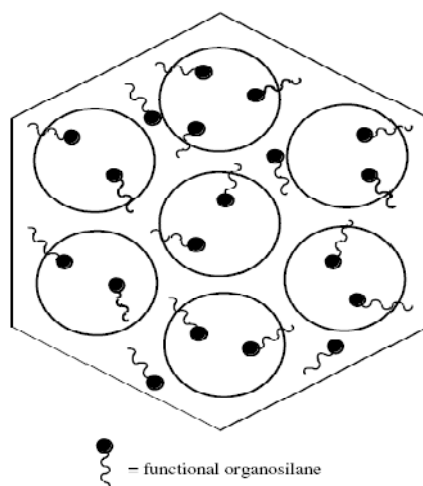
Fig.6: Schematic representation of distribution and placement of functional groups by co-condensation.

However, the co-condensation method also has a number of disadvantages: in general, the degree of mesoscopic order of the products decreases with increasing concentration of $(R'O)_3SiR$ in the reaction mixture, which ultimately leads to totally disordered products. Consequently, the content of organic functionalities in the modified silica phases does not normally exceed 40 mol%. Furthermore, the proportion of terminal organic groups that are incorporated into the pore-wall network is generally lower than would correspond to the starting concentration of the reaction mixture. These observations can be explained by the fact that an increasing proportion of $(R'O)_3SiR$ in the reaction mixture favors homocondensation reactions, at the cost of cross-linking co-condensation reactions with the silica precursors. The tendency towards homocondensation reactions, which is caused by the different hydrolysis and condensation rates of the structurally different precursors, is a constant problem because the homogeneous distribution of different organic functionalities in the framework cannot be guaranteed. Moreover, an increase in loading of the incorporated organic groups can lead to a reduction in the pore diameter, pore volume, and specific surface areas.

Moreover, during template removal, it is important to not disrupt organic functionalities by chemical extraction, used also for the synthesis of mesoporous materials functionalized with dyes [12-14]. Have been investigated density effects of silanol functional charged and products stability, together to silanes concentration/composition effect on the morphology of particles obtained by co-condensation, used also for pore large materials [15]. By using this approach, have been incorporated cheland ligands in to mesoporous products [16] and observed interesting properties [17]. Have been prepared by direct synthesis mesoporous spheres functionalized with thiol [18], or also foams functionalized with amino acids [19]. Lin *et al.* used this method to prepare MCM-41 functionalized with ethylene diammine complexes, which they subsequently to polymerize 1,4 diethyl benzene into the pores, obtaining conductive polymer linearly aligned [20].

2.4 COMPARISON BETWEEN GRAFTING AND CO-CONDENSATION METHODS

The one-pot synthesis [21-23] presents several advantages compared to post-grafting: (i) the functionalisation and structuring of films take place at the same time, (ii) it generally induces a homogeneous distribution of organic probes within the network and (iii) the stoichiometry of the thin film is perfectly controlled and is equal to the composition of the initial solution.
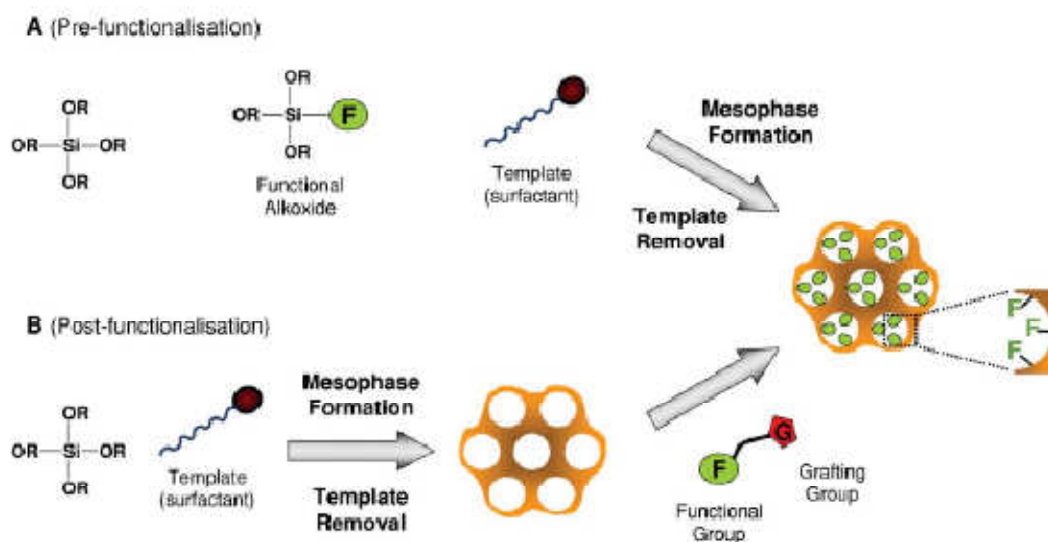
Fig.7: Comparison between grafting and co-condensation.

However, several difficulties exist: solubilization of the probes (organic functionalities) in the medium (addition of co-solvent or protonation); chemical reactions in the organic domain (polymerization of organic species); localization of the probes (organic, inorganic regions or interface); control of the mesophase (influence of the nature and/or amount of probes on the final mesophase); in some cases the organic functionalities cannot be stable in the conditions of one-pot synthesis. Products obtained by post-synthesis grafting are often structurally better defined and hydrolytically more stable than samples from the direct synthesis method. However, the grafting does not provide better control over the amount of organic groups incorporated in the structure, and doesn't allow a uniform surface coverage with organic groups.

2.5 PREPARATION OF PERIODIC MESOPOROUS ORGANOSILICAS (PMOs)

The synthesis of organic–inorganic hybrid materials by hydrolysis and condensation reactions of bridged organosilica precursors of the type $(R'O)_3Si-R-Si(OR')_3$ [24-28] allows the construction of a new class of mesostructured hybrid characterized by a periodically organized pore system and a very narrow pore radius distribution, in which the organic bridges are integral components of the silica network (**Fig.8**). The organic units in this case are incorporated in the three-dimensional network structure of the silica matrix through two covalent bonds and thus distributed totally homogeneously in the pore walls. These materials can have large inner surface areas of up to 1800 m^2/g as well as high thermal stability but generally exhibit completely disordered pore systems with a relatively wide distribution of pore radii. PMO materials are considered as highly promising candidates for a series of technical applications, for example, in the areas of catalysis, adsorption, chromatography, nanoelectronics, or the preparation of active compound release systems.
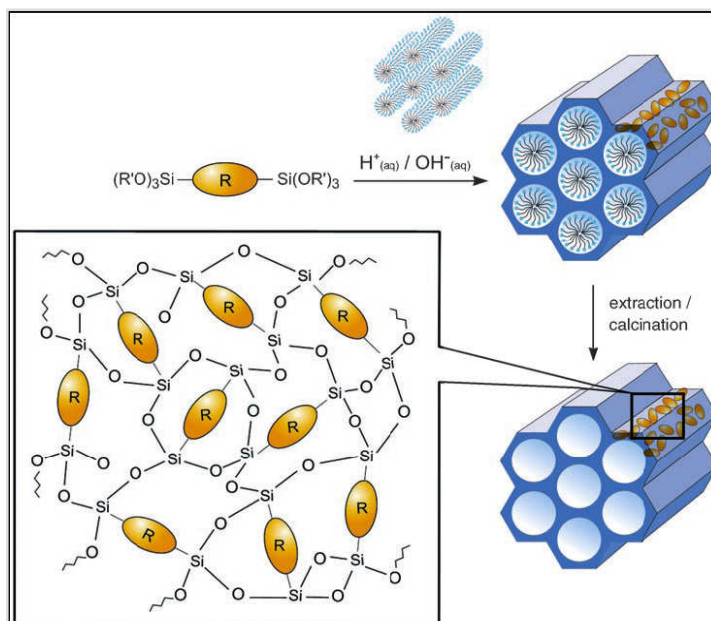
Fig.8: General synthetic pathway to PMOs that are constructed from bissilylated organic bridging units.

2.6 APPLICATIONS

2.6.1 CATALYSIS

During the last few years, hybrid mesoporous solids have been considered for a wide range of heterogeneous catalysis reactions [29]. The confinement of the catalyst within mesopores provides a means of introducing size and/or shape selectivity and thus greater specificity to a reaction. If functional groups are covalently attached to the surface, leaching is minimized. Reactions that have been studied using functionalized mesoporous solids include acid catalysis [30], base catalysis [31], oxidations [32], reductions, [33], enantioselective catalysis, [34], stereospecific polymerizations, [35], and other catalytic reactions that produce fine chemicals. In several investigations, confinement of the catalyst in the mesoporous solid improved the activity compared to attachment to amorphous or non-porous silica, either due to enhanced selectivity in a sterically homogeneous environment or due to higher catalyst turnover brought about by stabilization of the catalyst within the channels.

2.6.2 ENVIRONMENTAL APPLICATIONS

Several environmental issues are being addressed, employing hybrid mesoporous materials either for the generation of desired products without formation of waste, or for waste clean-up, including sorption of toxic heavy metal cations and anions, radionuclides, and organic solvents [37,38].The characteristics of suitable mesoporous sieves for environmental remediation include their high adsorption capacity and specificity for certain contaminants.

2.6.2.1 REMOVAL OF HEAVY METALS

Mesoporous sieves of interest for the removal of toxic heavy metals, such as mercury, cadmium, and lead, are based mostly on mesoporous silicates functionalized with mercaptopropyl surface groups. The thiol functionalities, which exhibit a high affinity for these metals have been incorporated either by grafting or by co-condensation techniques (**Fig. below**). Much of the development has been carried out by the groups of Liu, Pinnavaia, and Mercier [40-41].

Fig. 7. Heavy metal adsorption by thiol-functionalized mesoporous silicates. Adapted from [30].

Feng *et al.* attached MPTMS to large-pore MCM-41 by a wet coating technique, achieving a relative surface coverage up to 76 % [36]. Mercier and Pinnavaia grafted MPTMS onto an HMS support under dry conditions [40-41]. In a comparison between MPTMS-functionalized MCM-41 and HMS, more thiol groups could be attached to the surface of HMS, presumably because removal of the neutral surfactant template from HMS by solvent extraction

preserved more surface silanols than high-temperature calcinations of MCM-41. Thiol-functionalized HMS supports prepared by co-condensation of TEOS and MPTMS using a neutral amine template were equally effective.

2.6.2.2 SORPTION OF ORGANICS FROM AQUEOUS WASTE STREAMS

It is possible to change the wettability of mesoporous silicates by specific surface functionalization. This process can be used to separate liquids of different polarity. Mobil Oil Corporation has patented a sorption separation process using modified MCM-41 for purification of water [42]. Lim and Stein showed in a qualitative way that vinyl-modified MCM-41 exhibited interesting sorption properties [43]. For their affinity for non-polar solvents, vinyl-MCM-41and related materials may be useful for removing small amounts of organic fractions from water or for carrying out "dry" chemical reactions within the channels.

Zhao *et al.* have carried out a systematic study of the sorption properties of silylated MCM-41 to develop selective adsorbents for the removal of volatile organic compounds present in high-humidity gas streams or waste water [44]. MCM-41 modified with trimethylsilyl groups is very hydrophobic, exhibiting a good adsorption capacity for non-polar organic compounds while excluding water in the whole vapor pressure range. Mann and co-workers quantified benzene and water sorption of phenyl-MCM-41 [45]. Corma *et al.* [39] exploited the increase in hydrophobicity and increased stability of trimethylsilylated Ti-MCM-41 to improve the catalytic activity and selectivity in the epoxidation of olefins.

2.6.3 OPTICAL APPLICATIONS

Suitably functionalized hybrid mesoporous silicates are promising candidates for optical applications, including lasers, light filters, sensors, solar cells, pigments, optical data storage, photocatalysis, and frequency doubling devices [46]. Huo *et al.* demonstrated that mesoporous silica fibers can function as optical waveguides [47]. Modification of the mesoporous fibers by incorporation of appropriate dyes would allow tuning of the optical properties. A number of dyes have been integrated in mesoporous solids. Lebeau *et al.* incorporated a photochromic azo dye or a fluorescent laser dye (sulforhodamine B) in MCM-41 by co-condensation of TEOS with (3-aminopropyl)triethoxysilane coupled to the dye [48-49]. The dye molecules were anchored to the

surface and could not be extracted, either during or after surfactant removal. Kinski *et al.* investigated the nonlinear optical properties and polarization of para-nitroaniline entrapped in MCM-41 via the vapor phase or from alcoholic solution [50].

One-dimensional ordering of guest molecules depended on the sorption procedure, post-treatment, and annealing of the sample. Zhou *et al.* incorporated photosensitive copper phthalocyanine or the photosynthetic chlorophyll molecule in mesoporous silicates as well as mesostructured V_2O_5, WO_3, or MoO_3 [51,52]. In some of their experiments a specially functionalized surfactant (11-ferrocenyltrimethylundecylammonium bromide) was used to synthesize hexagonal and lamellar mesostructured silicates with redox active micelles. The ferrocenyl dye encapsulated in the channel structure provided optical absorptions in the visible wavelength region, corresponding to the oxidized and reduced states of the dye. Several pyridine, phthalocyanine, phenanthroline, and quinoline complexes in mesoporous solids were mentioned in the recent review by Moller and Bein [53].

2.6.4 POLYMER SYNTHESES

Mesoporous silicates have been used as hosts or reactors for a variety of polymerization reactions. Wu *et al.* synthesized conducting filaments of polyaniline in aluminosilicate MCM-41 [54]. Llewellyn *et al.* [55] studied the gas phase polymerization of vinyl acetate, styrene, and methyl methacrylate within MCM-41 and noted several confinement effects, including an increase in chain length of poly(methylmethacrylate) with decreasing pore size due to less facile termination processes. Aida *et al.* [57] provided an exciting demonstration of extrusion polymerization by a nanofabrication process [56] modifying the channels (27 Å diameters) of mesoporous silica fibers with titanocene and using these materials as nanoscopic reactors to grow linear polyethylene fibers. The polymerization product consisted of crystalline fibers with high molecular weights and diameters between 30 and 50 nm. The polymer chains formed inside the mesopores at the activated titanocene sites and were then extruded into the solvent phase where they grew into longer crystalline fibers.

2.6.5 FUTURE OPPORTUNITIES

During the last decade much progress has been made in controlling the architecture of porous inorganic solids by using organic molecules or molecular aggregates as structure directors, space fillers, or templates. Functional porous nanostructures can now be designed with a high degree of complexity by combining processes from a number of fields, including sol-gel chemistry, zeolite chemistry, surfactant chemistry, colloid chemistry, and polymer chemistry. Structuring can be carried out on multiple length scales [58]. For example, co-condensation methods combined with colloidal crystal templating have been applied to produce organically functionalized silicates with pore sizes of a few hundred nanometers [59].

In the future one can expect increasingly complex structures that combine hierarchical pore sizes with multiple organic or inorganic functional groups that are strategically placed on the internal or external surfaces and may provide synergistic influences on bulk properties and host-guest interactions. Surface functionalization will make it easier to interface the mesoporous sieves with substrates that may be necessary in device applications (e.g., silicon substrates in the electronics industry). Several procedures have been developed to control the product morphology and to produce larger uniform particles for chromatographic packing materials, shaped particles, fibers, and films for membranes or sensor applications [60,61]. Introduction of organic moieties within the silicate framework may increase the flexibility of mesoporous films and fibers and reduce the brittleness of monoliths. The flexibility in choosing organic, inorganic, or hybrid building blocks and combinations of templates allows one to control the material's properties and to optimize them for each desired application.

REFERENCES

1. S. Inagaki, S. Guan; Y. Fukushima, T. Oshuna, O. Terasaki, *J. Chem. Soc. Chem. Commun*., **1999**, 121, 9611;

2. S. Inagaki, S. Guan, T. Oshuna, O. Terasaki, *Nature*, **2002**, 416, 303;

3. N. K. Mal, M. Fujiwara, Y. Tanaka, *Nature*, **2003**, 421, 350; N.K. Mal, M. Fujiwara, Y. Tanaka, T. Taguchi, M. Matsukata, *Chem. Mater*., **2003**, 15, 3385;

4. C. Tournè-Peteilh, D. Brunel, S. BLgu, B. Chiche, F. Fajula, D. A. Lernera, J.-M. Devoisselle, *New J. Chem*., **2003**, 27, 1415;

5. Q. Fu,G. V. R. Rao, L. K. Ista, Y.Wu, B. P. Andrzejewski, L. A.Sklar, T. L. Ward, G. P. Lopez, Adv. Mater., **2003**, 15, 1262;

6. D. L. Rodman, H. Pan, C.W. Clavier, X. Feng, Z.-L. Xue, *Anal. Chem*., **2005**, 77, 3231;

7. X. S. Zhao, G. Q. Lu, *J. Phys. Chem. B*, **1998**, 102, 1556;

8. T. Tatsumi, K. A. Koyano, Y. Tanaka, S. Nakata, *Stud. Surf. Sci. Catal*., **1998**, 117, 143;

9. M. H. Lim, A. Stein, *Chem. Mater*., **1999**, 11, 3285;

10. D. S. Shephard, W. Zhou, T. Maschmeyer, J. M. Matters, C. L. Roper, S. Parsons, B. F. G. Johnson, M. J. Duer, *Angew. Chem. Int. Ed*., **1998**, 37, 2719;

11. F. de Juan, E. Ruiz-Hitzky, *Adv. Mater*., **2000**, 12, 430;

12. B. Lebeau, C.E. Fowler, S. Mann, C. Farcet, B. Charleux, C. Sanchez, *J. Mater. Chem*., **2000**, 10, 2105;

13. C.E. Fowler, B. Lebeau, S. Mann, *Chem. Commun*., **1998**, 1825;

14. A.S.M. Chong, X.S. Zhao, A.T. Kustedio, S.Z. Qiao, *Microp. Mesop. Mater*., **2004**, 72, 33;

15. A. Walcarius, C. Delacote, Chem. Mater., **2003**, 15, 4181;

16. S. Huh, J.W. Wiench, J.C. Yoo, M. Pruski, V.S.Y. Lin, *Chem. Mater*., **2003**, 15, 4247;

17. M.C. Burleigh, S. Dai, C.E. Barnes, Z.L. Xue, *Sep. Sci. Technol*., **2001**, 36, 3395;

18. K. Kouge, T. Murakami, N. Kikukawa, M. Takemori, *Chem. Mater*., **2003**, 15, 3184;

19. I. Diaz, J. Perez-Pariente, *Chem. Mater*., **2002**, 14, 4641;

20. V.S.Y. Lin, D.R. Radu, M.K. Han, W. Deng, S. Kuroki, B.H. Shanks, M. Pruski, *J. Am. Chem. Soc*., **2002**, 124, 9040;

21. S. Huh, H.T. Chen, J.W. Wiench, M. Pruski, V.S.Y. Lin, *J. Am. Chem. Soc*., **2004**, 126, 1010;

22. N. Yu, Y. Gong, D. Wu, Y. Sun, Q. Luo, W. Liu, F. Deng, *Microporous Mesoporous*

Materials, **2004**, 72, 25;

23. G. Wirnsberger, B.J. Scott, G.D. Stucky, *Chem. Commun*., **2001**, 119;

24. D. A. Loy, K. J. Shea, *Chem. Rev*., **1995**, 95, 1431;

25. K. J. Shea, D. A. Loy, *Chem. Mater*., **2001**, 13, 3306;

26. S. Inagaki, S. Guan, Y. Fukushima, T. Ohsuna, O. Terasaki, *J. Am. Chem. Soc*., **1999**, 121, 9611;

27. B. J. Melde, B. T. Holland, C. F. Blanford, A. Stein, *Chem. Mater*., **1999**, 11, 3302;

28. T. Asefa, M. J. MacLachlan, N. Coombs, G. A. Ozin, *Nature*, **1999**, 402, 867;

29. J. H. Clark, D. J. Macquarrie, *Chem. Commun*., **1998**, 853;

30. M. H. Lim, C. F. Blanford, A. Stein, *Chem. Mater*., **1998**, 10, 467; Y. V. Subba Rao, D. E. De Vos, P. A. Jacobs, *Angew. Chem. Int. Ed. Engl*., **1997**, 36, 2661;

31. C. J. Liu, S. G. Li, W. Q. Pang, C. M. Che, *Chem. Commun*., **1997**, 65;

32. R. Anwander, C. Palm, G. Gerstberger, O. Groeger, G. Engelhardt, *Chem. Commun*., **1998**, 1811;

33. N. Bellocq, S. Abramson, M. LaspØras, D. Brunel, P. Moreau, *Tetrahedron: Asymmetry*, **1999**, 10, 3229;

34. D. J. Macquarrie, *Green Chem.*, **1999**, 195;

35. D. J. Macquarrie, *Philos. Trans. R. Soc. London*, A **2000**, 358, 419,

36. X. Feng, G. E. Fryxell, L.-Q. Wang, A. Y. Kim, J. Liu, K. M. Kemner, *Science,* **1997**, 276, 923;

37. J. Tudor, D. O'Hare, *Chem. Commun*., **1997**, 603;

38. D. Brunel, *Microporous Mesoporous Mater*., **1999**, 27, 329;

39. A. Corma, J. L. Jorda, M. T. Navarro, F. Rey, *Chem. Commun*., **1998**, 1899;

40. L. Mercier, T. J. Pinnavaia, *Adv. Mater*., **1997**, 9, 500;

41. L. Mercier, T. J. Pinnavaia, *Environ. Sci. Technol*., **1998**, 32, 2749;

42. J. S. Beck, D. C. Calabro, S. B. McCullen, B. P. Pelrine, K. D. Schmitt, J. C. Vartuli, US Patent 5 220 101, Mobil Oil Corporation, USA **1993**;

43. M. H. Lim, A. Stein, *Chem. Mater*., **1999**, 11, 3285;

44. X. S. Zhao, G. Q. Lu, *J. Phys. Chem. B,* **1998**, 102, 1556;

45. C. M. Bambrough, R. C. T. Slade, R. T. Williams, S. L. Burkett, S. D. Sims, S. Mann, J.

Colloid Interface Sci., **1998**, 201, 220;

46. C. M. Bambrough, R. C. T. Slade, R. T. Williams, *J. Mater. Chem*., **1998**, 8, 569;

47. Q. Huo, D. Zhao, J. Feng, K. Weston, S. K. Buratto, G. D. Stucky, S. Schacht, F. Schüth, *Adv. Mater*., **1997**, 9, 974;

48. B. Lebeau, C. E. Fowler, S. R. Hall, S. Mann, *J. Mater. Chem*., **1999**, 9, 2279;

49. C. E. Fowler, B. Lebeau, S. Mann, *Chem. Commun*., **1998**, 1825;

50. I. Kinski, H. Gies, F. Marlow, *Zeolites,* **1997**, 19, 375;

51. H. S. Zhou, H. Sasabe, I. Honma, *J. Mater. Chem*., **1998**, 8, 515;

52. I. Honma, H. S. Zhou, *Adv. Mater*., **1998**, 10, 1532;

53. K. Moller, T. Bein, *Chem. Mater*., **1998**, 10, 2950;

54. C.-G.Wu, T. Bein, *Science,* **1994**, 264, 1757.

55. P. L. Llewellyn, U. Ciesla, H. Decher, R. Stadler, F. Schueth, K. Unger, *Stud. Surf. Sci. Catal*., **1994**, 84, 2013;

56. S. A. Johnson, D. Khushalani, N. Coombs, T. E. Mallouk, G. A. Ozin, *J. Mater. Chem*., **1998**, 8, 13;

57. K. Kageyama, J. Tamazawa, T. Aida, *Science*, **1999**, 285, 2113;

58. G. A. Ozin, S. Oliver, *Adv. Mater*., **1995**, 7, 943;

59. S. Oliver, A. Kuperman, N. Coombs, A. Lough, G. A. Ozin, *Nature*, **1995**, 378, 47;

60. M. Grun, I. Lauer, K. K. Unger, *Adv. Mater*., **1997**, 9, 254;

61. J. E. Martin, M. T. Anderson, J. Odinek, P. Newcomer, *Langmuir*, **1997**, 13, 4133.

EXPERIMENTAL SECTION I

The synthesis of mesoporous materials powders has been carried out in the Laboratory of Applied Chemistry of University of Calabria, with the supervision of Prof. Rosario Aiello and Prof. Flaviano Testa and in the "Laboratoire Chimie de la Matière Condensée" of University of Paris VI (France), with the supervision of Prof. Florence Babonneau and Dott. Thierry Azais. Two projects related to synthesis and characterization of mesoporous materials functionalized with different guest molecules have been developed. Important the choice of functional molecules has been to be used as guest species of porous hosts, providing highly advanced products for optoelectronic and photovoltaic devices. A new organometallic zinc(II) complex was used, interesting for its fluorescence properties, synthesized in the Laboratory of Inorganic and Coordination Chemistry of University of Calabria, directed by Prof. Mauro Ghedini and with the supervision of Dr. Iolinda Aiello. Commercial products were used, as phenyl phosphonic acid and benzoic acid, the first useful for the synthesis of hybrid materials, and the second known as model molecule to evaluate the use of mesoporous materials in the system for drug delivery.

The Experimental part I has regarded the synthesis and characterization of mesoporous materials powders, with different organizations and structural characteristics (mesophase type, periodicity, pore dimension, etc.). Have been, in particular, synthesized mesoporous materials powders type MCM-41, MCM-48 and SBA-15, different for structure and pore dimension to evaluate possible surface and structural differences, at the same processing conditions. These materials have been functionalized with amino groups by two different synthetic techniques.

Experimental part II and III have concerned the synthesis and characterization of mesoporous material with hexagonal geometry (MCM-41 and SBA-15 materials) functionalized and not and loaded with phenylphosphonic and benzoic acid, in order to create specific systems host-guest with potential applications in several fields.

EXPERIMENTAL PART I

MESOPOROUS MATERIALS INCORPORATING A ZINC(II) COMPLEX: SYNTHESIS AND DIRECT LUMINESCENCE QUANTUM YIELD DETERMINATION

3.1 INTRODUCTION

New luminescent inorganic-organic hybrid materials incorporating the luminescent zinc(II) complex (ZnL_2) covalently bonded to different types of mesoporous silica hosts (namely MCM-41, MCM-48 and SBA-15), were prepared via both the methods of grafting post-synthesis (GPS) and one-pot synthesis (OPS).

These materials are different from one another in the order of channels in their structures. MCM-41 and SBA-15 materials (**Fig.1**) have a hexagonal phase coming from silica condensation around surfactant micelles with cylindrical morphology and unidirectional pores. MCM-48 material exhibits a three-dimensional pore system, formed by intersected longitudinal pores along the three directions in space.
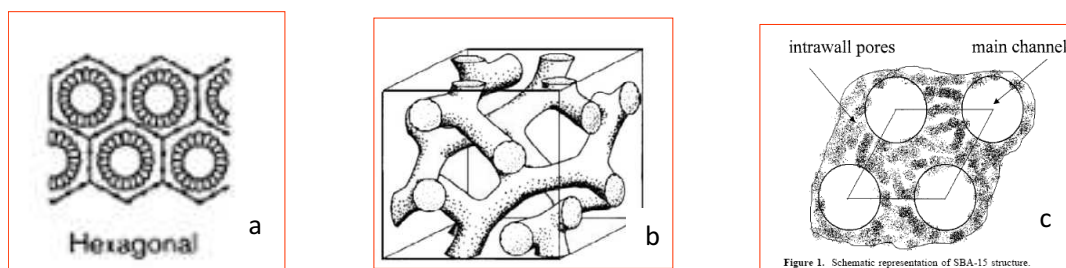
Fig.1: Three structure types observed for silica-surfactant mesophases: (a) MCM-41 (Hexagonal, 1-D); (b) MCM-48 (Cubic, bi-continuous, 3-D); (c) (hexagonal, 3-D). In each type there is a periodic arrangement of pores (or layers), but the inorganic walls (or sheets) are amorphous. All these materials have narrow pore size distributions and high surface areas.

The pore morphology determine the type of molecules that can fit into it and, therefore, those that are eligible, for example, for the adsorption process. The maximum amount accepted depends on the pore volume. The pore walls in these matrices can be functionalized with a wide range of chemical species in order to modify their adsorption properties.

These features make them suitable to host different species for long periods of time, under appropriate conditions. Therefore, the functionalization of the mesoporous walls is another important aspect to consider in these systems. The walls of the matrices of ordered mesoporous materials of silicon oxide contain large amounts of silanol groups, which could facilitate certain interactions. The immobilization of guest species into porous inorganic solids has extensively been investigated to construct functional supramolecular materials [1]. The resulting materials can exhibit unique physicochemical properties controlled by the states of guest species as well as the nature of the porous solids. The mesoporous silica prepared by supramolecular templating method possess advantages such as controlled pore openings, large surfaces area and low dimensional pore geometry for the guest organization. The potential applications of this class of materials include adsorbents, catalysts and their supports, and optoelectronics materials [2,3].

In the field of optical materials, mesostructured materials fall in the range between nanoporous host such as zeolites that can align small molecules and patterned micron-scale photonic band gap materials [4]. However, the mesopore size range presents several possible advantages for optical applications. The high surface area creates the potential to dope materials at higher concentrations without self-interactions. Besides, the meso size range, 2-30 nm, is attractive for producing size-confined structures such as quantum dots [5] or nanowires [6]. Numerous studies have been performed on modification of mesoporous materials to increase their potential applicability. It was demonstrated that the direct introduction of functional molecules during of the one-pot synthesis of mesoporous materials and grafting post-synthesis techniques were two efficient processes.

These two techniques have been utilized to incorporate fluorescent dyes into mesoporous materials, obtaining the so-called luminescent hybrid mesoporous silica (LHMS) [7]; in fact, the advantage of an inorganic matrix embedded with functional chromophores [8-13] is the more rigid environment which stabilizes the luminescent complexes and significantly increases material photostability [12,14,15]. In the last five years many research groups have studied lanthanides complexes embedded into mesoporous materials [16-23]; these studies are connected with the major subject of lanthanide-doped organic–inorganic hybrid materials, within the development of optical materials such as high efficiency and stable solid-state lasers, new fiber amplifiers and sensors, devices with high conversion, fast photochromic and non-linear

responses, *etc*. Their interest relies on the possibility of combining properties of hybrid materials (shaping, tunable refractive index and mechanical properties, corrosion protection, specific adhesion, etc.) and the well-known luminescence of lanthanide ions [24].

LHMS include materials incorporating the well-studied Ru-bipy derived complexes [25,26], organic dyes [27,7], Schiff-base groups chelating Zn^{2+} or Cu^{2+} [13]. The photophysical characterization of LHMS on film or solid is mainly performed by means of emission spectroscopy and lifetime measurement. If LHMS embeds europium complexes, then the evaluation of the emission quantum yield (EQY) can be performed; in fact, on the basis of the corrected emission spectrum and the observed luminescence lifetime of the $^5D_0$ emitting level of Eu^{3+} ion, the EQY of the sample can be calculated according to the method described elsewhere [20,28,29]; in the cases of LHMS films or solids embedding other metals, up to now, no emission quantum yield (EQY) is reported.

This should be ascribed to the difficulty in determining the EQY on solid or film samples, which is a more complex procedure than the corresponding solution measurement and requires an integrating sphere and proper excitation sources. Nevertheless, the lack of this value does not allow a comparison among the photophysics of different chromophore embedded in LHMS, or between the same chromophore before and after immobilization in mesoporous materials, or the evaluation of the photophysical properties of LHMS with a fluorophore incorporated using two different methods, *e.g.* one-pot synthesis and grafting post-synthesis.

We are currently involved in the synthesis and characterization of photoactive materials [30] and recently we have extended our interests to light emitting species supported on inorganic mesoporous materials. Aim of this research is to compare two different synthesis protocols, grafting post-synthesis (GPS) and one-pot synthesis (OPS), which allow for the incorporation of the blue-emitting ZnL_2 complex on different mesoporous hosts, MCM-41, MCM-48 and SBA-15 materials.

MCM-41 has a one-dimensional, hexagonally ordered, unconnected but regular cylindrical pore structure (S_{BET} ~1100 m^2/g, D_{pore} ~30 Å); MCM-48 consists of an uniform array of tubular pores which are 3D connected (S_{BET} ~1500 m^2/g, D_{pore} ~33 Å); SBA-15 exhibits a regular two-dimensional array of tubular channels (S_{BET} ~800 m^2/g, D_{pore} ~50 Å). Because of the differences in their pore dimension and structure, these materials are suitable hosts for

investigating the effect of confinement or incorporation of organic and inorganic guest molecules [31,32]. The properties of the mesoporous solid products obtained by grafting post-synthesis [GPS series: (GPS)(Zn/MCM-41), (GPS)(Zn/MCM-48), (GPS)(Zn/SBA-15)] were compared with those directly synthesized through one-pot synthesis [OPS series: (OPS)(Zn/MCM-41), (OPS)(Zn/MCM-48), (OPS)(Zn/SBA-15)].

The emission spectra are reported and the EQY is measured by means of an integrating sphere. Topology and photophysical properties of both series of products were examined and the differences arising from the different synthesis methods are discussed with reference to the effect of spatial pore arrangement on the host product.

3.2 EXPERIMENTAL SECTION

3.2.1 MATERIALS

Tetraethyl orthosilicate 99% (TEOS; Aldrich) and 3-aminopropyltriethoxysilane 97% (APTES, Aldrich) were used as silica source and siloxane functionalization agent, respectively. Hexadecyltrimethylammonium bromide (CTABr, Fluka) and triblock copolymer Pluronic P123 (EO_{20}-PO_{70}-EO_{20}, Carlo Erba) were used as template agents. Salicyaldehyde 99% and zinc(II) acetate dehydrate were other reagents. Ethanol 99% and ultrapure water, obtained from Milli-Q equipment by Millipore, were used as solvents.

3.2.2 GRAFTING POST-SYNTHESIS (GPS) METHOD

3.2.2.1 PREPARATION OF THE LIGAND HL

Salicylaldehyde (21 mmol, 2.32 g) was added to 4.44 ml of APTES (19 mmol, 4.21 g) in ethanol (4 ml). The solution was refluxed for 5 hours under constant stirring The crude product obtained after evaporation of the solvent under reduced pressure was suspended in chloroform and filtered through a Celite column. The HL ligand obtained was a green-yellow oil which was stored at -15°C (5.85 g, 90% yield).

Elemental analysis, calc. for $C_{16}H_{27}NO_4Si$: C, 59.04; H, 8.36; N, 4.30; found: C, 58.72; H, 8.12; N, 4.10. IR (KBr) ν: 1634 (C=N) cm^{-1}. ^{1}H-NMR ($CHCl_3$) δ: 13.5 (s, 1H, -OH), 8.32 (s, 1H, -CH=N), 7.25 (m, 2H, Ph), 6.96 (d, 1H, Ph), 6.85 (t,1H, Ph), 3.85 (q, 6H, $-OCH_2$), 3.60

(t, 2H, -NCH$_2$), 1.85 (q, 2H, CH$_2$), 1.22 (t, 9H, CH$_3$), 0.68 (t, 2H, -SiCH$_2$) ppm. UV/Vis: λ_{max} (CH$_2$Cl$_2$) 325 nm.

3.2.2.2 PREPARATION OF THE ZINC(II) COMPLEX (ZnL$_2$)

Zinc(II) acetate dihydrate (0.50 mmol, 0.11 g) and HL (1 mmol, 0.33 g) were mixed in 30 ml of ethanol and stirred at room temperature. The reaction mixture was checked by absorption UV-Vis spectroscopy which, after a reaction time of 4 hours, clearly showed that the imine band at 325 nm disappeared and a band at 361 nm appeared, concurrent with the formation of ZnL$_2$.

This reaction product was not separated from the reaction mixture and in the subsequent reactions with the mesoporous silica hosts, ZnL$_2$ was reacted using 1 ml of the described reaction mixture. The workup of the reaction mixture, removing part of the solvent under reduced pressure, gave a solid yellow-green product, (ZnL$_2$)*, in a 45% yield which account for the hydrolyzed ZnL$_2$ derivative containing two -Si(OH)$_3$ groups instead of the initial two -Si(OEt)$_3$ groups. Mp >350°C. Elemental analysis, calc. for C$_{20}$H$_{28}$N$_2$O$_8$Si$_2$Zn: C, 43.99; H, 5.17; N, 5.13; found: C, 44.54; H, 5.44; N, 5.02. IR (KBr) ν: 1619 (C=N) cm^{-1}.

As the complex was insoluble in common solvents, no ^{1}H-NMR analysis was carried out. The luminescence properties of Zn(II) imine complexes arise from the Zn(II) coordination sphere [33-35]. Therefore, the (ZnL$_2$)* photophysical data $\lambda_{em} = 457$ nm and $\Phi = 4.4\%$, as recorded on a powder sample, were used to compare the luminescence of materials synthesized using GPS and OPS.

3.2.2.3 PREPARATION OF MCM-41 MATERIAL

MCM-41 material was prepared from a gel with the following molar composition: TEOS : NH$_4$OH : CTABr : H$_2$O = 1 : 1.64 : 0.15 : 126. In a typical synthesis, 2.40 g of CTABr were dissolved in 120 ml of ultrapure water and stirred until the washed solution was homogeneous and clear. After adding 8 ml of ammonium hydroxide (32 wt%), the mixture was stirred for 5 min, then after 10 g of TEOS were added. The solution was stirred overnight, filtered and washed with water and ethanol. For template removal and access to porosity, the solids were calcined at 823 K for 5 hours.

3.2.2.4 PREPARATION OF MCM-48 MATERIAL

MCM-48 material was prepared from gel with the following molar composition: TEOS : NaOH : CTABr : H_2O = 1 : 0.25 : 0.65 : 62. In a typical synthesis, 23 g of CTABr was dissolved in 111 ml of ultrapure water, then 1 g of sodium hydroxide and 20.80 g of TEOS were added. The solution was stirred for 1 hour, transferred into a polypropylene bottle and heated at 383 K for 3 days. The solid was recovered by filtration, washed with distilled water, and calcined at 823 K for 6 hours.

3.2.2.5 PREPARATION OF SBA-15 MATERIAL

Triblock copolymer was used as surfactant in the synthesis of SBA-15 material. The molar composition of the gel for 4.0 g of Pluronic P123 was: TEOS : HCl : H_2O = 1 : 5.85 : 162.7. In a typical synthesis the block polymer was dissolved in 30 ml of water and 120 ml of chloride acid (2M) solution and stirred constantly. Then 8.50 g of TEOS were added to the solution and stirred at 308 K for 20 hours. The mixture was aged at 353 K overnight without stirring. The solid product was recovered, washed, and air-dried at room temperature. The template was removed by calcination at 773 K for 5 hours.

Because in the following the properties of these starting materials will be compared with those of the grafted samples, MCM-41, MCM-48 and SBA-15 will be indicated, for clarity, as (GPS)(MCM-41), (GPS)(MCM-48) and (GPS)(SBA-15), respectively.

3.2.2.6 PREPARATION OF (GPS)(HL/MCM-41), (GPS)(HL/MCM-48) AND (GPS)(HL/SBA-15)

The procedure of grafting post-synthesis is the same for all the selected mesoporous silica solid products. The incorporation of HL was performed on surfactant-free materials, by adding, under nitrogen atmosphere, an ethanolic solution containing the amount of HL (1 ml) required for a HL/SiO_2 molar ratio $\cong$ 3, to a suspension of 1 g of calcined mesoporous powder in 100 ml of ethanol. This mixture was refluxed under stirring for 17 hours and the resulting solid was filtered, washed with ethanol and acetone, and dried in an oven at 333 K overnight.

IR (KBr) ν: 1647 cm^{-1} [C=N for (GPS)(HL/MCM-41)]; 1647 cm^{-1} [C=N for (GPS)(HL/MCM-48]; 1637 cm^{-1} [C=N for (GPS)(HL/SBA-15)] cm^{-1}. [HL/SiO_2: for (GPS)(HL/MCM-41) =0.08; for (GPS)(HL/MCM-48)= 0.40; (GPS)(HL/SBA-15)=0.43].

3.2.2.7 PREPARATION OF (GPS)(ZN/MCM-41), (GPS)(ZN/MCM-48) AND (GPS)(ZN/SBA-15)

The procedure of grafting post-synthesis is the same for all the selected mesoporous silica solids produced. The incorporation of Zn(II) chromophore was performed on the surfactant-free materials, by addition, under nitrogen atmosphere, of 1 ml of the above described ethanolic solution containing ZnL_2, to a suspension of 1 g of calcined mesoporous powder in 100 ml of ethanol (ZnL_2/SiO_2 molar ratio $\cong 3$).

This mixture was refluxed under stirring for 17 hours. The resulting solid was filtered, washed with ethanol and acetone, and dried in oven at 333 K overnight. IR (KBr) ν: 1631 [C=N for (GPS)(Zn/MCM-41)]; 1634 [C=N for (GPS)(Zn/MCM-48); 1634 (C=N for (GPS)(Zn/SBA-15)] cm^{-1}.

3.2.3 ONE-POT SYNTHESIS (OPS) METHOD

3.2.3.1 PREPARATION OF (OPS)(ZN/MCM-41)

CTABr (2g, 0.0055 mol) was dissolved in 84 ml of distilled water. Then 23.88 ml of sodium hydroxide (1 M) was added to the solution and stirred for 10 min. Successively 9.40 g (0.045 mol) of TEOS and 1 ml of the above described ethanolic solution containing ZnL_2 was added (ZnL_2/SiO_2 molar ratio $\cong 2$). The mixture was stirred for 48 hours at room temperature and the resulting solid was recovered by filtration, washed with ultrapure water, extracted twice with ethanol (1 g of solid for 500 ml of ethanol) and dried at 333 K overnight. IR (KBr) ν: 1634 (C=N) cm^{-1}.

3.2.3.2 PREPARATION OF (OPS)(ZN/MCM-48)

CTABr (2.40g, 0.0066 mol) was dissolved in a mixture of 100 ml of distilled water and 50 ml of EtOH. Then 12 ml of ammonium hydroxide (32 wt%), 3.40 g (0.0163 mol) of TEOS and 1 ml of the ethanolic solution containing ZnL_2 (ZnL_2/SiO_2 molar ratio $\cong 2$) were added. The mixture was stirred for 5 hours at room temperature. After reaction, the solid was recovered by filtration, washed with distilled water, extracted twice with ethanol (1 g of solid for 500 ml of ethanol) and dried at 333 K overnight. IR (KBr) ν: 1634 cm^{-1} (C=N).

3.2.3.3 PREPARATION OF (OPS)(ZN/SBA-15)

Pluronic P123 (4.0 g) was dissolved and stirred in 30 ml of water and 120 ml of chloridric acid (2M). Then 8.50 g (0.041 mol) of TEOS and 1 ml of the above described ethanolic solution containing ZnL_2 were added (molar ZnL_2/SiO_2 molar ratio $\cong 2$) to the mixture and stirred for 20 hours. The solid product was recovered, washed with distilled water, extracted twice with ethanol (1 g of solid for 500 ml of ethanol) and air-dried at 333 K overnight. IR (KBr) ν: 1634 cm^{-1}(C=N).

3.2.3.4 PREPARATION OF (OPS)(MCM-41), (OPS)(MCM-48) AND (OPS)(SBA-15)

In order to compare the properties of materials before and after functionalization, three reference samples were prepared using the same synthesis procedure of one-pot method (see 3.2.3.2), without adding ZnL_2.

3.2.4. CHARACTERIZATION

Elemental analysis was performed using a Perkin Elmer CHNS/O 2400 apparatus and thermogravimetric data (TGA) were obtained with a Netzsch 409 analyzer. The infrared spectra were recorded on a KBr pellet using a Perkin Elmer Spectrum One FT–IR spectrophotometer equipped for reflectance measurements. ^{1}H-NMR spectra were recorded on a Bruker WM spectrometer at 300 MHz. Compounds were dissolved in deuterated chloroform ($CDCl_3$), and tetramethylsilane (TMS) was used as internal standard. X-ray diffraction (XRD) patterns of the powder samples were obtained with CuKα radiation on a Philips PW 1730/10 instrument.

Measurements were performed in a 2θ range of 1-15° range with a step size of 0.005° and a step time of 0.5 s. Nitrogen adsorption-desorption measurements are performed at 77 K on a Micromeritics ASAP 2010. After template removal, the samples were pre-treated under vacuum at 623 K, or at 387 K for the functionalized samples, for 6 hours before analysis. The specific surface area of samples was calculated using the BET model. Pore size distribution curves were obtained with the BJH (Barrett-Joyner-Halenda) method based on the desorption branch of the isotherms. Corrected luminescence spectra were obtained on a Horiba Jobin Yvon Fluorolog 3 spectrofluorimeter, equipped with a Hamamatsu R-928 photomultiplier tube. The emission quantum yields (EQY) of powder samples were obtained by means of a 102 mm diameter

integrating sphere coated with Spectralon® and mounted in the optical path of the spectrofluorimeter using, as excitation source, a 450 W Xenon lamp coupled with a double-grating monochromator for selecting wavelengths. The experimental uncertainties were 1 nm for the band maxima for the luminescence spectra and 5% for EQY.

3.3 RESULTS AND DISCUSSION

Chemically functionalized mesoporous materials incorporating ZnL_2 as a guest molecule were successfully obtained from both the method of grafting post-synthesis (GPS) as well as the one-pot synthesis (OPS) procedure (**Fig.2**).
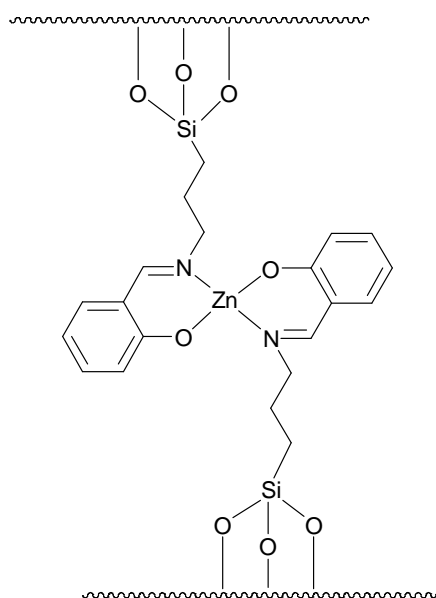
Fig.2: Sketch of a possible chemical structure of the mesoporous-matrix-linked ZnL_2 complex.

3.3.1 GRAFTING POST-SYNTHESIS PRODUCTS:
(GPS)(ZN/MCM-41), (GPS)(ZN/MCM-48) AND (GPS)(ZN/SBA-15)

The GPS method consists of two subsequent steps. In the first, once surfactant has been removed by calcination, the host silica-based mesoporous material formed by silica-surfactant self-assembling [12] occurs simultaneously with the condensation of the inorganic species (TEOS). The second step is the post-synthesis incorporation of the ZnL_2 guest molecule onto the selected mesoporous supports, MCM-41, MCM-48 or SBA-15.

Successful grafting of the ZnL_2 was evidenced by the infrared (IR) spectra of the (GPS)(Zn/MCM-41), (GPS)(Zn/MCM-48) and (GPS)(Zn/SBA-15) products which show the absorption bands characteristic of the C=N stretching at 1631 cm^{-1} for (GPS)(Zn/MCM-41) or at 1634 cm^{-1} for both (GPS)(Zn/MCM-48) and (GPS)(Zn/SBA-15).

These bands are shifted by ca. 10 cm^{-1} to lower values with respect to the corresponding (GPS)(HL/MCM-41), (GPS)(HL/MCM-48) and (GPS)(HL/SBA-15) reference compounds, thus reproducing the trend usually observed with metal complexation to an imino ligand [36]. The amount of the ZnL_2 loading can be conveniently represented by the ZnL_2/SiO_2 molar ratio.

These values are obtained from the experimental TGA data (**Tab.1**) of GPS samples and similar ZnL_2/SiO_2 ratios ranging from 0.09 for (GPS)(Zn/MCM-41) to 0.13 for (GPS)(Zn/SBA-15) were found. Since the reacted ZnL_2 was in large excess with respect to SiO_2 ($ZnL_2/SiO_2 \cong 3$), these results show that ZnL_2 can be successfully grafted on all three host materials used regardless of their different structures.

Tab.1: ZnL_2/SiO_2 ratio obtained through thermogravimetric analysis.

Sample	Ratio ZnL_2/SiO_2	
	(GPS)	(OPS)
(Zn/MCM-41)	0.09	0.14
(Zn/MCM-48)	0.12	0.42
(Zn/SBA-15)	0.13	0.45

The pore structure and channel arrangement of the synthesized materials were studied with XRD powder diffraction (**Fig.S1-S3**), comparing the peaks pattern of the host (GPS)(MCM-41), (GPS)(MCM-48) or (GPS)(SBA-15) starting materials with those of the corresponding (GPS)(Zn/MCM-41), (GPS)(Zn/MCM-48) and (GPS)(Zn/SBA-15) derivatives (**Tab.II**).

The (GPS)(MCM-41) and (GPS)(MCM-48) materials did not exhibit high angle diffraction peaks, but only a broad band alongside the main reflection peak *(100)*. The absence of high angle peaks is typical of poorly ordered long range porous systems.

Tab.II: XRD *d*-spacing of the synthesized siliceous mesoporous samples.

Sample	(GPS)			(OPS)		
	d_{100}	d_{110}	d_{200}	d_{100}	d_{110}	d_{200}
(MCM-41)	4.2			3.9		
(Zn/MCM-41)	4.5			4.2		
(MCM-48)	3.3			3.4		
(Zn/MCM-48)	3.4			3.8		
(SBA-15)	9.2	5.5	5.6	9.1	5.5	5.5
(Zn/SBA-15)	9.5	4.7	5.3	9.7	5.2	5.7

The XRD pattern of (GPS)(SBA-15) showed peaks corresponding to the *(100)*, *(110)* and *(200)* reflections which are diagnostic of the *p*6*mm* hexagonal symmetry. After chemical modification, the *(100)* reflection was still detectable for all of the (GPS)(Zn/MCM-41), (GPS)(Zn/MCM-48) and (GPS)(Zn/SBA-15) series and approximately in the same position of the corresponding parent species (**Tab.II**), suggesting that the pore arrangement of the grafted materials do not undergo significant modification.
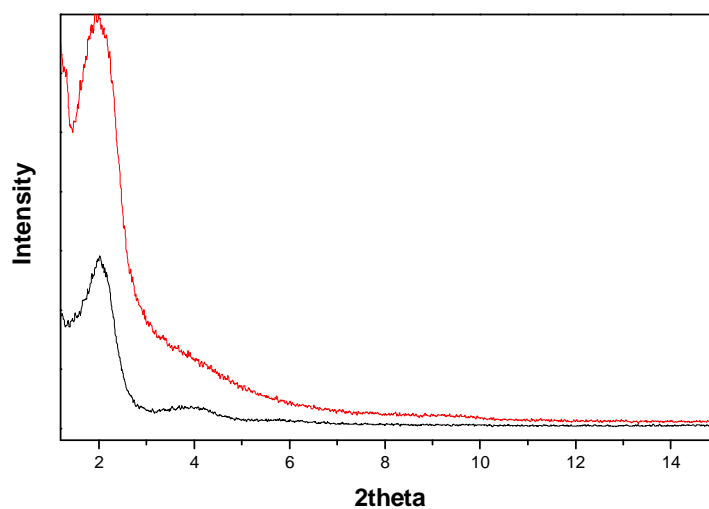
Fig.S1: XRD patterns of (GPS)(MCM-41) (——) and (GPS)(ZnL/MCM-41) (——).
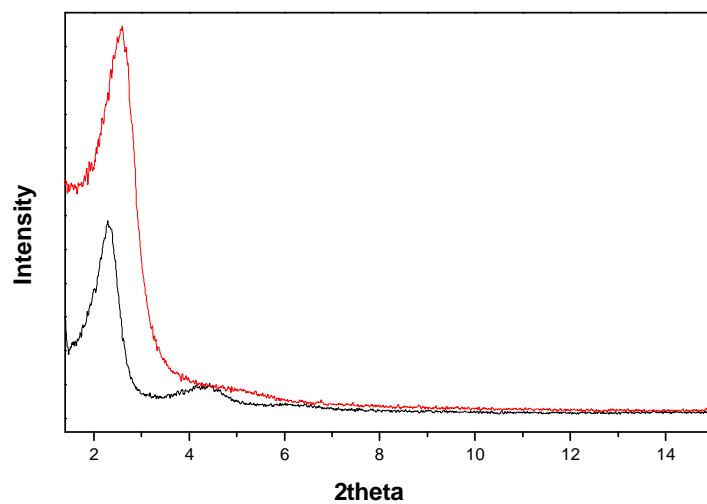
Fig.S2: XRD patterns of (GPS)(MCM-48) (——) and (GPS)(ZnL/MCM-48) (——).
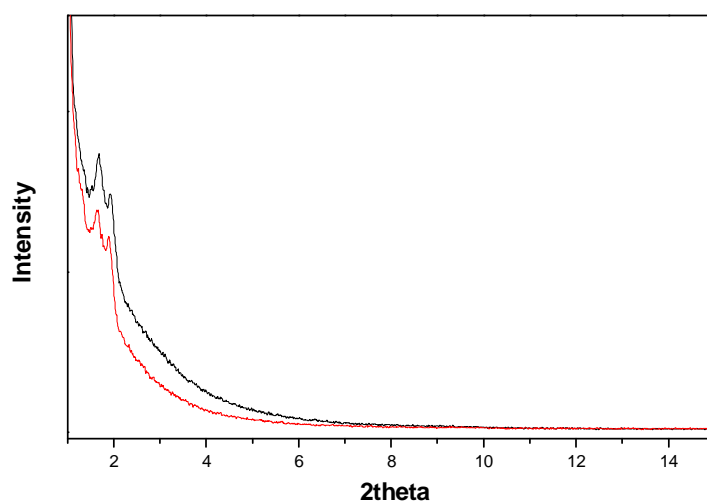
Fig.S3: XRD patterns of (GPS)(SBA-15) (——) and (GPS)(ZnL/SBA-15) (——).

Surface areas and pore volumes were analyzed using the nitrogen adsorption/desorption technique (**Tab.III**). The N_2 adsorption isotherms of (GPS)(Zn/MCM-41) and

(GPS)(Zn/MCM-48) exhibit typical Type IV reversible isotherms while (GPS)(Zn/SBA-15) showed Type IV irreversible isotherms with a hysteresis loop (**Fig.S7-S9**). The shift in nitrogen uptake, together with a decrease in pore volume, suggests that ZnL_2 occupies only part of the available space in the materials.

Table III. Specific surface area calculated with the BET model (S_{BET}), nitrogen adsorption/desorption data (V_p), pore diameter (D_{pore}) of mesoporous materials.

Sample	S_{BET} (m^2/g)		V_p at (cm^3/g) P/P$_0$=0.8		D_{pore}(Å)	
	(GPS)	(OPS)	(GPS)	(OPS)	(GPS)	(OPS)
(MCM-41)	1135	1057	0.68	0.68	30	29
(Zn/MCM-41)	963	898	0.60	0.61	28	27
(MCM-48)	1357	1238	0.79	0.72	33	28
(Zn/MCM-48)	953	912	0.66	0.52	26	26
(SBA-15)	860	822	0.89	0.80	47	41
(Zn/SBA-15)	578	538	0.61	0.66	40	37
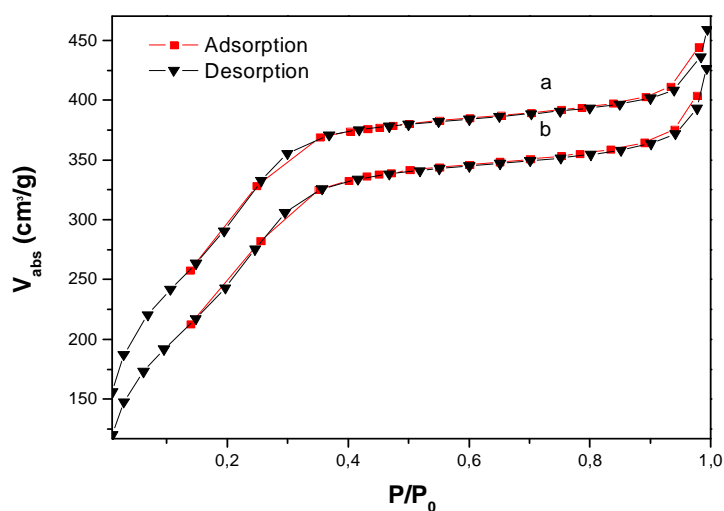
Fig.S7: Absorption/desorption isotherms of (GPS)(MCM-41) (a) and (GPS)(ZnL/MCM-41) (b).
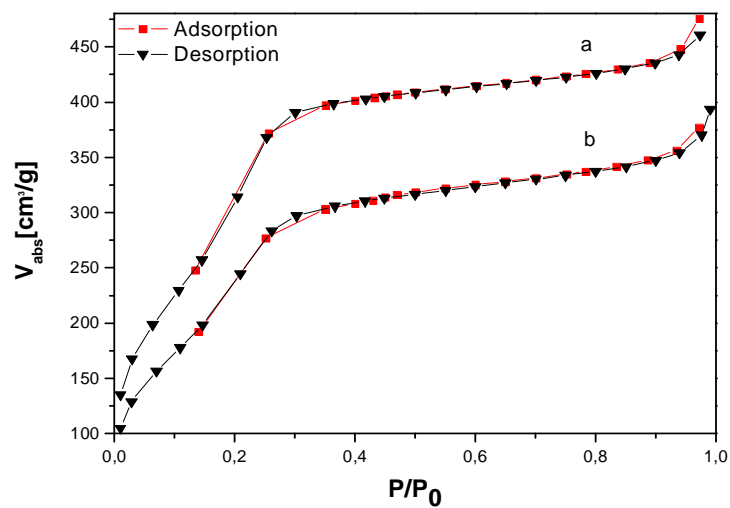
Fig.S8: Absorption/desorption isotherms of (GPS)(MCM-48) (a) and (GPS)(ZnL/MCM-48) (b).
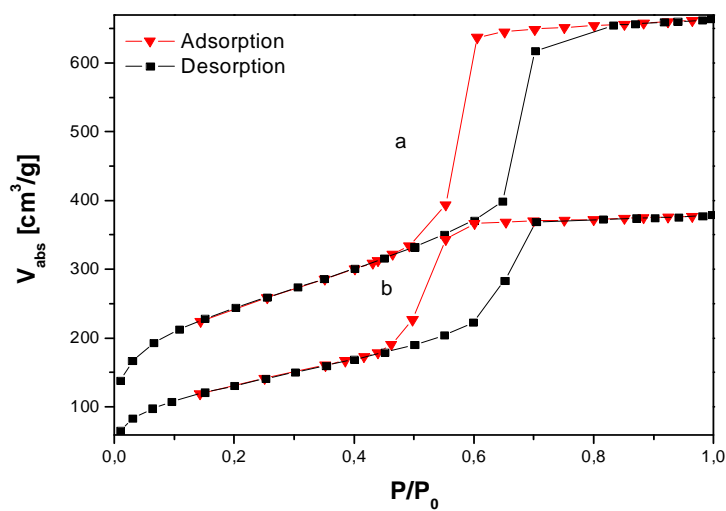
Fig.S9: Absorption/desorption isotherms of (GPS)(SBA-15) (a) and (GPS)(ZnL/SBA-15) (b).

The physical properties of the investigated samples, compared in **Tab.III**, demonstrate that ZnL_2 incorporation influences the adsorption properties and show that ZnL_2 incorporation is governed by the topology of the starting material.

In fact, the specific surface area of the Zn complex-containing materials is reduced as a function of the pore dimensions of the starting material: the greatest degree of reduction (32%) was found with (GPS)(Zn/SBA-15) ($D_{pore} \approx 50$ Å), a 30% reduction for (GPS)(Zn/MCM-48) ($D_{pore} \approx 35$ Å), and only 15% for (GPS)(Zn/MCM-41) ($D_{pore} \approx 30$ Å). Considering the limited ZnL_2 loading (TGA) in the grafted materials and the reduction of both surface area and pore volume, it can be supposed that grafting post-synthesis loading allows for a distribution of the guest species probably most on the external surface of the mesoporous hosts or near the channel openings. The luminescent properties of functionalized samples by grafting were investigated using emission spectra of powder samples sandwiched between two quartz windows (**Fig.3**). Mesoporous materials without zinc(II) complex do not show luminescence, while the samples hosting the Zn(II) species (GPS)(Zn/MCM-41), (GPS)(Zn/MCM-48) and (GPS)(Zn/SBA-15) exhibited an emission maximum at 485 nm and an intense shoulder at about 530 nm.
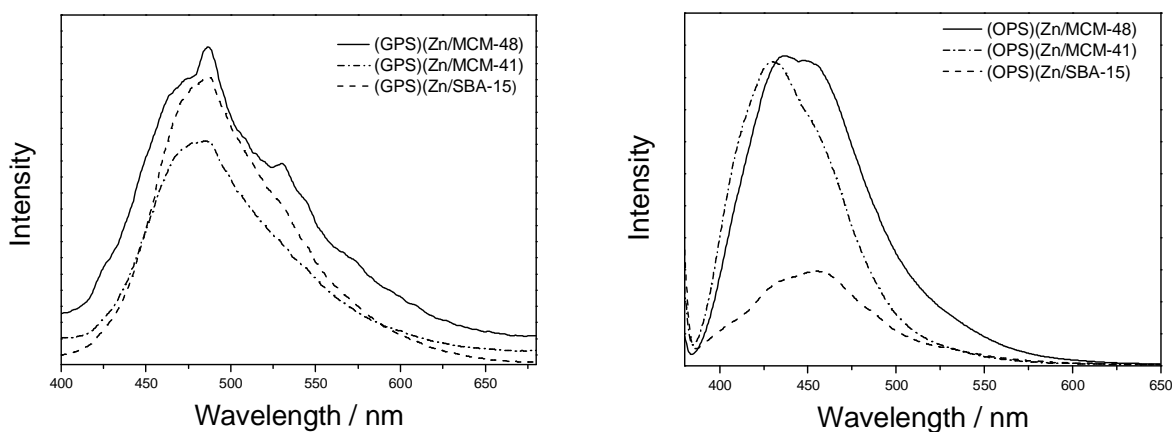
Fig.3: Fluorescence emission spectra of mesoporous hybrid samples, (GPS) and (OPS) series.

The emission quantum yield (EQY) of the GPS samples are independent of the type of mesoporous support, showing similar values, i.e. about 2% (**Tab.IV**). ZnL_2 emission peak is at 457 nm, while the spectral bands of the GPS samples are red-shifted.

The bands shape and the comparison with similar compounds [13,33] indicate that luminescence originates from singlet π-π^* ligand-centered excited state, which is lowered in energy respect to the non-emissive n-π^* iminic state as a consequence of the metal complexation. The spectral red-shift and the decreasing of the EQY of the GPS samples respect to reference compound (2% vs. 4.4%, respectively) could be due to a distortion of the geometry around the metal centre, which implies a mixing between and n-π^* and π-π^* related states; owing to this, the EQY reduces and the Franck-Condon shift enlarges. Moreover, the presence of two principal bands (at 485 and 530 nm) with different red-shift probably accounts for two principal types of confinement, whereby ZnL_2 is grafted on both the external surface and near the opening of the channels. Because these types of immobilization are independent of the type of mesoporous supports used, the EQY is expected to remain almost constant.

Tab. IV: Emission quantum yield (EQY) of the Zn(II) complex-containing mesoporous materials.

Sample	Φ	
	(GPS)	(OPS)
(Zn/MCM-41)	2%	22%
(Zn/MCM-48)	2%	10%
(Zn/SBA-15)	2%	5%

3.3.2. ONE-POT SYNTHESIS PRODUCTS:
(OPS)(ZN/MCM-41), (OPS)(ZN/MCM-48) AND (OPS)(ZN/SBA-15)

The syntheses of the materials functionalized using the one-pot method, (OPS)(Zn/MCM-41), (OPS)(Zn/MCM-48) and (OPS)(Zn/SBA-15), were carried out in a single step (Experimental Section) by reacting ZnL_2 and TEOS, in a molar ratio for $ZnL_2/SiO_2 \cong 2$. The incorporation of ZnL_2 was confirmed by IR spectroscopy, which showed the C=N stretching at values 1648 cm^{-1} for (OPS)(Zn/MCM-41) and 1634 cm^{-1} for both (OPS)(Zn/MCM-48) and (GPS)(Zn/SBA-15), comparable with those recorded for the corresponding compounds of the

GPS series. Quantitatively, the amount of loaded ZnL_2, given by the ZnL_2/SiO_2 ratios calculated from the TGA data (**Tab.I**) is 0.14 for (OPS)(Zn/MCM-41), 0.43 for (OPS)(Zn/MCM-48) and 0.45 for (OPS) (Zn/SBA-15). Interestingly, these values, compared with those obtained for the GPS series, confirm that the ZnL_2 loading obtained from the one-pot method is more efficient that that obtained from grafting post-synthesis. TGA data (**Tab.I**) also show differences among these mesoporous "hosts" as a function of their structure and pore dimensions. The sample with higher amount of ZnL_2 is (OPS)(Zn/SBA-15) due to its larger pore size; samples of (OPS)(Zn/MCM-48) also contained a high amount of ZnL_2 due to the interconnected and three-dimensional channel network of the precursor material.

       In fact, such 3-dimensional channels is more efficient in loading than the one- and bi-dimensional channel of MCM-41 and SBA-15 materials, respectively. X-Ray diffraction, N_2 adsorption/desorption and emission spectroscopy were used to investigate the topology of functionalized mesoporous materials. As seen with the GPS method, XRD patterns showed that functionalization did not alter the texture of the solids, as the hybrid samples exhibited the same structures as the reference samples MCM-41, MCM-48 and SBA-15 materials. The incorporation of the chromophore molecules into the framework was confirmed by an increase in intensity of XRD patterns (**Fig.S4-S6**).
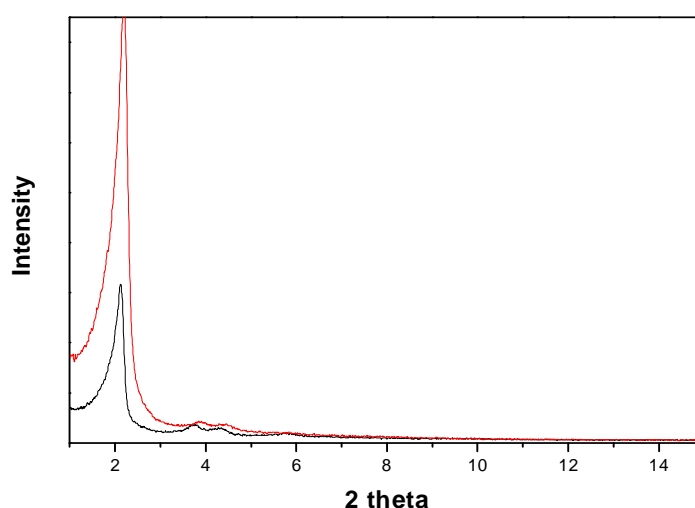
Fig.S4: XRD patterns of (OPS)(MCM-41) (——) and (OPS)(ZnL/MCM-41) (——).
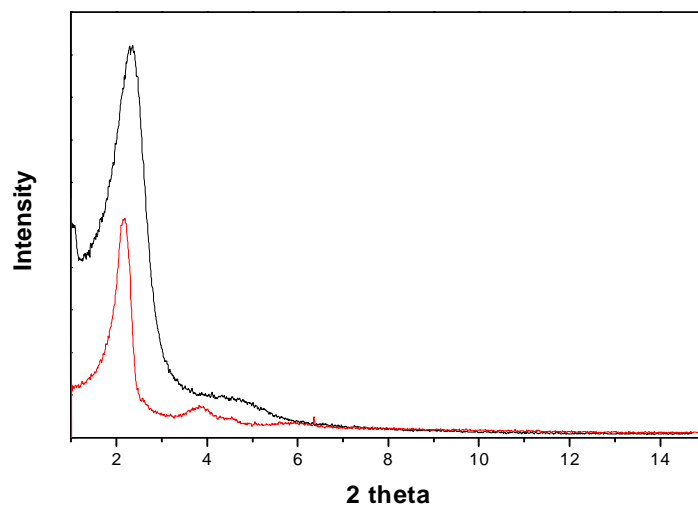
Fig.S5: XRD patterns of (OPS)(MCM-48) (──) and (OPS)(ZnL/MCM-48) (──).
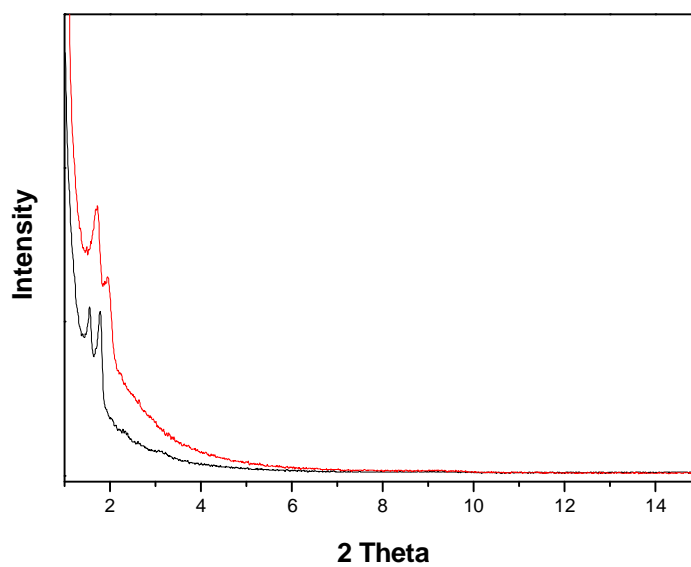
Fig.S6. XRD patterns of (OPS)(SBA-15) (──) and (OPS)(ZnL/SBA-15) (──).

Samples (OPS)(Zn/MCM-41), (OPS)(Zn/MCM-48) and (OPS)(Zn/SBA-15) exhibited adsorption/desorption isotherms (**Fig.S10-S12**) similar to the grafted samples. In the OPS samples, however, the decrease in surface area and pore volume was greater in the ZnL_2-free reference samples than the GPS products. This result is in agreement with the TGA data, corresponding to a higher ZnL_2 content (**Tab.I**).
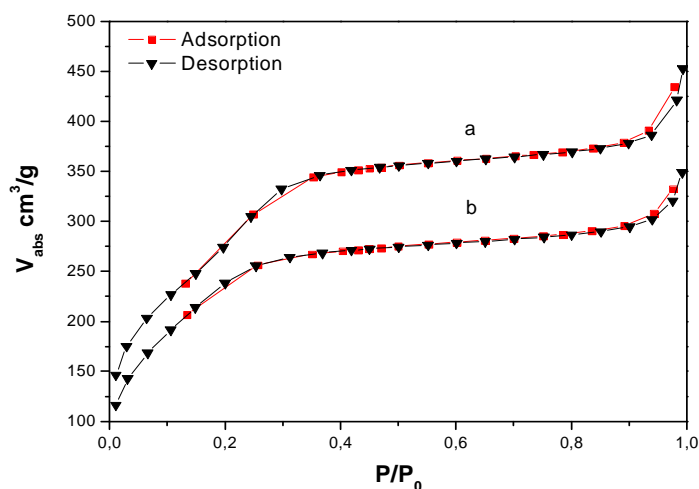
Fig.S10: Absorption/desorption isotherms of (OPS)(MCM-41) (a) and (OPS)(ZnL/MCM-41) (b).
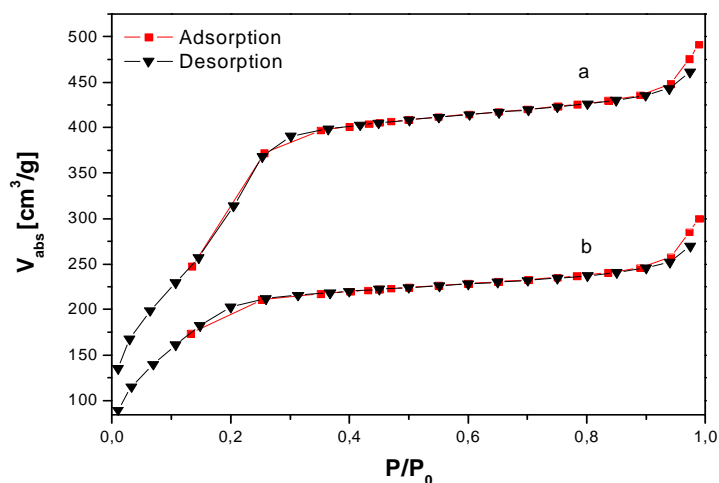
Fig.S11: Absorption/desorption isotherms of (OPS)(MCM-48) (a) and (OPS)(ZnL/MCM-48) (b).
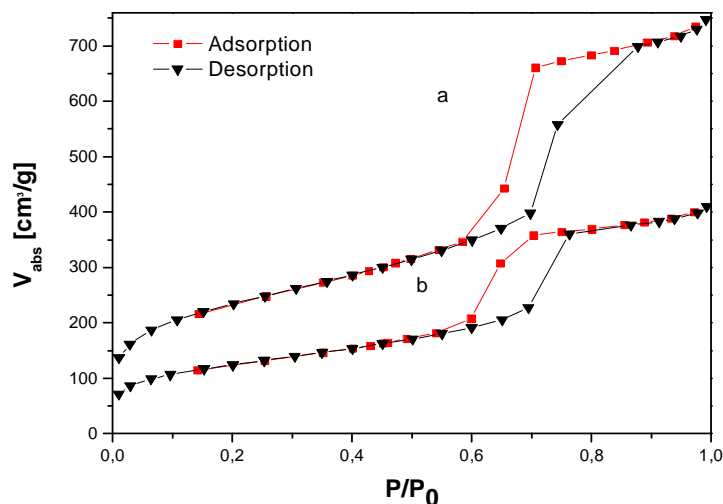
Fig.S12: Absorption/desorption isotherms of (OPS)(SBA-15) (a) and (OPS)(ZnL/SBA-15) (b).

The emission spectra for OPS samples (**Fig.3**) showed an intense peak at 455 nm, and, with respect to spectra from the GPS samples, no relevant shoulders at higher wavelengths were detected. Furthermore, in this case, the EQY was dependent on the mesoporous topology, increasing as pore diameters decreased: (OPS)(Zn/MCM-41) with smaller pores exhibited highest EQY value (22%), while (OPS)(Zn/SBA-15) with large channels showed the lowest EQY (5%). The blue-shift of the emission maximum, related to a greater Frank-Condon shift respect to GPS samples, and the close resemblance with the free ZnL_2, reflect the minor distortion of the chromophore in samples obtained via OPS with respect to GPS.

Considering the trend of EQY, the intense emission of the OPS mesoporous materials could be attributed to the confinement of the chromophores in the walls of the silica matrix and within the channels since in this way, pore size reduction could confers to the luminophore an increased rigidity and a more efficient radiative deactivation.

Similar conclusions have been reported for analogous systems in which conformational restriction of the rigid conjugate system gives rise to fluorescence enhancement [38,39].

3.4 CONCLUSIONS

The covalent incorporation of a luminescent Si(OEt)$_3$-functionalized Schiff base ZnL$_2$ in silica-based mesoporous materials has been successfully accomplished with two different synthetic procedures: grafting post-synthesis and one-pot synthesis. The structural properties and luminescent behavior of these host-guest complexation systems were studied using XRD, N$_2$ adsorption/desorption, TGA and UV/Vis spectroscopy.

In particular, for the first time the luminescent behavior of a LHMS solid samples was quantitatively investigated by direct measurement of the EQY utilizing an integrating sphere coupled with a spectrofluorimeter. Using this method has been possible to evidence a correlation between luminescence intensity and structure of mesoporous materials.

In summary, the photophysical characterization coupled with the usual investigation of the samples does informations about the chromophore distribution in doped mesoporous materials. The ZnL$_2$ amount and the EQY in GPS samples is constant, regardless of the type of starting mesoporous material, suggesting that ZnL$_2$ is principally anchored on the external walls and near the opening of the channels.

Besides, reduction of the S$_{BET}$ after grafting (which was proportional to the pore diameter) indicates that the channel openings are involved in the grafting of the chromophore. In OPS samples, the blue-shift of the emission band respect to GPS samples, the increase in EQY and the decrease in ZnL$_2$ loading which reflects the reduced pore diameter of the starting material, could be referred to an anchorage of ZnL$_2$ principally into the walls and within the channels. With respect to grafting, the one-pot method is simpler in terms of synthesis protocols, offering a better control of organosilane ZnL$_2$ complex-loading and as a result a high homogeneous distribution of organic groups. The best luminescent properties have been obtained in materials synthesized from the one-pot synthesis. Since a tight chromophore confinement can significantly increase the EQY, the present data suggest that MCM-41, which presents a honeycomb-like structure of uniform mesopores is the most suitable host, providing the best fit for the zinc(II) chromophores used here. These results clearly indicate that one-pot synthesis is a reliable procedure for preparing high performing luminescent materials. It should also be mentioned that utilization of ZnL$_2$-loaded MCM-41 is advantagous for the fabrication of organic light emitting devices (OLEDs).

Since the pathways open for n/p migration-recombination are limited essentially to only one dimension, it may be possible to obtain a grater degree of order on electroluminescent processes by utilizing porous, channel-type materials containing light-emitting and electronically interacting guest molecules [37, 38].

REFERENCES

1. F. Hoffmann, M. Cornelius, J. Morell, M. Fröba, *Angew. Chem. Int. Ed.* 45 (**2006**) 3216;

2. G.J.A.A. Soler-Illia, P. Innocenzi, *Chem. Eur. J.* 12 (**2006**) 4478;

3. S. Angelos, E. Johansson, J. F. Stoddart, J. I, Zink, *Adv. Funct. Mater.* 17 (**2007**) 2261;

4. B.J. Scott, G. Wirnsberger, G. D. Stucky, *Chem. Mater.* 13 (**2001**) 3140;

5. H. Parala, H. Winkler, M. Kolbe, A. Wohlfart, R. A. Fischer, R. Schmechel, H. von Seggern, *Adv. Mater.* 12 (**2000**) 1050;

6. Y. J. Han, J. M. Kim, G. D. Stucky, *Chem Mater* 12 (**2000**) 2068;

7. D. Chandra, T. Yokoi, T. Tatsumi, A. Bhaumik, *Chem. Mater.* 19 (**2007**) 5347;

8. C. J. Brinker, G.W. Scherer, *Sol-Gel Science*; Academic Press, New York, **1990**;

9. C. J. Brinker, D.E. Clark, D.R. Ulrich (Eds.), *Better Ceramics through Chemistry*, North-Holland, New York, **1984**, 1;

10. J.D. Mackenzie, D.R. Ulrich (Eds.), *Ultrastructure Processing of Advanced Ceramics*, Wiley, New York, **1988**, 1;

11. R. K. Iler, *The Chemistry of Silica*, Wiley-Interscience, New York, **1979**, 1;

12. R. Reisfeld, C. K. Jørgensen, *Chemistry, Spectroscopy and Applications of Sol-Gel Glasses, Structure and Bonding,* Springer, Berlin, **1992**, 77;

13. H. Zhang, P. Zhang, K. Ye, Y. Sun, S. Jian, J. Wang, W. Pang, *J. Lumin.* 117 (**2006**) 68;

14. Y. Lu, H. Fan, N. Doke, D. A. Loy, R. A. Assink, D. Lavan, C. J. Brinker, *J. Am. Chem. Soc.* 112 (**2000**) 5258;

15. T. Asefa, M. J. MacLachlan, N. Coombs, G. A. Ozin, *Nature* (**1999**) 867;

16. E. DeOliveira, C. R. Neri, O. A. Serra, A. G. S. Prado, *Chem. Mater.* 19 (**2007**) 5437;

17. L.-N. Sun, J.-B. Yu, H.-J. Zhang, Q.-G. Meng, E. Ma, C.-Y. Peng, K.-Y. Yang, *Microporous and Mesoporous Materials* 98 (**2007**) 156;

18. S. Bo, X. Liu and Z. Zhen, *Journal of Luminescence* (**2008**), doi:10.1016/j.jlumin.2008.03.020;

19. L.-N. Sun,Y. Zhang, J.-B.Yu, C.-Y. Peng, H.-J. Zhang, *Journal of Photochemistry and Photobiology A: Chemistry* (**2007**), doi:10.1016/j.jphotochem.2008.04.015;

20. S. Quici, M. Cavazzini, M C Raffo, L. Armelao, G Bottaro, G Accorsi, C Sabatini, F Barigelletti, *J. Mater. Chem.* 16 (**2006**) 741;

21. L. C. Cides da Silva, T. S. Martins, M. Santos Filho, E.E.S. Teotonio, P.C. Isolani, H.F. Brito, M.H. Tabacniks, M.C.A. Fantini, J.R. Matos, *Microporous and Mesoporous Materials* 92 (**2006**) 94;

22. A. Fernandes, J. Dexpert-Ghys, A. Gleizes, A. Galarneau, D. Brunel, *Microp. Mesop. Mater.* 83 (**2005**) 35;

23. Q.G. Meng, P. Boutinaud, A.C. Franville, H.J. Zhang, R. Mahiou, *Microp. Mesop. Mater.* 65 (**2003**) 127;

24. P. Escribano, B. Julian-Lopez, J. Planelles-Aragò, E. Cordoncillo, B. Vianab, C. Sanchez, *J. Mater. Chem.* 18 (**2008**) 23;

25. M. Ogawa, T. Nakamura, J.-I. Mori, K. Kuroda, *Microp. Mesop. Mater.* 48 (**2001**) 159;

26. B. Lei, B. Li, H. Zhang, W. Li, *J. Phys Chem C* 111 (**2007**) 11291;

27. A. B. Descalzo, M. Dolores Marcos, C. Monte, E. Martinez-Manez, K. Rurack, *J. Mater. Chem.*, 17 (**2007**) 4716;

28. S.-J. Seo, D. Zhao, K. Suh, J. H. Shin, B.-S. Bae, *J. Lumin.* 128 (**2008**) 565;

29. M. H. V. Werts, R. T.F. Jukes, J. W. Verhoeven, *Phys. Chem. Chem. Phys.* 4 (**2002**) 1542;

30. A. Crispini, I. Aiello, M. La Deda, I. De Franco, M. Amati, F. Lelj, M. Ghedini, *Dalton Trans.* 43 (**2006**) 5124;

31. K. Moller, T. Bein, *Chem. Mater.* 10 (**1998**) 2950;

32. G. A. Ozin, E. Chomski, D. Khushalani, M. J. MacLachlan, *Curr. Opin. Colliod Interface Sci.* 3 (**1998**) 181;

33. M. La Deda, M. Ghedini, I. Aiello, A. Grisolia, *Chem. Lett.* 3 (**2004**) 1060;

34. T. Sano, Y. Misho, Y. Hamada, H. Takahashi, T. Vsuky, K. Ghibata, *J. Mater. Chem.* 10 (**2000**) 157;

35. P. Wang, Z. Hang, Z. Xie, S. Tang, O. Wong, C.-S. Lee, N. Wong, L. Hung, S. Lee, *Chem. Commun.* (**2003**) 1664;

36. T. Yu, W. Su, W. Li, Z. Hong, R. Hua, M. Li, B. Chu, B. Li, Z. Zhang, Z. Z. Hu, *Inorg. Chim. Acta* 359 (**2006**) 2246;

37. L. Z. Zhang, Y. Xiong, P. Cheng, G.-Q. Tang, D.-Z. Liao, Chem. Phys. Lett. 358 (2002) 278.

38. L. Gao, Y. Wang, J. Wang, L. Huang, L. Shi, X. Fan, Z. Zou, T. Yu, M. Zhu, Z. Li, *Inorg. Chem.* 45 (**2006**) 6844.

EXPERIMENTAL PART II

SYNTHESIS AND CHARACTERIZATION OF PHENYLPHOSPHONIC ACID TRAPPED INTO MESOPOROUS SILICA-BASED MATERIALS

3.1 INTRODUCTION

Mesoporous materials [1] are one of the most studied inorganic materials known till date because of their interesting 2-D and 3-D open framework structures and widespread applications as ion-exchanger, adsorbent, support, film, acid–base, oxidation catalysts, etc. Among these, phosphate-based molecular sieves [2,3] have attracted considerable attention from academia and industry because of their high potential to various applications, especially in biological utilizations [4]. Although varieties of pure and binary mesoporous metal phosphates such as Ti [5], Al [6], Zr [7], Nb [8], Sn [9], In, W, Ce, V [10] have been reported, only few phosphate based hybrid materials have been used in catalysis [5,11,12].

The syntheses of organic–inorganic hybrid mesoporous silica materials have attracted widespread attention in this context [13-16]. These functionalized mesoporous materials are of great interest due to their range of potential applications in electronics, optics, catalysis, adsorption, etc. These hybrid materials having mesoporous structures with exceptionally high surface area allow the binding of a large number of surface chemical moieties leading to their unique properties associated with the surface functional groups. In this work we have succeeded in the syntheses of mesoporous [17] phosphates, by using neutral and cationic surfactants. The presence of phenyl group in the hybrid mesoporous materials [18] may have many advantages: (a) hydrophobicity of the material can be increased; (b) acid sites can be generated for their use as proton conductor in anode or cathode catalyst and as membrane in fuel cell technology; (c) shape selective acid catalysis is also expected because this material possesses definite pore size, which will allow the passage of molecules smaller than its pore size.

Here is reported the synthesis of mesoporous hybrid (organically modified) materials by using phenylphosphonic acid (**Fig.1**) as the source of phosphorus in the presence of cationic and neutral surfactants. The main interest in studying phenylphosphonic acid are its chelation properties, which allow the synthesis of hybrid materials either by surface modification of metal

oxides [19] or by sol-gel processing [20] and its use as a precursor in the synthesis of alumino-titanophosphonate clusters [21] that can be considered as good starting point in the so-called "building block strategy". Detailed characterizations were performed to understand surface properties of these novel mesoporous materials.
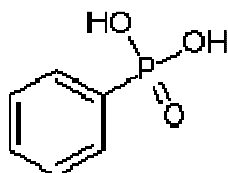
Fig.1: Phenylphosphonic acid.

3.2 EXPERIMENTAL SECTION

3.2.1 MATERIALS

Tetraethyl orthosilicate 99% (TEOS, Aldrich) and 3-aminopropyltriethoxysilane 97% (APTES, Aldrich) were used as silica source and silane functionalization agent, respectively. As template agents were used hexadecyltrimethylammonium bromide (CTABr) and triblock copolymer Pluronic P123 (EO_{20}-PO_{70}-EO_{20}). As guest molecule, phenylphosphonic acid and ethanol 99% were used and ultrapure water as solvents.

3.2.2 SYNTHESIS OF MCM-41 MATERIAL

MCM-41 material was prepared using a procedure adapted from a work of Lesaint *et al.* [22]. 0.8 mL of CTAB ($C_{16}H_{33}N^{+}(CH_3)_3Br^{-}$; Fluka) was stirred with 42.8 mL of a 0.1 M NaOH aqueous solution (Aldrich) at 40°C and after complete dissolution, 3.81 g of TEOS (tetraethoxysilane; Aldrich) were added. The final molar ratios were TEOS: CTAB: NaOH: H_2O = 1:0.12:0.23:130. The solution was kept for three days at room temperature under magnetic stirring, then was recovered, washed with deionised water and dried at 70°C overnight.

The surfactant was removed from this silica-based material by chemical extraction [23], suspending 1 g of sample in a mixture of 300 mL of ethanol and 25 mL of HCl (37% in weight). The mixture was kept under reflux overnight and the solid was recovered by filtration and dried at 70°C.

3.2.3 SBA-15 SAMPLE SYNTHESIS

The preparation of the silica-based SBA-15 material was similar to that described by Zhao *et al.* [24]. The template solution was prepared dissolving 4.0 g of Pluronic $^{®}$ P123 (Fluka) in 104 mL of deionized water and 20 mL of 37 wt% HCl with stirring at 35°C. Then, 9.16 mL of TEOS were added under magnetic stirring for 12 hours at room temperature. The molar composition of final gel mixture was:

$$TEOS/HCl/P123/H_2O = 1:6.03:0.017:145.$$

The white precipitate was aged at 100°C for 24 hours, then filtered, washed with deionised water and dried at 60°C for 12 hours. Calcination was carried out on this sample by increasing the temperature with heating rate of 10°C/min to 550°C in 8 hours in air.

3.2.4 POST-SYNTHESIS GRAFTING OF MCM-41 AND SBA-15 MATERIALS

1 g of the mesoporous materials (MCM-41 and SBA-15 free template, previously activate in oven at 120°C for 2 hours) with 1.33 mL of APTES $((C_2H_50)_3Si(CH_3)_3NH_2$; Aldrich) were put in 20 mL of toluene (Fluka) under magnetic stirring. The mixture was heated under reflux at 110°C overnight and the product was filtered, washed with toluene and dried at 100°C. Amine-functionalized mesoporous silica materials were denoted MCM41-NH_2 and SBA15-NH_2.

3.2.5 LOADING PHENYLPHOSPHONIC ACID

The free template (MCM-41, SBA-15) and amine-functionalized samples (MCM41-NH_2, SBA15-NH_2) were activate at 100°C for 12 hours. The encapsulation process was performed by incipient wetness procedure [25], soaking 0.500 g of sample in a solution of phenylphosphonic acid $(C_6H_7O_3P$; Fluka; 0.012 g cm^{-3}) in ethanol for 24 hours. This procedure was repeated three successive times, and after each impregnation, the solvent was removed by heating at 70°C overnight. After third impregnation, the samples were washed with 4 ml of ethanol, under vacuum, and dried in oven at 70°C overnight. The samples loaded were labelled as MCM41-AF, MCM41-NH_2-AF, SBA15-AF and SBA15-NH_2-AF, where AF stands for phenylphosphonic acid.

3.3 CHARACTERIZATION

The infrared spectra were recorded on a KBr pellet using a Perkin Elmer Spectrum One FT–IR spectrophotometer, in the 4000-500 cm^{-1} range (256 scans with a 4 cm^{-1} resolution). The spectra were recorded in transmission using anhydrous KBr powder, with the background recorded using KBr pellet. XRD patterns were recorded with a Philips PW 1830 diffractometer equipped with a Cu-Kα source. Measurements were performed in a 2θ range of 1-6° range with a step size of 0.002° and a step time of 3 s.

Nitrogen adsorption-desorption measurements were conducted at 77 K on a Micromeritics ASAP 2010. The samples free template were out-gassed under vacuum at 350°C, and the amine-functionalized samples at 115°C for 6 hours before analysis. Micrographs of the cross section of selected calcined and impregnated materials were obtained with a transmission electron microscope (TEM) JEOL 100 CX II apparatus. Mesoporous powders were deposited on a carbon-coated copper grid. EDX analysis were achieved using EDAX Genesis software.

3.4 RESULTS AND DISCUSSION

3.4.1 N$_2$ ADSORPTION/DESORPTION ISOTHERMS

Nitrogen adsorption/desorption isotherms on different SBA-15 materials are presented in **Fig.2**. According to the IUPAC classification, SBA-15 free template material exhibits type IV isotherms with the H2 type hysteresis loops characteristic of a mesoporous solid having shape and size pore slightly different. This loop became more narrow for the samples SBA15-AF, SBA15-NH$_2$ and SBA15-NH$_2$-AF, with parallel adsorption and desorption branches corresponding to a narrow distribution of pores. According to the IUPAC classification, type IV isotherms can be observed for MCM41, MCM41-AF and MCM41-NH$_2$ samples (**Fig. 2**), with pore filling in the range 0.25-0.40 *P/P$_0$*. However, a type II isotherm, typical of non porous materials is observed for MCM41-NH$_2$-AF.
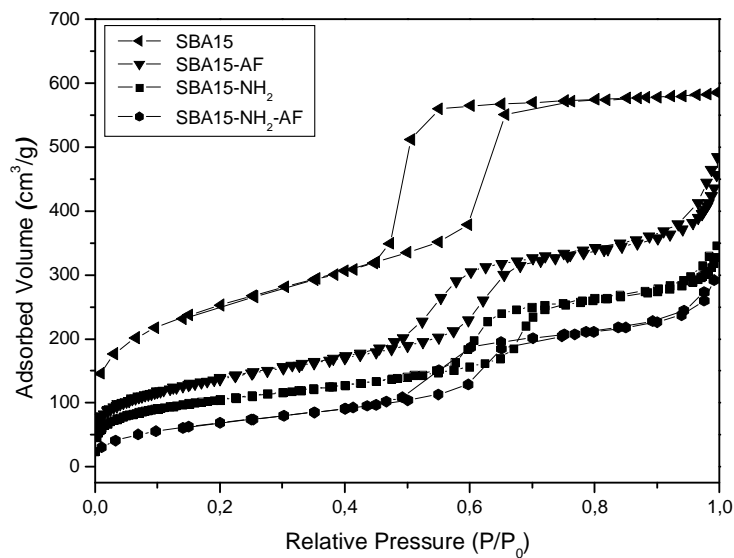
Fig.2: Nitrogen adsorption/desorption isotherms of SBA-15 materials
before and after amine functionalization and further phenylphosphonic acid loading.
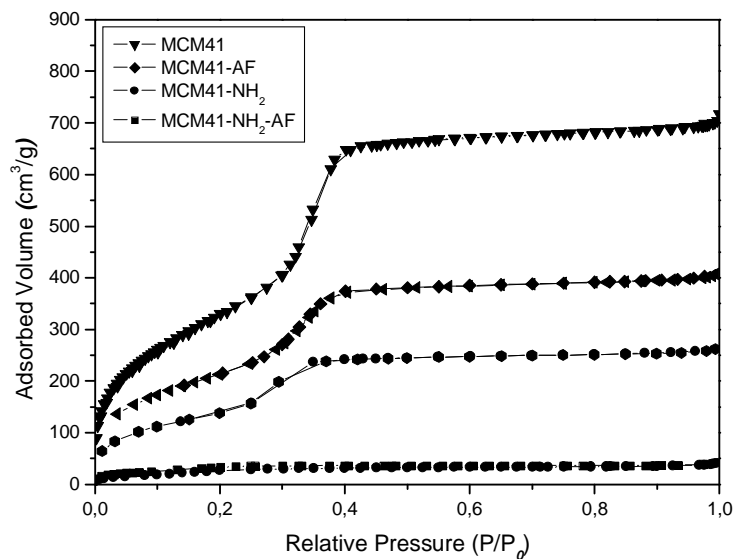
Fig.3: Nitrogen adsorption/desorption isotherms of MCM41 materials
before and after amine functionalization and further phenylphosphonic acid loading.

Tab.1 and Tab.2 summarize the specific surface areas, pore volumes and pore size of all materials prepared. The specific surface area of samples was calculated using the BET model [26]. The pore size was obtained with the BJH (Barrett-Joyner-Halenda) method based on the desorption branch of the isotherms [27]. Specific surface areas of 1477 m^2/g and 766 m^2/g were measured on the MCM41 and SBA15 samples, respectively. For the relative samples functionalized and loaded, a drastic decrease of the specific surface area and pore volume was observed, suggesting the incorporation of these functionalities in the pore channels.

In particular, for the MCM41-NH_2-AF, the immobilization of phosphonic acid within the pore system showed a significant decrease in the surface area and pore volume, probably due to a quasi complete blocking of the pore openings. With the grafting of organic amino groups onto parent silica based materials, the pore size is reduced from 6.0 to 5.4 nm for SBA15 and from 3.2 to 2.5 nm for MCM41 materials. The pore volumes decrease with the similar trend for both series. These changes indicate that amine groups have been introduced into the mesoporous channels.

Tab.1: Summary of Porosity Characteristics for SBA15 mesoporous material
before and after amine functionalization and loading with phenylphosphonic acid.

	S_{BET} (m^2/g)	V_P (cm^3/g)	D_P (Å)	Isotherm type	Amount of phosphonic acid (mg/g)
SBA15	766	0.48	60	IV	
SBA15-AF	425	0.43	57	IV	0.322
SBA15-NH_2	355	0.43	54	IV	
SBA15-NH_2-AF	250	0.31	49	IV	0.380

Tab.2: Summary of Porosity Characteristics for MCM41 mesoporous materials
before and after amine functionalization and loading with phenylphosphonic acid.

	S_{BET} (m^2/g)	V_P (cm^3/g)	D_P (Å)	Isotherm type	Amount of phosphonic acid (mg/g)
MCM41	1477	1.03	32	IV	
MCM41-AF	1002	0.70	31	IV	0.363
MCM41-NH_2	543	0.45	25	IV	
MCM41-NH_2-AF	60	0	-	II	0.341

3.4.2 XRD DIFFRACTION

Fig.3 shows the powder X-ray patterns of MCM-41 and SBA-15 series, before and after amine-functionalization and phenyl phosphonic acid encapsulation, indicating that the mesoscopic ordering was almost completely retained. The MCM41 sample shows two diffraction peaks around 2° and 3.5° 2θ angle, corresponding to (100) and (110) planes, which indicate hexagonally ordered mesoporous structure of the powder.
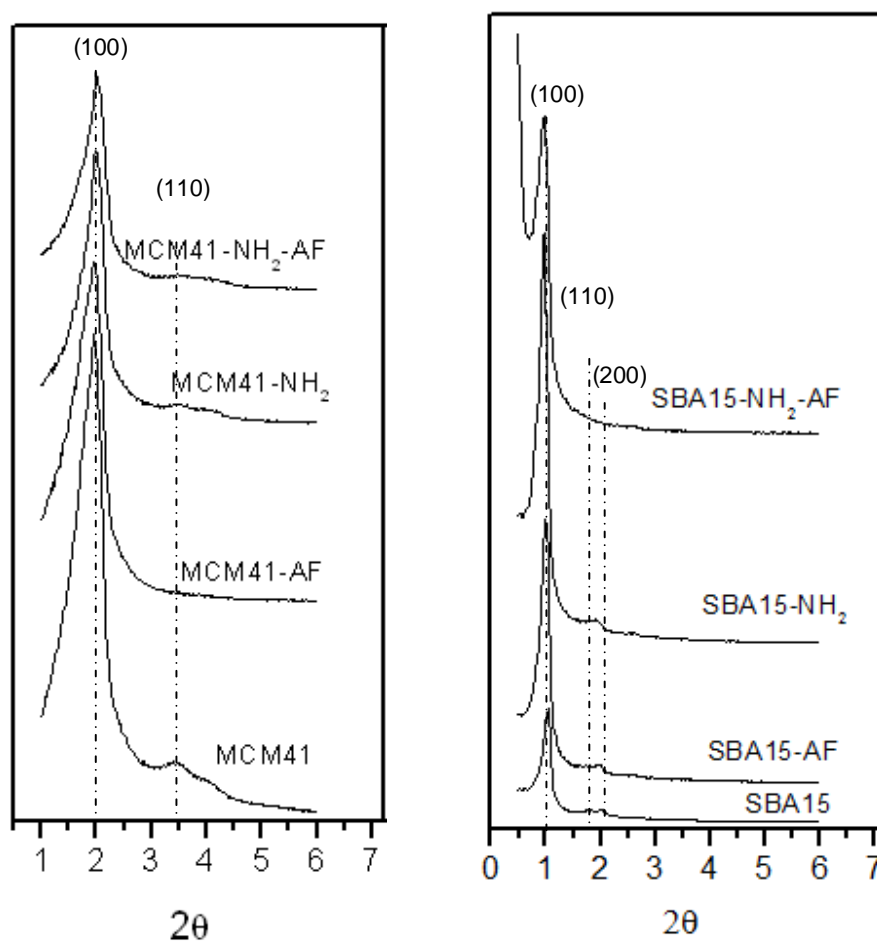
Fig.4: Powder XRD patterns of MCM41 and SBA15 materials
before and after amine functionalization and further phosphonic acid loading.

After amine-functionalization and phosphonic acid loading, the position of (100) reflection remained virtually constant in all the samples, suggesting that the hexagonal pore arrangement is intact. However, the disappearance of the peak around 3.5° 2θ angle was observed. This could happen because the ordered structure partially collapses after the chemical modification and encapsulation process. The collapse probably is promoted by the presence of organic groups and their interactions with inorganic silica framework [28], according with nitrogen adsorption/ desorption data. The pure SBA-15 material has a single intensive reflection (100) at 2θ angle around 1°, and the reflection is related to regular pore size and ordered pore arrangement. Two additional diffraction peaks, corresponding to the high length-scale order, (110) and (200) reflections, typical of a well ordered hexagonal structure, are also observed. After the introduction of amine groups (SBA15-NH$_2$ sample) and phosphonic acid loading (SBA15-AF sample), the XRD pattern is still retained, indicating that these processes not influence completely the structure of pure siliceous SBA-15. For SBA15-NH$_2$-AF and MCM41-NH2-AF materials, XRD patterns show a single peak indicating that the amino groups and phosphonic acid loaded form a material with lower long range order.

3.4.3 ELEMENTAL ANALYSIS

The amounts of organic material (amine groups and phosphonic acid) present in the solids and determined by elemental analysis are showed in **Tab.1** and **Tab.2**. The amounts of phosphonic acid introduced for a gram of silica-based materials are comparable. When the phosphonic acid is encapsulated in the amine-functionalized sample, the amount is greater for SBA-15 material, probably due to more large pore dimension and more adapted confinement system. In the sample without amino groups a higher content for MCM41 sample is found, probably for its good confinement environment and a better fitting of guest molecule in MCM41 pores.

3.4.4 FTIR SPECTROSCOPY

Functional groups were identified using FTIR spectroscopy (**Fig.4** and **Fig.5**). In the calcined and extracted silica-based samples (SBA-15 and MCM-41), typical bands were observed at 800 cm^{-1} (Si-O-Si, symmetric vibration), a large band between 1100 and 1200 cm^{-1} (Si-O-Si,

asymmetric vibrations) and at 950 and 3500 cm^{-1} (Si-OH and SiO-H, respectively) [29]. The incorporation of amine groups in the SBA-15 and MCM-41 silicate frameworks can be qualitatively confirmed by data shown in figures: 1510 cm^{-1}, weak peak due to the symmetrical –NH$_3^+$ bending, indicating the existence of amine groups; 1650 cm^{-1}, peak assigned to N-H bending.
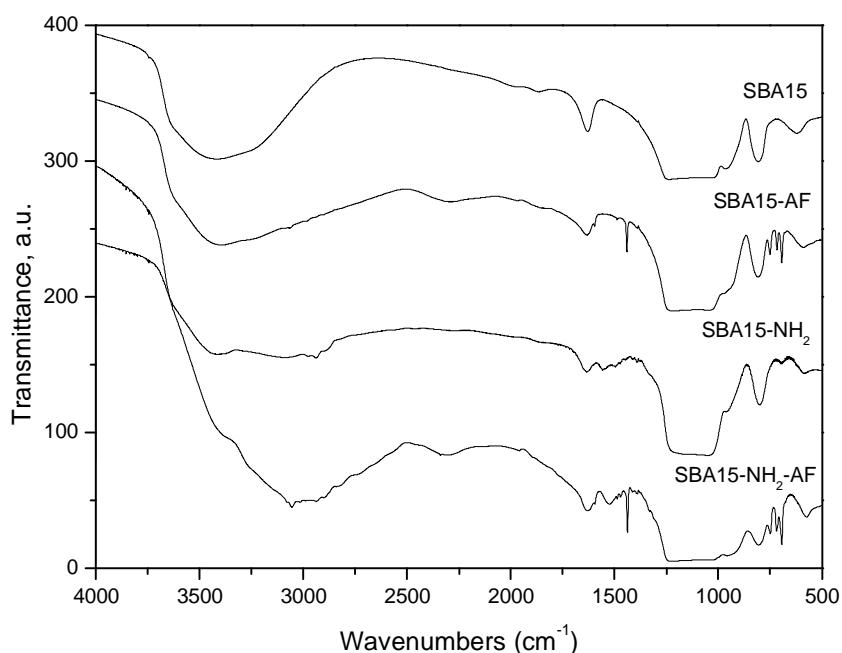
Fig.4: FTIR spectra of SBA-15 materials before and after amine modification and further phosphonic acid loading.

In the spectra of samples functionalized and loaded (SBA15-NH$_2$-AF and MCM41-NH$_2$-AF), are present characteristic peaks of phenylphosphonic acid: 1438 cm^{-1} (sharp): P–C stretching vibration; 753, 723, 694 cm^{-1} (medium intensity): characteristic bands of the mono-substituted phenyl ring. In particular, the typical signal of phosphonic acid at 1438 cm^{-1} is more intense in the amino modified samples, indicating that a great amount of guest molecule is covalently bonded to the silica walls and external surface by triethoxysilane functions.
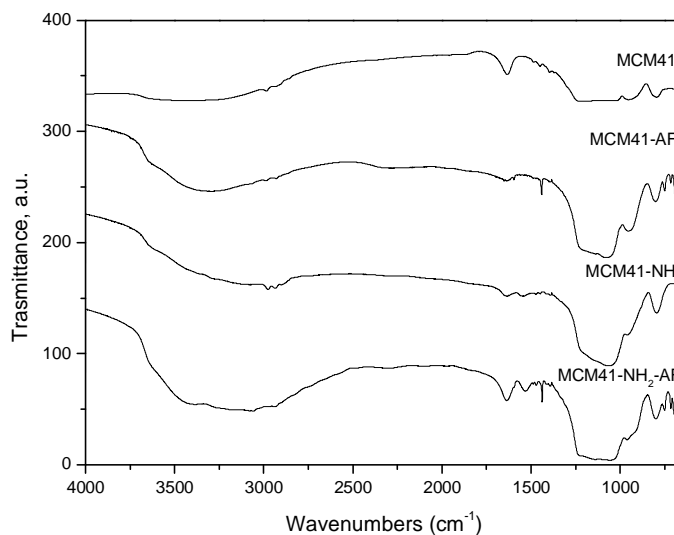
Fig.5: FTIR spectra of MCM41 materials before and after amine modification and further phosphonic acid loading.

3.4.5 TEM MEASUREMENTS

The TEM images of SBA-15 and MCM-41 series are compared in **Fig.6** and **7**. The hexagonal arranged pore arrays of the MCM-41 sample was partially disrupted by the incorporation of amine and phosphonic functionalities, showing amorphous places according with N_2 sorption data. For the SBA15 series, TEM images confirm that the samples preserve the hexagonal structure also after amine-functionalization and phosphonic acid loading. The pore diameter estimated from TEM images are in good agreement with that estimated from the BJH adsorption isotherms.
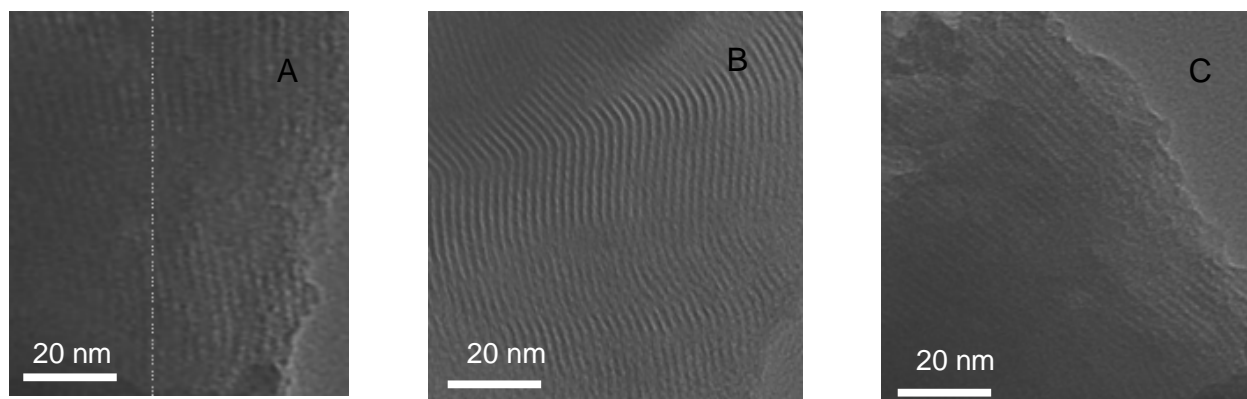
Fig.6: TEM images and magnifications of A) free template MCM41; B) MCM41-AF; C) MCM41-NH$_2$-AF
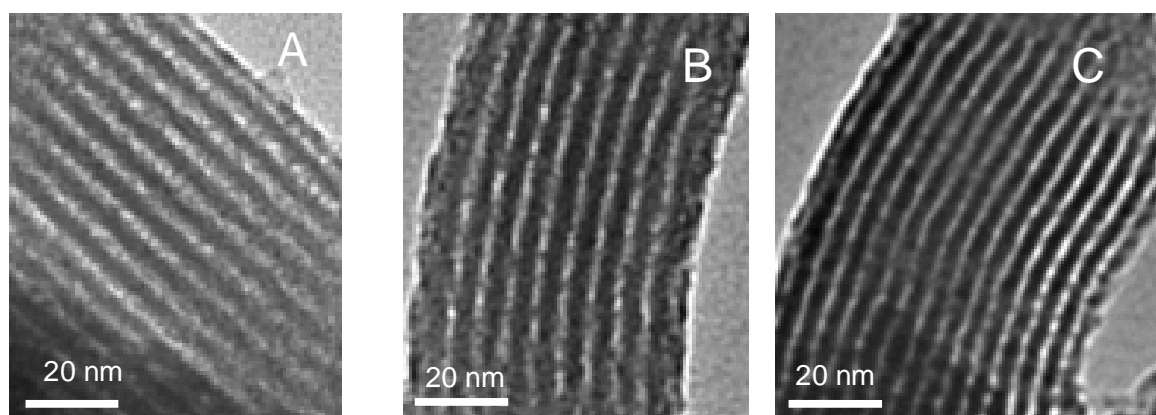
Fig.7: TEM images and magnifications of A) free template SBA15; B) SBA15-AF; C) SBA15-NH$_2$-AF.

3.5 CONCLUSIONS

Hybrid mesoporous materials have been prepared by incorporation of phenylphosphonic acid on the silica matrix partly with triethoxysilane functions anchored to the internal external surface partly by physical confinement in the pore system. The introduction effects on the silica framework have been analyzed by surface characterization in order to verify significant changes before and after loading process. Two types of samples have been synthesized: MCM-41 and SBA-15 materials, both of the M41S family, with well-ordered hexagonal arrays of channel structure. The functionalization with amino groups have produced a decrease of the initial structural parameters as confirmed by N_2 sorption data and XRD diffractions, with a similar trend for SBA-15 and MCM-41 series.

However, TEM images show that the SBA15-NH$_2$ material contains well ordered pore structure similar to that of the pure SBA-15. The loaded samples produce a high change of porosity characteristics, correlated to a large amount of phenylphosphonic acid encapsulated in the silica matrix. This result is confirmed by elemental analysis and FTIR spectroscopy, that show an increase of typical peak of guest species for the sample loaded and modified with amino groups. In particular the samples loaded after chemical functionalization permit to incorporate more quantities of guest molecules, by triethoxysilane functions acting as anchorages to the internal and external surface. The samples loaded but not functionalized show a lower degree of encapsulation, as confirmed by elemental analysis data.

MCM41-NH$_2$-AF materials show a drastic change of both surface area and pore volume and also a partial collapse of the structure. This is probably due to confinement environment smaller respect to SBA-15 sample, inducing a blocking of the pore openings. The SBA-15 materials after loading with or without amino groups maintain an ordered pore arrangement as confirmed by TEM images notwithstanding large amounts of phosphonic acid encapsulated in the silica framework.

REFERENCES

1 R. Szostak, *Molecular Sieves: Principles of Synthesis and Identification*, Van Nostrand Reinhold, New York **1989**;

2 S.T. Wilson, B.M. Lok, C.A. Messina, T.R. Cannan and E.M. Flanigen, *J. Am. Chem. Soc.* **1982**, 104, 1146;

3 M.E. Davis, C. Saldarriaga, C. Montes, J. Garces and C. Crowder, *Nature,* **1988**, 331, 698;

4 T. Kokubo, H.M. Kim, M. Kawashita and T. Nakamura, *J. Mater. Sci. Mater. Med.,* **2004**, 15, 99;

5 A. Bhaumik and S. Inagaki, *J. Am. Chem. Soc.,* **2001**, 123, p. 691;

6 B.T. Holland, P.K. Isbester, C.F. Blanford, E.J. Munson and A. Stein, *J. Am. Chem. Soc.,* **1997**, 119, 6796;

7 J. Jimenez-Jimenez, P. Maireles-Torres, P. Olivera-Pastor, E. Rodriguez-Castellon, A. Jimenez-Lopez, D.J. Jones and J. Roziere, *Adv. Mater.,* **1998**, 10, 812;

8 N.K. Mal, A. Bhaumik, P. Kumar and M. Fujiwara, *Chem. Commun.,* **2003**, 872;

9 N.K. Mal and M. Fujiwara, *Chem. Commun.*, **2002**, 2702; C. Serre, A. Auroux, A. Gervasini, M. Hervieu and G. Ferey, *Angew. Chem. Int. Ltd. Ed.,* **2002**, 41, 1594;

10 T. Doi and T. Miyake, *Chem. Commun.,* **1996**, 1635;

11 J.E. Haskouri, C. Guillem, J. Latorre, A. Beltran, D. Beltran and P. Amoros, *Eur. J. Inorg. Chem.,* **2004**, 1804;

12 T. Kimura, *Chem. Mater.,* **2005**, 17, 337;

13 S. Inagaki, S. Guan, Y. Fukushima, T. Ohsuna and O. Terasaki, *J. Am. Chem. Soc.,* 1999, **121**, 9611;

14 T. Asefa, M.J. MacLachlan, N. Coombs and G.A. Ozin, *Nature,* **1999**, 402, 867;

15 B.J. Melde, B.T. Holland, C.F. Blanford and A. Stein, *Chem. Mater.,* **1999**, 11, 3302;

16 M.P. Kapoor, A. Bhaumik, S. Inagaki, K. Kuraoka and T. Yazawa, *J. Mater. Chem.,* 2002, 3078;

17 N.K. Mal and M. Fujiwara, *Chem. Commun.,* **2002**, 2702;

18 N.K. Mal, M. Fujiwara and M. Matsukata, *Chem. Commun.,* **2005**, 5199;

19 J. Randon, P. Blanc, R. Paterson, *J. Membr. Sci.*, **1995**, 98, 119; P. Pechy, FP. Rotzinger, MK. Nazeeruddin, O. Kohle, SM. Zakeeruddin, R. Humphrybaker, M. Gratzel, *Chem. Soc. Chem Commun.*, **1995**, 65;

20 P.H. Mutin, C. Delenne, D. Medoukali, R. Corriu, A. Vioux, *Mater. Res. Soc. Symp. Proc.*, **1998**, 519, 345;

21 T. Azais, L. Bonhomme-Coury, J. Vaissermann, P. Bertani, J. Hirshinger, J. Maquet, C Bonhomme, *Inorg. Chem.*, **2002**, 41, 981;

22 C. Lesaint, B. Lebeau, C. Marichal, J. Patarin, *Microporous and Mesoporous Materials,* 83, **2005**, 76;

23 C.-Y. Chen, H.-X. Li, M.E. Davis, *Micropor. Mater.*, **1993**, 2, 17;

24 D. Zhao, J. Feng, Q. Huo, N. Melosh, G.H. Fredrickson, B.F. Chmelka, G.D. Stucky, *Science*, **1998**, 279, 548;

25 C. Charnay, S. Begu, C. Tourne-Peteilh, L. Nicole, D.A. Lerner, J.-M., Devoisselle, *Eur. Pharm. Biopharm.*, **2004**, 57, 533;

26 S. Brunauer, P.H. Emmett, E.J. Teller, *J. Am. Chem. Soc.*, 60, **1938**, 309;

27 P. Barrett, L.G. Joyner, P. Halenda, *J. Am. Chem. Soc.*, 73, **1951**, 373;

28 M.H. Lim, C.F. Blanford, A. Stein, *J. Am. Chem. Soc.*, 119, **1997**, 4090;

29 A.L. Smith, *Spectrochim. Acta,* 16, **1960**, 87.

EXPERIMENTAL PART III

SYNTHESIS AND CHARACTERIZATION OF BENZOIC ACID TRAPPED INTO MESOPOROUS SILICA-BASED MATERIALS

3.1 INTRODUCTION

There is a growing interest for hydrophobic drugs release systems based on mesoporous materials [1]. It has been shown by Vallet-Regi *et al.* [2] that some molecules, interesting from a pharmaceutical point of view, can be confined in large amount in the silica matrices type MCM-41 and SBA-15. The obtained composite material allows and it is possible to control release kinetics of the drug [3-6]. A variety of organic compounds can be adsorbed onto the surface of porous materials due to their peculiar adsorptive properties. SBA-15 mesoporous silica can be easily and reproducibly prepared within a wide range of temperatures (35–130 °C) using tetraethylorthosilicate or sodium silicate. It is a hexagonally ordered silica material with tailorable uniform mesopores and micropores in the mesopore walls.

It has thick pore walls (2–6 nm), leading to improved thermal and hydrothermal stability and may exhibit a large variety of morphologies depending on the synthesis conditions [7-10].

These remarkable characteristics make SBA-15 as highly promising model adsorbents for fundamental adsorption studies and for pharmaceutical use. SBA-15 is usually synthesized at low temperature and mild conditions by the sol-gel process, which allows the incorporation of sensitive molecules, like proteins or therapeutics into the gel. Moreover, these materials can be utilized in the future as supports of active principles to control the diffusion of the molecules in the human body, to increase the solubility of the hydrophobic active principles and to direct these active biologically molecules. In the present study, we used benzoic acid (**Fig.1**) as a model compound for drugs, possessing as the 80% of active principles an aromatic ring and a carboxylic group. Thus, benzoic acid encapsulated in mesoporous SBA-15 material is a good reference sample for the study of silica-based drug delivery systems [5].

This opens the possibility to develop heteronuclear correlation NMR methods (e.g., ^{29}Si, ^{13}C) through using ^{13}C-labeled benzoic acid to better characterize the possible interactions of the encapsulated molecules with silica surfaces with and without modification.

The object is to encapsulate by a simply impregnation procedure this model molecule in order to characterize its physical state, that is strongly dependent on the environment effect. For example, a substance can be a crystalline solid at room temperature but also it can act as liquid when it is encapsulated.

The surface of MCM-41 material has been also modified by reaction with the organosilanes [11,12]. This modification allows the selection of the appropriate group depending on the drug and its application. The characterization of the synthesized samples was done by X-ray diffraction, N_2 adsorption-desorption measurements, TEM and FTIR spectroscopy, elemental analysis.
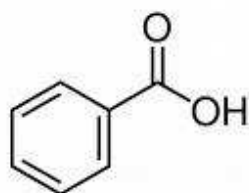
Fig.1: Benzoic acid.

3.2 EXPERIMENTAL SECTION

3.2.1 MATERIALS

Benzoic carboxy ^{13}C acid, 99% (AB; Isotec) was used without further purification. Surfactant P123 (EO$_{20}$-PO$_{70}$-EO$_{20}$, M_{av} = 5800) was purchased from Aldrich and the other chemicals of reagent grade were from Fluka. All chemicals were used as received.

3.2.2 SYNTHESIS OF SBA-15

SBA-15 materials were prepared using a procedure adapted from that described by Zhao *et al* [13]. 4 g of Pluronic P123 were dissolved in 104 mL of deionized water and 20 mL of 37 wt% HCl under magnetic stirring. After complete dissolution, 9.16 mL of TEOS were added to the template solution. The starting molar ratio was 1.0TEOS:0.017P123:6.03HCl:145H_2O. The resulting mixture was kept under magnetic stirring for 12 h at room temperature and subsequently aged at 373K for 24 h. After reaction, the solid silica material was recovered by filtration, washed with deionised water and dried at 333K for 12 h. The surfactant was removed from the as-synthesized material by heating the samples at 823K under air for 6 h.

3.2.3 POST-SYNTHESIS GRAFTING OF AMINO GROUPS ONTO SBA-15 MATERIALS (SBA15-NH₂)

Aminopropyl-functionalized SBA-15 material (denoted as SBA15-NH$_2$) was prepared by a post-synthesis grafting method. The process was carried out on the template-free silica SBA-15 materials previously activated in oven at 423K for 2 h, by adding 1.33 g of 3-aminopropyltriethoxysilane (APTES) to 500 mg of pure materials in 20 mL of toluene. The reaction was performed under reflux conditions at 383K for 8 h and the products were filtered and washed with toluene. The grafted samples were dried at 373K for 12 h in air.

3.2.4 BENZOIC ACID LOADING PROCEDURE (SBA15-AB, SBA15NH₂-AB)

The impregnation of the host-silica materials (with or not amino groups) was performed by soaking 500 mg of the mesoporous sample in 4 mL of a solution of 50 mg of benzoic acid in ethanol, through the incipient wetness procedure [14]. Four successive impregnations were carried out, with a small amount of solution just allowing the powder to be wetted. Samples are dried in the oven at 330K for 12 h to remove the solvent.

Finally, the samples were washed with 4 mL of ethanol to remove the excess of crystallized benzoic acid, and finally dried at 373K for 12 h. The samples with and without amine function loaded with benzoic acid are labelled SBA15NH$_2$-AB and SBA15-AB, respectively.

3.3 CHARACTERIZATION

X-Ray diffraction (XRD) patterns were obtained with CuKα radiation on a Philips PW 1730/10. Measurements were achieved for 2θ values in the 0-6° range with a step size of 0.005° and a step time of 0.5 s. Nitrogen adsorption-desorption measurements were conducted at 77 K on a Micromeritics ASAP 2010. The calcined samples were pre-treated under vacuum for 6 h at 623 K, or at 388 K for the functionalized samples. The specific surface area of samples was calculated by the BET model.

The pore size distribution curves were obtained by the BJH (Barrett-Joyner-Halenda) method based on the desorption branch of the isotherms. Infrared spectra were measured with a Nicolet Nexus spectrophotometer and recorded in reflectance in the 450-4000 cm^{-1} range. Analyses were performed using KBr as the blank. The content of amino groups and benzoic acid in the mesoporous materials was determined by the CHN elemental analysis using a Perkin Elmer

2400 apparatus, and by thermogravimetric analysis, using a NETZSCH 409 analyzer. A thermogravimetric analysis of all samples was conducted in air from room temperature to 820°C with a heating rate of 10°/minute.

3.4 RESULTS AND DISCUSSION

3.4.1 N_2 ADSORPTION/DESORPTION ISOTHERMS

Nitrogen gas adsorption/desortion isotherms of the samples are shown in **Fig**.**2**. According to the IUPAC classification, the pure (SBA-15), the impregnated with benzoic acid (SBA15-AB) and the functionalized with amino groups (SBA15-NH_2) samples exhibit type IV isotherms, characteristic of mesoporosity, indicating that the obtained samples and as-made SBA-15 possess similar structure. Pure SBA-15 shows an hysteresis type H1, associated with mesoporous materials and typical of uni-modal pore distribution (**Fig.2**), while other samples show an hysteresis type H2 which is related to a distribution of pore size and shape not well defined.

The functionalized sample impregnated with benzoic acid (SBA15NH_2-AB) exhibit type II isotherms characteristic of materials that are no porous and indicate that the mesoporous system is completely filled with the benzoic acid. Characteristic porosity parameters of the samples before and after impregnation with benzoic acid are listed in **Tab.1**.

The BJH pore diameter, BET surface area and pore volume of SBA15 after modification and impregnation processes decrease with the aminopropyl and benzoic acid amount. The pure material as-synthesized exhibits a surface area of 886 m^2/g, a pore volume of 0.97 cm^3/g, with an uni-modal pore size distribution that exhibit sharp peak ~35 Å. The others samples show a marked decrease of surface properties respect to the starting material, specially SBA15NH_2-AB, which presents a drastic reduction of specific surface area and pore volume. These results are attributed to the occupation of organic molecules on the surface of the pores, which determine a blocking of opening pores, as confirmed also by XRD diffraction patterns.
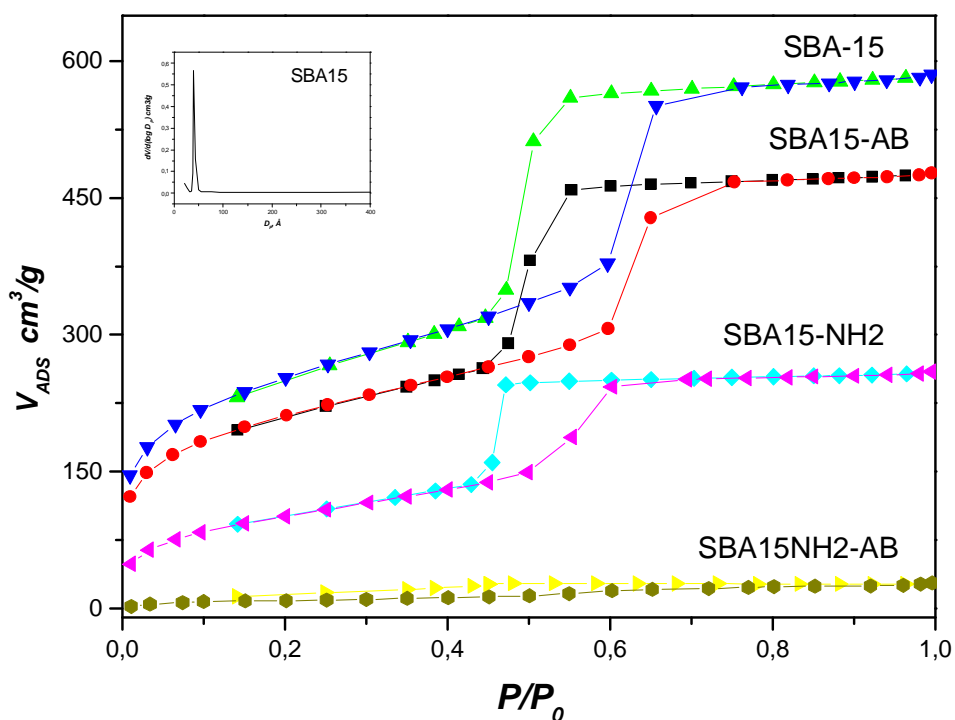
Fig.2: Nitrogen gas adsorption/desorption isotherms of SBA-15 materials before and after
amine functionalization and benzoic acid encapsulation.

Tab.1: Structural Properties of mesoporous materials (with amino groups or not) before
and after impregnation with benzoic acid

Sample	Isotherm type	BET surface area (m^2/g)	Total pore volume (cm^3/g)	Pore size maximum (nm)	d_{100} spacing (nm)
SBA-15	IV	886	0.97	4.0	7.9
SBA15-AB	IV	738	0.80	3.9	7.2
SBA15-NH$_2$	IV	368	0.42	3.5	7.2
SBA15NH$_2$-AB	II	61	0.05	2.7	-

3.4.2 XRD DIFFRACTION

Small-angle X-ray diffraction patterns of impregnated and functionalized materials are shown in **Fig.3, 3'**. The diffraction patterns of the calcined SBA-15, the amino-functionalized SBA15-NH$_2$ and the impregnated SBA15-AB materials exhibit stronger intensities than the corresponding as-synthesized ones. However, they show an intense diffraction indexed to (100) plane and two poorly-resolved weak diffraction peaks corresponding to (110) and (200) planes.

However, the peak intensity decrease and the slight shift of the (100) diffraction peak of the modified samples toward larger 2θ angles indicates a minor shrinkage of the cell dimension. Moreover, the (110) and (200) diffractions become unperceivable in the SBA15NH$_2$ sample, showing that the mesopore ordering decreases with the successive structure modification.

For the SBA15NH$_2$-AB sample, a collapse of the structure takes place due to the full filling of the pore system, as confirmed also by N$_2$ sorption data. The loading on the mesoporous functionalized matrix affects the hexagonal order of the mesopore channels. This is confirmed by elemental analysis and TG data about the amount of benzoic acid encapsulated, which is much higher for the SBA15NH$_2$-AB respect to SBA15-AB. The triethoxysilane functions allow a high anchoring of guest species on the internal and external surface of silica matrices.
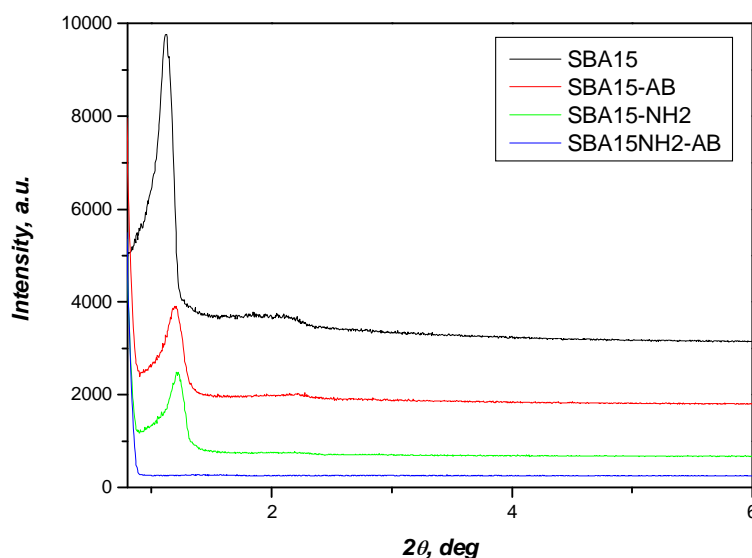
Fig.3: XRD patterns of SBA15 before (a) and after (b) template removal.

3.4.3 FTIR FOURIER TRANSFORM INFRARED

Qualitative identification of the benzoic acid has been achieved with diffuse reflectance infrared Fourier transform spectroscopy. The absorption band observed at 1700 cm^{-1} in the spectrum of benzoic acid crystals was assigned to the carbonyl-stretching vibration (C=O), where benzoic acid molecules formed a centrosymmetric hydrogen-bonded dimer in the crystal [15]. Others characteristic peaks of benzoic acid are localized at 1430-1450 cm^{-1} (C=C aromatic) and a 700 cm^{-1} (C-H). These peaks are present in all spectra of mesoporous samples without amino groups impregnated four times (**Fig.4**).

This gives the evidence that carboxylic acid molecules are trapped into the material. After washing with 4 mL of ethanol, the peaks at 1585 cm^{-1} and 1450 cm^{-1} are less intense, indicating that a low amount of benzoic acid remains in the mesoporous matrix.

The presence of N-H bending vibration around 687 cm^{-1} and the symmetric –NH$_2$ bending vibration at 1510 cm^{-1} in the spectrum of the sample functionalized with APTES (**Fig.5**) confirms the incorporation of amino groups.
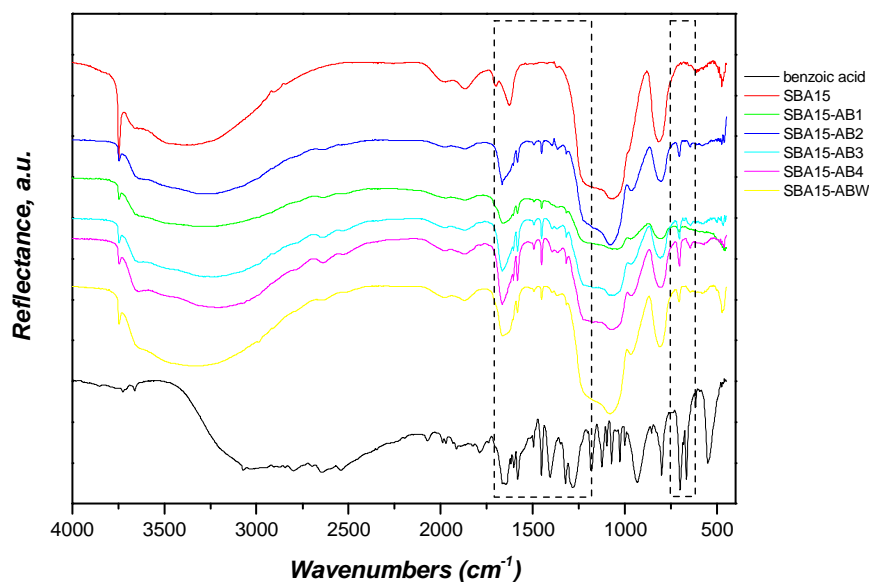
Fig.4: FTIR absorption spectra of SBA-15 after four impregnation and washing.
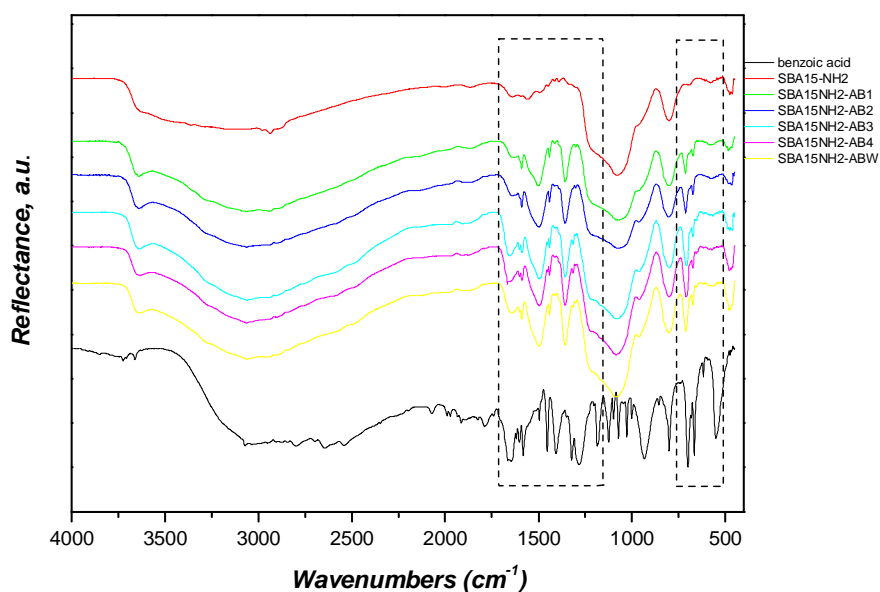
Fig.5: FTIR absorption spectra of SBA15-NH$_2$ after four impregnation and washing.

Obviously, the intensity of these peaks increases with aminopropyl content. The absorbance of the C-N stretching vibration is normally observed around 1000-1200 cm^{-1} [16]. The presence of aminopropyl groups in the modified SBA-15 was further corroborated by a broad band at 2700-3400 cm^{-1} attributed to the NH$_3^+$ stretching vibration. Other characteristic peaks at 1367cm^{-1}, 1450 cm^{-1}, 1497 cm^{-1}, 1585 cm^{-1} are present in these functionalized samples.

3.4.4 THERMOGRAVIMETRIC AND ELEMENTAL ANALYSIS

The amount of benzoic acid were determined by thermogravimetric and by elemental analysis (EA) through the determination of carbon percentage. The SBA-15 sample pure does not show indication of any residual surfactant. The SBA15-AB sample exhibits a weight loss of 9.24% from 120 to 600°C due to matrix decomposition containing the benzoic. The functionalized sample (SBA15-NH$_2$) exhibit a first weight loss associated to the presence of the solvent (toluene) and a second weight loss from 250 to 600 °C due to the decomposition of the silica with functional groups. Over the peak at 303.7°C attributable to amino groups, it is possible to note an other peak at 420,4°C, which it meets also in the sample SBA15NH$_2$-AB. This sample

shows a significant weight loss from 290 to 600 °C to attribute to decomposition the framework silica-amino groups-benzoic acid. By termogravimetric and elemental data (**Tab**.2), it is possible to determine the amount of benzoic acid encapsulated in mesoporous matrix.

The benzoic acid contents analyzed by EA are slightly higher than those by TG. From results of both techniques, it infers that SBA15NH$_2$-AB material is the host sample with higher amount of guest species, due to presence of triethoxysilane functions which permit a higher incorporation of benzoic acid by covalent bonds to the silica walls and external surface.

Tab.3: Incorporation of organic groups in SBA-15 materials.

Sample	Amount of benzoic acid (mg/g)	
	by TG	by EA
SBA15	0	0
SBA15-AB	0.11	0.21
SBA15-NH$_2$	0.13	0.13
SBA15NH$_2$-AB	0.21	0.24

3.4.5 EDX ANALYSIS

The amount of benzoic acid encapsulated into SBA-15 samples functionalized or not with amino groups has been valuate also by EDX analysis, together with elemental analysis and TG data. This measure is rather qualitative, and gives an indication of the presence of guest molecules by percentage of atoms relative to interesting species. In **Tab.4** the percentages of C, O and Si calculated for the SBA15-AB and SBA15NH$_2$-AB samples are reported. The amount of carbon (% Wt) is related to the presence of amino groups and benzoic acid molecules (**Fig.6**). Obviously, the amount of carbon is higher for sample SBA15NH$_2$-AB, considering both benzoic acid and amino groups with respect SBA15-AB sample where only benzoic acid is present. These results are in agreement with elemental analysis and TG data.

Tab.4: Incorporation of organic groups in SBA-15 materials.

Sample	C (%Wt)	O (%Wt)	Si (%Wt)
SBA15-AB	21.6	43.60	34.80
SBA15NH$_2$-AB	30.72	40.58	28.70
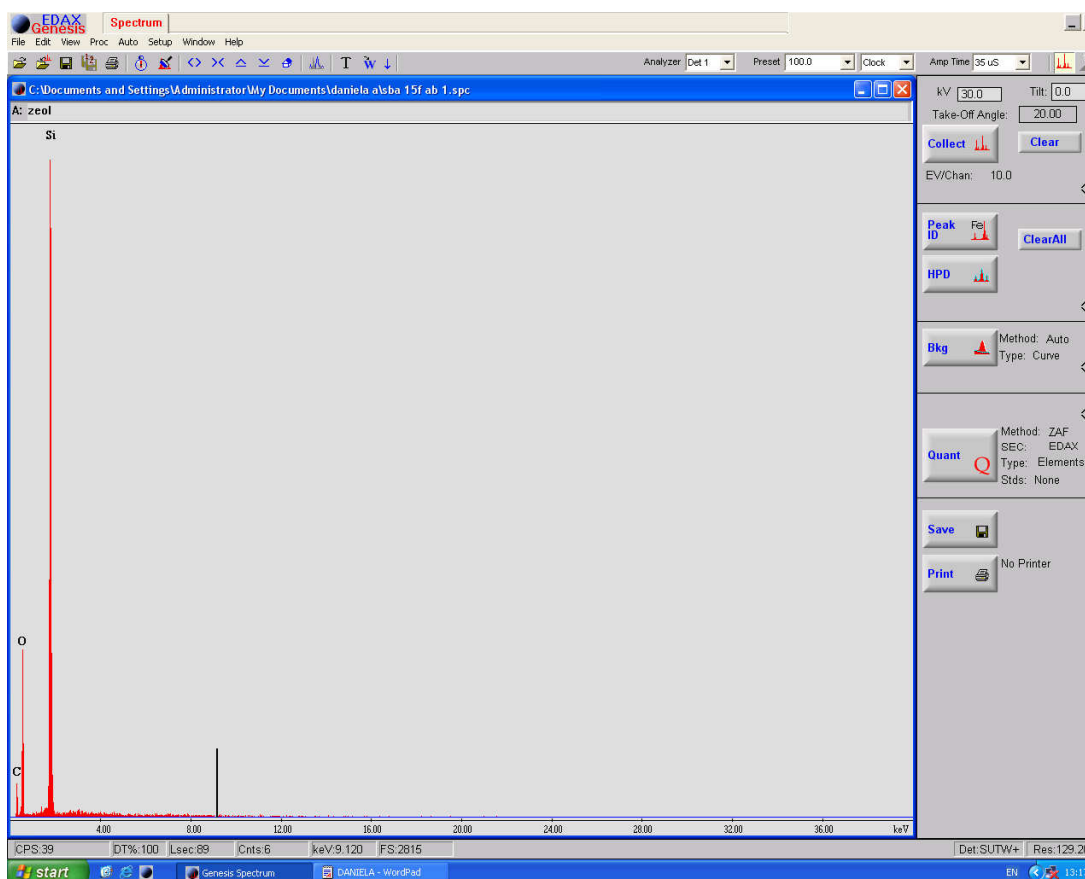
Fig.6: EDX analysis of SBA15NH$_2$-AB.

3.5 CONCLUSIONS

Aminopropyl functionalized and not SBA-15 materials loaded with benzoic acid as guest molecule were synthesized by grafting post-synthesis using P123 as pore directing agent under acid conditions. The resultant samples are characterized by several techniques to verify the entire effects on the mesostructure due to the incorporation of benzoic acid and chemical functionalization with amino groups.

N_2 sorption data evidences that all samples suffer a noteworthy change of structural parameters, as area surface and pore volume indicating a partial occlusion of opening pores. This result is highly evident for SBA15NH$_2$-AB, which shows a dramatic reduction of surface area and pore diameter, due the presence of amino groups and benzoic acid molecules covalently bonded to the internal and external pore surface or simply confined in the opening pores.

This is confirmed by XRD diffraction, which shows a decrease in long-range ordering of all samples, and in particular of SBA15NH$_2$-AB. This is correlated to a higher content of organic groups (benzoic acid and amino groups) in the samples, as confirmed by elemental analysis, TG data and EDX analysis.

All samples exhibit diffraction patterns typical of poorly ordered hexagonal mesostructure. FTIR spectra show typical peaks of benzoic acid more marked for functionalized sample. This confirms the importance of covalent anchoring to incorporate high quantities inside silica matrices.

REFERENCES

1. Unger K.; Rupprecht H.; Valentin B.; Kircher W. *Drug DeV. Ind. Pharm.* **1983**, *9* (1-2), 69.

2. M. Vallet-Regi, F. Balas, D. Arcos, *Angew. Chem. Int. Ed.*, **2007**, 46, 7548;

3. M. Vallet-Regi, A. ramila, RP del Real, J. Perez-Pariente, *Chem. Mater.*, **2001**, 13, 308;

4. J.M. Devoiselle, C. Tournè-Peteilh, D.A. Lerner, C. Charnay, L. Nicole, S. Begù, *Chem. Phys. Chem.*, **2003**, 3;

5. M. Vallet-Regì, P. Horcajado, A. Ramila, J. Perez-Pariente, *Microporous and Mesoporous Materials*, **2004**, 68;

6. M. Vallet-Regi, B. munoz, A. Ramila, J. Perez-Pariente, J. diaz, Chem. Mater, 2003, 15;

7. Morishige, K.; Kawano, K. *J. Chem. Phys.* **2000**, *112* (24), 11023

8. Gedat, E.; Schreiber, A.; Albrecht, J.; Emmler, T.; Shenderovich, I.; Findenegg, G. H.; Limbach, H-H.; Buntkowsky, G. *J. Phys. Chem. B* **2002**, *106*, 1977.

9. Dosseh, G.; Y. Xia, C. Alba-Simionesco, *J. Phys. Chem. B* **2003**, *107*, 6445.

10. Morineau, D.; Xia, Y.; Alba-Simionesco, C. *J. Chem. Phys.* **2002**, *117* (19), 8966.

11. K.A. Utting, D.J. Macquarry, *New J. Chem.*, **2000**, 24, 591;

12. D. Brunel, F. Fajula, J.B. Nagy, B. Deroide, M.J. Verhoef, L. Veum, J.A. Peters, H.Van Bekkum, *Appl. Catal. A: General*, **2001**, 213, 73;

13. Zhao, D. Y.; Feng, J.L.; Huo, Q.S.; Melosh, N.; Fredricksson, G.H.; Chmelka, B.F.; Stucky, G.D.; *Science*, **1998**, 279, 548;

14. T. Azais, C. Tourne-Petheil, F. Aussenac, N. Baccile, C. Coelho, J.M. Devoisselle, F. Babonneau, *Chem. Mater.*, **2006**, 18, 6382;

15. G.A. Sim, J.M. Robertson, T.H. Goodwin, *Acta Crystallogr.*, *1955*, 157;

16. Shriner, R. L.; Hermann, C. K. F.; Morril, T. C.; Curtin, D. Y.; Fuson, R. C. *The Systematic Identification of Organic Compounds*, 7th ed.; John Woley & Sons: New York, **1998**.

CHAPTER IV

MESOPOROUS THIN FILM

4.1 INTRODUCTION

Among the various shapes and morphologies of mesoporous materials (powders, monoliths, fibers, films, etc.), thin films are particularly suitable for applications in optical, electronic, sensing devices [1] and separation. A comparison between dimensions and morphologies of mesoporous silica is shown in **Fig.1**.
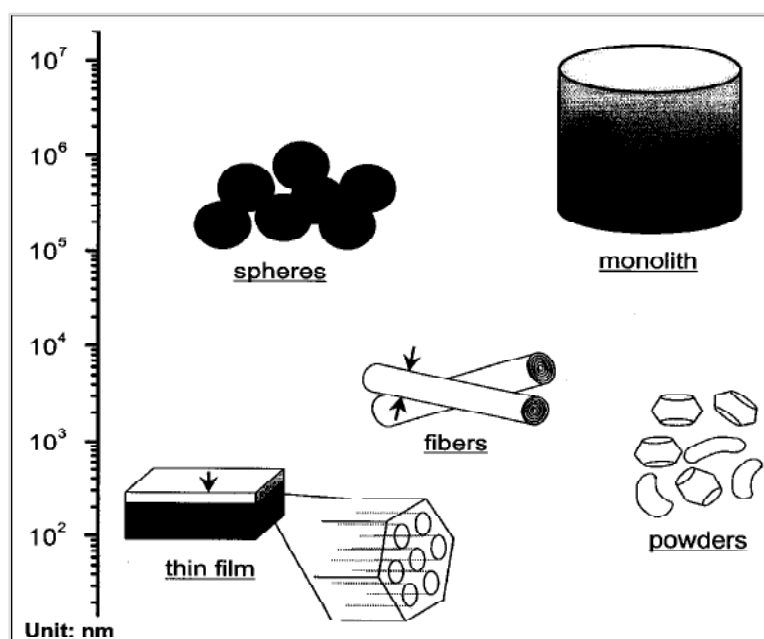
Fig.1: Schematic representation of different dimensions and morphologies of mesoporous silica.

Thin solid films can be prepared through a great number of different techniques that can be classified in three main categories, chemical, physicochemical, and physical. While physical deposition techniques are preferred for the preparation of dense thin films, chemical deposition approaches are much more appropriated for the preparation of porous layers.

The chemical factors govern the relative amounts of surfactant and inorganic precursor and the kinetics of hydrolysis–condensation reactions. The processing conditions control the diffusion of volatile EtOH, H_2O and HCl molecules inside or outside of the film, fixing the dry film composition and its final thickness.

The preparation of reproducible mesoporous organized thin films with optical homogeneity and transparency requires the understanding and control of three main levels, namely, the chemistry associated with the initial solution, the processes linked to the layer deposition technique, and the thermal, washing or UV post-treatments. Different methods used to prepare the MTF are illustrated in **Fig.2**.
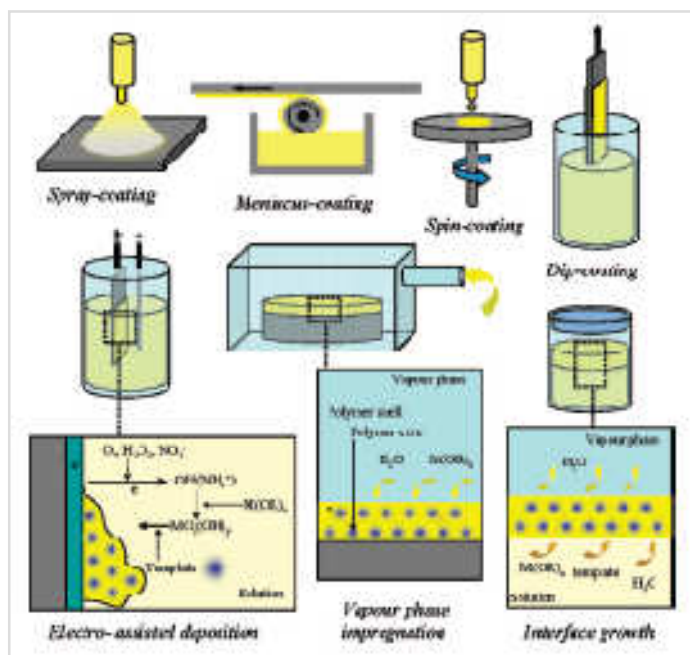
Fig.2: Various processing methods used to prepare *MTF*.

4.2 INITIAL SOLUTION

The optimal sols are composed of ethanol, due to its high volatility, high wettability properties with hydrophilic substrates and miscibility with the inorganic source (metal alkoxides, chloride alkoxides or metallic salts). Homogeneous thin films are obtained only if the solvent perfectly wets the substrate and is highly volatile.

Moreover, the nanostructures formed involve pore and wall dimensions that are in the range of 1-10 nm, suggesting that the dimensions of the inorganic entities to stabilize in the initial solution should not exceed this order of magnitude. Since the organization is partly governed by the interactions between the surfactant head group and the inorganic entities [2], the nature and the

density of the chemical groups present at the surface of the inorganic entities has to be known and controlled. The initial solutions must thus fulfill all the requirements of a perfectly controller sol-gel system. It must be pointed out that the hydrolysis and condensation steps of the inorganic precursors have to be adjusted by selecting the appropriate components and their relative quantities (water content, pH, dilution, etc.) [3]. The relative amounts of organic and inorganic components have to be reasonably fixed so to permit the organization to be stable in the intermediate hybrid state ($V_{CTAB}/(V_{CTAB} + V_{SiO2})$) and after removal of the template ($V_{pore}/(V_{pore}+ V_{SiO2})$). Taking conventional phase diagrams as simplified models, it is well established that the final mesostructure of the film depends on the quantity of surfactant that shares the volume with the other constituents [4,5].

The template volume ratio is usually taken as 20% and 80% and may be derived from classical phase diagrams free of inorganic components (CTAB [6], block copolymer [7]). The range of surfactant/inorganic precursor molar ratio is between 0.08 and 0.35. In order to favour fast hydrolysis and slow condensation, promoting the formation of small oligomers controled and stabilized in a short period of time, the pH is fixed close at the isoelectric point $Si(OH)_4$ ($H^+/Si \approx$ 0.14÷0.004), while the hydrolysis ratio ($h = H_2O/Si$) is around at 5. Hydrochloric acid is the preferred acid because its volatility allows it to depart from the film during evaporation, after having fulfilled its catalytic role in the sol. For low-acidified sols (aqueous 10^{-2} M HCl solution) [8,9], only the formation of a 2D hexagonal mesophase (*plane group p6m*) is observed. For acidified sol, different behaviors are noticed. Short aging times of the sols always lead to a 3D hexagonal mesophase (*space group P6$_3$/mmc*) whereas, for longer aging times of the sols, and depending on dip-coating conditions, either the previous mesophase (or a cubic mesophase (Pm*3*n) are obtained. The aging time of the sol has to be controlled, because it was reported that the degree of condensation of the inorganic oligomers can greatly influence the mesostructuring [4,10].

4.3 EISA (*EVAPORATION INDUCED SELF-ASSEMBLY*)

One of the main parameters that governs the entire film-formation process is evaporation. As soon as a layer of the initial sol is deposited on the substrate, evaporation of volatile components (ethanol, water, and hydrochloric acid) takes place at the air/film interface. The

evaporation leads to the fast and progressive (10-30s) enrichment of the film in silica oligomers and template molecules. When the surfactant concentration has reached the equivalent of the critical micelle concentration (***cmc***) for the system, micelles start to form by hydrophobic segregation of alkyl chains. An organized mesostructure with respect to the physical-chemical properties of the surfactant molecule in the actual medium is eventually formed.

Previous works have been dedicated to the influence of packing parameter *g* ($g = V/a_0 l$, where *V* is the total volume of the surfactant chain, a_0 is the effective head-group area and *l* is the surfactant chain length) [11] and to the concentration effect (V_{CTAB}/V_{total}, dove $V_{total} = V_{CTAB} + V_{SiOx(OH)y} + V_{H2O} + V_{EtOH}$) on the final mesostructure [4,5,12-14]. Recently, synthesis routes have been developed in which the accent is put in using polymeric surfactant templates with a greater solubility difference between the hydrophilic and hydrophobic domains [7,15]. Water contents in the system or the hydrolysis degree of the inorganic species have been proved important features [16,17], as they can enhance the formation of ordered micelle arrays, and control the interactions between the template and the inorganic network at the hybrid interface. It is clear that more accurate diagrams taking into account these factors are needed. The Sanchez group recently introduced a quaternary "texture diagram", in an attempt to better explain and locate these stability domains (**Fig.3a, Fig.3b**) [18].

The evolution of an EISA system as a function of time (i.e., the kinetics of the system) can be understood plotting a system trajectory in the phase diagrams containing the main actors of the system. If the concentration of the inorganic and template species in the initial dilute solutions is low, no liquid crystalline species will be formed; even micelle formation is difficult under these conditions, because the critical micelle concentration (***cmc***) of the template in the solvent (often a mixture of low weight alcohols and lower water quantities) is relatively high. When solvent evaporates, the self-assembly properties of the template enter the scene, and aggregation processes (i.e., micellization) begin to take place (**Fig.4**).

When higher concentrations are reached, a liquid crystalline phase is formed, due to micelle aggregation. In the ideal case, micelles pile up in ordered structures and the inorganic building blocks locate themselves in the outside (polar) fraction of the organic liquid crystal formed. A hybrid mesostructure (inorganic skeleton surrounding an organic liquid-crystalline phase) is thus formed. EISA can thus be described by competitive processes related to the

kinetics of condensation versus the kinetic of organization, both influenced by the kinetics of diffusion of the volatile species.
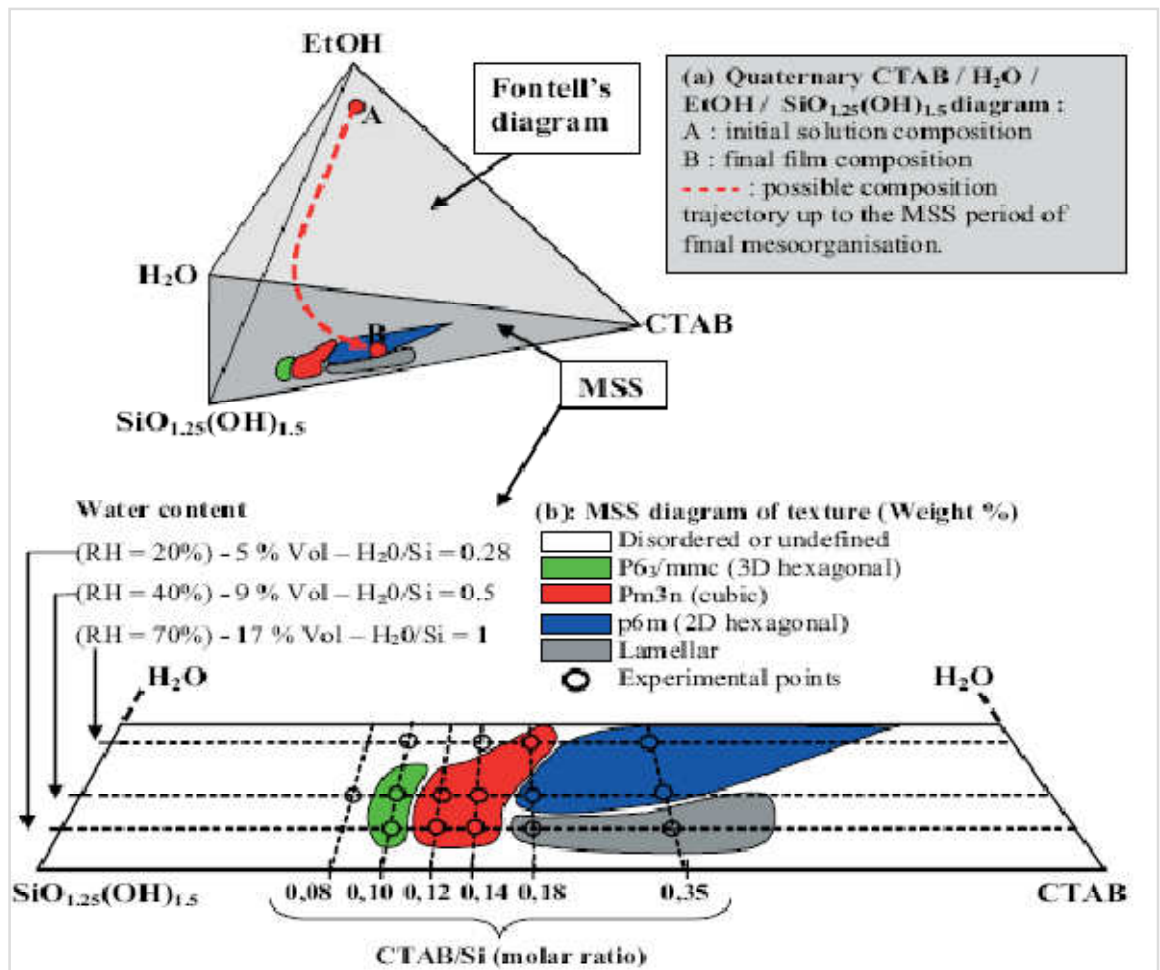
However, these processes are difficult to control and thus difficult to predict if they occur successively or simultaneously during drying. A scheme of the process occurring in a thin film and its correlation with a simple ternary phase diagram is shown in **Fig.5**.

For the CTAB/TEOS system, the MSS (*modulable state steady*) lasts from a few seconds at low humidity to 10 min at high relative humidity [19]. For TMO-based films prepared under highly acidic conditions to prevent extend condensation, the MSS can last several hours [13,20].
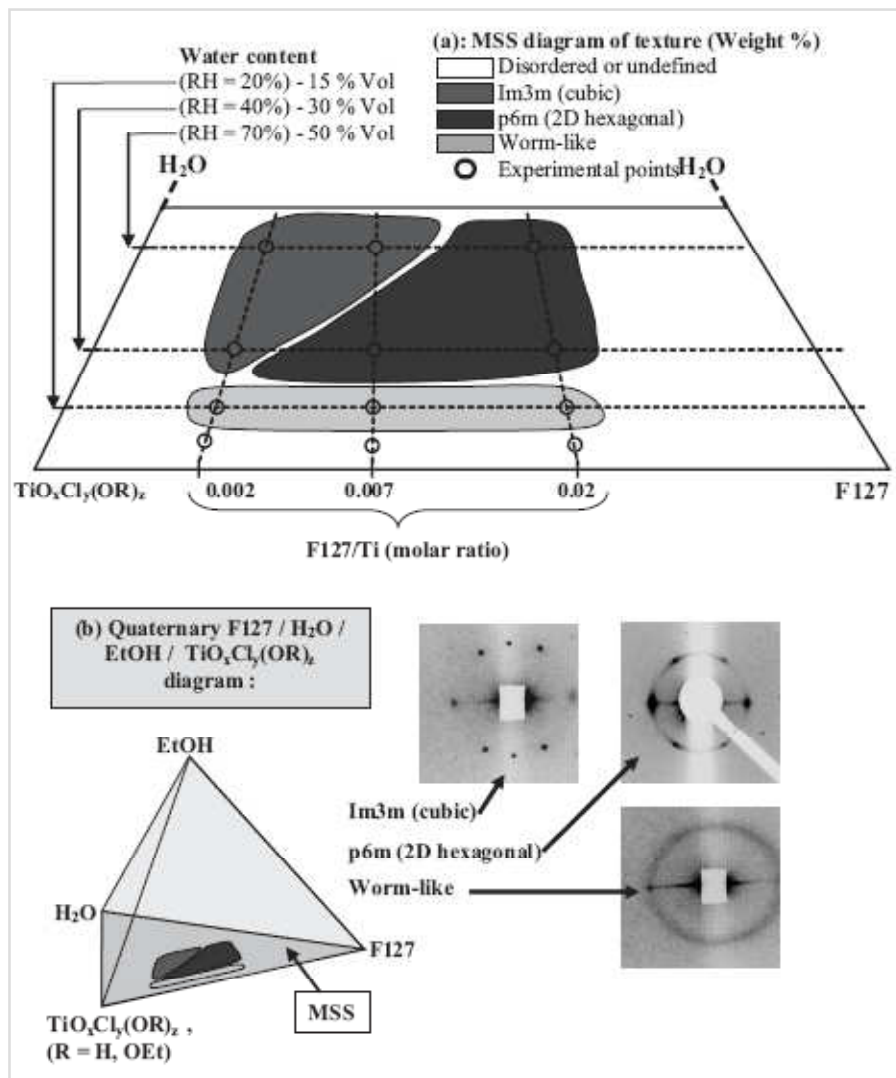
Fig.3a,3b: Texture diagram EISA.

In-situ SAXS experiments coupled with interferometry shed light into these complex assembly processes [4,14,21,22]. In most of the cases, the mesostructure appears after the drying line (i.e., when practically all the solvent is evaporated and the film attains more or less its final thickness). In the case of cationic surfactants such as CTAB, well-defined mesostructures are formed upon drying, and a number of phase transitions have been reported between them, before reaching the final mesophase [14,23].
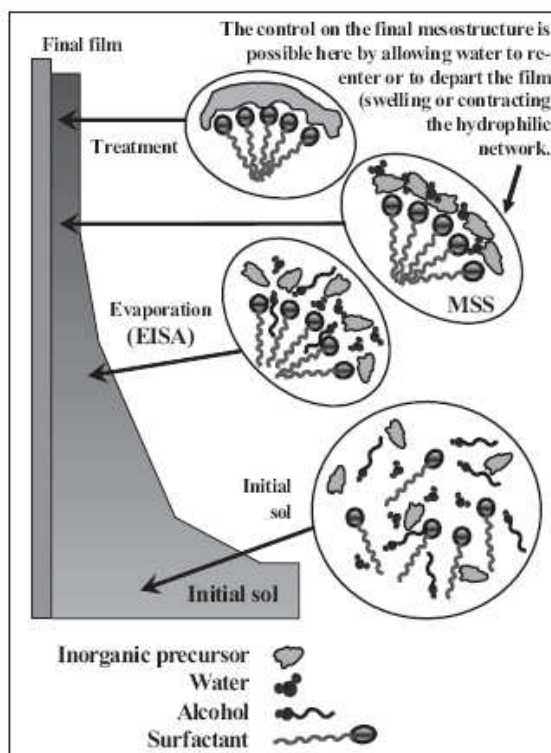
Fig.4: Formation of mesostructured thin film by dip-coating. *Step 1*: presence of isotropic initial sol in which the condensation is slowed. *Step 2*: evaporation proceeds and the micelles start to form above *cmc*. *Step 3*: evaporation is completed; the film is in equilibrium witt environment (MSS) and the mesostructure is fixed by relative humidity (RH) before inorganic condensation. *Step 4*: inorganic network is condensed; hybrid mesostructure is stabilized.
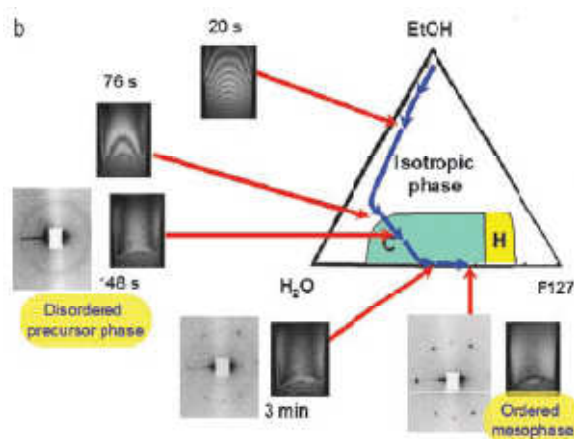
Fig.5: Simplified system trajectory of the formation of a mesostructured TiO_2 film (F127).

This multiplicity of mesophases upon mesostructure formation has been observed by in-situ X-ray reflectometry experiments on silica/cationic surfactant films grown at the air–water interface [24]. In the case of nonionic templates, the formation of a short-range order phase (often called a "wormlike phase") precedes the formation of an organized and well-oriented product mesophase. This kind of "disorder-to-order" transition has also been observed in the initial stages of formation of thick films or xerogels [25].
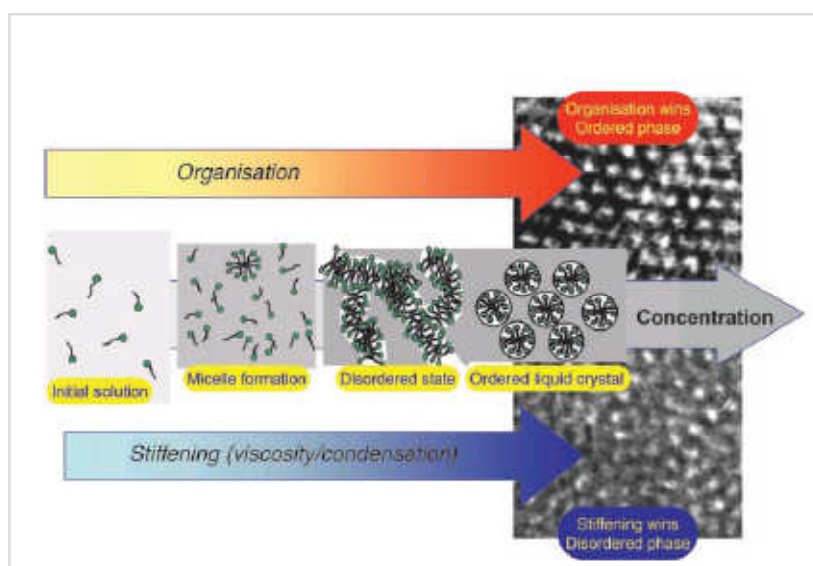
Fig.6: Scheme of the "race towards order" concept. The forces leading to order are predominantly thermodynamic ones (i.e., optimization of self-assembly).

When a well-defined organization at the mesoscale is desidered, the system has to be designed to separate phases and organize completely before the medium becomes rigid enough to "freeze" a disordered phase, or even to "freeze" before any phase separation, leading to a non-mesoporous, or poorly ordered film. In other words, the "race towards order" must be won [7].

If the thermodynamic differences between ordered or disordered mesophase are not significant at ambient temperature [26], the "race can be won" if 1) the nucleation rate for an organized mesophase made upon the self-assembly of micelles and inorganic counterparts (i.e., the NBBs of the hybrid mesophase) is important and 2) the medium is compliant enough to permit rearrangement of the NBBs. The kinetic phenomena involved in the "race towards order" (**Fig.6**) are analogous to those involved in phase separation at the micron scale [27-29].

Some clues of the condensation kinetics can be obtained by applying in-situ spectroscopic techniques, such as ATR-FTIR spectroscopy [18], FTIR ellipsometry [30], and IR synchrotron radiation.

In summary, film formation by EISA is a "chemical symphony" that implies the coordinated interplay of the following phenomena:

1) Sol–gel chemistry (shape, size, hydrophilicity and connectivity of the inorganic or hybrid NBBs).

2) Self-assembly between template molecules, to form micelles, between micelles, to form extended liquid crystalline domains, and between micelles and inorganic or hybrid NBBs.

3) A "race towards order" in which the processes of gelling and order from phase separation compete.

4) Mass transport, which controls the homogeneity of the processes (and thus the mesostructure) along thickness.

Different mesostructered film prepared by EISA method are reported in **Tab. 1-2**.

Tab. 1

Ordered mesostructured films prepared by dip-coating

Thin film structure	Precursors	Support	Reference
Three-dimensional cubic silica	TEOS, ethanol, HCl, CTAB	Alumina	[37]
Hexagonal and three-dimensional cubic silica ∥	TEOS, ethanol, HCl, PEO-PPO-PEO	Silicon wafers and glass slides	[38]
Two-dimensional hexagonal silica ∥	TEOS, PEO-PPO-PEO, ethanol, HCl, pluronic F-127	Si(1 0 0) wafers	[39]
Two-dimensional hexagonal and rectangular titania ∥	$TiCl_4$, ethanol, pluronic F-127, Brij 58	Glass or silicon substrates	[40]
Disordered tungsten oxide	WCl_6, pluronic P-123, ethanol	Tin-doped indium oxide (ITO)-coated glass	[41]
Hexagonal silica	TEOS, 3-(2,4-dinitrophenylamino)propyltriethoxysilane, CTAB	Glass slides	[42]
Two-dimensional hexagonal and two-dimensional rectangular ZrO_2	$ZrCl_4$, $C_{16}H_{33}(CH_2CH_2O)_{20}OH$ ethanol, H_2O	Silicon	[43]
Two-dimensional hexagonal aluminum oxide normal to the substrate	$AlCl_3$, $C_{16}H_{33}(CH_2CH_2O)_{20}OH$ ethanol, H_2O, NH_4OH	Glass plates or silicon wafers	[44]
Hexagonal silica ∥	TEOS, CTAB, ethanol, H_2O, HCl	Glass slide	[45]
Hexagonal silica	TMOS, NaOH, NH_3, H_2O, CTABr	Silicon wafers, borosilicate glass	[46]
One-dimensional hexagonal silica	TEOS, HCl, H_2O, F-127, EtOH	Glass and silicon	[47]
One-dimensional hexagonal and cubic silica ∥	TEOS, HCl, H_2O, EtOH, Brij 56	Silicon with oxide overlayer (SiO_2/Si) and Au	[48]
Three-dimensional hexagonal silica, c-axes ⊥	TEOS, HCl, H_2O, CTABr, EtOH	Silicon wafers	[49]
Hexagonal and cubic silica ∥	TEOS, HCl, H_2O, CTABr	Silicon	[50]
One-dimensional hexagonal, three-dimensional hexagonal, lamellar and cubic silica	TEOS, CTAB, Brij 56, HCl, H_2O	Silicon	[51]
Two-dimensional hexagonal silica membranes ∥	TEOS, HCl, H_2O, alkyl trimethyl ammonium bromides (C_{12}–C_{16})	Glass or silicon	[52]
Three-dimensional hexagonal and cubic silica ∥	TEOS, HCl, H_2O, gemini surfactants	Silicon wafers or glass	[53]
One- and two-dimensional hexagonal silica ∥	TEOS, EtOH, HCl, H_2O, CTAB, F-127	Glass or silicon wafers	[54]
Cubic and three-dimensional hexagonal silica ∥	TEOS, HCl, EtOH, CTAB	Silicon wafers	[55]

∥: Parallel to interface; ⊥: normal to interface.

Tab. 2

Ordered mesostructured films prepared by spin-coating

Thin film structure	Precursors	Support	Reference
Hexagonal silica ‖	TMOS, HCl, CnTAC	Pyrex glass	[65]
Hexagonal silica ‖	TEOS, CTACl, HCl	Glass	[66]
Three-dimensional hexagonal silica *c*-axis ⊥ to the film plane	TEOS, HCl, CTAB, ethanol	Glass plates	[67]
Three-dimensional hexagonal silica ⊥	TEOS, CTAB, HCl, ethanol	Glass plates	[68]
Hexagonal titania	Ti(OCH(CH$_3$)$_2$)$_4$, HCl, propanol	Glass slides	[69]
Hexagonal silica ‖	TEOS, CTAC, HCl, pluronic P-123	Microslide glass, titanium, silicon	[70]
Hexagonal disordered titania	Ti(OC$_4$H$_9$)$_4$, ethanol, HCl, CTAC, BTAC	Soda lime silica glass plates	[71]
Disordered silica	TEOS, pluronic P-123, ethanol, polypropylene glycol	Si(1 0 0) single crystal wafers or at-cut piezoelectric crystalline quartz	[72]
Oriented lamellar silica	TEOS, ethanol, HCl, Fe-TMA	Glass	[73]
Hexagonal silica	Sodium silicate solution, H$_2$SO$_4$, CTACl	ITO-coated glass	[74]
Hexagonal and cubic SiO$_2$ ‖	TEOS, P-123, F-127, ethanol, H$_2$O, HCl	N-type silicon with SiO$_2$ and Si$_3$N$_4$	[75]
Disordered tungsten oxide	WCl$_6$, ethanol, P-123	ITO-coated glass, Pyrex glass	[76]
Hexagonal silica	TMOS, NaOH, NH$_3$, H$_2$O, CTABr	Silicon wafers, borosilicate glass	[46]
One-dimensional hexagonal silica ‖	TEOS, HCl, H$_2$O, P-123	Glass	[77]
Hexagonal silica ‖	TEOS, HCl, H$_2$O, P-123	Glass	[78]
One-dimensional hexagonal and cubic silica ‖	TEOS, HCl, H$_2$O, EtOH, Brij 56	Silicon with oxide overlayer (SiO$_2$/Si) and Au	[48]
Hexagonal silica	TEOS, HCl, H$_2$O, CTABr, EtOH	Surface aluminum hydroxide on glass	[79]
One-dimensional hexagonal silica ‖	TEOS, HCl, H$_2$O, CTACl, PrOH	Glass	[80]
Lamellar, one-dimensional hexagonal silica ‖	TEOS, HCl, H$_2$O, CTACl, PrOH	Glass	[81]
Hexagonal and cubic silica ‖	TEOS, HCl, H$_2$O, CTABr	Silicon	[50]
Disordered titania	Ti(OC$_4$H$_9$)$_4$, EtOH, HCl, CTACl	Glass plates	[82]
Lamellar, hexagonal and cubic silica ‖	TMOS, CTACl, HCl, H$_2$O	Glass	[83]

‖: Parallel to interface; ⊥: normal to interface.

4.4 FILM FORMATION

Mesoporous materials are rigid solids and cannot be easily shaped into thin films at the post-synthesis stage. Thus, the reactive mixture has to be deposited as a thin film, or the synthesis conditions should favour the formation of a thin interfacial layer.

Mesoporous Thin Film (MTF) were produced at air-water and oil-water interfaces. In both cases, the films were observed to grow by the transport of material from the solution towards the interface. MTF were formed on different types of solid supports by a variety of preparation methods [31]. The methods may be classified by the role played by the surface in the growth process. Thus, we distinguish between surfaces which nucleate MTF growth, and surfaces which are coated by the film. In the first case, the films were grown on mica and exhibited hexagonal ordering with the pores aligned parallel to the support (**Fig.7**).

The films can be prepared also on hydrophobic, amorphous and stainless steel supports [32]. The specific interactions of the surfactant molecules with the support were observed to affect the structure of the resulting films [33]. In MTFs grown on amorphous supports the pores were aligned perpendicular to the support and the film exhibited distorted hexagonal packing. Films grown on crystalline substrates exhibited in-plane orientation ordering of the surfactant rods. Other conventional methods for thin film formation, i.e. spin- and dip-coating, were applied for their preparation [34,35]. In these methods an oligomeric solution of silica is prepared prior to the addition of surfactant. In many cases, coating is carried from a solution containing a highly volatile liquid so as to enhance the rate of film formation by rapid solvent evaporation.
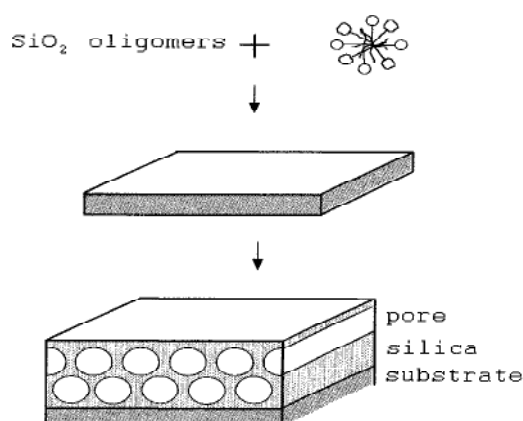
Fig.7: Mechanism of MTF formation at support-water interface.

4.4.1 SPIN-COATING

Spin coating [36,37] is a procedure used to apply uniform thin films to flat substrates. An excess amount of a solution is placed on the substrate, which is then rotated at high speed in order to spread the fluid by centrifugal force. A machine used for spin coating is called a spin coater, or simple spinner (**Fig.8**).

Rotation is continued while the fluid spins off the edges of the substrate, until the desired thickness of the film is achieved. The applied solvent is usually volatile, and simultaneously evaporates. The thickness of the film also depends on the concentration of the solution and the solvent. There are four distinct stages to the spin coating process [38]:

- Deposition of the coating fluid onto the wafer or substrate. This can be done by using a nozzle and pouring the coating solution or by spraying it onto the surface. A substantial excess of coating solution is usually applied compared to the amount that is required.
- The substrate is accelerated up to its final, desired, rotation speed .
- The substrate is spinning at a constant rate and fluid viscous forces dominate the fluid thinning behavior.
- The substrate is spinning at a constant rate and solvent evaporation dominates the coating thinning behavior.
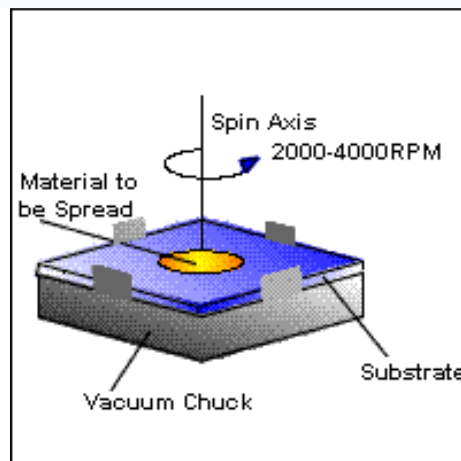
Fig.8: Spin-coater.

Mathematic treatment imposes balancing between viscous forces and centrifugal force. Moreover it is important to keep in mind that, because of solvent evaporation, the viscosity changes in function of the time.

The final formula is:

$$h_f = c_0 \cdot \left(\frac{e}{2 \cdot (1 - c_0) \cdot K} \right)^{\frac{1}{3}}$$

h_f = thickness of film;

c_0 = concentration of solid in the solution;

e (speed of evaporation) = $C \sqrt{\omega}$

$K = \rho\omega^2/3\eta$

The instrument is formed by a small rotating support pierced in the center; through this opening, was produced vacuum to keep adherent to the support the substrate covering. By two grips, it is possible to control either the speed or the time of rotation. A cover guarantees the operator's security.

4.4.2 DIP-COATING

Fig.9 shown the dip-coating process, which may be divided in five stages: immersion, start-up, deposition, evaporation and drainage. The substrate is slowly dipped into and withdrawn from a tank containing the sol, with a uniform velocity, in order to obtain a uniform coating [39,40]. The thickness of film depends on various parameters: viscosity of solution, gravity force, extraction speed, surface tension between liquid and vapor, etc.
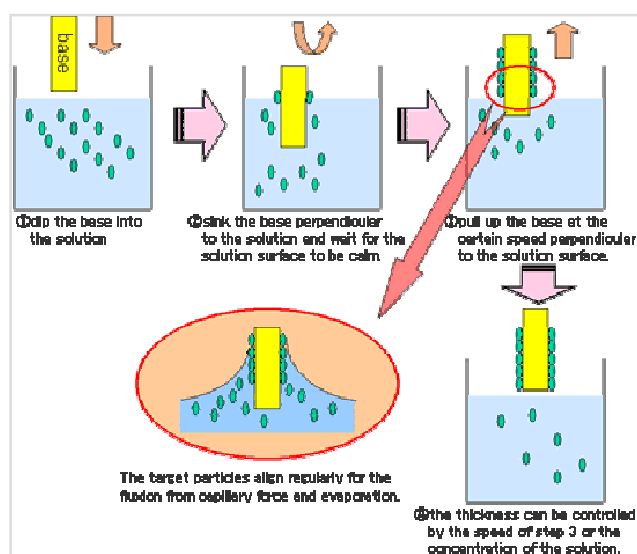
Fig.9: Deposition of thin film by dip-coating.

The substrates are withdrawn from a homogeneous precursor solution and the dip-coated solution is allowed to drain to a particular thickness. The thickness of the film is mainly determined by the rate of evaporation of the solvent and the viscosity of the solution. When the velocity of substrate and the viscosity of liquid aren't very high, the thickness of film can be obtained from Landau and Levich equation:

$$h = \frac{0.94(\eta U)^{2/3}}{\gamma_{LV}^{1/6}(\rho g)^{1/2}}$$

where U is the speed of extraction, η is the viscosity, γ_{LV} is the surface tension liquid-vapor. It is important to observe that for polymeric systems the thickness of film change with $U^{2/3}$.

This equation assumes constant viscosity and Newtonian behavior, without effects of evaporation. Landau and Levich equation is effective for sol prepared in acid catalysis.

4.4.3 ALTERNATIVE DEPOSITION TECHNIQUES

Casting [41] is an alternative solvent evaporation method that has been used for the preparation of mesostructured films. In this method, the solution is dropped on to the substrate and allowed to solidify, resulting in much thicker films. Electrodeposition of mesoporous thin films is employed to create continuous thin films of mesostructured materials on a variety of substrates. This method has been reported by Attard *et al*., Elliott *et al*. [42,43].

All the authors used a direct liquid crystal templating method, which requires a high surfactant concentration (>30 wt.%) to provide a homogeneous liquid crystal phase during the entire electrodeposition process. Pulsed laser deposition (PLD) is another alternative deposition technique for creating continuous mesoporous thin films on non-planar surfaces producing good quality ordered mesoporous films.

4.5 CONSOLIDATION TREATMENTS

Consolidation treatment aims to stabilize the inorganic network by further condensation and to increase the porosity through template elimination. The fresh film (low-condensed molecular species plus template and remaining solvent) is liquid-like enough to allow rearrangements and therefore is readily soluble in solvents such as alcohols or water. In this way, the inorganic condensation is encouraged (e.g., by moderate thermal treatment, T>150°C, or alkalinization by exposure to NH_3 vapors) [4,22,44,45].

These treatments produce a densification of the pore walls and a uni-axial contraction. Consolidation treatments are very important and necessary in order to obtain reproducible products. Residual wall porosity can be eliminated and the crystalline nature of the inorganic wall

can be tailored by an adequate set of post-synthesis conditions [46]. In transition-metal-derived thin films, treatment conditions can be set to create open porosity, therefore improving pore accessibility [13,47,48]. It is possible to combine mild-temperature treatment, basic treatment (NH$_3$ atmosphere) [44], solvent extraction [44,49] and degradation of organics by UV-O$_3$ [50]. Thus, there are a great variety of possible treatments that can be adapted to the type of materials and the targeted application.

4.6 APPLICATIONS

Mesoporous Thin Films (MTF) with their unique properties, e.g., versatile framework nature (single or multioxides, crystalline or amorphous structure, hybrid organic-inorganic, etc.), high surface area, modulable pore dimension and shape (cylindrical, spherical, ellipsoidal, etc.), tailored surface (organic or inorganic, inert or active), and high processing and handling abilities have offered to scientists a land of opportunities [51-53]. Mesoporous thin films or membranes are characterized by bulk properties, such as symmetry, pore diameter, surface area and stability, and film-related parameters, such as pore orientation, film thickness, continuity and surface roughness [54-56]. The interest in mesoporous thin films originates from the appreciation of their technological potential as membranes [68], sensors [64-67], heterogeneous catalysts and insulating layers of low dielectric constant for microelectronics [57-60], photonic devices [61-63]. These applications require the ordered material in the form of thin film.

Stucky *et al.* [69] synthesized optically transparent mesoporous silica films doped with fluorescein entities, which function very effectively as pH sensors. Cheng *et al.* [70] reported the electrochromic properties of mesoporous tungsten oxide films. Innocenzi *et al.* [71] synthesized mesoporous silica films deposited on alumina substrates. The films exhibited a change in the current intensity as a function of relative humidity indicating its potential use as humidity sensors. Domansky *et al.* [72] studied the dielectric response of mesoporous silica films as a function of several gas-phase chemical species. The dielectric constant and dissipation factor of partially dehydroxylated films were highly sensitive to water vapor and ammonia in air showing their potential as chemical sensors.

Dag *et al.* [73] reported the preparation of silicon clusters inside hexagonal mesoporous silica films displaying photoluminescence and nanosecond luminescence lifetimes. These composites

are promising as light-emitting diodes, optical interconnections and chemical sensors. Yu *et al.* [74] prepared silica mesoporous thin films with low dielectric constant via sol–gel method. Preliminary results on these silica films show a very positive prospective for intermetal dielectric applications. Hu *et al.* [75] synthesized mesoporous silica films with block copolymers showing very low dielectric constant (<2.3) which makes them useful for current and future microelectronic applications.

4.6.1 SENSORS

Mesoporous thin film are commonly used as supports in the development of optical sensor devices because they are transparent, chemically inert, thermally and mechanically robust, photostable, easily processed and they allow the embedding/grafting of molecular probes [64,76,77]. Mesostructured thin films with their larger porosity and high surface area should improve analytes diffusion and accessibility towards supported probes.

Moreover, both their unimodal narrow pore size distribution and their controlled porous connectivity make them much more resistant to the huge capillary stresses usually responsible for the instability and the collapsing of mesoporous xerogels in liquid work conditions.

The choice of the mesophase (2D or 3D geometry) could be adjusted to specific properties of the sensor (i.e. diffusion, accessibility, mechanical stability). In addition to that, the leaching of the functionality which is one of the greatest problems in hybrid sensor applications, is prevented by the anchorage of the sensing probe to/within the framework. Highly ordered mesoporous transparent thin films with high mechanical robustness are well-suited materials for fast response optical sensors. Future applications in this area also might use patterning methods such as ink-jet and micro-pen printing of mesostructures in order to generate optical multi-sensor arrays.

4.6.2 PHOTOCHROMIC MATERIALS

Mesostructured materials can host photochromic dyes, i.e. dyes which change their color upon light illumination. It is desirable that the reverse reaction (thermal bleaching) is fast allowing rapid switching between two states (high/low transmission in a certain wavelength range). For purely inorganic host materials, the response times are slow in comparison to solution and undesired reverse photochromism is often observed. In organic matrices, on the other hand,

the response can be much faster (in the order of seconds). In these matrices more than one site is available for the dye which then results in a multiple distribution of response times. The properties can be improved, however, by blending inorganic and organic components on a molecular level.

4.6.3 LOW-K DIELECTRIC MATERIALS

Mesoporous films are particularly suited as insulators in the semiconductor industry [78]. Currently the industry is working on the development of materials that are suitable for new more efficient and fast chips. These insulating materials must have relative permittivity values significantly lower than that of silicon dioxide ($\varepsilon_r \approx 3.8$) and for components smaller than the typical size of 0.1 mm. Materials with ε_r values less than 2 are often necessary (ultralow-k materials).

Owing to their large pore volumes (ε_r (air) ≈ 1) and their comparatively high organic fraction, mesoporous films, whose atoms are lighter and less extensively polarizable than those of silicon dioxide, are in principle very suitable as low-k dielectrics.

The various attempts to prepare mesoporous silica films with low permittivities for use as insulators in microelectronic applications are very promising. Lower permittivity values could be achieved through a better control of the structure and porosity.

4.6.4 LASER MATERIALS

It is possible to use the mesostructure architecture to construct new optical materials with high reliability by one-step silica/block-copolymer/dye co-assembly. It has been done by processing mesostructured thin films, waveguides as well as thin films on optical fibers and simultaneously doping these materials with rhodamine 6G, a well-investigated laser dye of the xanthene family. In order to achieve lasing, the mesostructured materials have to be patterned into the appropriate shape.

One way is to pattern waveguiding structures by soft lithography. Feedback for proper lasing can be introduced by fabricating a resonator structure, for example by coating the ends of the waveguides with a metal.

4.6.5 PHOTONIC APPLICATIONS

Most of the described examples of mesostructured films using luminescent molecules were designed to probe the film formation, to elaborate waveguides or laser arrays or to study the energy transfer between two organic dyes located in the micelles [62,79]. However, the localization of the probes in the micellar part of thin films could limit their potential applications mainly due to leaching of the dye. In 1999 Lebeau *et al.* [62] reported for the first time the ''one-pot'' synthesis of functionalized mesoporous silica thin films using 3-(2,4-dinitrophenylamino)propyltriethoxysilane in the presence of the surfactant (CTAB).

Optical properties of the dye-functionalized surfactant-extracted mesoporous materials were investigated by UV-vis and fluorescence spectroscopies. The optical activity of the dye moiety was retained when it was covalently linked to the silica network of the mesostructure. The well-organized local separation of organic/inorganic regions in mesostructured composites provides substantial versatility for adjusting host/guest optical properties. The hydrophobic regions are compatible environments for organic dopants, enhancing their overall solubilities and preventing their aggregation. In addition, the rigid inorganic framework protects and stabilizes the included species but could also incorporate other functionalities. The position of probes inside the three mains regions constituting mesostructured materials can be controlled by several factors. It has been shown that philicity and the number of trialkoxysilane groups per dopant molecule can affect the placement of the probes in mesostructured thin films. The philicity operates by placing hydrophobic organic molecules inside the surfactant micelles.

Zink *et al.* [80] used this preferential placement of probes to study the energy transfer between two luminescent dyes located in two different spatially-separated regions. It is interesting to point out that for these films, the fluorescence peak of the mesostructured film is 27 times more intense than that of the amorphous film, and the excitation peak intensity of the mesostructured film is 42 times more intense than the excitation peak of the amorphous film. The higher fluorescence intensity of R6G in nanostructured films relative to amorphous films shows that the presence of CTAB affects R6G luminescence.

4.6.6 OLEDs

Mesoporous thin film can be used as emitting layers in which coordination complexes with luminescent properties for OLED preparation are grafted. OLEDs (**Organic Light Emitting Diodes**) are electro-optics devices based on luminescent organic compounds with significant advantages with respect to the more common and widely used inorganic based devices (LEDs): [82]: low operating voltage, low production cost, easy color modulation obtained through suitable structural modifications, possibility of multicolor emission, high resolution, easy processing, possibility of making wide and flexible panel displays [83]. Vacuum-deposited Organic Light Emitting Devices (OLED) technology has developed rapidly since the first report by Tang and VanSlyke of low voltage green electroluminescence (EL) from the hexacoordinated complex tris(8-hydroxyquinolinato) aluminium(III) (AlQ_3). In this type of devices the design of efficient emitter materials requires the optimization of several properties including high photoluminescence efficiency, sublimation without chemical degradation, appropriate energy-level matching with the cathode and hole-transport layer for balanced charge injection and transport and the ability to form structurally stable films.

These properties are strongly coupled to the molecular and electronic structure of the molecules, as well as the bulk packing of molecules achieved by vapours deposition. Nowadays, one of the major issues which can prevent the commercialization of this new technology is the easy degradation of these devices. The device lifetime depends on numerous factors, and can vary from several minutes to thousand of hours depending on the nature of the materials used into the devices. The weak stability of OLEDs can be correlated to: the degradation of the electrodes with time, the chemical and/or thermal and/or morphologic instability of the organic materials, undesirable secondary reactions due to the presence of impurities even in small quantities, crystallization of the film initially amorphous.

Based on these premises, it is necessary to develop thermally and morphologically stables amorphous organic electroluminescent materials which can allow the formation of uniform, defect-free, thin films [84]. The properties of OLEDs can be potentially enhanced through their confinement as "guests" in a matrix characterized by an ordered length scale. The length scales defining structure and organization of a material determine its fundamental properties. From this point of view, mesoporous thin film, in which coordination complexes of suitable photo or

electro-activity can be covalently and non-covalently grafted envisaging their use in the production of OLEDs, are an excellent support. This new class of materials should allow the development of a new general procedure able to increase (in the working conditions of the devices) the resistance to chemical degradation (oxidation and/or hydrolysis) and also to prevent their crystallisation.

4.7 CHARACTERIZATION TECHNIQUES

Mesostructured thin films are made of a very small amount of matter (usually between 10 and 500 μg/cm^2 of film) spread onto a substrate. Their characterization, more difficult than for bulk materials, is thus limited to spectroscopic investigations and very sensitive techniques. At microscopic level, the chemical composition is determined by Fourier transform infrared spectroscopy (FTIR), Rutherford back scattering (RBS), energy dispersive X-ray analysis (EDX), and X-ray photoelectron spectroscopy (XPS). The microstructure is obtained by Raman scattering (RS) and wide angle X-ray diffraction (XRD). The mesostructure is probed by electron microscopies (SEM and (HR)TEM) and diffusion and reflectometry techniques (SANS, SAXS, XRR, neutron reflectometry). The porous texture (often required for applications) can be described by gas adsorption, monitored by gas consumption (Krypton adsorption), spectroscopic ellipsometry (ellipsometric porosimetry, EP), X-ray reflectomety, surface acoustic wave (SAW).

For porous or hybrid nonporous films, the texture can be investigated by following the diffusion of a chemical probe through the porous (organic) mesoscopic network by electrochemical characterization or spectroscopy. Because of its high sensitivity, fluorescence spectroscopy is also used for characterizing locally the environment of a probe, collecting information on the organic domains of a hybrid film, on the organic/inorganic interface or on the symmetry and chemistry of an emitting inorganic center of the inorganic matrix. Finally, the mechanical properties of the thin films can be obtained by nanoindentation (NI), ellipsometric porosimetry, or acoustic waves analyses (SAW).

4.7.1 STRUCTURAL CHARACTERIZATIONS

Most of the papers reported in the literature conventional 1D XRD technique (Bragg-Brentano geometry) were used to assess the mesostructure but in most cases, it is insufficient to

correctly define the structure as a result of the mono-orientation of the ordered domains with respect to the substrate interface. Indeed, a straightforward and no ambiguous characterization of the structural periodic organization of the mesoporous network can only be visualized by 2D-SAXS [44]. Even if the very few number of laboratory SAXS equipements available and the difficulties to access synchrotron SAXS lines make such investigations difficult to perform, it remains the absolute tool. When access to GI-SAXS is possible, one of the most common way of assessing the proper structure is to combine 2D diffraction patterns and TEM images [13,44,88-92], which provides a direct observation of the mesoporous network and the measurement of its periodicity, space group, and potential network contraction. **Fig.12** illustrates the high complementarity of both techniques.

4.7.1.1 GI-SAXS (GRAZING INCIDENCE SMALL ANGLE X-RAY SCATTERING)

GI-SAXS is based on angular distribution of X-ray coherent scattering intensity and is well suited to the characterization of thin mesoporous films since it allows to evaluate the entire thickness and gives informations about the periodicity, the orientation, and the space group of the ordered domains [93,94]. Diffusion scattering (and potentially diffraction) is observed at low angles when electron density inhomogeneities exist in the nanometer range. The experimental setup is usually a film irradiated by a narrow X-ray beam at very low angle ($\alpha < 1°$). The angular distribution of the scattered X rays is collected onto a 2D detector as shown in **Fig.12**.

For mesoporous thin films, the obtained diffusion diagrams exhibit diffraction spots characteristic of the periodical mesostructure of the film. From the complete 2D diffraction pattern, the packing geometry of the mesophase can be identified. The structure attribution should be made with much care by coupling 2D diagrams with TEM. GI-SAXS allows the determination of the mesostructure, the anisotropy of a mesostructure (needed for accurate pore size determination by other techniques described hereafter), and the coexistence of several mesophases (either due to a lack of homogeneity of the film or by stacking of different mesostructured layers).
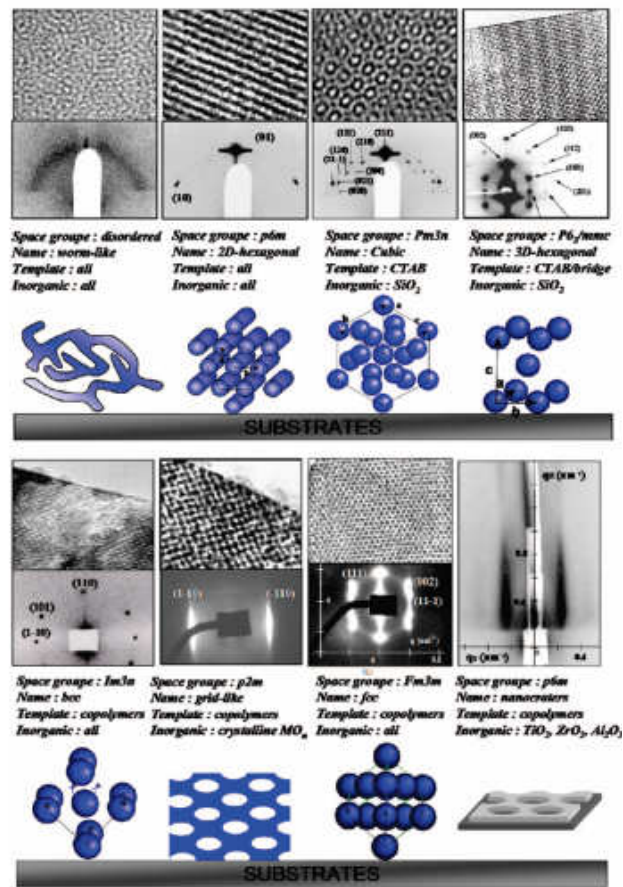
Fig.12: 2D SAXS patterns corresponding to the various types of mesostructures obtained.

4.7.1.2 X-Ray Reflectometry (XRR)

XRR is a scattering technique allowing the non-destructive determination of the electronic density, the thickness and the interfacial rugosity of a thin film. A film is irradiated by a narrow X-ray beam at low incidence angle ($<1.5°$). The incident and detecting angle are similar and the detector is punctual. For such configuration, only electronic density variations along the (z) axis can be observed. The resulting reflectometric diagram is produced by the interferences of the beam reflected at the surface of the film and the beam reflected by the other interfaces of the system (the film-substrate interface and the "high electronic density"-"low electronic density" interfaces of the mesostructure).

At low wave vector the critical angle of penetration of the beam into a homogeneous film is measured. The refractive index of the film is determined according to the Snell-Descartes law:

cos θ_C = n_{FILM}. For angles $\theta > \theta C$, interference fringes appear: these fluctuations can be described by the extended Bragg law.

4.7.2 TEXTURAL CHARACTERIZATIONS

4.7.2.1 GAS PHYSISORPTION POROSIMETRY

Although the determination of the mesostructural parameters is a first necessity for materials scientists, many applications involving porous films are crucially depending on the accurate knowledge of the pore size distribution (PSD), pore connectivity of the network and the ability to determine matter exchange and matter adsorption capacities of the porous network and the film environment. Adsorption porosimetry is considered the reference analytical approach for the description of micro and mesoporous parameters.

By analyzing the multilayer physisorption and capillary condensation of a gas within the pores, a plot of the adsorbed volume of gas versus the partial pressure P/P_0 of gas is obtained. The mono- and multilayer physisorption of the gas observed at low P/P_0 can be plotted by the Brunauer-Emmett-Teller (BET) equation (**eq.1**)

$$\frac{P}{n(P_0 - P)} = \frac{1}{n_m C} + \frac{C - 1}{n_m C} \frac{P}{P_0} \qquad (eq.\,1)$$

It allows the determination of the surface area, with n_m being the number of molecules needed to cover the accessible surface with a monolayer of molecules, n, the number of molecules adsorbed at the partial pressure P/P_0, and C, a parameter characteristic of the net heat of adsorption of the molecule at the surface [95,96]. The gas uptake observed at higher $P/P0$ values, defined as capillary condensation, is used for the determination of the PSD between 2 and 50 nm via the Kelvin equation (**eq.2**)

$$RT \ln\left(\frac{P}{P_0}\right) = -\gamma V_L \frac{G}{r_P} \qquad (eq.\ 2)$$

that describes the condition of appearance of the capillary condensation at a given value of $P/P0$, with γ, the condensed liquid surface tension, VL the molar volume of the liquid adsorbate, r_P the radius of the pore, and G, a geometrical factor characteristic of the liquid-air meniscus curvature

(BJH model) [97]. More sophisticated models taking into account the internal curvature of the liquid-solid interfaces [98-100] and the thickness of adsorbed gas layer before capillary condensation or taking a nonporous material of similar surface properties as the reference are advantageously employed. The micropores characterization is obtained by plotting the adsorption curve at very low partial pressure ($P/P_0 < 0.1$). Originally developed by Dubinin e Radushkevitch [95,96], the micropore size distribution determination is now being efficiently evaluated by the DFT approaches whenever a realistic description of the surface can be given. The physisorption can be monitored by measuring various physical parameters (adsorbed gas volume pressure, electronic density, refractive index, weight of gas adsorbed, spectroscopic absorbance of the adsorbed gas, etc.).

4.7.2.2 KRIPTON AND NITROGEN ABSORPTION

Nitrogen physisorption is difficult to apply to thin films attending the very limited amount of porous matter available on one film deposited onto a substrate of several square centimeters surface. Only a few examples of nitrogen adsorption onto MTFs have been reported. In these cases, the authors have used several tens of films to collect the minimum amount of porous matter needed. This fastidious work pushed scientists to develop alternative porosimetry techniques implying only one film.

Replacing N_2 by Kr (sublimation pressure at 77 K is ~1.7 torr) reduces drastically the amount of un-adsorbed molecules in the dead volume. The adsorbed amount of gas is then monitored with an improved accuracy (about ten times less matter is needed in this case to obtain adsorption-desorption isotherms as shown in **Fig.13**). However, unless special conditions are applied, mesopores larger than approximately 6 nm cannot be studied for fundamental reasons at 77 K using Kr, because for these pore size Kr does not condense to a liquid.
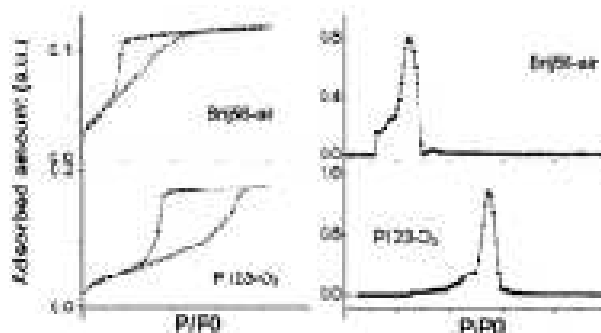
Fig.13: Kr physisorption isotherms of periodically organized silica films
prepared with different structuring agent.

4.7.2.3 SPECTROSCOPIC ELLIPSOMETRY POROSIMETRY

The spectroscopic ellipsometry is a nondestructive optical technique based on the analysis of the change of polarization state of a polarized light beam after reflection onto a surface. The ellipsometric parameters (Ψ e Δ), obtained from the Fresnel coefficients of the reflected beam, are very sensitive to the presence of a superficial layer of optical properties different from those of the substrate [101]. This technique is routinely used to assess the physical thickness of the film and its optical density. For the porosimetry measurements, two types of apparatus exist.

Ellipsometric porosimeter (EP) is constituted by a vacuum chamber. A partial pressure of gas is applied over the film for a controlled physisorption, in the same way of usual N_2 porosimetry. In the second type of apparatus (Environmental Ellipsometric Porosimetry) the analysis is performed at atmospheric pressure by applying onto the film a dynamic flux of air containing a controlled relative pressure of gas (usually water or alcohol).

The physisorption of a gas into the porous network of a MTF gives several types of very interesting data. First, the isotherm of the variation of the refractive index of the film can be plotted versus the relative pressure of gas (**Fig.14**) allowing the determination the porous volume of the film (optical properties of the skeleton are needed) and the determination of the adsorbed volume of gas at each relative pressure (the optical properties of the adsorbant in liquid state are needed).
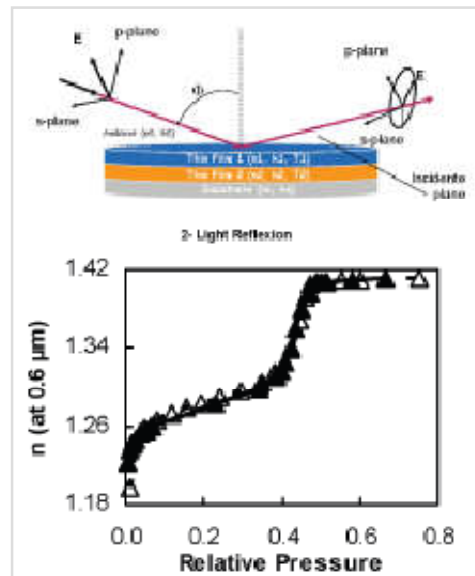
Fig.14: (top) Scheme of the reflection of a linearly polarized light beam onto a substrate coated with two layers of matter of real and imaginary parts of the refractive index of *ni* and *ki* and of thickness *Ti*; (bottom) example of adsorption-desorption of ethanol into a P.O. mesoporous silica film.

So, only one analysis is needed for the complete characterization of a multilayer periodically organized system such as those described by Soler-Illia *et al*. [102-104]. Moreover, EP and EEP analysis allow the determination of variation of film thickness versus the adsorbate partial (relative) pressure. The observed swelling and contraction of the MTFs are very informative on the adsorption mechanisms taking place. A low pressure swelling is characteristic of micropores with molecular adsorption mechanism. On the other hand, the contraction observed whenever mesopores are analyzed is due to capillary forces (a collective effect of the adsorbed molecules forming a liquid meniscus). From this contraction isotherm, the transverse Young's modulus E of the film can be easily determined at pressure higher than the capillary condensation with the general (**eq.3**), in which T_0 is the film thickness, V_L is the molar volume of the liquid adsorbate, $cos \theta$ is the adsorbate-film wetting angle at high partial (relative) pressure of adsorbate, and k is the variation of film thickness versus the logarithm of the partial (relative pressure) during the relaxation of capillary stress.

4.7.2.4 Transmission electron microscopy (TEM)

TEM technique is usually conducted with ED or Fourier Transformation (FT) simulation for a direct view of pore structures of mesoporous materials. In order to observe preferred orientation of mesoporous grain to the substrate and the pore morphology of mesochannels affected by substrate and anisotropic shrinkage from heat treatment, thin film specimen should always be together with its host substrate. At the thin section of a TEM specimen containing the interface of mesoporous silica and substrate, electron transparency can be achieved. A top-view TEM can also be examined using on-substrate sample, which, in turn, has been polished to achieve good electron transparency. It is to be noted that TEM result is localized; therefore, it is desirable to further examine its consistency with XRD investigation.

4.7.2.5 In Situ Fourier Transform Infrared

FTIR is a powerful routine characterization technique analyzing the absorption of IR wavelength by local vibrational states and chemical bonds (bending, stretching, or rotating), usually in the energy range 400-4000 cm^{-1}.

FTIR is then used for quantification of organic functions (assessment of structuring agent departure, grafting of organic functions, organic molecule adsorption-desorption isotherms, or less often, inorganic matrix hydroxylation and condensation states). In situ FTIR is a very interesting evolution of this widespread technique.

Employed to double the GISAXS experiments, a synchrotron source is used for rapid scan time-resolved FTIR to analyze the chemical composition of the film cast during the evaporation and mesostructuration processes. The dynamic water content of the film can then be monitored (the time needed to equilibrate the water composition of the film with the environment relative humidity) and followed until the inorganic network was rigid.

Although very little work was reported so far, time-resolved in situ FTIR investigations will probably develop very quickly in the optimization of the evaporation and post-treatment of organic-inorganic films (**Fig.15**).
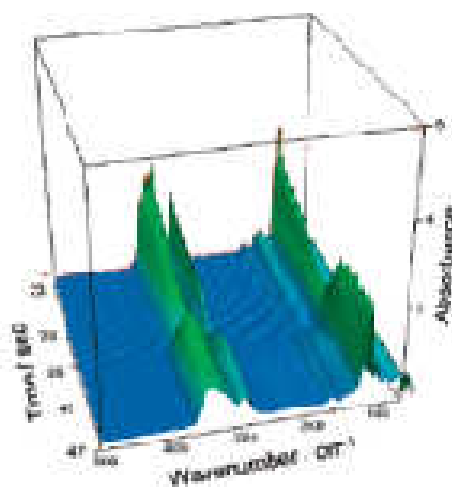
Fig.15: Rapid scan time-resolved FTIR monitoring of the formation of
a periodically organized silica thin film by EISA.

REFERENCES

1. G. Ogawa, *Curr. Opin. Colloid Interface Sci.*, **2001**, 4, 209;

2. Q. Huo, D.I. Margolese, U. Ciesla, D.G. Demuth, P. Feng, T.E. Gier, P. Sieger, A. Firouzi, B.F. Chmelka, F. Schuth, G.D. Stucky, *Chem. Mater.*, **1994**, 6, 1176;

3. C.J. Brinker, G.W. Scherer, *Sol-Gel Science, Academic Press*, San Diego, CA, **1990**;

4. D. Grosso, F. Babonneau, P.A. Albouy, H. Amenitsch, A.R. Balkenende, A. Brunet-Bruneau, J. Rivory, *Chem. Mater.*, **2002**, 2, 931;

5. S. Besson, T. Gacoin, C. Ricolleau, C. Jacquiot, J.P. Boileau, *J. Mater. Chem.*, **2003**, 13, 404;

6. K. Fontell, A. Khan, B. Ldstrom, D. Maciejweska, S.P. PuangNgerm, *Colloid Polym. Sci.*, **1991**, 269, 7;

7. G.J. de A.A. Soler-Illia, E.L. Crepaldi, D. Grosso, C. Sanchez, *Curr. Opin. Colloid Interface Sci.*, **2003**, 8, 109;

8. B. Alonso, P.A. Albouy, D. Durand, F. Babonneau, *New J. Chem.*, **2002**, 26, 988;

9. B. Alonso, A.R. Balkenende, P. A. Albouy, H. Amenitsch, M.N. Rager, F. Babonneau, *J. Sol-Gel Sci. Technol.*, **2003**, 26, 587;

10. P. Innocenzi, P. Falcaro, D. Grosso, F. Babonneau, *J. Phys. Chem. B*, **2003**, 107, 4711;

11. J. Israelachvili, *Intermolecular and Surface Forces*, 2nd ed., Academic Press, New York, **1992**;

12. A. Gibaud, D. Grosso, B. Smarsly, A. Baptiste, J.F. Bardeau, F. Babonneau, D.A. Doshi, Z. Chen, C.J. Brinker, C. Sanchez, *J. Phys. Chem. B*, **2003**, 107, 6114;

13. E.L. Crepaldi, G.J.A.A. Soler-Illia, D. Grosso, F. Cagnol, F. Ribot, C. Sanchez, *J. Am. Chem. Soc.*, **2003**, 125, 9770;

14. D.A. Doshi, A. Gibaud, V. Goletto, M. Lu, H. Gerung, B. Ocko, S.M. Han, C.J. Brinker, *J. Am. Chem. Soc.*, **2003**, 125, 11646;

15. D. Grosso, C. Boissiere, B. Smarsly, T. Brezesinski, N. Pinna, P.A. Albouy, H. Amenitsch, M. Antonietti, C. Sanchez, *Nat. Mater.*, **2004**, 3, 787;

16. G.J.A.A. Soler-Illia, C. Sanchez, B. Lebeau, J. P, *Chem. Rev.*, **2002**, 102, 4093;

17. G.J.A.A. Soler-Illia, E.L. Crepaldi, D. Grosso, D. Durand, C. Sanchez, *Chem. Commun.*, **2002**, 2298;

18. D. Grosso, F. Cagnol, G.J.A.A. Soler-Illia, E.L. Crepaldi, H. Amenitsch, A. Brunet-Bruneau, A. Burgeois, C. Sanchez, *Adv. Funct. Mater.*, **2004**, 14, 309;

19. F. Cagnol, D. Grosso, G.J.A.A. Soler-Illia, E.L. Crepaldi, F. Babonneau, H. Amenitsch, C. Sanchez, *J. Mater. Chem.*, **2003**, 13, 61;

20. D. Grosso, F. Babonneau, C. Sanchez, G.J. A.A. Soler-Illia, E.L. crepaldi, P.A. Albouy, H.Amenitsch, A.R. Balkenende, A. Brunet-Bruneau, *J. Sol-Gel Sci. Technol.*, **2003**, 26, 561;

21. D. Grosso, P.A. Albouy, H. Amenitsch, A.R. Balkenende, F. Babonneau, *Mater. Res. Soc. symp. Proc.*, **2000**, 628, CC6.17.1;

22. D. Grosso, A.R. Balkenende, P.A. Albouy, A.Ayral, H. Amenitsch, F. Babonneau, *Chem. Mater.*, **2001**, 13, 1848;

23. D. Grosso, F. Babonneau, G.J.A.A. Soler-Illia, P.A. Albouy, H.Amenitsch, *Chem. Commun.*, **2002**, 748;

24. J.L. Ruggles, S.A. holt, P.A. Reynolds, J.M. White, *Langmuir*, **2000**, 16, 4613;

25. N. Yao, A.Y.Ku, N. Nakagawa, T. Lee, D.A. Saville, I.A. Aksay, *Chem. Mater.*, **2000**, 12, 1536;

26. F. Siperstein, K.E. Gubbins, *Mol. Simul.*, **2001**, 27, 339;

27. K. Nakanishi, *J. Porous Mater.*, **1997**, 4, 67;

28. G.J.A.A. Soler-Illia, A. Louis, C. Sanchez, *Chem. Mater.*, **2002**, 14, 750;

29. N.A. Melosh, P. Davidson, B.F. Chmelka, *J. Am. Chem. Soc.*, **2000**, 122, 823;

30. A. Brunet-Bruneau, S. Besson, T. Gacoin, J.P. Boilot, J. Rivory, *Thin Solid Films*, **2004**, 447/448;

31. H. Yang, A. Kuperman, N. Coombs, S. Mamiche-Afara, G.A. Ozin, *Nature*, **1996**, 379, 703;

32. N. Nishiyama, A. Koide, Y. Egashira, K. Ueyama, *J. Chem. Soc. Chem. Commun.*, **1998**, 19, 2147;

33. I.A. Aksay, M. Trau, S. Manne, *Science*, **1996**, 273, 892;

34. B.A. McCool, N. Hill, J. Di Carlo, W.J. De Sisto, *J. Membr. Sci.*, **2003**, 218, 55;

35. D.Y. Zhao, J.L. Feng, N. Melosh, G.H. Fredriekson, B.F. Chmelka, *Adv. Mater.*, **1998**, 10, 1380;

36. C.J. Brinker, G.W. Scherer, *Sol-Gel Science, Academic Press*,**1990**;

37. M. Ogawa, T. Igarashi, K. Kuroda, *Bull. Chem. Soc. Jpn.*, **1997**, 70, 2833;

38. http://www.chim.unipr.it/lab-vetro/spin.htm

39. V. Bekiari, M.L. Ferrer, P. Lianos, *J. Phys. Chem. B*, **1999**, 103, 9085;

40. M.H. Huang, B.S. Dunn, H. Soyez, J.I. Zink, *Langmuir*, **1998**, 14, 7331;

41. L. Huang, S. Kawi, K. Hidajat, S.C. Ng, *Microp. Mesop. Mater*., **2006**, 88, 245;

42. G.S. Attard, P.N. Bartlett, N.R.B. Coleman, J.M. Elliot, J.R. Owen, J.H. Wang, *Science*, **1997**, 278, 838;

43. J.M. Elliot, G.S. Attard, P.N. Bartlett, N.R.B. Coleman, *Chem. Mater*., **1999**, 11, 3602;

44. D. Grosso, A.R. Balkenende, P.A. Albouy, M. Lavergne, F. Babonneau, *J. Mater. Chem*., **2000**, 10, 2085;

45. D. Kundu, H.S. Zhou, I. Honma, *J. Mater. Sci. Lett*., **1998**, 17, 2089;

46. F. Schuth, *Chem. Mater*., **2001**, 13, 3184;

47. E.L. Crepaldi, G.J.A.A. Soler-Illia, A. Bouchara, D. Grosso, D. Durand, C. Sanchez, *Angew. Chem*., **2002**, 3, 347;

48. D. Grosso, G.J.A.A. Soler-Illia, E.L. Crepaldi, F. Cagnol. C. Sinturel, A. Bourgeois, A. Brunet-Bruneau, H. Amenitsch, P.A. Albouy, C. Sanchez, *Chem. Mater*., **2003**, 24, 4562 ;

49. Z.L. Hua, J.L. Shi, L. Wang, W.H. Zhang, *J. Non-Cryst. Solids*, **2001**, 292, 177;

50. T. Clark, J.D. Ruiz, H. Fan, C.J. Brinker, B.I. Swanson, A.N. Parikn, *Chem. Mater*., **2000**, 12, 3871;

51. S. Baskaran, J. Liu, K. Domansky, N. Koheler, X. Li, C. Coye, G. E. Fryxell, S. Thevuthasan and R. E.Williford, *Adv. Mater.,* **2000**, 12, 291;

52**.** S. Seraji, Y. Wu, M. Forbess, S. J. Limmer, T. Chou and G. Cao, *Adv. Mater*., **2000**,12, 1695;

53**.** J. S. Beck, J. C. Vartuli, W. J. Roth, M. E. Leonowicz, C. T. Kresge, K. D. Schmitt, C. W. Chu, D. H. Olson, E. W. Sheppard, S. B. McCullen, J. B. Higgins and J. L. Schlenker, *J. Am Chem. Soc.,* **1992**, 114, 10834;

54. G. Wirnsberger, P. Yang, B.J. Scott, B.F Chmelka and G. Stucky, *Spectrochim. Acta A*, **2001**, 57, 2049;

55. F.K. de Theijle, A.R. Balkenende, M.A. Verheijen, M.R. Balkanov, K.P. Mogilnikov and Y. Furukawa, *J. Phys. Chem B*, **2003**, 107, 4280 ;

56. G. Wirnsberger, P. Yang, H.C. Huang, B. Scott, T. Deng, G.M. Whitesides, B.F. Chmelka, G. D. Stucky, *J. Phys. Chem. B*, **2001,** 105, 6307;

57. Y.F.Lu, H.Y. Fan, N. Doke, D.A. Loy, R.A. Assink, D.A. LaVan, C.J. Brinker, *J. Am. Chem. Soc.*, **2000**, 122, 5258;

58. K. Domansky, J. Liu, L.Q. Wang, M.H. Engelhard, S. Baskaran, *J. Mater. Res.*, **2001**, 16, 2810;

59. F.K. de Theije, A.R. Balkenende, P.A. Albouy, H. Amenitsch, M.N. Rager, F. Babonneau, *J. Sol-Gel Sci. Technol.*, **2003**, 26, 587;

60. J.I. Jung, J.Y. Bae, B.S. Bae, *J. Mater. Chem.*, **2004**, 14, 1988;

61. P. Innocenzi, P. Falcaro, S. Schergna, M. Maggini, E. Menna, H. Amenitsch, I.J.A.A. Soler-Illia, D. Grosso, C. Sanchez, *J. Mater. Chem.*, **2004**, 14, 1838;

62. B. Lebeau, C.E. Fowler, S.R. Hall, S. Mann, *J. Mater. Chem.*, **1999**, 9, 2279;

63. P.N. Minoofar, B.S. Dunn, J.I. Zink, *J. Am. Chem. Soc.*, **2005**, 127, 2656;

64. H.Y. Fan, Y.F. Lu, A. Stump, S.T. Reed, T. Baer, R. Schunk, L.V. Perez, G.P. Lopez, C.J. Brinker, *Nature*, **2000**, 405, 56;

65. G. Wirnsberger, B.J. Scott, G.D. Stucky, *Chem. Commun.*, **2001**, 119;

66. H. Fan, S. Reed, T. Baer, R. Schunk, G.P. Lopez, C.G. Brinker, *Microp. Mesop. Mater.*, **2001**, 44, 625;

67. A. Cabot, J. Arbiol, A. Cornet, J. R. Morante, F. Chen and M. Liu, *Thin Solid Films*, **2003**, 463, 64;

68. G. Xomeritakis, S. Naik, C. M. Braunbarth, C. J. Cornelius, R. Pardey and C. J. Brinker, *J. Membrane Sci.*, **2003**, 215, 225;

69. G. Wirnsberger, Scott B.J., Stucky G.D., *Chem. Commun.*, **2001**, 119;

70. W. Cheng, E.Baudrin, B.Dunn, J.I. Zink, *J. Mater. Chem.,* **2001**, 11, 92;

71. P. Innocenzi, A. Martucci, M. Guglielmi, A. Verzotti, E. Traversa, *Sens. Actuators B*, **2001**, 76, 299;

72. K. Domansky, J. Liu, L. Wang, Engelhard, S. Baskaran, *J. Mater. Res.,* **2001**, 16, 2810;

73. O. Dag, G.A. Ozin, H. Yang, C. Reber, G. Bussiere, *Adv. Mater.,***1999**, 11, 474;

74. S. Yu, T. Wong, K. Pita, X. Hu, *Microelectron. Nanometer Struct..*, **2002**, 20, 2046;

75. S. Yu, T. Wong, K. Pita, X. Hu, **,** *J. Appl. Phys.*, **2002**, 92, 3338;

76. C. Sanchez, B. Lebeau, F. Chaput, J.P. Boilot, *Adv. Mater.*, **2003**, 15, 1969;

77. A. Soler-Illia, C. Sanchez, B. Lebeau, J. Patarin, *Chem. Rev.,* **2002**, 102, 4093;

78. R.D. Miller, *Science*, **1999**, 421, 286;

79. P.N. Minoofar, B.S. Dunn, J.I. Zink, *J. Am. Chem. Soc*., **2005**, 127, 2656;

80. W. Cheng, E. Baudrin, B. Dunn, J.I. Zink, *J. Mater. Chem.,* **2001**, 11, 92;

81. C.J. Brinker, G.W. Scherer, *Sol-Gel Science, Academic Press*, 1990;

82. P.E. Burrows, Z. Shen, V. Bulovic, D.M. McCarty, S.R. Forrest, J.A. Cronin, M.E.Thompson, *J.Appl.Phys*., **1996,** *79*, 7991;

83. W. Stampor, J. Kalinowski, G. Marconi, P. Di Marco, V. Fattori and G. Giro, *Chem.Phys. Lett.,* **1998,** 183, 373;

84. R. Treush, F.J. Himpsel, S. Kakar, L.J. Terminello, C. Heske, T. Van Buuren, V.V. Dinh, H.W.Lee, K. Pakbaz, G. Fox, I. Jimenez, *J.Appl. Phys.,* **1999***, 86, 88;

85. B.J. Chen, W.Y. Lai, Z.Q. Gao, C. S. Lee, S.T. Lee, W.A. Gambling, , *Appl. Phys. Lett.*, **1999**, *75*, 4010;

86. Tang S.W., *Appl. Phys. Lett*., **1987**, 51, 913;

87. Caria S., Murgia M., Zamboni R., Melpignano P., Biondo V., *Appl. Phys. Lett.*, in press;

88. M. Klotz, P.A. Albouy, A. Ayral, C. Menager, D. Grosso, A. Van der Lee, V. Cabuil, F. Babonneau, C. Guizard, *Chem. Mater*., **2000**, 12, 1721;

89. K. Yu, X. Wu, C.J. Brinker, J. Ripmeester, *Langmuir*, **2003**, 19, 7282;

90. C. Renard, C. Ricolleau, E. Fort, S. Besson, T. Gacoin, J.P. Boilot, *Appl. Phys. Lett*., **2002**, 80, 300;

91. S. Besson, T. Gacoin, C. Jacquiod, C. Ricolleau, F. Babonneau, J.P. Boilot, *J. Mater. Chem*., **2000**, 10, 1331;

92. S. Besson, C. Ricolleau, T. Gacoin, C. Jacquiod, J.P. Boilot, *J. Phys. Chem. B*, **2000**, 104, 12095;

93. P. Falcaro, S. Costacurta, G. Mattei, H. Amenitsch, A. Marcelli, M.C. Guidi, M. Piccinini, A. Nucara, L. Malfatti, T. Kidchob, P. Innocenzi, *J. Am. Chem. Soc.*, **2005**, 127, 3838;

94. http://www.ncnr.nist.gov/programs/crystallography/software/cmpr/

95. S.J. Gregg, K.S.W. Sing, Adsorption, surface area and porosity, 2nd ed., Academic Press; New York, 1982;

96. F. Rouquerol, J. Rouquerol, K. Sing, *Adsorption by Powders and Porous Solids*; Academic Press; New York, **1999**;

97. E.P. Barett, L.G. Joyner, P.P. Halenda, *J. Am. Chem. Soc*., **1951**, 73, 373;

98. J. Broekhoff, J.H. De Boer, *J. Catal*., **1967**, 9, 8;

99. J. Broekhoff, J.H. De Boer, *J. Catal*., **1969**, 10, 368;

100. A. Galarneau, D. Desplantier, R. Dutartre, F. Di Renzo, *Microp. Mesop. Mater*., **1999**, 27, 297;

101. F. Abeles, *Opt. Acta*, **1957**, 4, 42;

102. M.C. Fuertes, F.J. Lopez-Alcaraz, M.C. Marchi, H.E. Troiani, V. Luca, H. Miguez, G.J.A.A. Soler-Illia, *Adv. Funct. Mater*., **2007**, 37, 575;

103. M.C. Fuertes, S. Colodrero, G. Lozano, A. Rodriguez, D. Grosso, C. Boissiere, C. Sanchez, G.J.A.A. Soler-Illia, H. Miguez, *J. Phys. Chem. C*, **2008**, submitted;

104. P.C. Angelome, L. Andrini, M.E. Calvo, F.G. Requejo, S.A. Bilmes, G.J.A.A. Soler-Illia, *J. Phys. Chem. B*, **2007**, 111, 10886;

REFERENCES TAB.1-2

37. B.A. McCool, N. Hill, J. DiCarlo, W.J. DeSisto, *J. Membr. Sci*., **2003**, 218, 55;

38. D. Zhao, P. Yang, N. Melosh, J. Feng, B.F. Chmelka, G.D. Stucky, *Adv. Mater*., **1998**, 10, 1380;

39. D. Grosso, A.R. Balkenende, P.A. Albouy, A. Ayral, H. Amenitsch, F. Babonneau, *Chem. Mater*., **2001**, 13, 1848 ;

40. D. Grosso, G.J. Soler-Illia, F. Babonneau, C. Sanchez, P. Albouy, A. Brunet-Bruneau, A.R. Balkenende, *Adv. Mater*., **2001**, 13, 1085;

41. W. Cheng, E. Baudrin, B. Dunn, J.I. Zink, *J. Mater. Chem*., **2001**, 11, 92;

42. B. Lebeau, C.E. Fowler, S.R. Hall, S. Mann, *J. Mater. Chem*., **1999**, 9, 2279;

43. E.L. Crepaldi, G.J. Soler-Illia, D. Grosso, P. Albouy, C. Sanchez, *Chem. Commun*., **2001**, 1582;

44. L. Pidol, D. Grosso, G.J. Soler-Illia, E.L. Crepaldi, C. Sanchez, P.A. Albouy, H. Anenitsch, P. Euzen, , *J. Mater. Chem*., **2002**, 12, 557;

45. Z. Hua, J. Shi, L. Wang, W. Zhang, *J. Non-Cryst. Solids*, **2001**, 292, 177 ;

46. M.T. Anderson, J.E. Martin, J.G. Odinek, P. Newcomer, *Mater. Res. Symp. Proc*., **1996**, 431, 217;

47. D. Grosso, A.R. Balkenende, P.A. Albouy, F. Babonneau, *Stud. Surf. Sci. Catal.*, **2000**, 129, 673;

48. T. Clark Jr., J.D. Ruiz, H. Fan, C.J. Brinker, B.I. Swanson, A.N.Parikh, *Chem. Mater.*, **2000**, 12, 3879;

49. D. Grosso, P.A. Albouy, H. Amenitsch, A.R. Balkenende, F. Babonneau, *Mater. Res. Soc. Symp. Proc.*, **2002**, 628, CC6.17.1–CC6.17.6 ;

50. Y. Goto, N. Sugimoto, Y. Fukushima, Y. Imada, Y. Kubota, Y. Sugi, *Mater. Res. Soc. Symp. Proc.*, **2000**, 581, 423 ;

51. H. Fan, Y. Lu, R.A. Assink, G.P. Lopez, C.J. Brinker, *Mater. Res. Soc. Symp. Proc.*, **2000**, 628, CC6.41.1–CC6.41.7 ;

52. M. Klotz, A. Ayral, C. Guizard, L. Cot, *Sep. Purif. Technol.*, **2001**, 25, 71 ;

53. D. Zhao, P. Yang, D.I. Margolese, B.F. Chmelka, G.D. Stucky, *Chem. Commun.*, **1998**, 2500;

54. M. Klotz, P. Albouy, A. Ayral, C. Menager, D. Grosso, A. Lee, V. Cabuil, F. Babonneau, C. Guizard, *Chem. Mater.,* **2000**, 12, 1721 ;

55. Y. Lu, R. Ganguli, C.A. Drewien, M.T. Anderson, C.J. Brinker, W. Gong, Y. Guo, H. Soyez, B. Dunn, M.H. Huang, J.I. Zink, *Nature,* **1997**, 389, 364;

65. M. Ogawa, H. Ishikawa, T. Kikuchi, *J. Mater. Chem.*, **1998**, 8, 1783;

66. H. Miyata, K. Kuroda, *Chem. Mater.*, **1999**, 11, 1609 ;

67. S. Besson, T. Gacoin, C. Jacquiod, C. Ricolleau, D. Babonneau, J.P. Boilot, *J. Mater. Chem.*, **2000**, 10, 1331;

68. S. Besson, C. Ricolleau, T. Gacoin, C. Jacquiod, J.P. Boilot, *J. Phys. Chem. B*, **2000**, 104, 12095.

69. H. Yun, K. Miyazawa, H. Zhou, I. Honma, M. Kuwabara, *Adv. Mater.*, **2001**, 13, 18;

70. J.M. Gomez-Vega, M. Iyoshi, K.Y. Kim, A. Hozumi, H. Sugimura, O. Takai, *Thin Solid Films*, **2001**, 615, 398;

70 V.V. Guliants, *Journal of Membrane Science,* **2004**, 235, 53;

71. M.M. Yusuf, H. Imai, H. Hirashima*, J. Sol–Gel Sci. Technol.*, **2002**, 25, 65;

72. H. Fan, H.R. Bentley, K.R. Kathan, P. Clem, Y. Lu, C.J. Brinker, J. *Non-Cryst. Solids*, **2001**, 285, 79;

73. H. Zhou, I. Honma, *Jpn. J. Appl. Phys.*, **1999**,38, L958;

74. C. Song, G. Villemure*, Microporous Mesoporous Mater*., **2001**, 679, 44 ;

75. T. Yamada, H. Zhou, H. Uchida, M. Tomita, Y. Ueno, T. Ichino, I. Honma, K. Asai, T. Katsube, *Adv. Mater*., **2002**, 14, 812;

76. E. Ozkan, S. Lee, P. Liu, C.E. Tracy, F.Z. Tepehan, J.R. Pitts, S.K. Deb, *Solid State Ionics* , **2000**, 149, 139;

77. T. Yamada, K. Asai, A. Endo, H.S. Zhou, I. Honma, *J. Mater. Sci. Lett*., **2000**, 19, 2167;

78 T. Yamada, K. Asai, A. Endo, H.S. Zhou, I. Honma, *Stud. Surf. Sci. Catal.*, **2001**, 132, 631;

79. J.M. Berquier, L. Teysseedre, C. Jacquiod, *J. Sol–Gel Sci. Technol.* , **1998**, 13, 739;

80. D. Kunda, H.S. Zhou, I. Honma, *J. Mater. Sci. Lett*., **1998**, 17, 2089;

81. I. Honma, A. Endo, D. Kunda, H.S., *ZhouMater. Res. Soc. Symp. Proc.*, **1999**, 576, 235;

82. H.M. Yusuf, H. Imai, H. Hirashima, *J. Non-Cryst. Solids*, **2001**, 285, 90;

83. M. Ogawa, N. Masukara, *Microporous Mesoporous Mater*., **2000**, 38, 35.

CHAPTER V

NON-SILICA MESOSTRUCTURED MATERIALS

5.1 INTRODUCTION

Short after the discovery of periodically organized mesoporous silica, a number of efforts were devoted to extending the mesoporous family to non-silicate materials. These systems concern mainly oxides or phosphates of transition metals (TM), aluminum, tin, etc. interesting because of their varied framework properties, which should permit development of a plethora of applications, particularly in catalysis, photo catalysis, sensors, optics, separation techniques, smart coatings, etc. However, the reported work on transition metal mesostructured materials is ≈ 1 order of magnitude lower than its silica counterpart. Several main reasons can account for the slower advancement in this field:

1) The pioneer groups in mesoporous materials have a scientific background related to zeolites; therefore, they are mainly familiar with silicon and aluminum chemistry.

(2) The high reactivity toward hydrolysis and condensation of transition metal oxide precursors increases the extent of uncontrolled phase separation between organic and inorganic components, yielding non-mesostructured materials, but porous gels.

(3) The redox reactions, the possible phase transitions, and the crystallization processes are often accompanied by the collapse of the structural integrity.

(4) Synthesis procedures are extremely sensitive to many external parameters, leading in some cases to irreproducible results.

Therefore, most reviews covering overall synthesis and characterization of porous and mesoporous materials are mainly focused on silica- and alumina-based systems; however, recent reviews cover specifically non-silica systems [1-4].

The first studies concerning non-silica mesostructured materials have been presented by researchers of the University of Santa Barbara [5-8]. A great variety of oxide-based hybrids containing surfactant templates and metal cations have been synthesized in the form of powders or "bulk gels": non-silica main block (Al [9-11], Ga [12], Sn [13,14], Sb, Pb), transition metals (Ti [15-18], V [19-23], Fe [24,25], Mn [26,27], Zr [28-32], Hf [33], Nb [34,35], W [36]), Y[37] and rare earths [38]. Some methods can even be generalized for more than one metal cation

[39,40] or mixed oxides [40,41]. Production of organized films is also possible for Al [41,43], Ti [44,47], Zr [48], V [49] e W [50]. The films present the paramount advantage to be directly shaped in any substrate for a targeted application. The pioneering and/or relevant publications between 1994 and 2001 for each system are summarized in **Tab.1**, including the nature of the precursors (molecular species, clusters, nanoparticles), surfactants, synthesis conditions, nature of the obtained phases, post-treatment, specific surface, and pore diameter.

Fig.1 displays selected TEM micrographs of non-silica mesostructured and mesoporous materials (powders or films), obtained by different pathways: precipitation or solvent evaporation. Generally, hexagonal or wormlike mesophases are obtained, cubic symmetry being less. Metallic (TM, Al, Sn) alkoxide precursors are more reactive toward hydrolysis and condensation than Si alkoxides. Because of this high reactivity, inorganic polymerization has to be partially blocked. In some cases, clusters or nanoparticles may result, which aggregate upon drying. Thermal treatment of these randomly ordered aggregates can lead to textural mesoporosity, even if the overall solid presents little or no order at the mesoscopic scale. The mesostructure quality and the extension of the organized domains are often lower for TM than for silica-based systems. The obtained structures are often unstable toward template removal.

5.2 CONTROL OF THE FORMATION OF THE INORGANIC NETWORK

Inorganic hydrolysis and condensation have to be mastered to avoid the instantaneous formation of an inorganic network, which would irreversibly "freeze" an ill-organized structure. The reactivity of the precursors can be efficiently controlled by different means [51]: by carefully adjusting the pH and dilution of metal salt solutions; by using alkoxides or other salts in the presence of condensation inhibitors (acids, complexing agents); by working in non-aqueous solvents and limited quantities of water; by modifying the redox state, or by using preformed nano-objects.
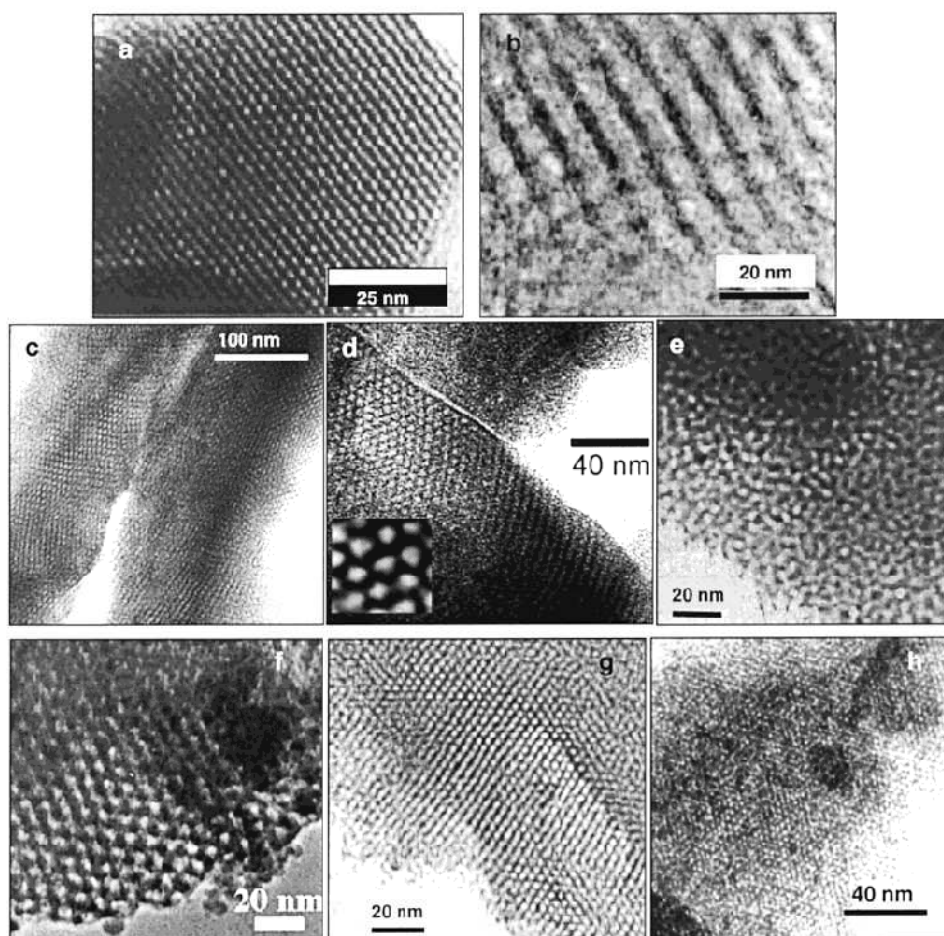
Fig.1: Bright field TEM images.

5.3 MINERAL PRECURSORS

The earliest approach, an extension of the methods applied for mesostructured silica, consisted in the dissolution of mineral salts in aqueous solutions containing surfactants (carrying ammonium, sulfate, or phosphate heads), in conditions of controlled pH. The use of these ionic templates produces mostly lamellar hybrid mesophases.

Highly charged metals [W, Sb(V)] known to yield polyoxometalates (POM) are capable of forming hexagonal or cubic meso-organized phases. The hybrid phases stemming from acidic aqueous solutions present a relatively low stability to thermal treatment, due to incomplete condensation of the inorganic network because of the low initial pH values. Detailed structural and in-situ characterization shows that the immediately formed mesostructured hybrids are

composed of an incompletely condensed inorganic framework that can evolve upon aging [52,53].

5.4 INHIBITION OF THE HYDROLYSIS-CONDENSATION PROCESS

There are two extensively used methods to control the hydrolysis and condensation processes of reactive alkoxides or chloroalkoxides, which usually lead to immediate precipitation: (1) Complexation of the metal centers (by means of phosphate, carboxylic acids, polyethanolamines, polyols, amines, etc.), which led to mesoporous TiO_2 can be directly performed by the polar head of the surfactant. 2) Mineral acids are added in an important H^+/M ratio.

5.5 NON-AQUEOUS SOLVENTS AND CONTROLLED WATER CONTENTS

To avoid massive precipitation of no structured phases is to conduct the synthesis in non aqueous media, in the absence of water, or low h values. A classical example is the first synthesis of mesostructured alumina phases, developed by Bagshaw and Pinnavaia, using nonionic surfactants as templates, in alcohol/water mixtures. The presence of low water quantities ($h \approx 1$-2) will have decisive effects, not only in the kinetics of the formation of the mineral phase but also in the chemical compatibility at the hybrid interface.

5.6 ORGANIZATION OF PREFORMED NANO-OBJECTS: ASSEMBLY OF NANOBUILDING BLOCKS

The assembly of mineral species of a given nature (clusters, aggregates, or nanocrystalline particles) permits other features, such as the reactivity of the inorganic precursors ("bricks") or the conservation of a pre-existent geometry, to be tailored. These can form an extended network, acting either as preformed nanobuilding blocks (NBB), which can be assembled around a hybrid interface, or as a mineral source, via dissolution- recondensation processes, according to their reactivity and the physical-chemical features of the reacting systems.

5.7 FORMATION MECHANISMS

Four types of mechanisms have been proposed in the literature, based on crossing different spectroscopic characterization techniques, such as NMR, fluorescence, RPE, or UV-vis

absorption: charge matching (CM), ligand-assisted templating (LAT), ion exchange/scaffolding, and modulation of the hybrid interface (MHI). The Charge Matching, based on the cooperative formation of LC hybrids, involves an extension could be made to non-silica materials. Subsequently, the cooperative organization in solution of anionic mineral species and cationic surfactants has been proposed to explain the formation processes of mesophases based on W or Sb. These assembly mechanisms rely on the cooperative association between surfactant molecules and mineral oligomers in solution. At moderate (ambient) temperatures, hybrid LC phases are formed (**Fig.2**).

The Ligand Assisted Templating mechanism is based on the formation of chemical coordination bonds between the template and the precursor inorganic species from the first stages of the synthesis path. This chemical bond is a Lewis acid-base reaction between the amine head of the template and the metallic center. The Ion Exchange followed by scaffolding has been proposed to explain the formation of mesostructured zirconia in alkaline conditions, in the presence of alkylammonium templates. The first stage involves the exchange of ammonium ions present in the precursor zirconium hydrated gel by alkylammonium species. The latter are adsorbed on the mineral surface, decreasing surface tension of the solution and minimizing gel deterioration upon solvent removal. The surface tension at the pore interface is decreased independently of the network organization; therefore, the surface area and the pore size of the dried and calcined materials are only proportional to the chain length.

The Modulation of the Hybrid Interface has been proposed to explain the different mesostructured TiO_2-based hybrid materials that can be obtained by hydrolysis-condensation of titanium alkoxides, in the presence of neutral PEO based surfactants. The model is focused on the competition between the hydrophobic/ hydrophilic character of the inorganic precursor and the template and the complexing power of the latter.

5.8 STABILITY OF THE INORGANIC NETWORK

An essential issue in the performance of non-silica mesoporous materials is the stability of the inorganic network. Most synthesis methods being based on avoiding fast and extended condensation, subsequent chemical, mild thermal, or hydrothermal processing is often needed to favor extended condensation.

This post-processing helps to consolidate the mineral walls. Template removal to obtain a porous oxide remains a fundamental issue, in view of promising applications. In principle, pore space can be liberated by thermal treatment or repeated washing, as in silica systems. In the case of non-silica systems, an irreversible deterioration of the mesostructure is often associated with template elimination.

However, high specific surface areas can be obtained, depending on the nature of the metal and the synthesis protocol. Unfortunately, most of these oxides cannot support temperatures >500 °C, which is a serious limitation for most catalysis applications.
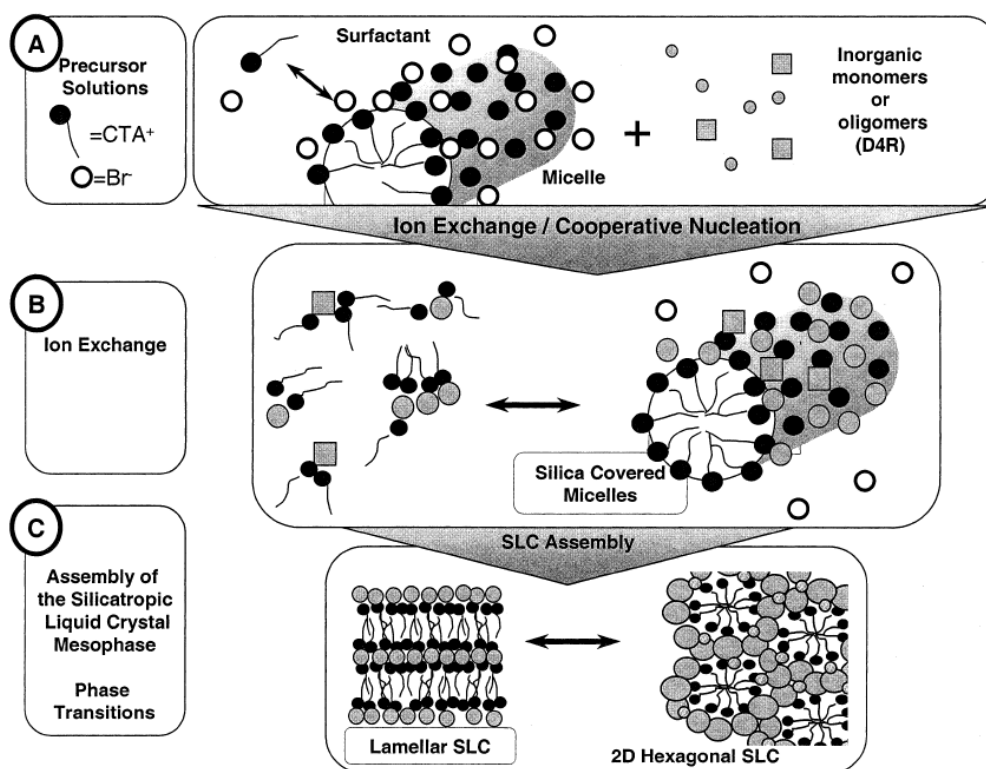
Fig.2: Schematic representation of cooperative mechanism.

The destruction of the mesoporous framework can be due to different reasons: the presence of an insufficiently condensed inorganic network, which bears residual stress or microporosity, modifications of the valence state via redox reactions, or crystallization of an inorganic phase.

However, aging the as-prepared hybrid phases in mild hydrothermal conditions permits a better consolidation of the inorganic walls. A gradual and rational thermal treatment, composed of consecutive stages, separates the different decomposition steps of the template (control of temperature ramps, atmosphere). A selective washing of the template can be done before thermal treatment.

REFERENCES

1. M. Tiemann,; Fro¨ba, M. *Chem. Mater*. **2001**, 13, 3211;

2. P. Behrens, *Angew. Chem., Int. Ed*. **1996**, 35, 515;

3. A. Sayari, Liu, P. *Microporous Mater.* **1997**, 12, 149;

4. F. Schuth, *Chem. Mater*. **2001**, 13, 3184;

5. Q. Huo, D. I. Margolese, U. Ciesla, D. K. Demuth, P. Feng, T. E. Gier, P. Sieger, A. Firouzi, B. F. Chmelka, F. Schuth, G. D. Stucky, *Chem. Mater*. **1994**, 6, 1176;

6. Q. Huo, D. I. Margolese, U.Ciesla, P. Feng, T. E. Gier, P.Sieger, R.Leon, P. M. Petroff, F.Schuth, G. D. Stucky, *Nature* **1994**, 368, 317;

7. U.Ciesla, Demuth, D.; Leon, R.; Petroff, P.; Stucky, G. D.; Unger, K. K.; Schuth, F. *Chem. Commun*. **1994**, 1387;

8. U. Ciesla, S. Schacht, G.D. Stucky, K.K. Unger, F. Schuth, *Angew. Chem., Int. Ed*. **1996**, 35, 541;

9. S. A. Bagshaw, E. Prouzet, T. J. Pinnavaia, *Science* **1995**, 269, 1242;

10. S. A. Bagshaw, T. J. Pinnavaia, *Angew. Chem., Int. Ed.* **1996**, 35, 1102;

11. F. Vaudry, S. Khodabandeh, M. E. Davis, *Chem. Mater*. **1996**, 8, 1451;

12. M. Yada, H. Takenaka, M. Machida, T. Kijima, *J. Chem. Soc., Dalton Trans.* **1998**, 1547;

13. T. Abe, A. Taguchi, M. Iwamoto, *Chem. Mater.* **1995**, 7, 1429;

14. V. Luca, D. J. MacLachlan, J. M. Hook Withers, R. *Chem. Mater.* **1995**, 7, 2220;

15. D. M. Antonelli, J. Y. Ying, *Angew. Chem., Int. Ed*. **1995**, 34, 2014;

16. M. Froba, O. Muth, A. Reller, *Solid State Ionics* **1997**, 101, 249;

17. R. L. Putnam, N. Nakagawa, K. M. McGrath, N. Yao, I. A. Aksay, S. M. Gruner, A. Navrotsky, *Chem. Mater.* **1997**, 9, 2690;

18. D. Khushalani, O. Dag, G. A. Ozin, A. Kuperman, *J. Mater. Chem.* **1999**, 9, 1500;

19. T. Abe, A. Taguchi, M. Iwamoto, *Chem. Mater.* **1995**, 7, 1429;

20. T. Doi, T. Miyake, *J. Chem. Soc., Chem. Commun.* **1996**, 1635;

21. P. Liu, I. Moudrakovski, J. Liu, Sayari, A. *Chem. Mater.* **1997**, 9, 513;

22. J. El Haskouri, Roca, M.; Cabrera, S.; Alamo, J.; Beltra´n-Porter, A.; Beltra´n-Porter, D.; Marcos, M. D.; Amoro´s, P. *Chem. Mater.* **1999**, 11, 1446;

23. N. Mizuno, Hatayama, H.; Uchida, S.; Aguchi, T. *Chem. Mater.* **2001**, 13, 179;

24. L. Michot, Mathieu, C.; Bouquet, E. *C. R. Acad. Sci. Paris, Ser. II C* **1998**, 167;

25. X. Guo, Ding, W.; Wang, X.; Yan, Q. *Chem. Commun.* **2001**, 709;

26. S. L. Suib, *Science* **1997**, 276, 926;

27. J. Luo Suib, S. L. *Chem. Commun.* **1997**, 1031;

28. (a) M. J. Hudson, Knowles, J. A. *Chem. Commun.* **1995**, 1083. (b) Hudson, M. J.; Knowles, J. A. *J. Mater. Chem.* **1996**, 6, 89;

29. A. Y. Kim, Bruinsma, P. J.; Chen, Y. L.; Liu, J. *Mater. Res. Symp. Proc.* **1996**, 435, 131;

30. Huang, Y. Y.; McCarthy, T. J.; Sachtler, W. M. H. *Appl. Catal. A* **1996**, 148, 135;

31. (a) Pacheco, G.; Zhao, E.; Garcı´a, A.; Sklyarov, A.; Fripiat, J. J. *Chem. Commun.* **1997**, 491; (b) Pacheco, G.; Zhao, E.; Garcı´a, A.; Sklyarov, A.; Fripiat, J. J. *J. Mater. Chem.* **1998**, 8, 219; (c) Zhao, E.; Herna´ndez, O.; Pacheco, G.; Hardcastle, S.; Fripiat, J. J. *J. Mater. Chem.* **1998**, 8, 1635;

32. M. S. Wong, Ying, J. Y. *Chem. Mater.* **1998**, 10, 2067;

33. P. Liu, Liu, J.; Sayari, A. *Chem. Commun.* **1997**, 577;

34. D. M. Antonelli, Ying, J. Y. *Chem. Mater.* **1996**, 8, 874;

35. Antonelli, D. M.; Ying, J. Y. *Angew. Chem., Int. Ed.* **1996**, 35, 426;

36. A. Stein, Fendorf, M.; Jarvie, T. P.; Mueller, K. T.; Benesi, A. J.; Mallouk, T. E. *Chem. Mater.* **1995**, 7, 304;

37. M. Mamak, Coombs, N.; Ozin, G. A. *Adv. Mater.* **2000**, 12, 198;

38. Yada, M.; Kitamura, H.; Ichinose, A.; Machida, M.; Kijima, T. *Angew. Chem., Int. Ed.* **1999**, 38, 3506;

39. Cabrera, S.; El-Haskouri, J.; Guillem, C.; Latorre, J.; Beltra´n- Porter, A.; Beltra´n-Porter, D.; Marcos, M. D.; Amoro´s, P. *Solid State Sci.* **2000**, 2, 405;

40. Yang, P.; Zhao, D.; Margolese, D. I.; Chmelka, B. F.; Stucky, G. D. *Nature* **1998**, 396, 512;

41. Yang, P.; Zhao, D.; Margolese, D. I.; Chmelka, B. F.; Stucky, G. D. *Chem. Mater.* **1999**, 11, 2813;

42. Kriesel, J. W.; Sander, M. S.; Tilley, T. D. *Adv. Mater.* **2001**, 13, 331;

43. Kriesel, J. W.; Sander, M. S.; Tilley, T. D. *Chem. Mater.* **2001**, 13, 3554;

44. Grosso, D.; Soler-Illia, G. J. A. A.; Babonneau, F.; Sanchez, C.; Albouy, P.-A.; Brunet-Bruneau, A.; Balkenende, A. R. *Adv. Mater.* **2001**, 13, 1085;

45. H. Yun, K. Miyazawa, H. Zhou, I. Honma, M. Kuwabara, *Adv. Mater.* **2001**, 13, 1377;

46. Y. K. Hwang, K.-C. Lee, Y.-U. Kwon, *Chem. Commun.* **2001**, 1738;

47. Alberius-Henning, P.; Frindell, K. L.; Hayward, R. C.; Kramer, E. J.; Stucky, G. D.; Chmelka, B. F. *Chem. Mater.* **2002**, 14, 3284;

48. (a) E. Crepaldi, D. Grosso, G. J. A. A. Soler-Illia, P.- A. Albouy, C. Sanchez, *Chem. Commun.* **2001**, 1582; (b) E. Crepaldi, G. J. A. A. Soler-Illia, A. Bouchara, D. Grosso, D. Durand, C. Sanchez, *Angew. Chem. Int. Ed.,* **2002**;

49. (a) E. Crepaldi, D. Grosso, G. J. A. A. Soler-Illia, P.- A. Albouy, H. Amenitsch, C. Sanchez, *Chem. Mater.,* **2002**, 14, 3316; (b) E. Crepaldi, G. J. A. A. Soler-Illia, D. Grosso, P.- A. Albouy, H. Amenitsch, C. Sanchez, *Stud. Surf. Sci. Catal.,* **2002**, 141,

50. (c) D. Grosso, G. J. A. A. Soler-Illia, E. Crepaldi, C. Sanchez, *Adv. Funct. Mater.* **2002**;

51. J. Livage, M. Henry, C. Sanchez, *Prog. Solid State Chem.,* **1988**, 18, 259;

52. M. Linden, J. Blanchard, S. Schacht, S. Schunk, F. Schuth, *Chem. Mater.,* **1999**, 11, 3002;

53. Ciesla, U.; Fro˙ba, M.; Stucky, G. D.; Schu¨ th, F. *Chem. Mater.* **1999**, 11, 227.

CHAPTER VI

MESOPOROUS HYBRID THIN FILMS

6.1 INTRODUCTION

Hybrid mesoporous materials are becoming an increasing subject of study, due to the possibility to combine inorganic, organic, and even biological functions in a tailored matrix or nanocomposite [1,2,4]. A great number of characteristics, including framework nature (composition, crystalline structure and crystallite size), high surface area, pore dimension, shape, surface, accessibility and pore array symmetry and interconnection can be tailored, and even tuned, in few finely controller synthesis steps. These materials present an increasing interest and potential in several fields in which a large functional interfacial area contained in a robust framework is required (e.g., for selective columns, exchangers, (bio)catalysts, nanocomposites for energy applications, etc.).

Moreover, a void or functionalised pore system is an opportunity to use these nanoconfined spaces as nanoreactors (for the construction of embedded nanoparticles or polymers), and thus creating advanced ordered nanocomposites with perfectly calibrated interfaces. The possibility of processing mesoporous hybrid materials as thin films is especially interesting, for the combined properties of a thoroughly tailored pore system and the inherent features of thin films (i.e., accurate control of thickness, composition, transparency, presence of electrodes, possibility of multilayer stacking etc.) [5]. Moreover, a wide variety of inorganic or hybrid frameworks can be easily obtained, as evaporation-based methods are usually more flexible than precipitation and can be thoroughly studied by in-situ techniques. The control of chemical and processing variables permit the easy creation and reproduction of an amazing collection of functional-pore arrays in which tailored diffusion of substrates is possible. These functions can be activated or modified by using light, current or changing environment. This makes mesoporous hybrid thin films (MHTFs) an exciting prospect for several nanotechnology applications (sensors, actuators, separation and interfacing devices, etc.) [5,6].

The need for mesoporous hybrid thin films (MHTF) has been driven historically by the demand of ultralow k dielectrics and low refractive index materials with a good mechanical stability and a hydrophobic nature. Hydrophobic or closed porosity can be used as a means to design new

materials with ultralow k values, in order to accomplish several very strict requirements to be integrated with the performance specifications by the microelectronics industry. Transparent films containing light-responsive functions can be combined with nonlinear optical chromophores to produce multifunctional photonic devices [7,8].

Several strategies that are already implemented for surfaces, polymers or even mesoporous hybrid powders and permit the precise positioning of functional groups in an accessible cavity should be explored (**Fig.1**). Hybrid mesostructured thin films could be classified into two general classes depending on the nature of the interaction existing between the organic and the inorganic parts. Class I corresponds to hybrid systems in which organic compounds (molecules, oligomers, or low molecular weight organic polymers) are simply embedded in inorganic matrixes. On the contrary, Class II corresponds to hybrid organic-inorganic in which organic and inorganic components were both bonded through stronger covalent or ion-covalent chemical bonds [9].

6.2 DOPED HYBRID MESOPOROUS THIN FILMS (CLASS I)

Examples of doped mesostructured hybrid films (class I), scarce compared to grafted films (class II) are obtained by in situ [10-13], or steady-state [14-17] preparations using fluorescent dyes on local environments provided by as synthesized thin films. These studies are based on specific spectroscopic responses of fluorescent dyes toward polarity, rigidity/microviscosity of their direct environment.

Hydrophobic dyes are incorporated in the hydrophobic part of micelles [10,12,14,16]. These dyes do or do not interact with the polar head groups of surfactant [15,17,18]. The specific localization of dyes in thin films was used to study the energy transfer occurring between two dyes localized in the organic part [15,19-21]. Even if these investigations involved low amount of probes usually, a high loading was reached without dye aggregation and without loss of mesostructure order [14,16]. These studies revealed that the mobility of dyes inside thin films are usually restricted especially when compared to free micelles in solution but increase with temperature [16]. This loss of mobility was assigned to the confined state of micelles in mesostructured thin films. However, it has been demonstrated recently [18,22,23] that a single dye could explore the mesostructure over a wide range in a relatively short time. Another approach to mesostructured

thin films of Class I consists in incorporating dyes molecules in calcined silica/titania mesoporous thin films. These films are synthesized via a simple immersion of films inside dye containing solutions [24,25-28]. To increase the loading and in some extent to limit leaching of the dyes, alumina-silica thin films were also tested [29].
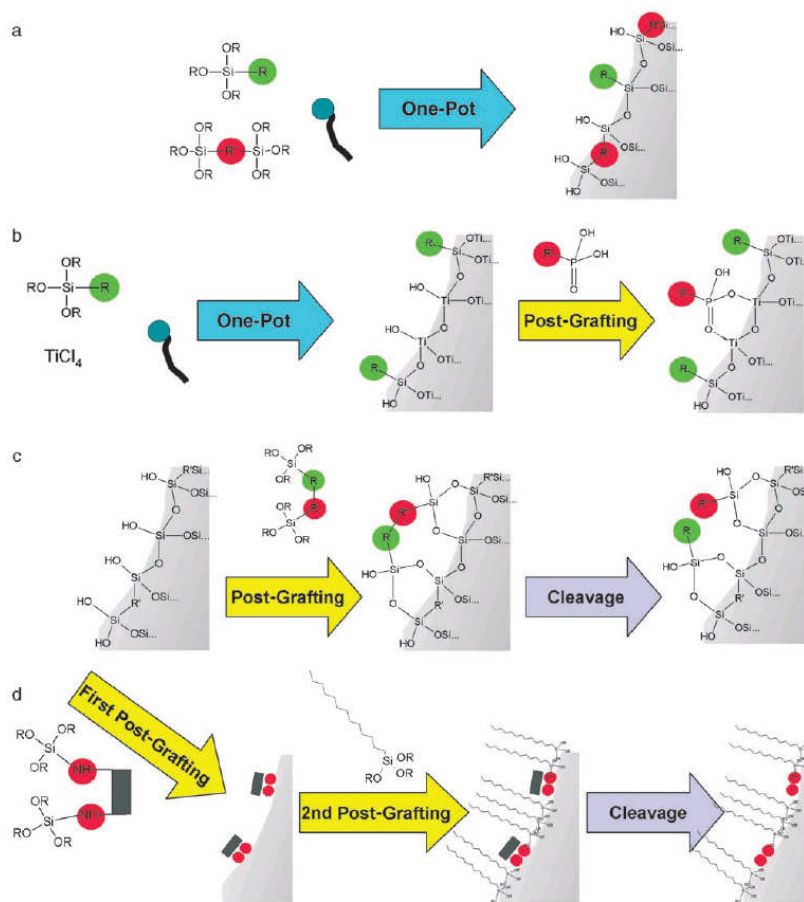
Fig.1: Different strategies to obtain "pore engineering" by location of organic functions inside the walls or the pore surfaces. a) One-pot synthesis by two different organo-alkoxysilanes; b) One-pot synthesis followed to post-grafting on residual surface sites; c) post-grafting of bridge functions, after washing and exposure to new functions; d) post-grafting followed to washing, inducing functional cavities with precise shapes and dimensions.

In addition, the concentration of the dye in thin films was higher than in solutions whatever was the solvent considered and without aggregation. Besides optical properties that mesostructured thin films could exhibit after dyes doping, these materials were successfully used as host matrixes

to elaborate new hybrid nanocomposites. The simplest reaction was the synthesis of rare earth ion complexes in the same time that mesostructuration occurs [30].

They were also used as an efficient template for the synthesis of carbon nanotubes [31-33]. The last way reported consists of a "one-pot" synthesis, that is, all the components of thin films (surfactant, inorganic precursors, solvents, catalysts, monomers) are mixed together in the same starting sol. This "one-pot" procedure has been also used to synthesis hybrid polymer-nanocomposite of Class II.

Despite all the potential applications described above of doped-mesostructured thin films (Class I), the localization of the organic components in the micellar part and/or the opened pores of mesostructured thin films could limit their potential applications mainly due to the high tendency of organic molecule leaching.

6.3 FUNCTIONALIZED HYBRID MESOPOROUS THIN FILMS: CLASS II

6.3.1 INTRODUCTION TO FUNCTIONALIZATION METHODS

Two grafting routes are commonly used to incorporate organic functionalities into MTFs: the "one-pot" synthesis and the post-functionalization. The first one, that is, "one-pot" synthesis, involves a co-condensation step between a functional inorganic precursor, generally an organosilane, with an inorganic in the presence of templates. In this case, the self-assembly process and functionalization take place at the same time.

In the second one, that is, post-functionalization, chemical modifications come off once self-assembly and calcination steps are achieved, via solution impregnation or vapor treatment through chemical bonds with silanol or M-OH groups covering the pore surface. The "one-pot" synthesis [34-39] is largely employed to functionalize silica MTFs, while post-functionalization is used with silica and TMOs matrixes. Despite the fact that post-functionalization has been widely used to modify properties of mesoporous powders, the most frequent route leading to functional MTFs is the "one-pot" synthesis. This approach allows the synthesis of MTFs bearing a large choice of organic functions (**Tab.1**). These functional groups could be chemically inert, such as, for example, alkyl chains [40-44] or aromatic groups [44], but also reactive as aminoalkyl [35, 45,46], or can present intrinsic properties such as silylated dyes [44,45,46] which can serve as sensors or more sophisticated materials as nanovalves [47,48].

The co-condensation route generally leads to a more homogeneous distribution of organic functionalities into mesoporous matrixes with a high control of the stoichiometry. The final materials exhibit a small decrease of the pore sizes and pore volume only.

The influence of organic functions generally limits the organic/metal molar ratio up to ca. 0.20 [49-54]. On the other hand, post-functionalization overcomes some difficulties related to the "one-pot" synthesis. Since mesostructuration process and grafting are two distinct steps, the influence of organic functionalities is seriously restricted.

Moreover, the thermal treatment at high temperature allowed by the absence of organic functionalities favours more stable matrices. However, this method often leads to a quite low loading, an inhomogeneous distribution of the functional groups inside matrixes, a decrease of the pore volume, and even in extreme cases, a complete closure of the pores [55]. Neat surfactant mesophases [56] or as-synthesized silica thin films [57,58] were first coated on a substrate and a subsequent organosilane or hexamethyl disilazene vapor treatment was then applied leading to functionalized MTFs. This subsequent vapor treatment has been also realized on calcined MTFs. Although the vast majority of functionalized mesostructured thin films are obtained via "one-pot" and post-functionalization pathways, combined routes have been investigated. This combined approach can occur when organosilanes are not commercially available.

Instead of synthesizing the desired organosilanes before film synthesis, some authors elaborated hybrid thin films through co-condensation or a post-functionalization procedure with an organosilane bearing a reactive function. After removal of surfactant, the post-modification involving the reactive function anchored into thin films and the organic molecule takes place. This combined approach presents the advantages both to avoid the synthesis of organosilanes and to limit the influence of organosilanes on the mesostructuration process.
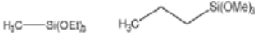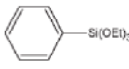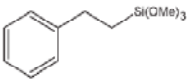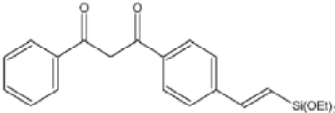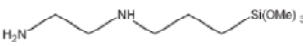
6.3.2 CO-CONDENSATION (ONE-POT SYNTHESIS)

The "one-pot" synthesis has been used to synthesize almost exclusively hybrid silica-based mesostructured thin film via co-condensation of organosilanes with TEOS or TMOS. However, Soler-Illia *et al.* [35,36] reported recently the one-pot synthesis of highly ordered hybrid mesoporous thin films obtained by co-condensation of organotrialkoxysilanes (R-Si(OEt)$_3$ with R= propylamine, propylthiol, and phenyl) with transition metal chloride (MCl$_4$ with M = Zr

or Ti). Such mixed oxide hybrid matrixes allow a further selective functionalization with metal chelating agent leading to bifunctional materials. Bifunctionalization could also be achieved with pure silica matrixes by a one step procedure.

Although the one-pot synthesis presents several advantages compared to post-grafting, this approach is somehow complicated and several difficulties exist in the control of the main parameters related to the EISA process.

Table 1 Functional organosilanes and properties of resultant thin film mesophases

Functional organosilanes	Experimental conditions and results	Properties/applications and references
1) Methyltriethoxysilane,[94,95,106,147] Propyltrimethoxysilane[98]	CTAB, F/TEOS = 0.25; 2D hex, 3D hex, cubic CTAB, F/TEOS = 0.11–0.43; 2D hex PS(35)-*b*-PEO(109); cubic CTAB, F/TEOS = 0.15; 2D hex	—[94,95] Low-*k* dielectric materials[147] —[104] Separation, catalysis, sensing[98]
2) Trimethylethoxysilane	TEOS, CTAB;2D hex post-grafting	Low-*k* dielectric materials[147]
3) Phenyltriethoxysilane	CTAB, F/TEOS = 0.25; 2D hex, 3D hex, cubic CTAB, F/TEOS = 0–0.15; cubic	—[94,95] Separation, catalysis, sensing[98] —[113]
4) (2-Phenylethyl)trimethoxysilane	CTAB F/TEOS = 0–0.02; cubic F/TEOS = 0.02–0.15; 2D hex	Separation, catalysis, sensing[98]
5) Triethoxydibenzoylmethane	CTAB F/TEOS = 0–0.01; cubic F/TEOS = 0.027–0.053; 2D hex F/TEOS > 0.053; lamellar	Heavy metals sensor[90]
6) Aminopropyltrimethoxysilane	Brij-56/CTAB, F/TEOS = 0.039–0.08; cubic CTAB, F/TEOS = 0.15; 2D hex (acidic form) Brij 56, F/TEOS = 0.25; cubic TEOS, CTAB; cubic post-grafting	Coupling of noble metals, dyes, and bioactive molecules[53,124] Separation, catalysis, sensing[98] Receptors for biomolecules[105] Sorption of heavy metals, coupling additional functionality[146] —[113]
7) 3-(2-Aminoethylamino)propyltrimethoxysilane	TEOS, CTAB; cubic post-grafting	Sorption of heavy metals, coupling additional functionality[146]

6.3.2.1 CHEMICAL AND PROCESSING PARAMETERS (EISA PARAMETERS)

The EISA method, which is used in almost all the syntheses of functionalized and mesostructured silica thin films, implies a homogeneous starting sol. However, when the silylated probe is poorly soluble or insoluble in the alcoholic sol, segregation or aggregation can take place. This phenomenon may be due to an insufficient hydrolysis of the organosilane precursor, resulting in hydrophobic species. In some cases, the precursor can be insoluble regardless of the hydrolysis time.

To overcome these problems, a prehydrolysis step of the organosilane in a weak acidic medium and/ or the use of a co-solvent are required. The choice of co-solvents is limited: the co-solvent must not only dissolve the desired organo functional molecule but must also be miscible with the starting sol without causing organo-silane gelation and affecting neither the film optical quality nor the mesostructuration. Moreover, the co-solvent must present evaporation ability close to that of ethanol and ensure a good wettability toward coating substrates.

The presence of organo-silanes could also modify the hydrolysis-condensation rates of silica species. To avoid basic catalysis of silica species, amino groups are first usually neutralized with a strong acid before the addition of the silica precursor. A subsequent treatment of the films with ammonia can allow the recovery of the amino group through deprotonation of the ammonium. An alternative one-pot synthesis is based on a pre-hydrolysis-condensation step of TEOS followed by the addition of organo-silanes just prior the sol deposition.

These conditions limit considerably the condensation of organo-silanes before film deposition. This "delayed" synthesis modifies the main EISA parameters, surfactant/inorganic precursor molar ratio and the relative humidity, within the dip-coater.

6.3.2.2 LOCALIZATION OF GRAFTING COMPOUNDS

The localization of species inside the mesophase has been investigated either directly by spectroscopic techniques such as fluorescence, UV-visible absorption and micro-Raman spectroscopies and/or indirectly by studying structural changes induced by the incorporation of probes (e.g., variation of the lattice parameters, [44,59], phase transition, [44,59,60], formation of mesophase at very low surfactant/TEOS ratio [61]). With regards to mesostructured thin films made with ionic surfactants such as CTAB, the structure can be divided into three main regions

(**Fig.2**): the silica framework, the ionic interface formed by the charged surfactant heads, the hydrosylilated silica surface and the organic region composed by the hydrophobic core of the micelles. This organic/inorganic phase separation is also obtained with nonionic surfactants such as triblock copolymers (PEO-PPO-PEO)-based thin films.

However, in this case, the limits between the three phases, silica wall, hydrophobic PPO block, and hydrophilic PEO block are less defined mainly because of interpenetration of the PEO and silica networks [62].

The silylated functions can be classified into two categories:

1) Monosilylated compounds, F-S-Si(OR)$_3$, constituting the most common category studied (with -OR being condensable groups, F the functionality, and S the spacing group).

2) Multisilylated probes of general formula F(S-Si(OR)$_3$)$_n$, mainly composed of (OR)$_3$Si-F-Si(OR)$_3$ bridged silsesquioxanes and rare earth complexes with silylated organic ligands.

The localization of organosilanes is governed by their physicochemical properties. This structure of the mesostructured thin films (**Fig.2**) was made with (a) ionic surfactants and (b) nonionic surfactants. Several factors have to be taken into account such as the hydrophilic/hydrophobic balance of the organosilane molecule, the number of anchoring functions (-OR)$_3$, the length and the nature of the spacing group (group S between the functionality F and the anchoring function -Si(OR)$_3$), and the nature of the functionality F (hydrophobic, hydrophilic, ionic, polar, apolar, aromatic, etc.). The localization of the functionality F is mainly governed by the "philicity" concept but also by specific interactions such as cation-π [63] or ionic [64]. Generally, the solubilization of lipophilic molecules occurs in the hydrophobic micelle core and the placement of hydrophilic molecules either in the ionic interface or in the framework. The functionality and the spacing group may interact with the silica wall, with the surfactant headgroup and with its hydrocarbon tail, affecting in some cases the curvature of the hybrid interface. Two kinds of sites are available when a molecule is solubilized inside micelles: near the polar head and between alkyl chains in the hydrophobic core of the micelles. The first sites occupied by aromatic compounds are near the polar head of CTAB surfactants due to specific interaction between the π system and the quaternary ammonium.
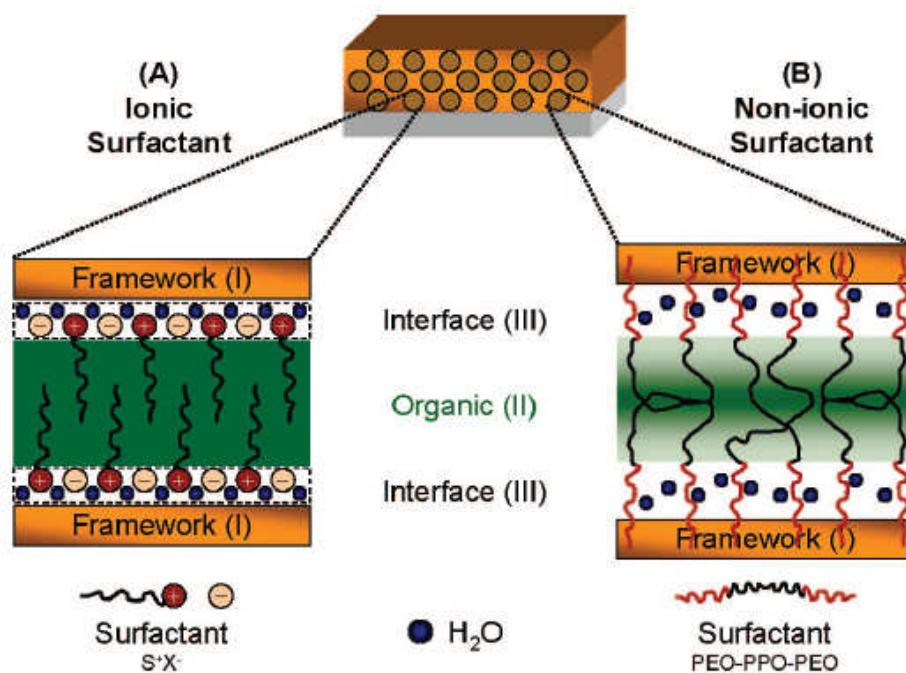
Fig.2: Structure of the mesostructured thin films made with (a) ionic surfactants and (b) nonionic surfactants.

When the first sites are saturated, the solubilization occurs in the hydrophobic part of the micelles, inducing a decrease of the curvature of the micelles and causing a phase transition. However, the length and the nature of the spacing group, S, could hinder the natural placement of hydrophobic functionality inside the micelles.

6.3.2.3 MESOSTRUCTURES MODIFICATIONS

The incorporation of compounds inside thin films can cause structural changes, from variations of the lattice parameters to phase transitions and even allows the formation of a mesophase for a molar ratio surfactant/silica very low leading to an amorphous thin film without organosilanes. All these changes give an indirect proof of the localization of the organosilane inside mesoporous thin films [44,59]. The incorporation of probes could also lead progressively to a destructuration of the mesophase with few changes in the lattice parameters [59-60]. The following sequence was observed: cubic phase (*Pm3n*) < mixture of cubic (*Pm3n*) and 2D-hexagonal (*p6m*) < pure 2D-hexagonal phase < lamellar phase (**Fig.3**).

Such phase transitions are explained in terms of variation in the packing parameter *g*. The increase of the packing parameter can be due to solubilization of large species preferentially in the hydrophobic part of micelles during evaporation of solvents, leading to an increase of the total volume associated to the surfactant chain. This mechanism is supported by the UV-visible experiments performed on hybrid thin films. In this case, the incorporation of large species causes direct phase transitions without modifications of the lattice parameters. This co-solvent effect allows the formation of a mesophase for conditions at which mesostructured thin films are not usually obtained (i.e., very low surfactant on silica ratio).
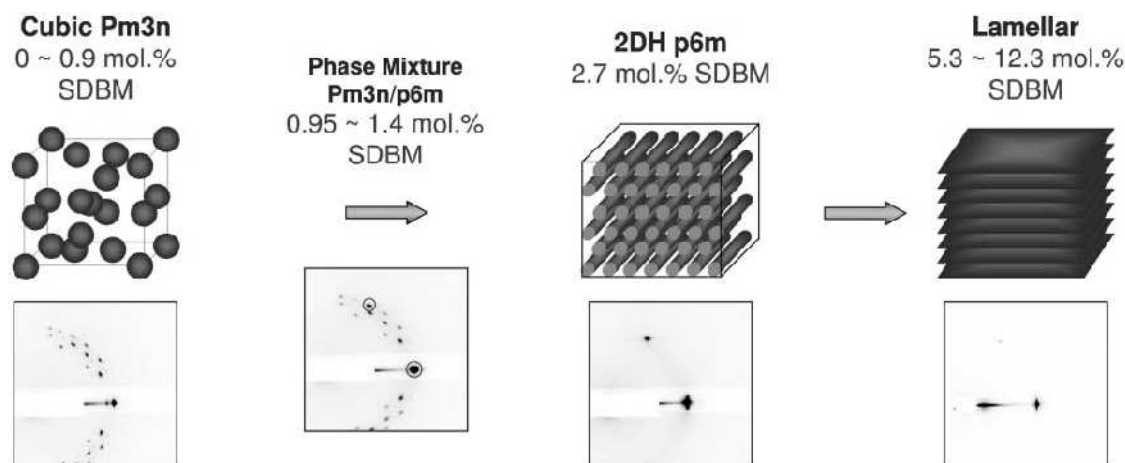
Fig.3: Phase transitions in mesoporous thin film.

6.3.3 POST-FUNCTIONALIZATION ROUTE

The other route leading to hybrid MTFs consists of post-grafting organic functions onto a stabilized inorganic network. Grafting on silica matrixes involves covalent bonds due to condensation reactions with organosilanes species which are also able to react on themselves. The strength of bonds, from ion-covalent to covalent, could influence dramatically the properties of the resulting hybrid matrixes in terms of diffusion, accessibility, and homogeneity.

It appears that two main parameters are of great importance for obtaining a homogeneous distribution of organic functions in MTFs: (i) the accessibility of the porosity (large diffusion of molecules inside the whole film) and (ii) the reactivity of the molecules toward matrixes and among themselves. The diffusion properties essentially depend on the mesophase (two
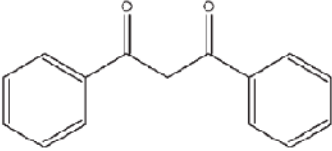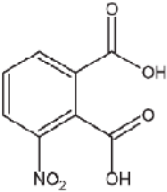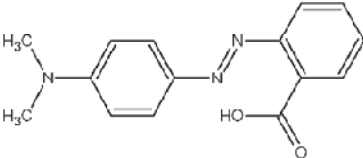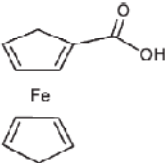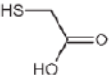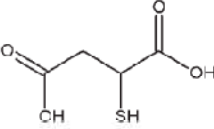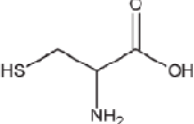
dimensional or three-dimensional), the pore interconnection (presence of restrictions or no interconnection, for example), the pore size, and the pore morphology (spherical, cylindrical, ellipsoidal, for instance).

6.3.3.1 POST-GRAFTING ON SILICA-BASED MATRICES

The most commonly employed method to functionalize mesostructured silica thin films is the one-pot synthesis. However, some studies employing post-functionalization have been reported either via vapor phase infiltration [51,57,58,65-69] or via immersion in a solution [70-72]. In the post-functionalization via immersion procedure, thin films have been calcined and stirred in dry toluene, ethanol, or dichloromethane solution containing organotrialkoxysilane or hexadimethylsilazane species under refluxing conditions. The reaction time varied from 4 to 24 h. Finally, thin films have been washed with solvent and dried at low temperature.

Before or after the calcination step, films are exposed to grafting molecule vapor in a closed vessel at moderate temperatures (150-165°C depending on the grafting molecule). Post-grafting in some cases led to materials presenting pore restriction (bottle ink pores) or to a total blocking of the porosity. The vapor infiltration techniques especially on as-synthesized MTFs prevent the usual shrinkage of pores due to calcination, allow densification of walls and thus an increase of mechanical and hydrothermal stabilities of MTFs, and limit the usual reduction of pores due to grafting.

Table 2 Modifiers and properties of resultant thin films mesophases

Functional organosilanes	Experimental conditions and results	Properties/applications and references
41) Dibenzoylmethane	ZrCl₄, Brij 58; 2D hexagonal	Hydrophobic[152]
42) 3-Nitrophthalic acid	ZrCl₄/TiCl₄, F127; cubic, 2D hexagonal	[150]
43) Methyl Red	ZrCl₄, Brij 58; 2D hexagonal	pH sensitive[152]
44) Ferrocenecarboxylic acid	ZrCl₄, Brij 58; 2D hexagonal	Redox properties[152]
45) Thioglycolic acid	ZrCl₄/TiCl₄, F127; cubic, 2D hexagonal	[151]
46) Mercaptosuccinic acid	ZrCl₄/TiCl₄, F127; cubic, 2D hexagonal	[150,151]
47) Cysteine	ZrCl₄/TiCl₄, F127; cubic, 2D hexagonal	[150]

REFERENCES

1. P. Gomez Romero, C. Sanchez, *Functional Hybrid Materials*, 2004; C. Sanchez, F. Ribot, *New J. Chem.*, **1994**, 18, 1007;

2. M. Antonietti, G. A. Ozin, *Chem. Eur. J.* **2004**, 10, 28;

3. G. J. A. A. Soler-Illia, C. Sanchez, B. Lebeau, J. Patarin, *Chem. Rev.*, **2002**, 102, 4093;

4. J. L. Shi, Z. L. Hua, L. X. Zhang, *J. Mater. Chem.*, **2004**, 14, 795;

5. L. Nicole, C. Boissiere, D. Grosso, A. Quach, C. Sanchez, *J. Mater. Chem.*, **2005**, 15, 3598;

6. D. Grosso, F. Cagnol, G.J.A.A. Soler-Illia, E. L. Crepaldi, H. Amenitsch, A. Brunet-Bruneau, A. Bourgeois, C. Sanchez, *Adv. Funct. Mater.*, **2004**, 14, 309;

7. N. Liu, D. R. Dunphy, P. Atanassov, S.D. Bunge, Z. Chen, G.P. Lopez, T. J. Boyle, C. J. Brinker, *Nano Lett.* **2004**, 4, 551;

8. E. Besson, A. Mehdi, V. Matsura, Y. Guari, C. ReyV, R.J.P. Corriu, *Chem. Commun.*, **2005**, 1775;

9. C. Sanchez, F. Ribot, *New J. Chem.,* **1994**, *18*, 1007;

10. Y. Lu, R. Ganguli, C.A. Drewien, M.T. Anderson, C.J. Brinker, W. Gong, Y. Guo, H. Soyez, B. Dunn, M.H. Huang, J.I. Zink, *Nature*, **1997**, 389, 364;

11. M. H, Huang, B. S. Dunn, H. Soyez, J. I. Zink, *Langmuir,* **1998**, 14, 7331;

12. M. H. Huang, B. S. Dunn, J.I. Zink, *J. Am. Chem. Soc.,* **2000**, 122, 3739;

13. A.C. Franville, B. Dunn, J.I. Zink, *J. Phys. Chem. B,* **2001**, 105, 10335;

14. M. Ogawa, *Langmuir,* **1995**, 11, 4639;

15. M. Ferrer, P. Lianos, *Langmuir,* **1996**, 12, 5620;

16. M. Ogawa, T. Igarashi, K. Kuroda, *Chem. Mater.,* **1998**, 10, 1382;

17. A. Yamaguchi, Y. Amino, K. Shima, S. Suzuki, T. Yamashita, N. Teramae, *J. Phys. Chem. B,* **2006**, 110, 3910;

18. C. Jung, C. Hellriegel, B. Platschek, D. Wohrle, T. Bein, J. Michaelis, C. Brauchle, *J. Am. Chem. Soc.,* **2007**, 129, 5570;

19. B.J. Scott, M.H. Bartl, G. Wirnsberger, G.D. Stucky, *J. Phys. Chem. A,* **2003**, 107, 5499;

20. N. Stevens, D.L. Akins, *Sens. Actuators B,* **2007**, 123, 59;

21. P.N. Minoofar, B.S. Dunn, J.I. Zink, *J. Am. Chem. Soc.,* **2005**, 127, 2656;

22. J. Kirstein, B. Platschek, C. Jung, R. Brown, T. Bein, C. Brauchle, *Nat. Mater.,* **2007**, 6, 303;

23. Y. Fu, F. Ye, W.G. Sanders, M.M. Collinson, D.A. Higgins, *J. Phys. Chem. B,* **2006**, 110, 9164;

24. M. Ogawa; H. Ishikawa; T. Kikuchi , *J. Mater. Chem.,* **1998**, 8, 1783;

25. T. Yui; T. Tsuchino, K. Akatsuka, A. Yamauchi, Y. Kobayashi, T. Hattori, M. Haga, K. Takagi, *Bull. Chem. Soc. Jpn.,* **2006**, 79, 386;

26. X.C. Wang; Yu, J. C., *Macromol. Rapid Commun.,* **2004**, 25, 1414;

27. K.S. Ahn, M.S. Kang, J. W. Lee, Y. S. Kang, *J. Appl. Phys.,* **2007**, 101;

28. W. Chen, X.D. Sun, Q. Cai, D. Weng, H.D. Li, *Electrochem. Commun.,* **2007**, 9, 382;

29. M. Ogawa, K. Kuroda, J. Mori, *Chem. Commun.,* **2000**, 24, 2441;

30. M.H. Bartl, B. J. Scott, H.C. Huang, G. Wirnsberger, A. Popitsch, B. F. Chmelka, G. D. Stucky, *Chem. Commun.* **2002**, 21, 2474;

31. M. Tamura, Y. Kemmochi, Y. Murakami, N. Chino, M. Ogura, S. P. Naik, M. Takai, Y. Tsuji, S. Maruyama, T. Okubo, *Appl. Phys. A,* **2006**, 84, 247;

32. K.Y. Shi, Y.J. Chi, H. T. Yu, B. F. Xin, H. G. Fu, *J. Phys. Chem. B,* **2005**, 109, 2546;

33. N. Petkov, S. Mintova, K. Karaghiosoff, T. Bein, *Mater. Sci. Eng. B,* **2003**, 23, 145;

34. X. Zhang, C.L. Liu, W.J. Wu, J. F. Wang, *Mater. Lett.,* **2006**, 60, 2086;

35. G.J.A.A. Soler-Illia, P.C. Angelome, P. Bozzano, *Chem. Commun.* **2004**, *2854*.

36. P.C. Angelome, , G.J.A.A. Soler-Illia, *J. Mater. Chem.* **2005**, *15*, 3903.

37. S. W. Boettcher, M.H. Bartl, J.G. Hu, G.D. Stucky, *J. Am. Chem. Soc.,* **2005**, 127, 9721;

38. M.H. Bartl, S.W. Boettcher, E.L. Hu, G.D. Stucky, *J. Am. Chem. Soc.,* **2004**, 126, 10826;

39. J. Livage, M. Henry, C. Sanchez, *Prog. Solid State Chem.* **1988**, 18, 259;

40. B. Alonso, P. A. Albouy, D. Durand, F. Babonneau, *New J. Chem.,* **2002**, 26, 1270;

41. B. Alonso, A.R. Balkenende, P.A. Albouy, H. Amenitsch, M.N. Rager, F. Babonneau, *J. Sol-Gel Sci. Technol.,* **2003**, 26, 587;

42. K. Yu, B. Smarsly, C.J. Brinker, *AdV. Funct. Mater.,* **2003**, 13, 47;

43. S. Tanaka, J. Kaihara, N. Nishiyama, Y. Oku, Y. Egashira, K. Ueyama, *Langmuir,* **2004**, 20, 3780;

44. F. Cagnol, D. Grosso, C. Sanchez, *Chem. Commun.,* **2004**, 15, 1742;

45. H.Y. Fan, Y.F. Lu, A. Stump, S.T. Reed, T. Baer, R. Schunk, L.V. Perez, G.P. Lopez, C. J. Brinker, *Nature,* **2000**, 405, 56;

46. H.Y. Fan, S. Reed, T. Baer, R. Schunk, G.P. Lopez, C.J. Brinker, *Microporous Mesoporous Mater.,* **2001**, 44, 625;

47. N.G. Liu, D. R. Dunphy, P. Atanassov, S.D. Bunge, Z. Chen, G.P. Lopez, T. J. Boyle, C. J. Brinker, *Nano Lett.,* **2004**, 4, 551;

48. N.G. Liu, Z. Chen, D.R. Dunphy, Y.B. Jiang, R. A. Assink, C.J. Brinker, *Angew. Chem., Int. Ed.,* **2003**, 42, 1731;

49. M. Matheron, A. Bourgeois, A. Brunet-Bruneau, P.A. Albouy, J. Biteau, T. Gacoin, J.P. Boilot, *J. Mater. Chem.* **2005**, 15, 4741;

50. M. Matheron, A. Bourgeois, T. Gacoin, A. Brunet-Bruneau, P.A. Albouy, J.P. Boilot, J. Biteau, P. Lacan, *Thin Solid Films,* **2006**, 495, 175;

51. M. Matheron, T. Gacoin, J.P. Boilot, *Soft Matter,* **2007**, 3, 223;

52. Y.F. LuFan, N. Doke, D.A. Loy, R.A. Assink, D.A. LaVan, C. J. Brinker, *J. Am. Chem. Soc.,* **2000**, 122, 5258;

53. O. Dag, I. C. Yoshina, T. Asefa, M. J. MacLachlan, H. Grondey, N. Coombs, G. A. Ozin, *AdV. Funct. Mater.,* **2001**, 11, 213;

54. F.K. de Theije, A.R. Balkenende, M.A. Verheijen, M.R. Baklanov, K.P. Mogilnikov, Y. Furukawa, *J. Phys. Chem. B,* **2003**, 107, 4280;

55. A. Stein, B.J. Melde, R.C. Schroden, *AdV. Mater.,* **2000**, 12, 1403;

56. N. Nishiyama, S. Tanaka, Y. Egashira, Y. Oku, K. Ueyama, *Chem.Mater.,* **2003**,15, 1006;

57. S. Tanaka, H. Tada, T. Maruo, N. Nishiyama, Y. Egashira, K.Ueyama, *Thin Solid Films* **2006**, 495, 186;

58. J.Y. Chen, F.M. Pan, L. Chang, A.T. Cho, K.J. Chao, *J. Vac. Sci. Technol. B,* **2005**, 23, 2034;

59. A. Gibaud, J.F. Bardeau, M. Dutreilh-Colas, V.V. Bellour, A. Balasubramanian, A. Robert, C. Mehdi, R.J. Corriu, *J. Mater. Chem.,* **2004**, 14, 1854;

60. L. Nicole, C. Boissière, D. Grosso, P. Hesemann, J. Moreau, C. Sanchez, *Chem. Commun.* **2004**, 2312;

61. J.I. Jung, J.Y. Bae, B.S. Bae, *J. Mater. Chem.,* **2004**, 14, 1988;

62. N.A.; Melosh, P. Lipic, F. S. Bates, F. Wudl, G. D. Stucky, G. H. Fredrickson, B. F. Chmelka, *Macromolecules,* **1999**, 32, 4332;

63. V. Goletto, V. Dagry, F. Babonneau, *Mater. Res. Soc. Symp. Proc.,* **1999**, 576, 229;

64. P. N. Minoofar, R. Hernandez, S. Chia, B. Dunn, J. I. Zink, A.C. Franville, *J. Am. Chem. Soc.,* **2002**, 124, 14388;

65. E. L. Crepaldi, G.J.A.A. Soler-Illia, D. Grosso, P.A. Albouy, CSanchez, *Chem. Commun.,* 2001, 1582;

66. P. C. Angelome, G.J.A.A. Soler-Illia, *Chem. Mater.,* **2005**, 17, 322;

67. P.C. Angelome, S. Aldabe-Bilmes, M. E. Calvo, E. L. Crepaldi, D. Grosso, C. Sanchez, G.J.A.A. Soler-Illia, *New J. Chem,* **2005**, 29, 59;

68. H. Fan, H. R. Bentley, K. R. Kathan, P. Clem, Y. Lu, C. J. Brinker, *J. Non-Cryst. Solids,* **2001**, 285, 79;

69. K. Kohmura, H. Tanaka, S. Oike, M. Murakami, N. Fujii, S. Takada, T. Ono, Y. Seino, T. Kikkawa, *Thin Solid Films,* **2007**, 515, 5019;

70. D. Fattakhova-Rohlfing, J. Rathousky, Y. Rohlfing, O. Bartels, M. Wark, *Langmuir,* **2005**, 21, 11320;

71. N. Petkov, S. Mintova, B. Jean, T. Metzger, T. Bein, *Mater. Sci. Eng. B,* **2003**, 23, 827;

72. A. Palaniappan, X. Li, F. E. H. Tay, J. Li, X.D. Su, *Sens. Actuators B,* **2006**, 119, 220.

Experimental Section II

The research work related to the preparation of mesoporous thin films has been developed in collaboration with the Laboratory of Material Science and Nanotechnologies, Nanoworld Institute and INSTM, of University of Sassari, with the supervision of Prof. Plinio Innocenzi. This laboratory is involved in the preparation of self-building of materials by supramolecular self-assembly techniques and control of the properties on nanometric scale.

The possibility of engineering advanced materials at atomic level (nanotechnology) is fundamental for our research work. The use of chemical innovative technologies allows to obtain materials able to self-build and self-organize in ordered structures through bio-mimetic process in which the material imitates self-building typical of natural structures at atomic scale. The Experimental part IV and V have regarded the synthesis of oxides thin film, in particular mesoporous titania and silica films, obtained by deposition from liquid phase, able to self-build and with organization of mesostructured porosity, in which it is possible to covalently graft luminescent coordination complexes and used, for example, as emitter layers in OLEDs.

These materials appear with ordered and organized porous structure and exhibit a topological pore structure with a precise spatial organization similar to a typical order of crystallographic structures. The possibility of obtaining highly pure materials is a key factor for these devices, whose properties can be improved by their confinement as guest in matrices at ordered length scale. The synthesized thin film have been modified through chemical treatments with organic functions with triethoxysilanes as covalent ligand to silanol network, then used to incorporate a particular guest species. This guest species is a luminescent zinc(II) complex, synthesized in the Laboratory of Chemistry Department under the supervision of Prof. Mauro Ghedini and Dr. Iolinda Aiello, and grafted in mesoporous matrices for applications in optic, electro-optic and photonic fields.

In Experimental part VI mesoporous silica films have been submitted to simple impregnations in solutions with a chromophore, rhodamine 6G, a well-know fluorescent dye, without covalent anchorage with the framework.

This to evaluate the response of the system, in terms of leaching of incorporated species and of structural variations and properties of the system after chemical modification.

Each sample has been characterized by spectroscopic and surface techniques to verify variations effects in the properties produced by the introduction in the structure of guest species. Mesoporous silica films have been used as chemical environment for the incorporation of rhodamine (R6G) to study its aggregation states into a mesostructured film.

The understanding of this process has important implications for the development of controlled solid-state luminescent devices.

Experimental Part IV

Blue-Emitting Mesoporous Films Prepared via Incorporation of Luminescent Schiff Base Zinc(II) Complex

7.1 Introduction

In the past years zinc complexes have received considerable attention for the preparation of electroluminescent thin films [1-5]. Luminescent zinc complexes are, in fact, promising key color components (as blue emitting molecules) for the fabrication of full-color displays [6]. The incorporation of luminescent complexes into a solid state matrix is a mandatory step for technological applications. The immobilization of luminescent organic molecules on rigid supports can lead, in fact, to an enhancement of the emission efficiency [7-13] and to a greater temporal stability of the fluorescence properties. Mesoporous silica [14-16] has been widely used as a matrix to host functional organic molecules since the ordered structure allows post-synthesis doping of the material and several types of multifunctional materials can be designed.

Mesoporous films are typically synthesized by evaporation-induced self-assembly (EISA) via dip- or spin-coating using inorganic precursors such as alkoxides, organo-alkoxides or chlorides, and organic templating agents such as low-molecular weight ionic surfactants or amphiphilic block copolymers [17-19]. Mesoporous films show large surface areas up to 1000 m^2 g^{-1}, and pore volumes up to 1.3 cm^3 g^{-1} [20]: these properties provide easy pore accessibility and functionalization of catalytic sites within the pores. Host-guest systems such as organic luminescent molecules in mesoporous silica films combine the chemical stability and mechanical strength of the inorganic matrix together with the functional properties of the active organic guests [21-25]. Grafting of metal complexes onto the inner walls of mesoporous silica can be obtained using three main approaches [26-29]: (i) direct grafting by reaction with surface silanol groups; (ii) indirect grafting via the functionalization of the silanol groups with silane coupling agents followed by the anchoring of metal complexes to the surface; (iii) ship-in-a-bottle immobilization of metal complexes. In the present work, we introduced a zinc(II) complex as light emitting guest species into a mesoporous silica film acting as host matrix. The goal was to incorporate a highly luminescent species in a mesoporous material preserving, at the same time, the ordered porosity and the high surface area of the matrix.

The synthesis of the luminescent material has been performed by addition to the zinc(II) complex of a Schiff base ligand bearing triethoxysilane functions; this allows grafting of the molecule directly to the surface of the mesoporous materials through covalent bonding. The structure of the anchoring groups gives high stability to the complex within the mesoporous matrix, avoiding leaching effects. In the present paper, we report the synthesis of a zinc(II) complex that has been obtained through the reaction between zinc(II) acetate and the Schiff base ligand which forms treating salicylaldehyde with (3-aminopropyl)triethoxysilane [21]. The chemical stability and the luminescence yield of this complex have been tested in functionalized mesoporous silica films.

7.2 EXPERIMENTAL SECTION

7.2.1 MATERIALS

Pluronic F127 $(OH(CH_2–CH_2O)_{106}(CHCH_3–CH_2O)_{70}(CH_2CH_2O)_{106}H)$, tetraethyl orthosilicate 99% (TEOS), (3-aminopropyl)triethoxysilane 97% (APTES) and salicylaldehyde 99% were all purchased from Aldrich and used as received. Zinc(II) acetate dihydrate was purchased from Alfa Aesar. Ethanol 99% (EtOH) was obtained from Fluka. [100] oriented, P-type/boron doped silicon wafers (Jocam) and silica slides were employed as the substrates. Silica slides were accurately washed by distilled water, ethanol and acetone. Ssilicon wafers were cleaned with ethanol and acetone.

7.2.2 PREPARATION OF SILICA SOL

The synthesis of mesoporous silica film (**Fig.1**) has been carried out at room temperature using a non-ionic surfactant as structure directing agent: linear triblock copolymer, Pluronic F127 $(EO_{106}\text{-}PO_{70}\text{-}EO_{106})$. Two different solutions have been prepared: a stock solution was prepared by adding ethanol, TEOS, water, and HCl. The initial molar composition was:

$$TEOS : EtOH : H_2O : HCl = 1 : 2.78 : 1.04 : 1.43 \cdot 10^{-2}.$$

The sol was left to react under stirring for 75 minutes at room temperature. A second solution was prepared by dissolving 1.3 g of Pluronic F127 in 15 ml of EtOH and 1.5 ml of HCl acid aqueous solution $(5.7 \cdot 10^{-2}$ M$)$. The final sol was obtained by adding 7.7 ml of the stock sol to the solution containing the block copolymer. The final molar composition was:

$$TEOS : EtOH : H_2O : HCl : Pluronic\ F127 = 1 : 16.3 : 5.4 : 1.88 \cdot 10^{-2} : 5 \cdot 10^{-3}$$

The sol was stirred at room temperature for 30 min and immediately used for film deposition, under controlled temperature and humidity conditions.
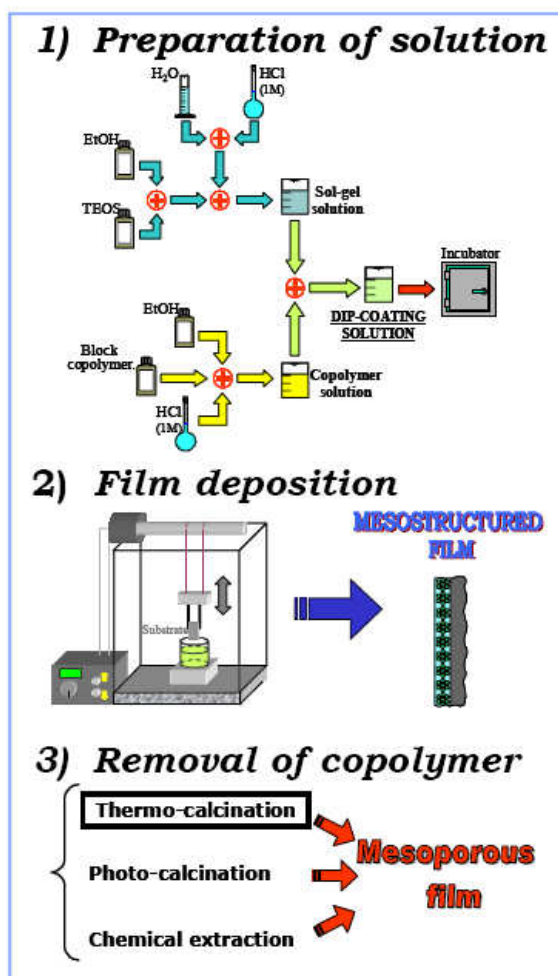

Fig.1: Synthesis protocol of mesoporous silica film.

7.2.3 PREPARATION OF SILICA FILMS

Silica film deposition has been carried out by dip-coating in controlled humidity and temperature conditions. Dip-coater is composed by a endless screw, moved by an electronic device by adjusting of rotation and extraction speeds (**Fig.2**). The substrate for film deposition is fixed to the end of screw. The instrument is boxed in a plexiglas transparent chamber,

hermetically closed, to guarantee stable and controlled conditions during deposition step from liquid sol. Relative humidity and temperature is carefully controlled.

Fig.2: Dip-coater instrument.

The film depositions were performed at 25°C and 24% of relative humidity (RH), at the withdrawal speed of 15 cm · min^{-1}. The substrates used for depositions are silicon wafers and silica slides, perfectly washed with soapy water, distilled water, acetone and ethanol to remove residuals on the surfaces. The dimensions of substrates were 3 cm x 1 cm. During extraction step of the substrate from beaker containing the sol, it observes the presence of interference fringes corresponding to "dewetting phase", are observed indicative of solvent evaporation phase and thin film formation on the substrate.

The fresh mesoporous silica thin film has been left few minutes inside the deposition chamber to permit complete evaporation of the ethanol. After the deposition, the films were dried in oven at 60 °C for 12 hours to stiffen the structure (**Fig.3**). Then, the films have been calcined in air for 60 min at 350°C for complete surfactant removal.

Fig.3: Thermal treatment of mesoporous silica thin film in oven.

7.2.4 GRAFTING POST-SYNTHESIS

Mesoporous silica films have been functionalized using a luminescent zinc(II) complex. The chemical modification reaction (**Fig.4**) has been carried out by grafting post-synthesis on the mesoporous calcined samples. The calcined mesoporous films were introduced into a beaker containing 45 cm^3 of tetrahydrofuran (THF) and ZnL$_2$ (0.21 mmol, 0.113 g) in EtOH (10 cm^3) and kept in the solution at different times. Impregnation time in the functionalization solution has been chosen as processing variable (0 ÷ 19 h). After reaction at room temperature, samples has been washed with ethanol, dried at 60°C in oven for 1 h and finally characterized. Hybrid film obtained have been designate as ZnL$_2$@SiO$_2$.
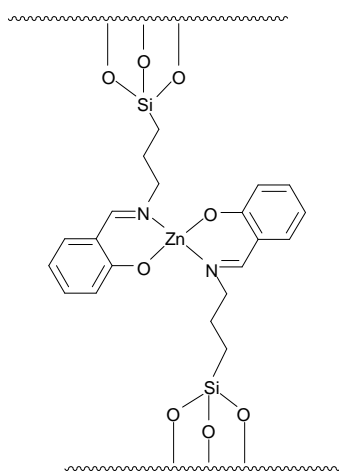
**Fig.4**: Sketch of a possible chemical structure of the ZnL$_2$@SiO$_2$ film.

7.2.5 CHARACTERIZATION OF LIGAND AND ZINC(II) COMPLEX

For the ligand and the corresponding zinc(II) complex, elemental analysis (C, H, N) were performed by a CHNS Perkin Elmer 2400 apparatus. The IR spectra were recorded on a KBr pellet using a Perkin Elmer FT 2000 spectrophotometer. The ^{1}H-NMR spectra were recorded by a Bruker WM spectrophotometer at 300 MHz, using deuterated chloroform (CDCl$_3$) and deuterated dimethyl sulphoxide (DMSO) in tetramethylsilane (TMS) as internal standard. UV-Vis analysis was performed by Perkin Elmer Lambda 900 spectrophotometer in the wavelength range 200-800 nm with a scan speed of 500 nm·min^{-1}.

7.2.6 PREPARATION OF THE LIGAND (HL)

Salicylaldehyde (21 mmol, 2.32 g) was added to 4.44 ml of APTES (19 mmol, 4.21 g) in ethanol (4 ml) (**Fig.5**). The solution was refluxed for 5 hours under constant stirring. The crude product obtained after evaporation of the solvent under reduced pressure was suspended in chloroform and filtered through a Celite column. The HL ligand obtained was a green-yellow oil which was stored at -15°C (5.85 g, 90% yield).
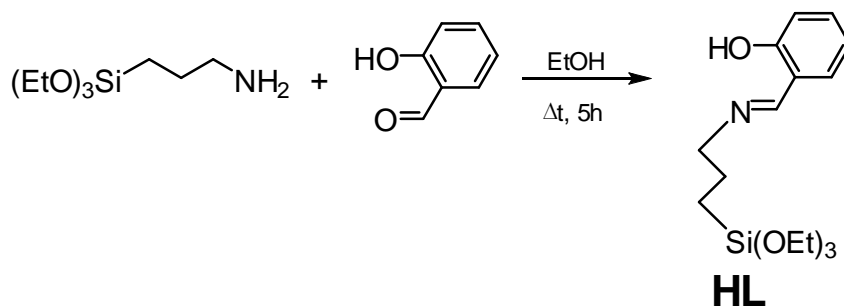
**Fig.5:** Scheme of the HL synthesis.

For HL ^{1}H-NMR, IR and also absorption and emission spectra have been registered. The ^{1}H-NMR spectrum recorded in CHCl$_3$ shows, in particular, the imine hydrogen signal at 8.32 ppm, which indicates the condensation reactions of the salicylaldehyde carbonyl group. The infrared spectra of the compound show two bands at 1281 and 1634 cm^{-1} that are attributed to

antisymmetric stretching of C–O and C=N groups, respectively [30,31], and a band at 757 cm^{-1} that is assigned to aromatic C–H [21]. The ligand purity has been verified by spectroscopic data and elemental analysis. From photophysical analysis on HL it infers that this species have good adsorption and no emission properties.

The UV-Vis spectra performed in CH_2Cl_2 solution show a strong absorption band at 325 nm and a second band of lower intensity at 425 nm, due to excitation n-π^* between only pair on the iminic hydrogen and an orbital π^* on the fragment C=N, while no luminescence was detected (**Fig.6**).
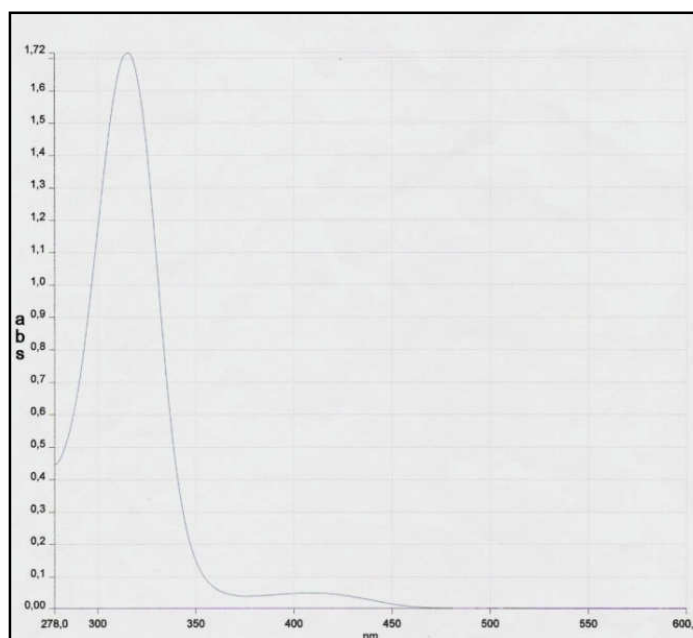

Fig.6: UV-Vis absorption spectrum of HL.

HL was used for the preparation of ZnL_2 complex, adapting the procedure described in literature (**Fig.7**) [21]. ^{1}H-NMR data are not available because of the low ZnL_2 solubility.

7.2.7 PREPARATION OF THE ZINC(II) COMPLEX (ZNL$_2$)

Zinc(II) acetate dihydrate (0.50 mmol, 0.11 g) and HL (1 mmol, 0.33 g) were mixed in 30 cm^3 of ethanol (**Fig.7**). The reaction mixture was checked by absorption UV/Vis spectroscopy. After 5 hours of reaction under reflux at 80°C, the imine band at 325 nm disappeared and at the

same time a band at 361 nm came out, confirming the formation of ZnL_2. This reaction product was not separated from the reaction mixture. Mesoporous silica host was added to 1 ml of the described reaction mixture containing ZnL_2. Part of the solvent was removed under reduced pressure, and a solid yellow-green product was obtained, $(ZnL_2)^*$, with a yield of 45% which account for the hydrolyzed ZnL_2 derivative containing two $-Si(OH)_3$ groups instead of the initial three-$Si(OEt)_3$ groups. Mp >350 °C.

With respect to HL, the ZnL_2 FTIR spectra show the shift of the C=N signal to lower frequencies (10-15 cm^{-1}) [21]. The bands (C=N) at 1539 cm^{-1} and 759 cm^{-1} are assigned to the stretching of bond C=N conjugated to aromatic ring and to the bending of C-H aromatics. As the complex was insoluble in common solvents, no ^{1}H-NMR analysis was carried out.
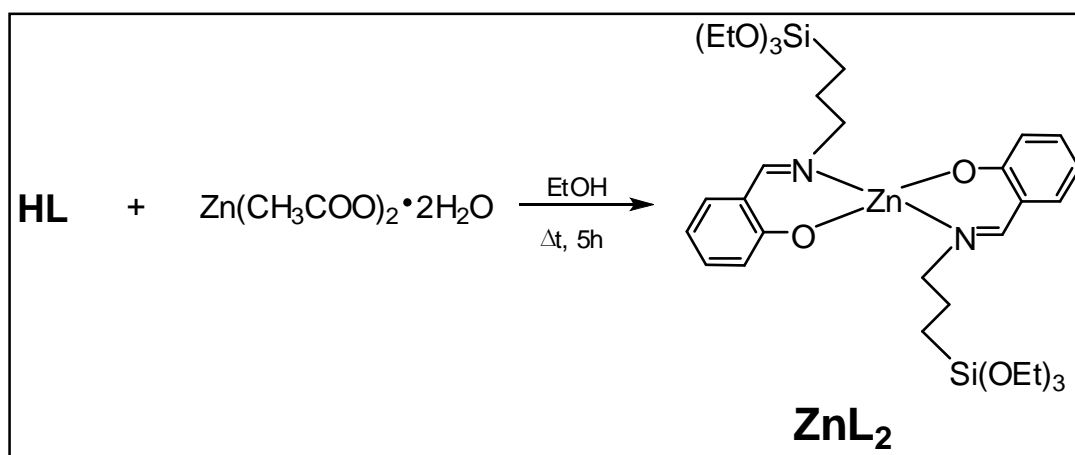
Fig.7: Scheme of the ZnL_2 synthesis.

Spectroscopic data and elemental analysis results confirms that the synthesized complex is pure. Zinc(II) complex show good emission properties, but for scarce solubility have been registered spectra in solution and on solid. From adsorption profile registered in CH_2Cl_2, it can identify a phase at 370 nm (**Fig.8**).
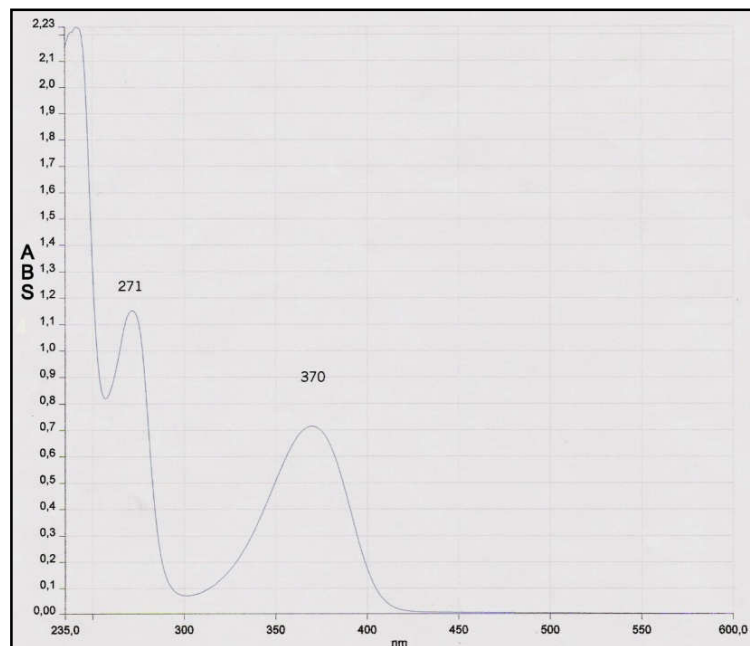
Fig.8: UV-Vis absorption spectrum of ZnL$_2$.

When the film is excited at 370 nm, an emission maximum at 450 nm is found with emission quantum yield (ϕ) of 30%. This emission frequency is in the range between 440 and 460 nm [5], typical for bi- e tetra-dentate Schiff base coordinated with zinc(II) ions and salicyaldehyde derivative. Emission properties of solution remain constant for several days.

7.2.8 STABILITY OF ZnL$_2$

The absorption spectra of ZnL$_2$ in EtOH show three main peaks at 361, 269 and 238 nm. The stability of ZnL$_2$ in EtOH was tested by monitoring the evolution of the absorption spectra with time. The complex appears very stable for 32 h. At longer times the ZnL$_2$ spectral intensities decrease in intensity and a precipitate, resulting from ZnL$_2$ condensation through the triethoxysilane functions is observed (**Fig.9**). A similar trend is shown for ZnL$_2$ in THF. The fluorescence spectra of a ZnL$_2$ ethanol solution show a strong emission band peaking at 457 nm (λ_{ex} = 360 nm).

The emission arises from the HL complexation to zinc(II) that hampers a non radiative decay pathway on binding the imine nitrogen electrons pairs involved in the metal coordination.
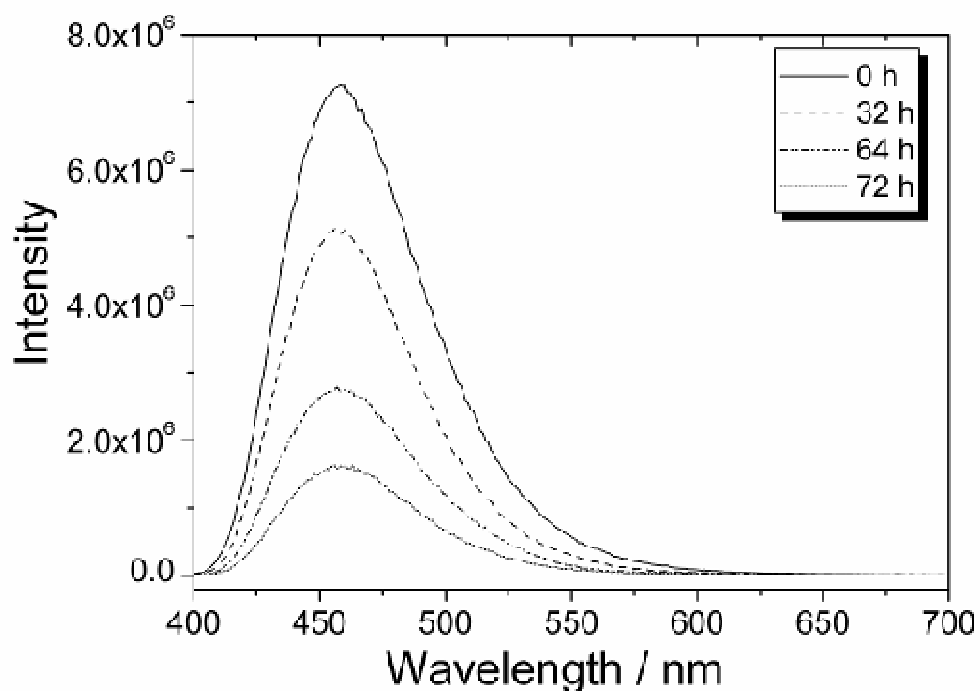
Fig.9: Fluorescence emission spectra (λ_{ex} = 360 nm) of the Schiff base zinc(II) complex
in ethanol as a function of time ($2.1 \cdot 10^{-7}$ ml/2 mL).

In fact, HL does not show emission, whilst the complex displays an intense emission band. The decrease in intensity with time of the band at 457 nm (**Fig.10**) reveals that the emission spectra are more sensitive than absorption spectra to aging of the complex, and after 72 h the emission intensity with respect to a freshly prepared solution, drop to 35%.
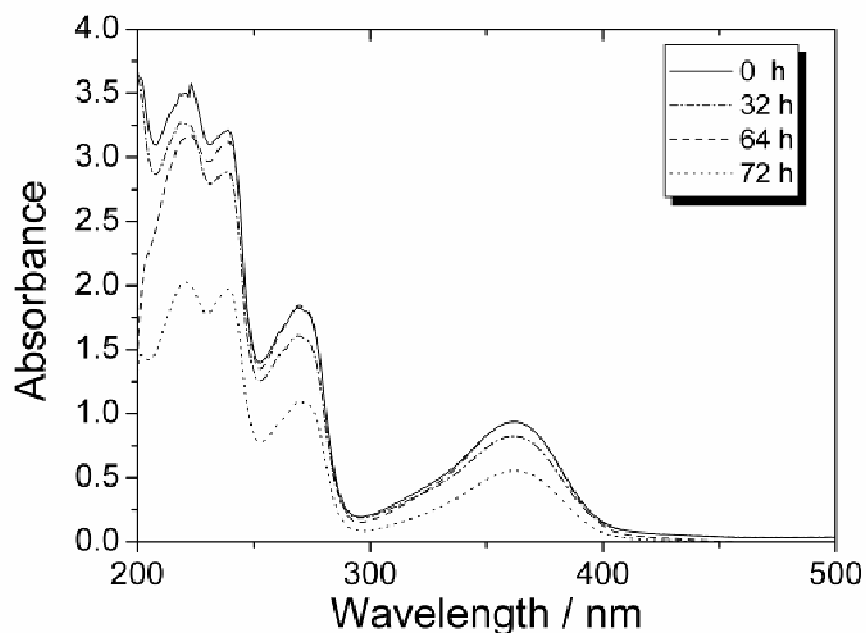
Fig.10: UV-Vis absorption spectra of the Schiff base zinc(II) complex
in ethanol as a function of time ($2.1 \cdot 10^{-7}$ ml/2 mL).

7.3 CHARACTERIZATION

For the film characterization, Fourier Transform Infrared (FTIR) analysis was performed using a Nicolet Nexus spectrophotometer. The spectra were recorded in transmission, in the 400-5000 cm^{-1} range by averaging 256 scans with 4 cm^{-1} of resolution. A silicon wafer was used as substrate to measure the background. Refractive index and thickness were measured by a α-SE™ Wollam spectroscopic ellipsometry. The measure was done at room temperature; n, k and the residual porosity were calculated by 2.03 α-SE™ Wollam software.

Transmission electron microscopy (TEM) images of mesostructured substrates were obtained in the bright field mode on a JEOL 200CX microscope equipped with a tungsten cathode operating at 200 kV. Samples for observations were prepared by depositing one drop of suspension containing scratched fragments of calcined mesoporous film in ethanol on a carbon coated copper grid and allowing solvent evaporation at room temperature.

UV-Vis analysis was performed on films deposited on silica substrates by UV-Vis Nicolet Evolution 300 spectrometer in the wavelength range 200-800 nm with a scan speed of 500 nm·min^{-1}.

Each acquisition is the average of 3 different scans collected with a bandwith of 1.5 nm. Fluorescence analysis was done using a FluoroMax-3 Horiba Jobin Yvon spectrofluorometer. The probing beam was set to impinge on one side of the sample (silica substrate, incidence angle of 2-3°) so that the sample acted as a waveguide for the incident light wave, while the luminescence was collected at 90° with respect to the incident beam. This configuration enhanced the signal-to-noise ratio and avoided reflection effects. Each acquisition is the average of 3 different accumulations.

7.4 RESULTS AND DISCUSSION

7.4.1 MESOPOROUS SILICA THIN FILM

#### 7.4.1.1 TEMPLATE REMOVAL AND FTIR SPECTROSCOPY

The mesostructure of the materials was mainly depended on the amount of the neutral surfactants template, instead of the molecular structure of the template itself, since it's the aggregation of the template, not the self-assembly of the template molecules themselves which direct the pore-forming in the silica matrix. Calcination is the most commonly used method for template removal in surfactant templated mesoporous materials. In our experiment, IR measurements showed the removal of Pluronic F127 was complete. FTIR spectroscopy is a simply and efficient analytic method to study structure of material obtained by sol-gel chemistry and self-assembled. Infrared absorption spectra give a direct and effective snapshot of the condensation state of the oxide network, give important informations about microstructural evolution with the temperature and about the influence of processing parameters on film microstructure. FTIR spectrum (**Fig.11,** black line) of mesoporous thin film as made shows typical signals of silica, surfactant and residual water. The presence of Pluronic F127 is revealed by a band around $2800 \div 3000$ cm^{-1}.

The three main peaks characteristic of Si-O-Si bonds vibrational modes are detected around 1070, 800, and 460 cm^{-1}. The lowest frequency mode (460 cm^{-1}) is assigned to transverse optical rocking motions. Near 800 cm^{-1}, a weak band due to Si-O-Si symmetric stretching is

observed. The highest frequency mode around 1070 cm^{-1}, whose intensity is the largest one, is assigned to antisymmetric stretching. A band of medium intensity centered near 940-960 cm^{-1} is attributed to Si-OH stretching vibrations.

Two main groups of bands can be found in this interval: around 3800-3650 cm^{-1}, stretching modes of isolated OH groups around 3740 cm^{-1} or OH groups partially involved in hydrogen bonding and around 3650-3200 cm^{-1}, stretching modes of strongly hydrogen-bonded OH groups in chains of different lengths.

   After calcination at 350°C, the surfactant is completely removed, as shown by the absence of any signal around 2700-3200 cm^{-1} (spectrum at 0 h). Water absorption is observed in the as prepared films (O-H stretching band around 3200 cm^{-1} and H-O-H bending at 1640 cm^{-1}). The films show also an absorption band around 3750 cm^{-1} due to isolated silanols which are produced by calcination process [32, 35-36].
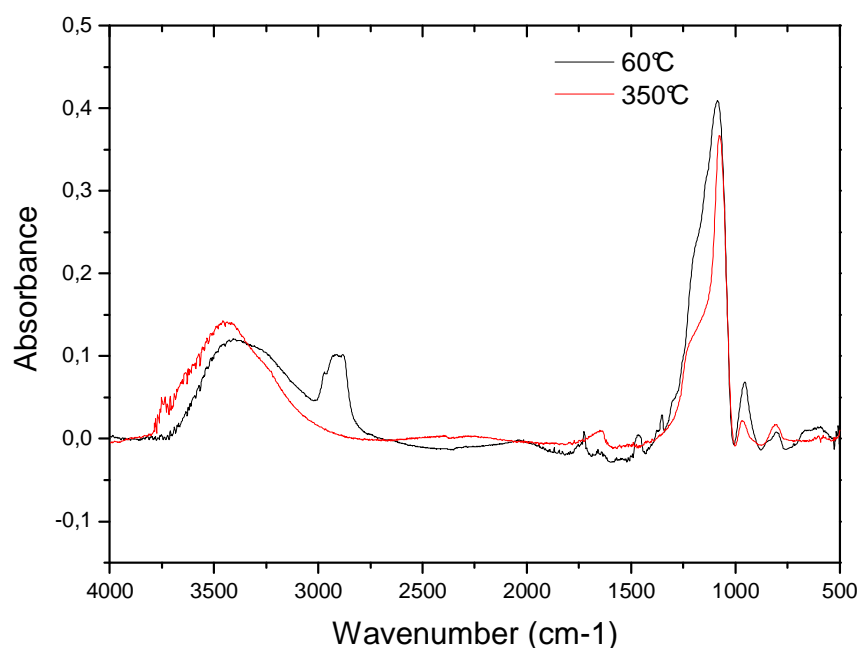

Fig.11: FT-IR absorption spectra of the mesoporous SiO2 film before (-) and after calcination (-).

7.4.1.2 TRANSMISSION ELECTRON MICROSCOPY

A "palette" of characterization techniques was adopted to study the incorporation of the ZnL_2 complex within the host mesoporous films. For the mesophase characterization of the resulting films, bright field TEM images were collected for samples calcined at 350°C. Fig.12 shows representative direct image of the deposited films. The snapshot suggests that the mesostructure is slightly distorted cubic. This periodicity is compatible with an orthorhombic *Fmmm* space group (Fig.13) that we have already observed by small angle X-ray scattering (SAXS) analysis [32].
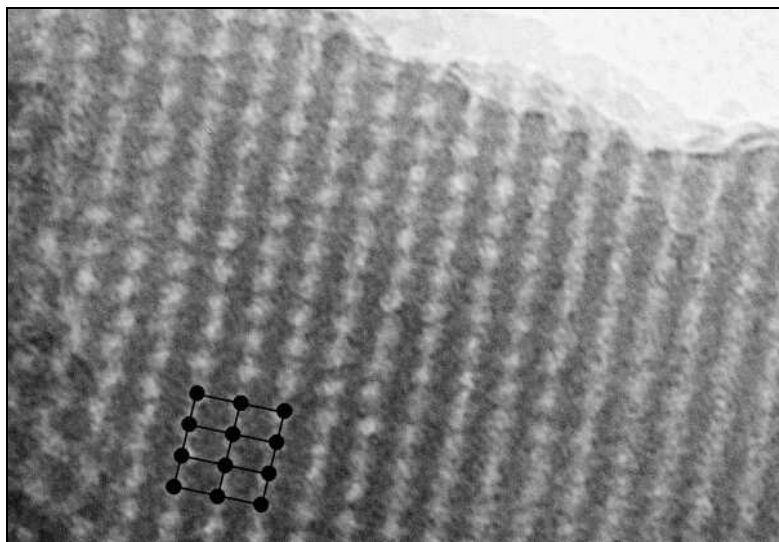
Fig.12: Bright field TEM image of the calcined mesoporous silica film.

This organization is due to structure distortion during thermal *shrinkage* produced by calcination. The organized interconnected porous structure is very suitable for post-synthesis grafting of doping molecules.

Several examples are reported in literature and show that after incorporation, both via physical adsorption or chemical bonding, the molecules maintain their activity and are well entrapped within the matrix without significant leakage [33].
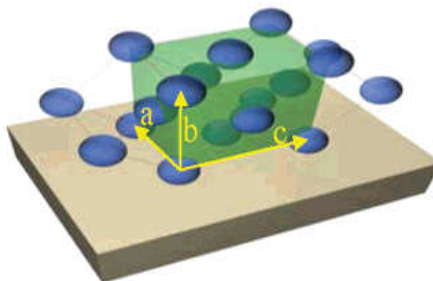
Fig.13: *Fmmm* mesophase.

7.4.2 HYBRID MESOPOROUS SILICA FILM

7.4.2.1 FT-IR SPECTROSCOPY

Infrared absorption spectra collected from a sample as a function of the impregnation time give a direct snapshot of the incorporation of the ZnL_2 together with the condensation state of the oxide network. The FTIR spectra of the films after impregnation (**Fig.14**) show the rise of new signals in the C–H stretching range (2700-3200 cm^{-1}). The intensity of this signal can be assumed as an indication of the quality of the impregnation of the porous film; the spectra show that the best result is obtained after 16 h of impregnation.

At times shorter than 16 h, the amount of complexes is much lower, whilst at longer times a decrease in the impregnation efficiency is observed. This is probably due to leakage effects caused by the hydrolysis of the silica bonds that anchor the zinc(II) complex to the surface of the film; on the other hand the stability of the film at the impregnation conditions is good; the silica bands do not show any significant change after the film is immersed in the doping solution.

The bands located in the range 2750-3050 cm^{-1}, in particular, are assigned to the stretching mode of –CH_2 group. The sharp bands at 1539 and 759 cm^{-1} are assigned to the vibration of C=N and C–H (aromatic), indicating the presence of ZnL_2 in the films.
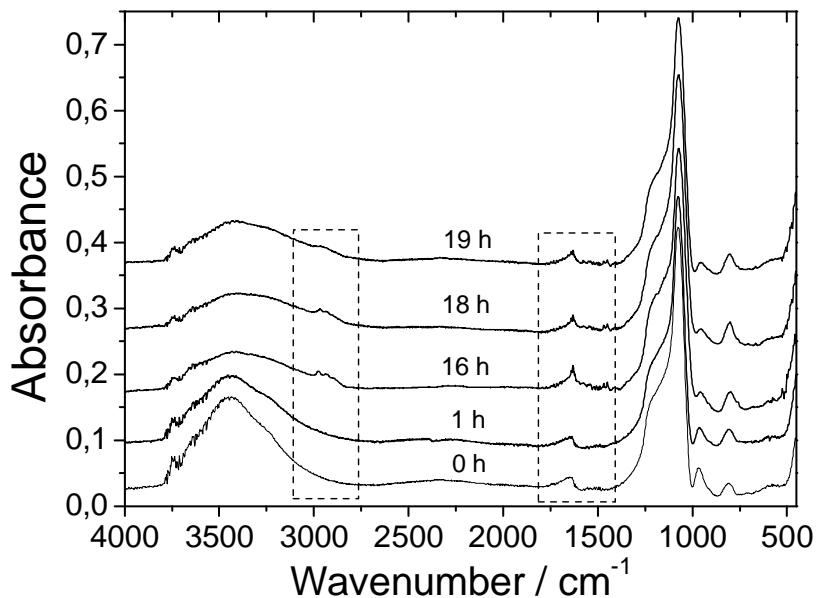
Fig.14: FT-IR spectra of silica film at different functionalization times.

7.4.2.1 ELLIPSOMETRIC SPECTROSCOPY

The effect of the introduction of the complex within the mesoporous film was also monitored by spectroscopic ellipsometry. Tab.I lists the thickness and the refractive index at λ = 632.8 nm of different samples before and after impregnation. The data were obtained assuming a fitting model based on the assumption of transparent films (the measure is done in the 390-900 nm range, in this interval the doped film doesn't absorb) on silicon (Cauchy dispersion relation) [37].

The quality of the fitting was evaluated on the ground of the mean square error (MSE). A Bruggeman Effective Medium Approximation (EMA) [38] layer with two components (silica and void) was used to evaluate the optical constants and the residual porosity of the films dried at 60 °C before impregnation; the fit gave a 24% of residual porosity.

This value is lower of the effective owing to model limitations. In as made film, the pore are largely full of adsorbed water and the silica walls are covered with silanol groups, as showed from FTIR data. The sample impregnated at higher times were, instead, modeled by a spline function.

Impregnation time	Thickness / nm		Refractive index $\lambda = 632.8$ nm	
	(before)	(after)	(before)	(after)
1 h	458 ± 10	448 ± 12	1.312	1.313
2 h	477 ± 19	473 ± 10	1.358	1.371
16 h	518 ± 16	530 ± 25	1.293	1.395
18 h	477 ± 13	470 ± 23	1.310	1.394
19 h	470 ± 15	490 ± 24	1.315	1.351

Tab.I: Thickness and refractive index of silica film before and after grafting.

The data from spectroscopic ellipsometry are well in accordance with the infrared spectra, in fact, only after 16 h a significant change in refractive index is observed, which indicates the successful impregnation of the film. The highest change in refractive index is observed in the films impregnated by ZnL_2 for 18 h, in accordance to the FTIR data.

It is also important to observe that the thickness is not affected by the doping process and this is a good indication about the stability of the host material in the present conditions of impregnation.

7.4.2.2 FLUORESCENCE SPECTROSCOPY

The fluorescence emission spectra ($\lambda_{ex} = 360$ nm) of the ZnL_2 grafted films as a function of the doping times are shown in **Fig.15**. At higher impregnation times the fluorescence peak shows a shift from 455 to 465 nm and a strong increase of emission intensity.

Emission in such zinc(II) diimino complex is due to the deactivation of the singlet π-π^* ligand-centred excited state, which is lowered in energy respect to the non- n-π^* as a consequence of the metal complexation.

The stability of the fluorescence emission has been tested as a function of aging time; in the case of a sample impregnated for 18 h with a ZnL_2 solution, the emission intensity after 7 days was around 80% of the initial one (**Fig.16**).
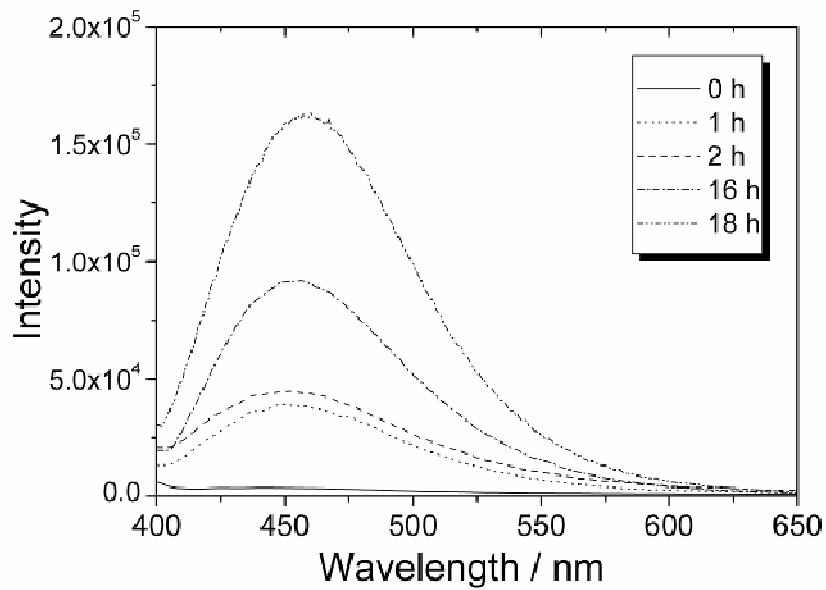
Fig.15: Fluorescence emission spectra of ZnL_2 doped SiO_2 mesoporous film as a function of the impregnation time.
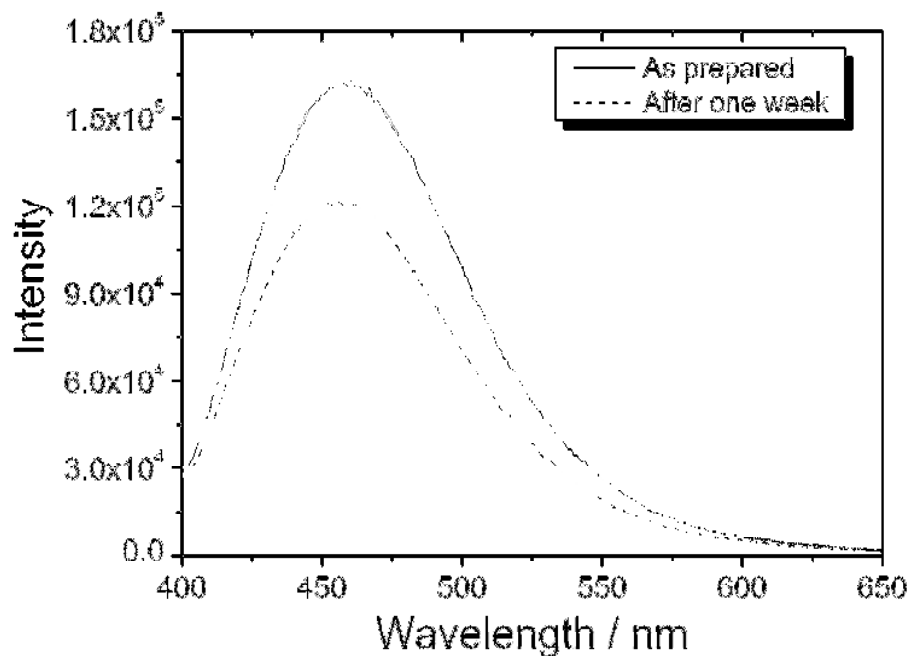

Fig.16: Fluorescence emission spectra of hybrid silica film after 1 week of aging time.

7.4.2.3 EMISSION QUANTUM YIELD DETERMINATION

The emission quantum yield of the silica thin films (measured by means of a 102 mm diameter integrating sphere coated Wight Spectralon mounted in the optical path of the spectrofluorimeter) remained at the constant value of $\Phi = 0.050$. the constancy of Φ-value of the grafted chromophore with respect to homologous reference species reveals that the photophysical properties of the confined specie did not change after grafting.

7.5 LEACHING EXPERIMENTS

To study the stability of ZnL_2 into the films, leaching experiments were carried out. The ZnL_2 doped films (nominal surface area ≈ 3 cm^2) were immersed in beakers containing 15 cm^3 of ethanol and then were taken out at different times. Finally, the samples were washed with ethanol and dried at 60°C for 1 h. The efficiency of the mesoporous host matrix in entrapping the ZnL_2 was tested by leaching experiments.

The entrapping of the complexes within the mesoporous films should involve the formation of direct silica bonds through the surface silanols (**Fig.7**). The formation of these bonds should be accompanied by a reduction in silanols, as indeed indicated in the present case by the reduction in intensity of the Si–OH signals in the FTIR spectra of impregnated samples.

To obtain a direct experimental evidence of the formation of a strong covalent bond between the matrix and the doping complexes in the films is difficult but leaching experiments can give some indirect indications. Leaching experiments were performed monitoring the change in intensity of the absorption and emission spectra of the ZnL_2 doped mesoporous films as a function of immersion in ethanol.

Fig.17 shows the emission spectra ($\lambda_{ex} = 360$ nm) of a film as a function of the leaching time. A decrease in emission intensity is observed in the first two hours, after 210 min the samples did not show anymore changes up to 7 days of measure. This result indicates, together with the FTIR data, that grafting of the complex to the silica mesoporous walls has been achieved.
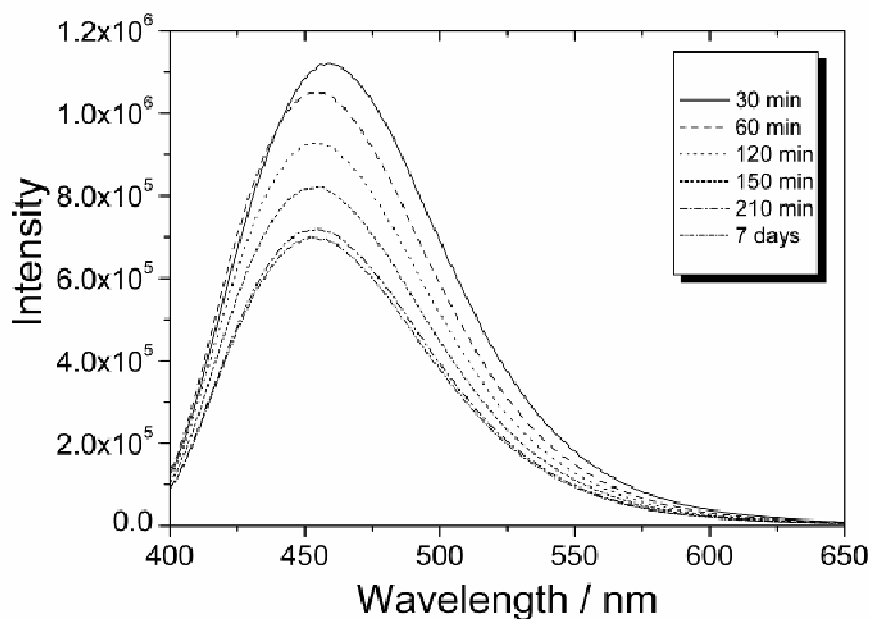
Fig.17: Fluorescence emission spectra of ZnL_2 doped SiO_2 mesoporous film as a function of the leaching time.

7.6 CONCLUSIONS

In this work, a properly functionalized luminescent zinc(II) complex has been synthesised with strong blue emitting properties. It was used to impregnate porous host materials, such as mesoporous silica films; after introduction of the complex, the films are highly fluorescencent and a good stability of the emitting properties is observed.

The incorporation into the film has been monitored by UV-Vis, Fourier transform infrared spectroscopy and spectroscopic ellipsometry. After 18 h of impregnation in the zinc(II) complex solution, the films showed strong blu emission and an increase in the refractive index.

Leaching experiments have shown that the complexes incorporated in the film are stable, no significant release has been, in fact, observed after several days of immersion of the samples in ethanol. This result indicates that complexes are attached to silica walls by surface silanols.

The luminescent behavior of this host-guest system has been studied, showing that it is more adapted to trap other luminescent complexes.

REFERENCES AND NOTES

1. Sheats JR, Antoniadis H, Hueshen M, Leonard W, Miller J, Moon R, Roitman D, Stocking A (**1996**) *Science,* 273, 884;

2. Karft A, Grimsdale AC, Holms AB (**1998**) *Angew Chem Int Ed* 37, 402;

3. Hamada Y, Sano T, Fujita M, Fujii T, Nishio Y, Shibata K (**1993**) *Jpn J Appl Phys* 32, 511;

4. Sano T, Nishio Y, Hamada Y, Takahashi H, Usuki T, Shibata K (**2000**) *J Mater Chem* 10, 157;

5. La Deda M, Ghedini M, Aiello I, Grisolia A (**2004**) *Chem Lett* 33, 1060;

6. Tao XT, Suzuki H, Wada T, Sasabe H, Miyata S (**1999**) *Appl Phys Lett* 75, 1655;

7. Yu T, Su W, Li W, Hong Z, Hua R, Li M, Chu B, Li B, Zhang Z,.Hu ZZ (**2006**) *Inorg Chim Acta* 359, 2246;

8. Zhang HJ, Fu LS, Wang SB, Meng QG, Yang KY, Ni JZ (**1999**) *Mater Lett* 38, 260;

9. Stein A, Melde BJ, Schroden RC (**2000**) *Adv Mater* 12, 1403;

10. Zhang WH, Shi JL, Wang LZ, Yan DS (**2000**) *Chem Mater* 12, 1408;

11. Xu W, Akkins DL (**2002**) *J Phys Chem B* 106, 1991;

12. Zhang MS, Yin W, Su Q, Zhang HJ (**2002**) *Mater Lett* 57, 940;

13. Wang H, Huang J, Wu S, Xu C, Xing , Xu L, Kann Q (**2006**) *Mater Lett* 60, 2662;

14. Kresge CT, Leonowicz ME, Roth WJ, Vartuli JC, Beck JS, (**1992**) *Nature* 359,710;

15. Wilson ST, Lok BM, Messina CA, Cannan TR, Flanigen EM (**1982**) *J Am Chem Soc* 104, 1146;

16. De Man JM., Van Santen RA, Vog ETC (**1992**) *J Phys Chem* 96, 10460;

17. Brinker CJ, Lu Y, Sellinger A, Fan H (**1999**) *Adv Mater* 11, 579 ;

18. Soler-Illia JAA, Sanchez C, Lebeau B, Patarin J (**2002**) *Chem Rev* 102, 4093;

19. Doshi DA, Gibaud A, Goletto V, Lu M, Gerung H, Ocko B, Han SM, Brinker CJ, (**2003**) *J Am Chem Soc* 125(38), 11646;

20. Soler-Illia G, Innocenzi P, (**2006**) *Chem: Europ J* 12(17), 4478;

21. Singh UG, Williams RT, Hallam KR, Allen CG, *J Sol State Chem* (**2005**) 178, 3405;

22. Zeleňák V, Hornebecq V, Llewellyn P (**2005**) *Microp Mesop Mater* 83:125

23. Fernandes A, Dexpert-Ghys J, Glezes A, Galarneau A, Brunel D (**2005**) *Microp. Mesop. Mater.* 83, 35;

24. Zhang H, Zhang P, Ye K, Sun Y, Jiang S, Wang Y, Pang W (**2006**) *J. Luminescence* 117, 68;

25. Baleizão C, Gigante B, Das D, Álvaro M, Garcia H, Corma A (**2004**) *J Catal* 223, 106;

26. Moller K, Bein T (**1998**) *Stud Surf Sci Catal* 117, 53;

27. Trong On D, Desplantier-Giscard D, Danumah C, Kaliaguine S (**2001**) *Appl Catal A Gen* 222, 299;

28. Pasqua L, Testa F, Aiello R, Madeo G, Nagy JB (**2002**) *Stud Surf Sci Catal* 142b, 1427;

29. Pasqua L, Testa F, Aiello R, Madeo G, Nagy JB (**2003**) *Phys Chem Chem Phys* (5), 640;

30. Tajmir-Riahi A (**1983**) *Polyhedron* 2, 723;

31. Torzilli MA, Colquhoun S, Kim J, Beer RH (**2002**) *Polyhedron* 21, 705;

32. Falcaro P, Grosso D, Amenistch H, Innocenzi P (**2004**) *J Phys Chem B* 108, 10942;

33. Scott BJ, Bartl MH, Wirnsberger G, Stucky GD (**2003**) *J Phys Chem A* 107, 5499;

34. Innocenzi P (**2003**) *J Non-Cryst Solids* 316, 309;

35. Innocenzi P, Falcaro P, Grosso D, Babonneau F (**2003**) *J Phys Chem B* 107, 4711;

36. Malfatti L, Kidchob T, Falcaro P, Costacurta S, Piccinini M, Cestelli Guidi M, Marcelli C, Corrias A, Casula M, Amenitsch H, Innocenzi P (**2007**) *Microp Mesop Mater* 103, 113;

37. The Cauchy dispersion equation: $n(\lambda) = An + Bn/\lambda 2 + Cn/\lambda 4$, allows calculating the refractive index as a function of the wavelength. An is a parameter related to the average refractive index of the material, while Bn and Cn are parameters that provide the shape or curvature of the $n(\lambda)$ curve.

38. For a two-components material, the refractive index in the Bruggemann approximation is expressed as:

$$f_v \frac{n_v^2 - n^2}{n_v^2 + 2n^2} + f_{SiO_2} \frac{n_{SiO_2}^2 - n^2}{n_{SiO_2}^2 + 2n^2} = 0$$

while f_v, n_v and f_{SiO2}, n_{SiO2} are the volume fractions and the refractive index of the pores void and silica, respectively.

EXPERIMENTAL PART V

ABSOLUTE EMISSION QUANTUM YIELD DETERMINATION OF SELF-ASSEMBLED MESOPOROUS TITANIA FILMS GRAFTED WITH A LUMINESCENT ZINC(II) COMPLEX

7.1 INTRODUCTION

Mesoporous titania films have attracted considerable attention due to their potential applications as photocatalysts, electrochemical sensors, photochromic and photovoltaic devices[1-10]. These highly ordered mesostructured materials offer a uniform and adjustable environment for encapsulating guest molecules and support a very homogeneous distribution of these molecules on the internal surface of the pores. Incorporation of luminescent guest species into these materials could offer the opportunity to modify the photophysical properties of the emitter by controlling its interaction with the host, as already experimented in silica-based mesoporous materials[11-15].

With this aim, in the last years several lanthanide containing complexes have been embedded in mesoporous titania thin films and powders using one-step sol-gel[16] and chemical modification methods[17], to exploit their characteristic luminescent properties such as long decay times, high quantum efficiency and narrow emission bands [18-20]. Furthermore, respect to the analogous luminescent hybrid mesoporous silica, these titania-based materials can exploit the semiconducting properties of TiO_2[21-24] to act as an effective antenna system for the excitation light[25,26]. Herein, is reported the preparation by post-synthesis[27-30] grafting of a luminescent hybrid mesoporous titania film obtained with incorporation of a properly functionalized blue-emissive Schiff base zinc(II) complex. The photophysical properties and the emission quantum yield of the material was quantified by using an integrating sphere.

7.2 EXPERIMENTAL SECTION

7.2.1 MATERIALS

The starting materials: Pluronic F127 ($OH(CH_2–CH_2O)_{106}(CHCH_3–CH_2O)_{70}(CH_2CH_2O)_{106}H$), tetraethyl orthosilicate 99% (TEOS), (3-aminopropyl)triethoxysilane

97% (APTES), $TiCl_4$ 99.9%, and salicylaldehyde 99% were purchased from Aldrich and used as received. Zinc (II) acetate anhydrous was purchased from Alfa Aesar.

Ethanol 99% (EtOH) and THF were obtained from Fluka. (100) oriented, P-type/boron doped silicon wafers (Jocam) and silica slides were employed as substrates. Silica slides were accurately washed by distilled water, ethanol and acetone before using; silicon wafers were cleaned with ethanol and acetone.

7.2.2 PREPARATION OF TITANIA SOL

Titania mesostructured films were synthesized using an EISA (evaporation induced self-assembly)-derived method, which allows for the generation of very ordered and porous films. Here, metal chlorides was used as the inorganic source, ethanol as the solvent, and triblock copolymer as the template.

Likewise to silica film, mesoporous titania thin film have two synthesis steps.The precursor solution was obtained by slowly adding $TiCl_4$ (0.660 ml) to a mixture of EtOH (14 ml) and block-copolymer Pluronic F127 [poly(ethylene oxide)-block-poly(propylene oxide)-block—poly(ethylene oxide), $(PEO)_{106}$ $(PEO)_{70}(PEO)_{106}$, Aldrich] (0.387g); water (1.04 ml) was added, drop by drop, after 5 min of mechanical stirring. This solution has a molar composition of $TiCl_4$: EtOH: H_2O at a relative ratio of 1: 40: 10 and a $TiCl_4$/Pluronic F127 ratio s~0.005. Using a low surfactant concentration, the mesostructure became more ordered.

7.2.3 DEPOSITION OF MESOPOROUS TITANIA THIN FILM

After stirring for few minutes, thin layers were deposited onto silicon and glass wafers by dip-coating in controlled temperature and humidity conditions. The plate was withdrawn from the solution at a speed of 15 cm·min^{-1}, resulting in a ~170 nm thick film which over an area of 1.5 x 3 cm^2. The relative humidity inside the deposition chamber was maintained at 20% at room temperature. After deposition, the films were dried at 60 °C for 12 h, at 130°C for 12 h, then the template was removed by calcination in air at 350°C for 30 min and then at 400°C for 3h (**Fig.18**).

Fig.18: Film sottili di titania mesoporosa depositati su wafer di silicio

7.2.4 GRAFTING OF MESOPOROUS TITANIA THIN FILM

The selected zinc emitter was successively incorporated into mesochannels by post-synthesis grafting (**Fig.19**). This process was performed by immersing the mesoporous titania thin films into an alcoholic solution of the complex (0.21 mmol, 0.113 g in 10 cm^3 of EtOH) and tetrahydrofuran (45 cm^3) at room temperature and for different impregnation times.

After impregnation, the final films were washed thoroughly with ethanol and characterized.
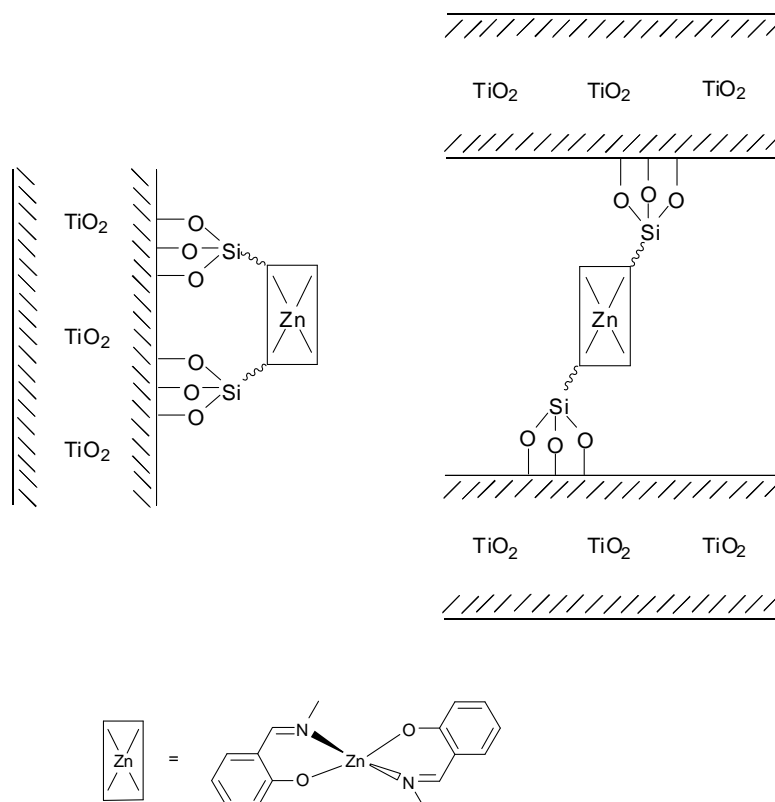
Fig.19: Sketch of some grafting modes of the zinc(II) complex to the titania mesoporous film.

7.3 CHARACTERIZATION

Fourier Transform Infrared (FTIR) analysis was performed using a Nicolet Nexus spectrophotometer. The spectra were recorded in transmission, in the 400-5000 cm^{-1} range by averaging 256 scans with 4 cm^{-1} of resolution. Refractive index and thickness were measured by a α-SE™ Wollam spectroscopic ellipsometry. n, k and the residual porosity were calculated by 2.03 α-SE™ Wollam software.

Transmission electron microscopy (TEM) images of mesostructured substrates were obtained in the bright field mode on a JEOL 200CX microscope equipped with a tungsten cathode operating at 200 kV. Fluorescence analysis was done using a FluoroMax-3 Horiba Jobin Yvon spectrofluorometer. The probing beam was set to impinge on one side of the sample (silica substrate, incidence angle of 2-3°) so that the sample acted as a waveguide for the incident light wave, while the luminescence was collected at 90° with respect to the incident beam.

This configuration enhanced the signal-to-noise ratio and avoided reflection effects. Each acquisition is the average of 3 different accumulations.

7.3.1 MESOPOROUS HYBRID TITANIA FILM

7.3.1.1 TRANSMISSION ELECTRON MICROSCOPY

For the mesophase characterization of the resulting films, bright field TEM images were collected for samples calcined at 40°C. **Fig.20** shows representative direct image of the deposited films. The snapshot suggests that the mesostructure is slightly distorted cubic. This periodicity is compatible with an orthorhombic *Fmmm* space group.
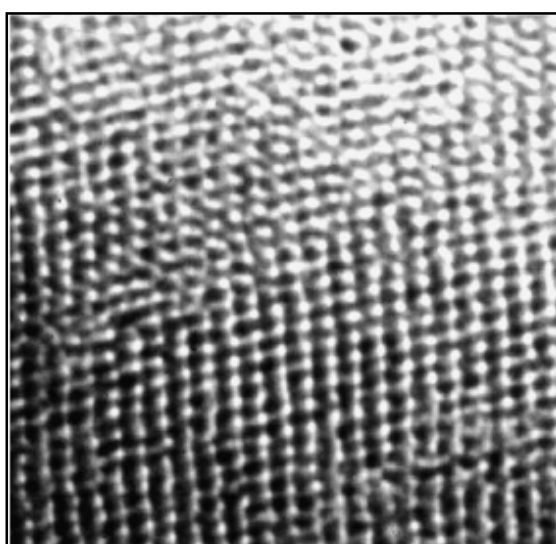
Fig.20: Immagine TEM del film di titania mesoporosa calcinato.

7.3.1.2 FTIR SPECTROSCOPY

Fourier transform infrared (FTIR) spectroscopy was used to follow the surfactant removal during calcination by monitoring the disappearance of the C-H vibrations in the range 2700-3200 cm^{-1} (**Fig. 21**). The incorporation of the chromophore (**Fig.19**) was assessed by FTIR and emission spectroscopies. In particular, in the FTIR spectrum recorded for the functionalized solid

film, it is noteworthy the appearance of a strong absorption band at about 1600 cm^{-1} attributed to the C=N stretching of the metal-bonded imino group[32].
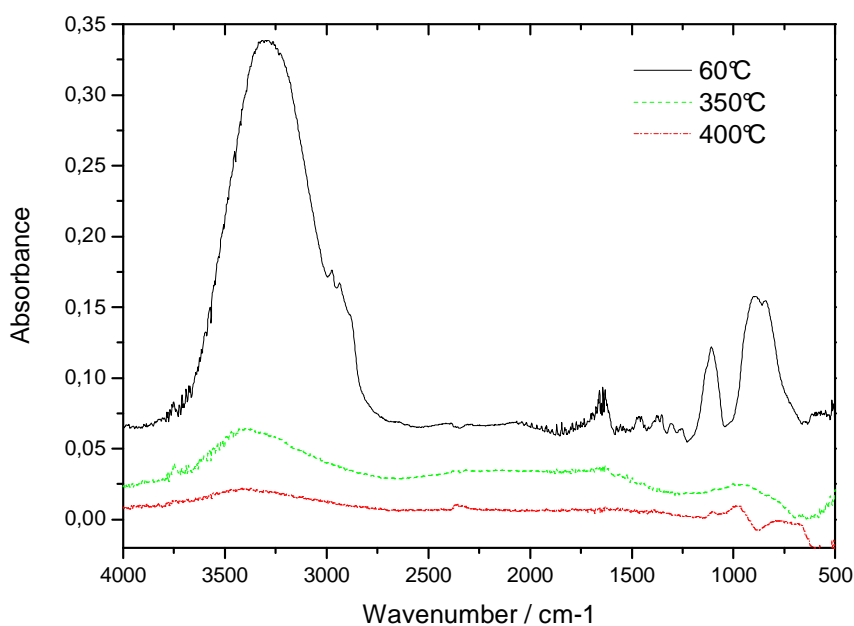
Fig.21: FT-IR spectra of titania film before and after calcination.

7.3.1.3 ELLIPSOMETRIC SPECTROSCOPY

The impregnation within the mesoporous film was also evaluated using spectroscopic ellipsometry by comparing the data collected before and after grafting (**Tab.1**). A Bruggeman Effective Medium Approximation (EMA) model with two components (titania and void) was used to evaluate the optical constants of the films calcined at 400 °C before the grafting process. The impregnated samples were modelled by an absorbing film on silicon model using a spline fit.

The increase in refractive index of the samples after impregnation gives a direct indication of the efficiency of the process, longer impregnation times giving a higher refractive index; an impregnation time of 24h seems not sufficient to give a significant incorporation of the chromophore.

The efficiency of the grafting process is reflected in the refractive index increase[31] with the impregnation time, which remains almost constant after 24h of impregnation, arises of 4.5% after 48h but decreases of 8.5% after 72h, according to emission data relative to simple deposition of Zn(II) emitter on the titania surface for high impregnation times.

Tab.1: Changes in thickness and refractive index of TiO$_2$ films deposited on silicon before and after grafting.

| Time of impregnation	Thickness / nm		Refractive index $\lambda = 632.8$ nm	
	(before)	(after)	(before)	(after)
1h	161 ± 1	163 ± 1	1.709	1.626
2h	157 ± 1	167 ± 1	1.710	1.629
24h	157 ± 1	195 ± 1	1.634	1.630
48h	161 ± 1	165 ± 1	1.702	1.778
72h	200 ± 1	210 ± 1	1.564	1.618

7.3.1.4 FLUORESCENCE SPECTROSCOPY

Fluorescence emission spectra (λ_{ex} = 360 nm) of the Zn(II) complex grafted films as a function of the doping times were measured using a Horiba Jobin Yvon Fluorolog 3 spectrofluorimeter, and shown in **Fig.22**. An intense peak was observed in the range 477 - 460 nm, and it is attributed to Zn(II) complexed chromophore incorporated into mesoporous titania, as evidenced by comparing these spectra with those recorded from a solid film of similar zinc Schiff base complexes[31].

Emission in such Zn(II) diimino complex is due to the deactivation of the singlet π-π* ligand-centred excited state, which is lowered in energy respect to the non-emissive n-π* iminic state as a consequence of the metal complexation[33].

The emission quantum yield of the thin film (measured by means of a 102 mm diameter integrating sphere coated with Spectralon® mounted in the optical path of the spectrofluorimeter) remained at the constant value of Φ = 0.060.

Increasing the impregnation time the emission intensity was not found to increase while a blue-shift was observed (**Fig.22**).
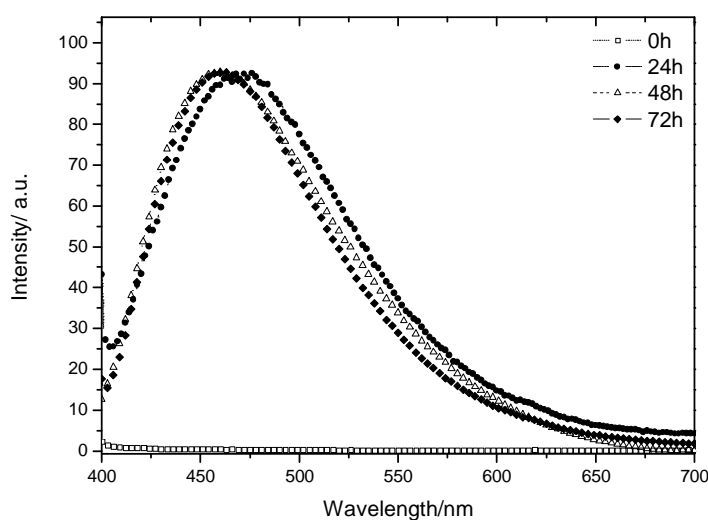
Fig.22: Fluorescence emission spectra of $ZnL_2@TiO_2$ films at different impregnation times.

This behavior is reasonable to account for an initial grafting of the Zn(II) emitter (emission recorded at 475 nm) to the titania support, thereafter, in a longer impregnation time, a blue-shift of the emission peak (*i.e.* toward a position which results closest to the position usually observed for unsupported Zn(II) Schiff bases complexes[33]), was observed, so suggesting that a simple deposition of a further amount of emitter occurred.

The constancy of Φ-value of the incorporated chromophore with respect to homologous reference species reveals that the photophysical properties of the confined chromophores did not change after embedding.

7.4 CONCLUSIONS

In summary, a properly functionalized luminescent zinc complex was successfully trapped in channels of titania thin films; the luminescent property of this host-guest nanostructured material was characterised with reference to the photophysical properties. The resulting films show an intense blue-fluorescence increasing with the functionalization time.

The photo/electroactive mesoporous titania films are advanced materials with potential applications in different fields, such as light emitting devices[34] or solar cells.[35] In order to test the actual performances of these materials it is very useful to recognize an appropriate figure of merits which makes possible a comparison among the different materials. In this context it is worthy to note that, according to the above described procedure, the emission quantum yield, a datum usually neglected for these hybrid organic/inorganic species, was quantitatively and accurately determined by an integrating sphere.

REFERENCES

1. V.F. Stone, R.J. Davis*, Chem. Mater*., 10 (**1998**) 1468;

2. K. Kalyanasundaram, M. Grätzel, *Coord. Chem. Rev*., 77 (**1998**) 347;

3. W. Goèpel, G. Rocker, R. Feierabend, *Phys. Rev. B*, 28 (**1983**) 3427;

4. L. D. Birkefeld, A.M. Azad, S.A. Akbar, *J. Am. Ceram. Soc*., 75 (**1991**) 2964;

5. T. Gerfin, M. Grätzel, L. Walder, *Prog. Inorg. Chem*, 44 (**1997**) 345;

6. J. S. Kim, H.K. Joo, T. K. Lee, K. Itoh, M. Murabayashi, *J. Catal*., 194 (**2000**), 484;

7. C. Sanchez, C. Boissière, D. Grosso, C. Laberty, L. Nicole, *Chem. Mater*., 20 (**2008**) 682;

8. G. J. A. A. Soler-Illia, P. Innocenzi, *Chem. Eur. J*., 12 (**2006**) 4478;

9. K. Ariga, A. Vinu, J. P. Hill, T. Mori, *Coor. Chem. Rev*., 251 (**2007**) 2562;

10. S. Angelos, E. Johansson, J. F. Stoddart, J. I. Zink, *Adv. Func. Mater*., 1, (**2007**) 2261;

11. K. De Witte, A.M. Busuioc, V. Meynen, M. Mertens, N. Bilba, G. Van Tendeloo, P. Cool, E. F. Vansant, *Microp. Mesopor. Mater*., 110 (**2008**) 100;

12. A. Fernandes, J. Dexpert-Ghys, A. Gleizes, A. Galarneau, D. Brunel, *Microp. Mesopor. Mater*., 83 (**2005**) 35;

13. H. Wang, J. Huang, S. Wu, C. Xy, L. Xing, L. Xu, Q. Kan, *Mater. Lett*., 60 (**2006**) 2662;

14. L. Z. Zhang, Y. Xiong, P. Cheng, G. Q. Tang, L. J. Wang, D. Z. Liao, *J. Mater. Chem*., 11 (**2001**) 2903;

15. Y. L. Sui, B. Yan, *Inorg. Mater*., 42 (**2006**) 144;

16. K. L. Frindell, M. H. Bartl, M. R. Robinson, G. C. Bazan, A. Popitsch, G. D. Stucky, *J. Solid State Chem.* 172 (**2003**) 81;

17. P. Liu, H. Li, Y. Wang, B. Liu, W. Zhang, Y. Wang, W. Yan, H. Zhang, U. Schubert, *J. Mater. Chem*., 18 (**2008**) 735;

18. C. Jia, E. Xie, A. Peng, R. Jiang, F. Ye, H. Lin, T. Xu, *Thin Solid Films* 496 (**2006**) 555;

19. N. Strataki, V. Bekiari, P. Lianos, *J. Hazardous Mat*., 146 (**2007**) 514;

20. Y. *Wang, L. wang, H. Li, P. Liu, D. Qin, B. Liu, W. Zhang, R. Deng, H. Zhang J*. Solid State Chem., 181 (**2008**) 562;

21. M. Murakami, Y. Matsumoto, K. Nakajima, *Appl. Phys. Lett*., 78 (**2001**) 2664;

22. A. Amtout, R. Lenoelli, *Phys. Rev. B*, 51 (**1995**) 6842;

23. J. S. Salafsky, *Phys. Rev. B*, 59 (**1999**) 10885;

24. O. Banakh, P.E. Schmid, R. Sanjines, F. Levy, *Surf. Coat. Technol*., 151/152 (**2002**) 272;

25. K. L. Frindell, M. H. Bartl, A. Popitsch, G. D. Stucky, *Angew. Chem. Int. Ed*., 41 (**2002**) 960.

26. K. L. Frindell, M. H. Bartl, M. R. Robinson, G. C. Bazan, A. Popitsch, G. D. Stucky, *J. Solid State Chem*.,172 (**2003**) 81;

27. C. Leisant, B. Lebeau, C. Marichal, J. Patarin, *Microp. Mesop. Mater*., 83 (**2005**) 76;

28. S. Zheng, L. Gao, J. Guo, *Mater. Chem. Phys*., 71 (**2001**) 174;

29. P.M. Price, J.H. Clark, D.J. Macquarry, *J. Chem. Soc., Dalton Trans*., (**2000**) 101;

30. K. Moller, T. Bein, *Stud. Surf. Sci. Catal*., 117 (**1998**) 53;

31. D. Aiello, L. Malfatti, T. Kidchob, R. Aiello, F. Testa, I. Aiello, M. Ghedini, M. La Deda, T. Martino, M. Casula, P. Innocenzi, J. *Sol-Gel. Sci Tech.,* (**2008**) 47, 283;

32. T. Yu, W. Su, W. Li, Z. Hong, R. Hua, M. Li, B. Chu, B. Li, Z. Zhang, Z. Z. Hu, *Inorg. Chim. Acta*, 359 (**2006**) 2246;

33. M. La Deda, M. Ghedini, I. Aiello, A. Grisolia, Chem. Lett., 33 (**2004**) 1060;

34. S. A. Haque, S. Koops, N. Tokmoldin, J. R. Durrant, J. Huang, D. D. C. Bradley, E. Palomares, *Adv. Mater*., 19 (**2007**) 683;

35. L. Malfatti, P. Falcaro, H. Amenitsch, S. Caramori, R. Argazzi, C. A. Bignozzi, S. Enzo, M. Maggini, P. Innocenzi, *Microp. Mesopor. Mater*., 88 (**2006**) 304.

EXPERIMENTAL PART VI

AGGREGATION STATES OF RHODAMINE 6G IN MESOSTRUCTURED SILICA FILMS

7.1 INTRODUCTION

Mesostructured films are an ideal material for incorporation of fluorescent dyes; controlling of the doping process is, however, a critical step because the dyes will be constrained in a complex chemical environment. We have incorporated Rhodamine 6G (**Fig.1**), a well known fluorescent dye, in silica mesostructured 2D-hexagonal films at different concentrations. We have used dense silica films as reference material to compare the effect of incorporation of Rhodamine 6G in mesostructured and dense materials.

We have also prepared mesostructured films at different surfactant concentrations to compare the surfactant effect on dye aggregation state. The dye doped films have been characterized by UV-Vis absorption spectroscopy, emission and excitation fluorescence spectroscopy. At high dye concentrations non-fluorescent sandwich H-type dimers are formed, but in mesostructured films the amount of this type of aggregates is reduced and the formation of fluorescent J-type dimers is favoured.

The presence of the surfactant within the mesopores gives rise to fluorescent dimers (J-type) at expenses of the non-fluorescent sandwich H-type.
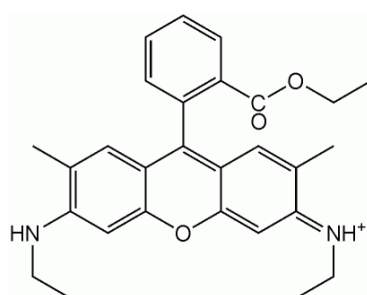
Fig.1: Rodamina 6G.

Rhodamine 6G (Rh6G) is one of the most popular fluorescent dyes and is widely used for its lasing ability to fabricate several types of luminescent materials [1,2]. Dye lasers are generally

based on dyes in solution (typically in ethanol, methanol, and less commonly water) or on dye-doped solids such as sol-gel materials [3,4].

Sol-gel route, because of the low processing temperature, is particularly suitable for incorporation of organic dyes in thin films; several examples of inorganic and hybrid organic-inorganic films doped by rhodamine 6G have been reported so far [1,3]. Different methods to introduce fluorescent dyes into solid materials via sol-gel processing have been developed, such as direct impregnation of a host porous matrix by dye solutions and "one-pot" synthesis [5,6].

One of the main difficulties which is encountered introducing fluorescent dyes, is controlling the aggregation states. Rhodamine 6G shows, in fact, a strong tendency to form aggregates when is dissolved in concentrated solutions or after incorporation into solid state matrixes. Stable ground state dimers are formed in water via π-π mixing of xanthene ring orbitals at concentrations around 10^{-5} M, and at 10^{-4} M the solution does not show any lasing capability. In alcohols, such as ethanol and methanol, the tendency to form dimers is much reduced and they are not observed before quite high concentrations (up to 0.1 M) are reached [7]. Rhodamine 6G (Rh6G) forms dimers through van der Waals dye-dye interactions and rhodamine – water (counterions) interactions [8]; coexistence of parallel and antiparallel dimers is also assumed [9].

Sandwich type (H-dimers) or head-to-tail dimers10 (J-type) are formed in accordance to the exciton theory. H-dimers are characterized by a strong absorption band of higher energy with respect to the monomer band, but this aggregated species is not fluorescent and is the main responsible of the monomer fluorescence quenching. J-aggregates are, instead, still fluorescent and have absorption and fluorescent bands at lower energy (J-band) with respect to the monomer band [11]. Controlling the aggregation state of Rh6G upon incorporation into a solid state matrix is, therefore, a very challenging task and has been the subject of several works [3,12].

Whilst incorporation of Rh6G in sol-gel materials [13,14] is now quite well understood and characterized, both in inorganic and in organic-inorganic hybrid host materials, the preparation of self-assembled mesoporous materials containing fluorescent dyes has still to be fully explored. In mesostructured porous materials an ordered porosity in the meso-scale is available; and the processing route by self-assembly through supramolecular templates should allow, in principle, to achieve a higher and more sophisticated control of the dye doping process.

A porous host material can be doped by Rh6G via post-synthesis impregnation [15,16], in this case a secondary bond is formed between the pore surface and the dye. Alternatively, organic dyes with alkoxy functionalities can be also used for post impregnation in order to obtain a direct covalent bonding to the pore surface. Post synthesis doping route is simple but not very effective, low controlling of the dye aggregation state, pore blocking, phase separation, and leaching effects are the main drawbacks [17].

Another possibility is represented by "one-pot" routes, the dye is introduced in the precursor solution during the synthesis and remains entrapped in the material after the film deposition. This route is widely used to incorporate organic dyes in hybrid organic-inorganic films but full controlling of aggregation state is still quite difficult. In the case of mesostructured thin films obtained via one-pot route, the presence of a surfactant plays a fundamental role and strongly affects the aggregation state of the dye [18]. It has been demonstrated that mesostructures thin films doped by Rh6G show stimulated emission and micron scale devices have been fabricated [19]. An interesting result is that the dye exhibited a lower tendency to aggregate after incorporation in mesostructured materials; the confinement effect in a nano-scale structure and the presence of the surfactant affect the aggregation state of the dye. In particular, dimer-to-monomer transformations have been reported for some types of rhodamine derivatives in micellar solutions of surfactants such as sodium dodecyl sulphate [20]. Tri-block copolymer surfactants, consisting of polyoxyethylene - polyoxypropylene- polyoxyethylene blocks (PEO – PPO – PEO) have been used to suppress the aggregation of Rh6G by emulsifying the monomeric dye and creating an effective partitioning in the solution [21]. In general, the chemical environment strongly affects the aggregation state of Rh6G, and a case by case study has to be performed. A fascinating feature of using mesostructured materials as hosts for optically active organic molecules is represented by the wide choice of environments [22].

The dye can be placed in specific regions, such as the pore walls, the micelles interior and the hybrid interface, and several strategies can be envisaged to differentiate the dye localization [23]. In the case of Rh6G, some studies indicate that during self-assembling by a supramolecular template the dye is incorporated within the hydrophobic core of the micelle. Prevention or limitation of aggregation has been observed but details of the process are not yet available.

In the present work we have studied the aggregation states of the dye after incorporation into a mesostructured film; understanding of this process has important implications for development of controlled solid state luminescent devices.

7.2 EXPERIMENTAL SECTION

Hybrid mesostructured silica films were prepared adding different amounts of rhodamine 6G and Pluronic F127 (EO_{106}–PO_{70}–EO_{106}) to a solution of tetraethoxysilane (TEOS), ethanol (EtOH), water and HCL. All the reagents were purchased from Aldrich and used without further purification. A precursor sol containing the silica source was prepared by adding in the following order: 3.08 cc of ethanol (EtOH), 4.26 cc of tetraethyl orthosilicate (TEOS), 0.355 cc of HCl aqueous solution (0.077 M).

This sol was stirred for 1 h at room temperature to allow pre-hydrolysis and slight condensation of the silicon alkoxide. Templating solutions were prepared dissolving different amounts of Pluronic F127 in a mixture of 10 cm3 EtOH and 1.5 cm^3 weakly HCl aqueous solution ($6·10^{-3}$ M). The amount of Pluronic F127 was varied from 0 to 1.3 g. After adding 7.7 cm^3 of the mother solution to the templating solutions, the final dipcoating solutions were obtained by introducing increasing amounts of Rh6G and stirring for 2 hours. All the solutions have been protected from the environmental light. At the end, the molar ratios of the dip coating solutions were TEOS : EtOH : H2O : F127 : Rh6G = 1 : 40 : 20 : s : c with s = $2.5 · 10^{-3}$ or $5·10^{-3}$ and c ranging from $5·10^{-5}$ to $5·10^{-2}$.

Silica sol-gel films doped with rhodamine 6G were prepared as reference, the precursor silica sol was prepared with the same procedure described for mesostructured films but without the addition of the surfactant. Thin films were obtained using a home made dip-coating system working at the pulling rate of 2 $mm·s^{-1}$; the relative humidity in the deposition chamber was set to $(27 ± 2)\%$. Fused silica slides (UV-grade, thickness 1 mm) were used as substrates for dip-coating. The substrates, previously cleaned with detergent solution, EtOH, and acetone, were dip-coated in the fresh solutions. The films, after deposition, were dried at 60 °C for 24 h. Absorption spectra were measured in 190-900 nm wavelength range using a UV-Vis Nicolet Evolution 300 spectrometer, at 500 $nm·min^{-1}$ scan rate.

Each acquisition is the average of 3 different scans collected with a bandwidth of 1.5 nm. Fluorescence analysis was performed using a FluoroMax-3 Horiba Jobin-Yvon spectrofluorometer. The probing beam was set to impinge on one side of the sample (incidence angle of 2-3°) so that the sample acted as a waveguide for the incident light wave, while the luminescence was collected at 90° with respect to the incident beam. This configuration enhanced the signal-to-noise ratio and limited the reflection effects. Each acquisition is the average of 3 different accumulations.

Emission spectra were collected between 495 and 800 nm, using an excitation wavelength of 480 nm. Excitation spectra were collected between 420 and 600 nm, using an emission wavelength of 620 nm. For 3D mapping, an excitation range from 420 nm to 620 nm and an emission range from 400 nm to 800 nm were used. For each sample, integration time and slit widths were optimized to maximize signal-to-noise ratio and to avoid saturation of the detector.

Mesostructured films were investigated by two-dimensional grazing incidence smallangle X-ray scattering (GISAXS) at the Austrian SAXS beamline of ELETTRA synchrotron (Trieste, Italy) [24]. The incident energy was set to 8 keV (wavelength 1.54 Å); the instrumental grazing angle between the incident radiation and the sample was set slightly above the critical angle (grazing incidence). A two-dimensional CCD detector (Photonic Science, UK) was used to acquire the scattering patterns; each measurement is the average of 10 acquisitions with integration time of 500 ms.

7.3 RESULTS AND DISCUSSION

7.3.1 GISAXS

Mesostructured silica films are obtained with different types of mesophase array, such as orthorhombic [25] or tetragonal [26]. In principle the mesophase formation depends on processing and synthesis parameters that can be, within some limits, adjusted to obtain a specific organization. The introduction of host functional molecules in mesostructured materials via one-pot synthesis does not produce, in general, a disruption of the mesophase [27,28].

We have used GISAXS to characterize the mesostructure of the films containing Rh6G at different concentrations; as a general trend we observed the same mesophase that does not change at different Rh6G concentrations. **Fig.2** shows a typical GISAXS pattern obtained from

an as deposited film with $s = 5 \cdot 10^{-3}$. The pattern has been indexed as 2d-hexagonal, *p6mm* in the space group; this mesophase is composed of ordered arrays of tubular micelles with hexagonal cross section [29].

Following this attribution, the cell parameter of the mesophase has been calculated as 6.6 ± 0.9 and 6.1 ± 0.8 nm in the in-plane (x) and out-of-plane (z) directions, respectively. Incorporation of rhodamine 6G into a solid state matrix is generally limited by aggregation effects, formation of non-fluorescent dimers (H-type dimers), is generally observed even at relatively low concentrations [3].
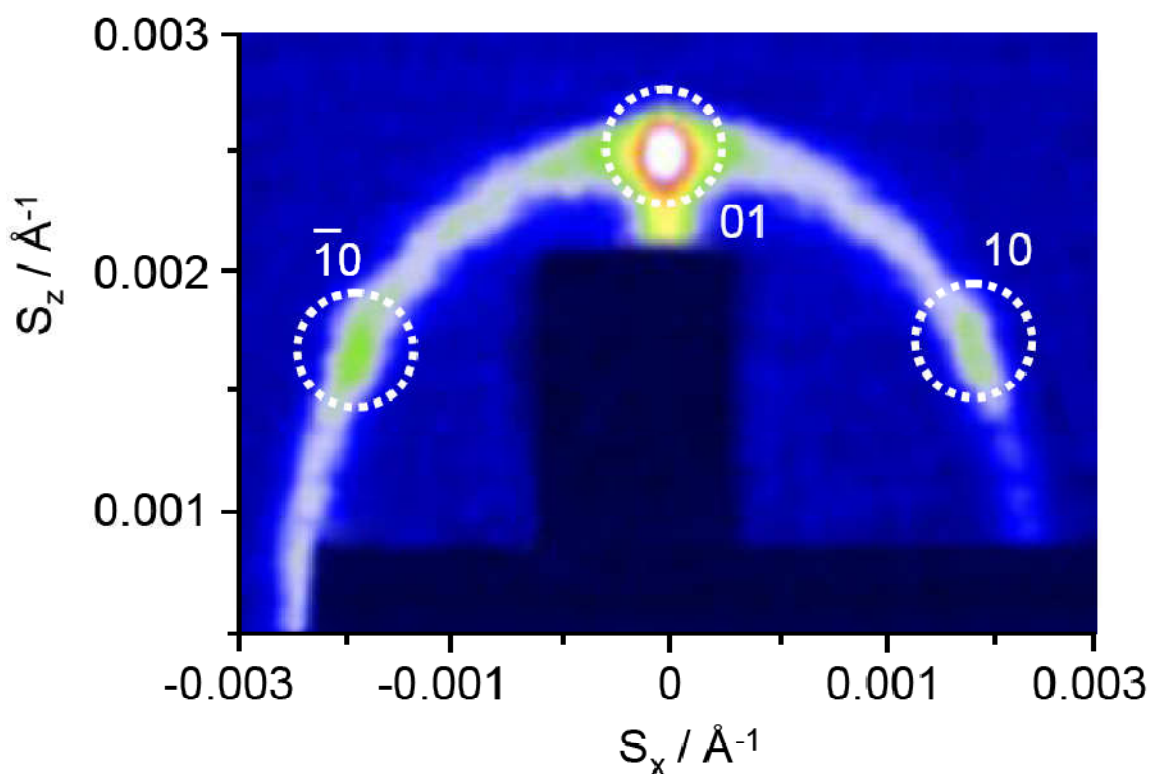

Fig.2: GISAXS pattern obtained an as deposited mesostructured Rh6g doped film with $s = 5 \cdot 10^{-3}$ and $c = 5 \cdot 10^{-2}$.

7.3.2 UV-VIS SPECTROSCOPY

The absorption spectrum of rhodamine 6G in the monomeric form is characterized by an absorption peak around 530 nm and a vibronic shoulder at lower wavelengths (~500 nm). The molecule is slightly solvathocromic and the absorption maximum red shifts in polar solvents; the

intermolecular aggregation strongly depends on the dye concentration and the chemical environment (polarity, charge, etc.) [7].

Rhodamine 6G dimers have two distinct absorption maxima, at higher (J-type dimers) and lower (H-type dimers) wavelengths with respect to the absorption peak of the monomer band (~530 nm). **Fig.3a, 3b and 3c** show the absorption spectra of the different types of films doped with rhodamine 6G at increasing concentrations (from 5.10^{-5} up to 10^{-3}).
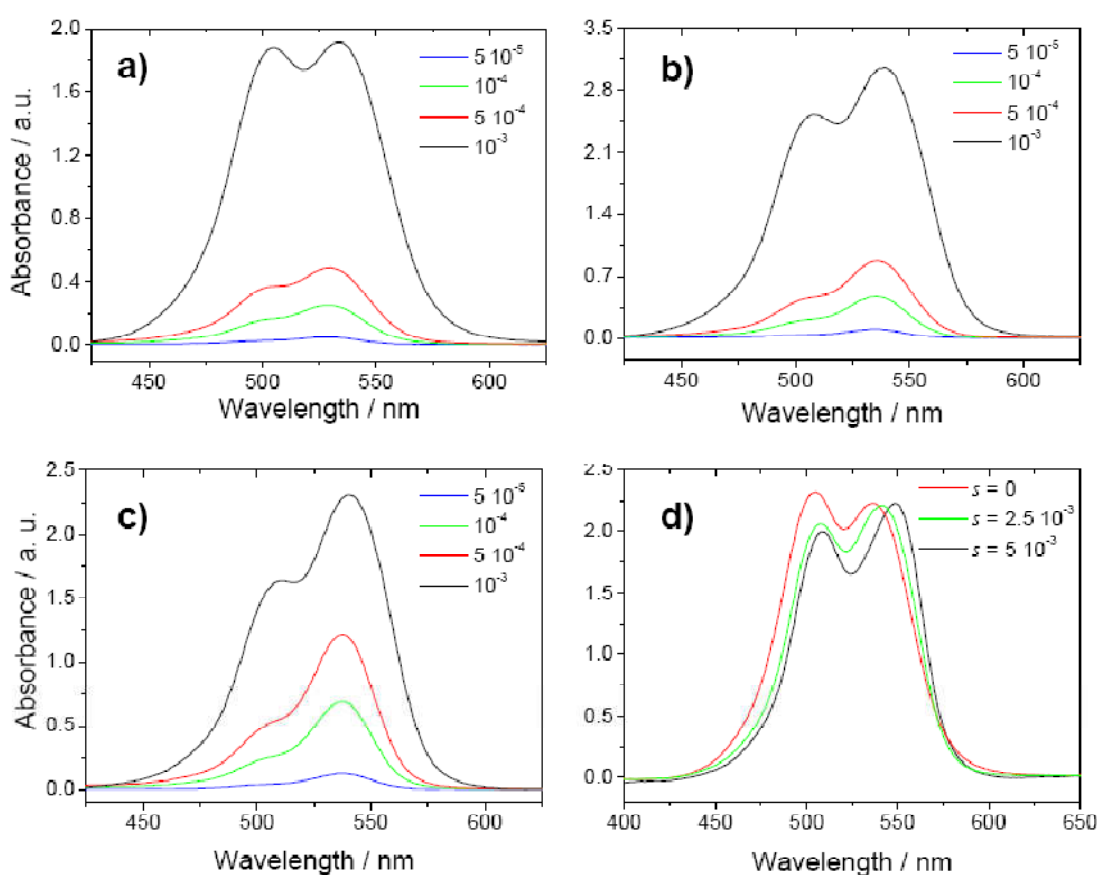
Fig.3: UV-visible absorption spectra of: (a) sol-gel silica films, (b) mesostructured silica films ($s = 2.5 \cdot 10^{-3}$), (c) mesostructured silica films ($s = 5 \cdot 10^{-3}$) doped with different amounts of rhodamine 6G. The rhodamine concentrations in the films are: $c = 5 \cdot 10^{-5}$, blue line; $c = 10^{-4}$, green line; $c = 5 \cdot 10^{-4}$ red line; and $c = 10^{-3}$, black line. (d) Difference spectra by subtracting the data of the films doped with $5 \cdot 10^{-4}$ Rh6G from those of 10^{-3} Rh6G concentration. The label in figure (d) indicates the surfactant concentration (red line, $s = 0$ sol-gel film; green line, $s = 2.5 \cdot 10^{-3}$; black line, $s = 5 \cdot 10^{-3}$).

We have evaluated the effect of the different amounts of dye intoduced in silica sol-gel films (**Fig.3a**) and in mesostructured films prepared with different surfactant concentrations: **Fig.3b**, $s = 2.5 \cdot 10^{-3}$ and **Fig.3c**, $s = 5 \cdot 10^{-3}$.

At the highest dye concentration (TEOS : Rh6G = 10^{-3} molar ratio), a H-dimer absorption band around 500 nm, is observed in all the samples. This dimer band is overlapped to the vibronic band, but can be clearly detected; the H-type dimer band has the highest relative intensity in the sol-gel silica sample and the lowest one in the mesostructured film prepared with the highest surfactant concentration. The formation of J-type dimers can not be evaluated from the absorption spectra because of the overlapping with the monomer band.

We have, therefore, subtracted the absorption spectra of the films with $c = 5 \cdot 10^{-4}$ from those with $c = 10^{-3}$ to separate the contributions of the different types of dimers. **Fig.3d** shows the spectra that resulted from the subtraction; two different absorption peaks are observed around 505 and 540 nm, which are assigned to H-type and J-type dimers, respectively [3,11].

The spectra have been normalized with respect to the J-dimer peak for comparison; it is interesting to observe that the relative intensity of the H-type and J-type dimer bands changes with a specific trend. The J-dimer band has the lowest relative intensity in the silica films and the highest in the sample with the highest surfactant concentration: this is an indication that the amount of J-dimers with respect to H-dimers is higher in mesostructured films with respect to the dense samples. The two dimer bands, H and J, appear partially overlapped, which is similar to what observed in the case of the dimer absorption spectrum in water [30] but differs from that in methanol [31] and ethylene glicol [11] where two well separated H and J bands are observed.

7.3.3 FLUORESCENCE SPECTROSCOPY

To get a better in sight of the effects of Rh6G aggregation on the optical properties we have recorded fluorescence emission spectra using an excitation at 480 nm on samples with different concentrations of rhodamine 6G, from $5 \cdot 10^{-5}$ up to $5 \cdot 10^{-2}$ M.

Fig.4a, 4b and **4c** show the normalized emission spectra, in the 500 – 800 nm range, of the different samples: sol-gel silica films (**Fig.4a**); mesostructured films with $s = 2.5 \cdot 10^{-3}$ (**Fig.4b**); and mesostructured films with $s = 5 \cdot 10^{-3}$ (**Fig.4c**).
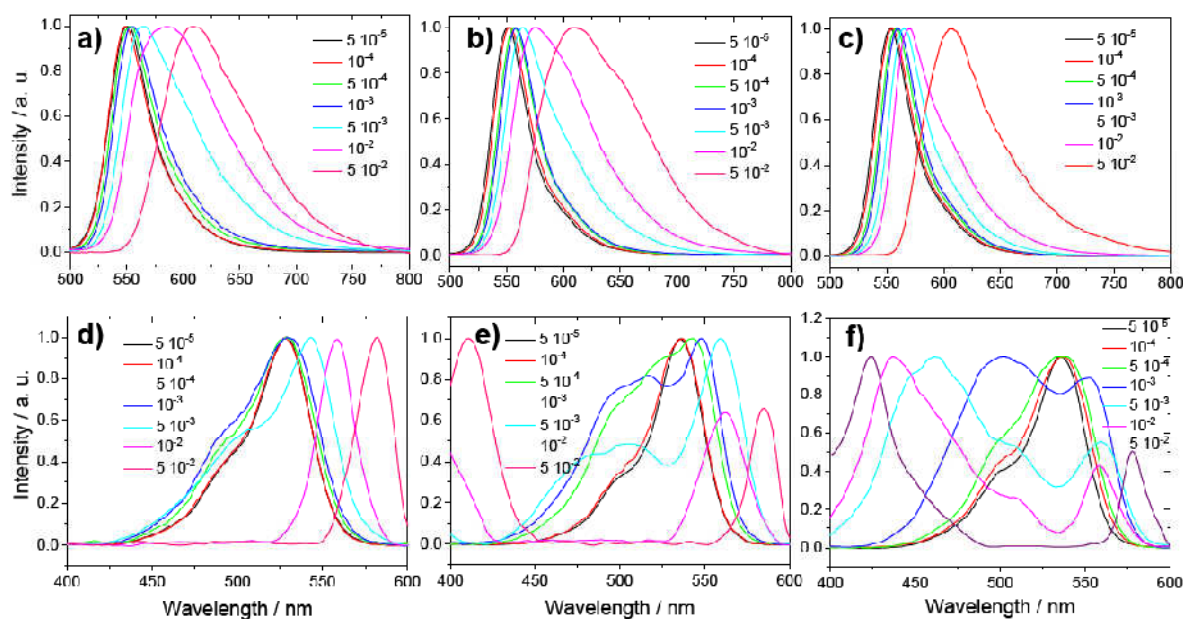
Fig.4: Emission spectra of rhodamine 6G doped sol-gel silica films (a); rhodamine 6G doped mesostructured silica films (s = 2.5·10^{-3}) (b); and rhodamine 6G doped mesostructured silica films (s = 5·10^{-3}) obtained by excitation at λ = 480 nm. Excitation spectra of rhodamine 6G doped sol-gel silica films (d); rhodamine 6G doped mesostructured silica films (s = 2.5·10^{-3}) (e) and rhodamine 6G doped mesostructured silica films (s = 5·10^{-3}) (f) obtained by emission λ = 620 nm.

The increase of rhodamine 6G concentration within the films has produced a broadening and red shift of the emission spectra. This effect is well in accordance with previous findings [10]; red shift and broadening of the emission band is characteristic of formation of fluorescent Jdimer species [32].

A red shift was observed in all the samples; the value of this shift, calculated from the samples at highest concentration (c = 5·10^{-2}) with respect to the samples at the lowest one (c = 5.10^{-5}), was 61 nm (**Fig.4a**), 58 nm (**Fig.4b**) and 53 nm (**Fig.4c**). A direct evidence of the red shift effect is given by the picture of the as prepared samples (**Fig.5**); the picture shows three doped mesostructured silica films (s = 5·10^{-3}) at decreasing rhodamine 6G concentrations (c = 5·10^{-2}, c = 5·10^{-3} and c = 5·10^{-4}), from left to right, illuminated by visible light (a) and by UV light at 365 nm (b). Upon exposure to UV light an intense coloration due to red shifted emission is observed.

In accordance with the literature the emission peak at 550 nm is assigned to the monomeric form of rhodamine 6G within the films, and the red shifted emission around 600 nm to fluorescent J-dimers [10,11,16].

The formation of rhodamine 6G aggregates (H-type) is clearly revealed by absorption spectra, they indicate also the presence of fluorescent dimers (J-type) whose formation is enhanced in mesostructured films; this evidence is well supported by the emission spectra (**Fig.4a, 4b, 4c**).
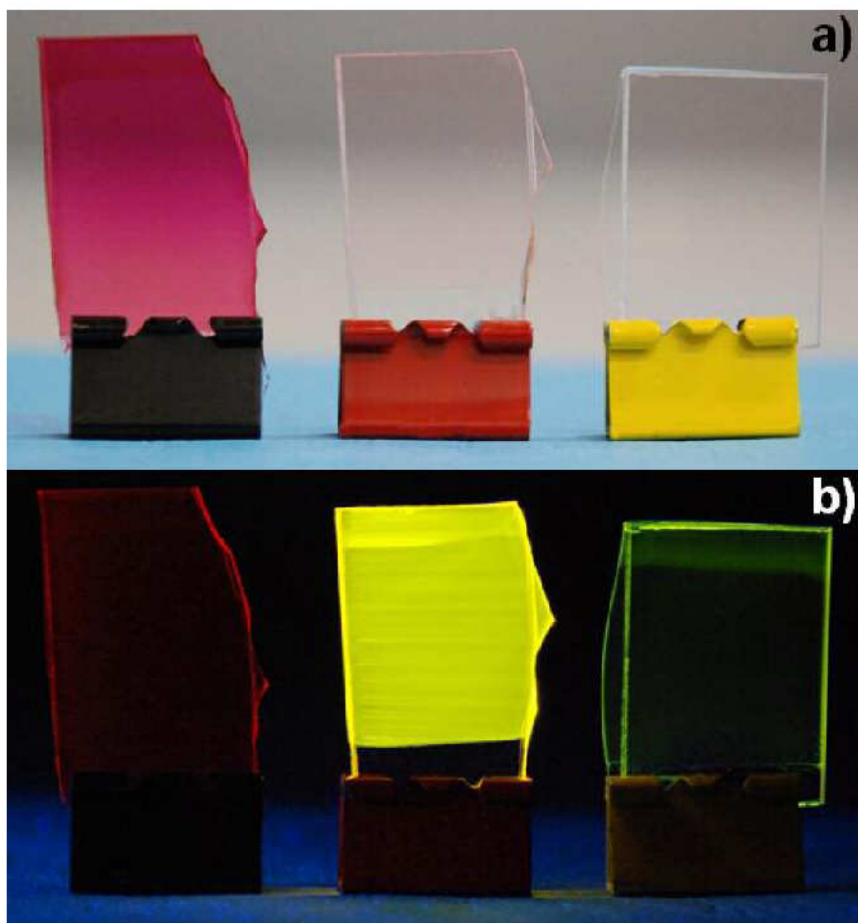
Fig.5: Picture of Rh6G doped mesostructured silica films (s = 5·10-3) at decreasing rhodamine 6G concentrations (c = 5·10-2, c = 5·10-3 and c = 5·10-4), from left to right, illuminated by visible light (a) and by UV light at 365 nm (b).

The extreme of these types of dyes is represented by a perfect sandwich structure (H-type) and a perfectly aligned head-to-tail dimer (J-type). This is, however, only an idealized configuration

and a distribution of dimer geometries is the most realistic description; a "magic angle" around 55° represents the limit between luminescent and non-luminescent dye aggregates [9,7].

Excitation spectra have been employed to follow the formation of fluorescent aggregates in the films as a function of the dye concentration.

Fig.4d, 4e, 4f show the excitation spectra recorded by monitoring the emission at 620 nm in the silica and mesostructured films doped with increasing concentrations of rhodamine 6G. The excitation spectra of silica films (Figure 3d) show one excitation band at 525 nm, which red shifts in the samples with the higher rhodamine 6G concentrations (c = $5 \cdot 10^{-3}$, 10^{-2}, $5 \cdot 10^{-2}$). The excitation spectra of the mesoporous films appear very different, they are characterized by three main excitation bands, one at 525 nm due to the monomer, a red shift excitation band and a blue shifted excitation band. The red and blue shift increases as a function of the rhodamine concentration, whilst the monomer excitation strongly decreases at concentrations around c = $5 \cdot 10^{-4}$.

A general overview of the response to excitation at different wavelengths is given by 3D excitation-emission-intensity spectra reported in **Fig.6** for the mesostructured sample prepared with the higher surfactant concentration (s = $5 \cdot 10^{-3}$) and six different rhodamine 6G concentrations (c = $5 \cdot 10^{-5}$, $5 \cdot 10^{-4}$, 10^{-3}, $5 \cdot 10^{-3}$, 10^{-2}, $5 \cdot 10^{-2}$). The spectra show the excitation (x-axis) vs emission (y-axis), intensity is reported in a colour scale; oblique lines in some images are due to scattering effects. The effect of rhodamine 6G concentration on the fluorescence emission and excitation can be clearly observed. At the lower concentrations the main contribution to the fluorescence is given by the monomeric form of rhodamine 6G, but the sligtly distorted shape of the image indicates that even at very low concentrations a contribution from different fluorescent species (Jdimers) is present.

The image of the sample with the lowest Rh6G concentration (c = $5 \cdot 10^{-5}$) shows that the emission has an intensity peak around 560 nm in correspondance to an excitation of 540 nm. The emission appears asymmetrically red shifted and the excitation ranges from 570 to 460 nm; this is an indication that the fluorescence is due to monomeric species as far as fluorescent aggregates. At c = $5 \cdot 10^{-4}$ Rh6G concentration the red shift of emission fluorescence increases and an asymmetric image is generated.
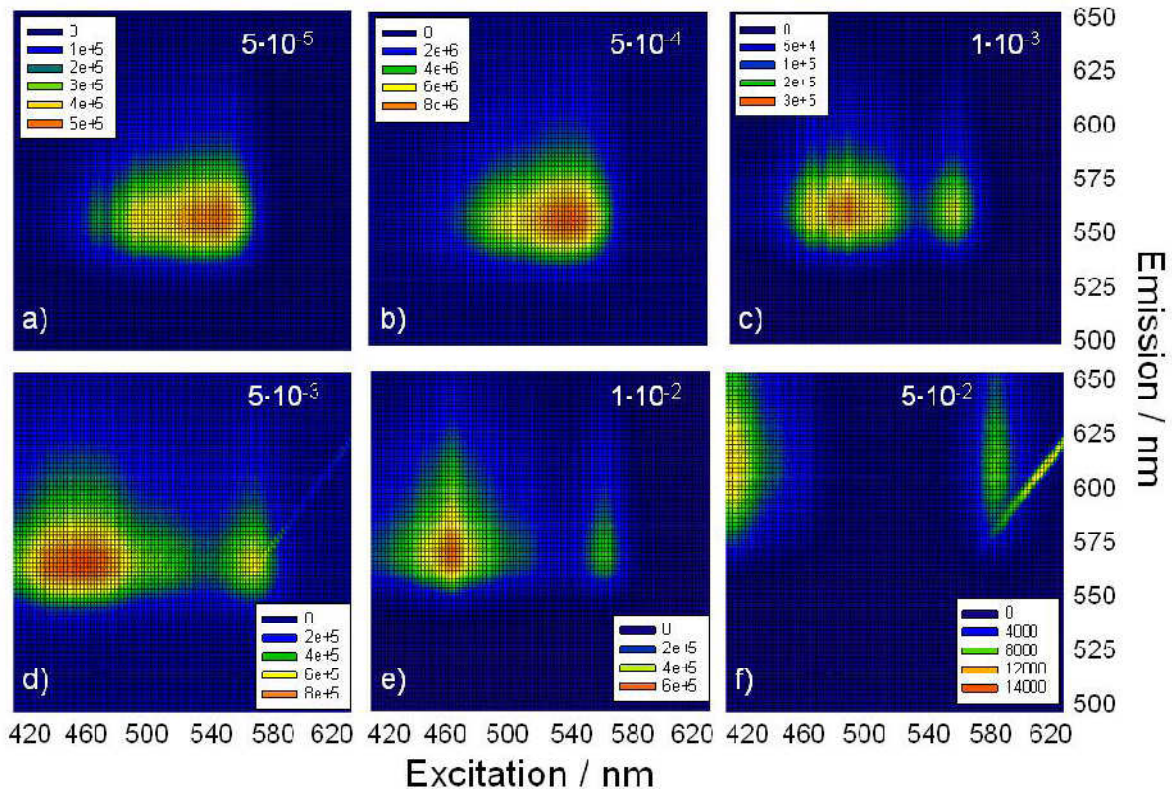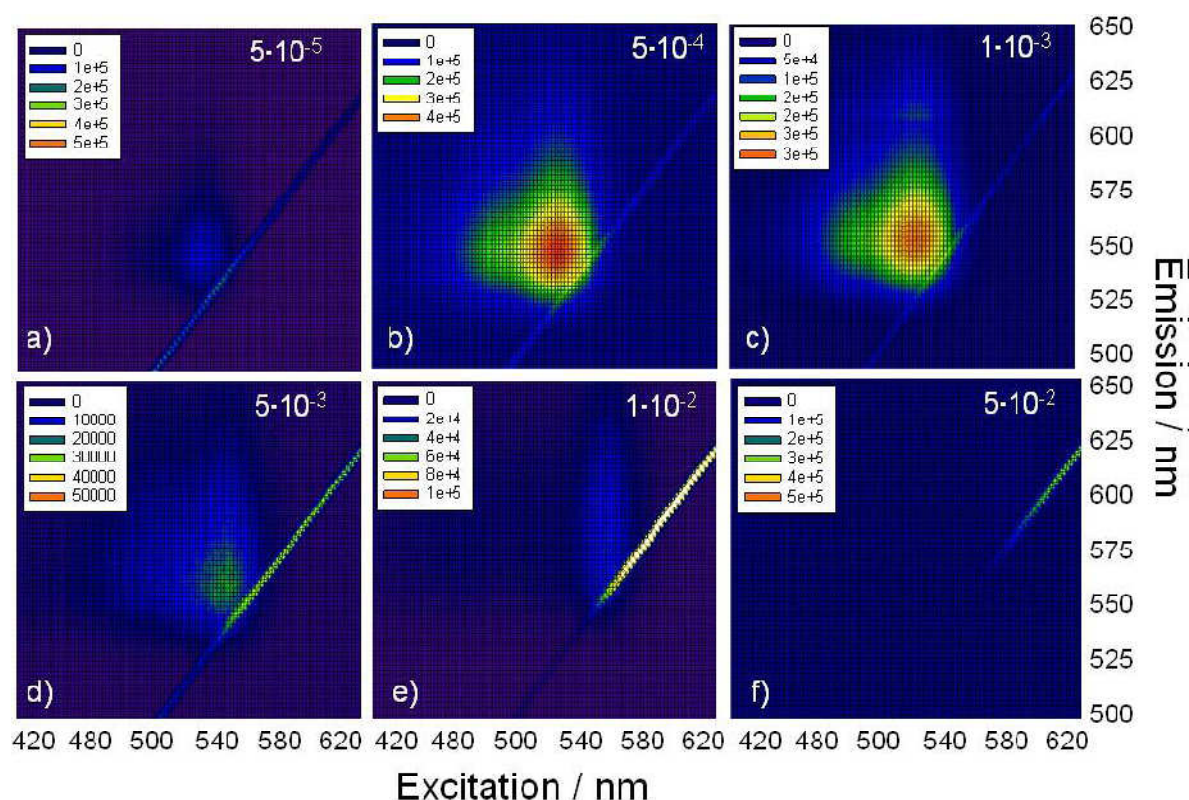
Fig.6: 3D excitation-emission-intensity spectra of rhodamine 6G doped mesostructured (s = 5·10^{-3}) silica films as a function of the dye concentration.

At c = 10^{-3} Rh6G concentration, exciton splitting is observed and the fluorescence emission is mainly due to J-type aggregates (**Fig.6c and 6f**). The maximum of J-dimer fluorescence is observed in the c = 5·10^{-3} sample, with a strong excitation splitting; the large excitation range indicates a large distribution of J-dimer aggregates.

At higher dye concentrations the fluorescence decreases in intensity and formation of H-dimer aggregates prevails. A comparison of the different fluorescence response shown by Rh6G doped mesostructured and silica sol-gel films can be done by observing the 3D spectra of the silica sol-gel samples in **Fig.7**.

Fig.1: 3D excitation-emission-intensity spectra of rhodamine 6G doped sol-gel silica films as a function of the dye concentration.

These excitation-emission-intensity images appear very different from those observed in mesostructured silica films. In this set of samples only a weak fluorescence is observed at the lowest dye concentration ($c = 5 \cdot 10^{-5}$). At $c = 5 \cdot 10^{-4}$ an intense fluorescence peaking at 550 nm in correspondance to an excitation at 520 nm is observed. The asymmetry of the image, which appears slightly distorted to red for emission and to blue for excitation, indicates that also in this sample a partial contribution to fluorescence emission due to J-type aggregates is present.

At higher concentrations ($c = 10^{-3}$) the fluorescence intensity only slightly decreases mantaining the asymmetric shape. Beyond this concentration the fluorescence abruptly decreases due to the formation of non-fluorescent aggregates.We have also to underline that an important effect that has be taken into account is the reabsorption of emitted light that could also cause red shift of the emission spectra. In the present case the partial overlapping of absorption (**Fig.3**) and emission (**Fig.4**) spectra indicates that this effect should be considered.

The changes of excitation spectra as a function of dye concentrations indicate, however, that the formation of fluorescent dye aggregates is the main responsible of the emission changes. The formation of non fluorescent aggregates (H-type) of rhodamine 6G upon incorporation is sol-gel films is a well known effect, which is the main responsible of the fuorescence quenching at high rhodamine 6G concentrations.

The aggregation state in these films depends on concentration and on the interactions with the pore walls and the presence of residual water and solvents. In the case of mesostructured films, rhodamine 6G can be introduced, such as the present case, using a "one-pot" synthesis and partecipates to the self-assembling process.

The presence of the surfactant in this case is very important, several studies have shown that introduction of surfactants in the sol-gel precursor solution reduces the aggregation of dyes [3]. It has been reported that when a dye is dissolved in aqueous surfactant solutions, the monomer associates to the hydrophobic chain of the surfactant and is included into the micelle [33]. The inclusion in the micelle core has the effect of preventing or limiting the dye aggregation, especially in presence of water that may bridge two monomers to form H-dimers.

In the case of mesostructured films the role of the surfactant is, however, quite complex, because it gives a special chemical environment to the guest dye but also acts as the templating agent of the mesostructure during the self-assembling process.

The guest dye, after film deposition, will be in a higly restricted environment which is, however, very different from that one of a corresponding sol-gel silica films. The previous data show several differences and give some indications on the origin of the fluorescence in the different samples:

(1) In sol-gel silica films the dyes aggregate mainly as non-fluorescent Hdimers and the origin of the fluorescence is mainly due to monomeric form of rhodamine 6G, the fluorescence disappears at concentrations much lower than the corresponding mesostructured films.

(2) The concentration of surfactant affects the dye aggregation, higher concentrations give more fluorescent films, but mainly from J-type dimers.

(3) The inclusion in a mesostructured film gives preferential formation of J-type with respect to H-type dimers.

(4) A distribution of dimers is present, corresponding to two extreme configurations, which we attribute to sandwich H-type dimers and head-to tail J-type aggregates.

(5) The formation of fluorescent aggregates is promoted by the presence of the surfactant that favors the formation within the micelles of head-to tail dimers, and introducing a constrained environment in which H-type dimers are distorted to give rise to oblique J-type aggregates.

7.4 CONCLUSIONS

Mesostructured silica films represent a peculiar environment for fluorescent dyes, such as rhodamine 6G. Incorporation of Rh6G in dense silica films favours preferential formation of H-type dimers, which are responsible of fluorescence quenching, even at quite low concentrations. "One-pot" doped mesostructured films show, instead, a very different property; fluorescent J-type dimers are formed and emission is still observed even at high dye concentrations.

The origin of this fluorescence is attributed to formation of fluorescent aggregates, such as J-type dimers. The presence of the templating micelles favours the formation of J-type aggregates at expenses of the nonfluorescent sandwich type H-dimers.

REFERENCES

1. Avnir, D.; Levy, D.; Reisfeld, R. *J. Phys. Chem.* **1984**, 88, 5956;

2. Knobbe, E. T.; Dunn, B.; Fuqua, P. D.; Nishida, F. *Appl. Opt.* **1990**, 29, 2729;

3. Innocenzi, P.; Kozuka, H.; Yoko, T. *J. Non-Cryst. Solids* **1996**, 201, 26;

4. Carbonaro, C. M.; Anedda, A.; Grandi, S.; Magistris, A. *J. Phys. Chem. B* **2006**, 110, 12932;

5. Laranjo, M.T.; Stefani, V.; Benvenutti, E. V.; Costa, T. M.H.; Ramminger, G. de O.; Gallas, M. R. *J. Non-Cryst. Solids* **2007**, 353, 24;

6. Narang, U.; Wang, R.; Prasad, P. N.; Bright, F. V. *J. Phys. Chem.* **1994**, *98*, 17;

7. Kemnitz, K. ; Yoshibara, K. *J. Phys. Chem.* **1991**, 95, 6095;

8. Daré-Doyen, S. ; Doizi, D. ; Guilbaud, P. ; Djedaini-Pilard, F. ; Perly, B. ; P. Millié *J. Phys. Chem. B* **2003**, 107, 13803;

9. Sasai, R.; Iyi, N.; Fujita, T. Arbeloa, F. L.; Martinez, V. M.; Takagi, K.; Itoh H. *Langmuir* **2004,** 20, 4715;

10. Del Monte, F.; Mackenzie, J.D.; Levy, D. *Langmuir* **2000**, 16, 7377;

11. Bojarski, P.; Matczuk, A.; Bojarski, C,; Kawski, A.; Kuklinski, B.; Zurkowska, G.; Diehl, H. *Chem. Phys.* **1996**, 210, 485;

12. Bujdak, J.; Iyi, N.; Kanko, Y.; Czimerova, A.; Sasai, R. *Phys. Chem. Chem. Phys.,* **2003**, 5, 4680;

13. McKiernan, J. M.; Yamanaka, S. A.; Dunn, B.; Zink, J. I. *J. Phys. Chem.* **1990**, 94, 5652;

14. Anedda, A.; Carbonaro, C. M.; Corpino, R.; Ricci, P. C.; Grandi, S.; Mustarelli, P. *J. Non-Cryst. Solids* **2007**, 353, 481;

15. Anedda, A.; Carbonaro, C. M.; Clemente, F.; Corpino, R.; Grandi, S.; Mustarelli, P.; Magistris, A. *J. Non-Cryst. Solids* **2005**, 351, 1850.

16. Anedda, A.; Carbonaro, C. M.; Clemente, F.; Corpino, R.; Ricci, P.C.; Rossigni, S. *Mater. Sci. Eng. C* **2005**, 25, 641;

17. Soler-Illia, G. J. A.; Innocenzi, P. *Chem.: A Europ. J.* **2006**, 12, 4478;

18. Vogel, R.; Meredith, P.; Harvey, M.D.; Rubinsztein-Dunlop, H. *Spectrochimica Acta Part A* **2004**, 60, 245;

19. (a) Yang, P.; Wirnsberger, G.; Huang, H. C.; Cordero, S. R.; McGehee, M. D.; Scott, B.; Deng, T.; Whitesides, G. M.; Chmelka, B. F.; Buratto, S. K.; Stucky, G. D. *Science,* **2000**, 287, 465; (b) Wirnsberger, G.; Stucky, G. D. *Chem. Mater.* **2000**, 12, 2525;

20. Pal, P.; Zeng, H.; Durocher, G.; Girard, D.; Giasson, R.; Blanchard, L.; Gaboury, L.; Villeneuve, L. *J. Photochem. Photobiol. A: Chem.* **1996**, 98, 65;

21. Vogel, R.; Harvey, M.; Edwards, G.; Meredith, P.; Heckenberg, N.; Trau, M.; Rubinsztein-Dunlop, H. *Macrom.* **2002**, 35, 2063;

22. Dunn, B.; Zink, J. I. *Acc. Chem. Res.* **2007**, 40, 747;

23. (a) Hernandez, R.; Franville, A. C.; Minoofar, P.; Dunn, B.; Zink, J. I. *J. Am. Chem. Soc.* **2001**, 123, 1248. (b) Minoofar, P. N.; Hernandez, R.; Chia, S.; Dunn, B.; Zink, J. I.; Franville, A. C. *J. Am. Chem. Soc.* **2002**, *124*, 14388. (c) Minoofar, P. N.; Dunn, B. S.; Zink, J. I. *J. Am. Chem. Soc.* **2005**, 127, 2656;

24. H. Amenitsch, M. Rappolt, M. Kriechbaum, H. Mio, P. Laggner, S. Bernstorff, *J. Sync. Rad.* **1998**, 5, 506;

25. Falcaro, P.; Grosso, D.; Amenitsch, H.; Innocenzi, P. *J. Phys. Chem. B* **2004**, 108, 10942;

26. Falcaro, P.; Costacurta, S.; Mattei, G.; Amenitsch, H.; Marcelli, A.; Cestelli Guidi, M.; Piccinini, M.; Nucara, A.; Malfatti, L.; Kidchob, T.; Innocenzi, P. *J. Am. Chem. Soc.* **2005**, 127, 3838;

27. Innocenzi, P.; Falcaro, P.; Schergna, S.; Maggini, M.; Menna, E.; Amenitsch, H.; Grosso, D.; Soler A.A. Illia, G.; Sanchez, C.; *J. Mater. Chem.* **2004**, 14, 1838;

28. Wirnsberger, G.; Scott, B. J.; Chmelka, B. F.; Stucky, G. D. *Adv. Mater.* **2000**, 12, 1450;

29. Grosso, D. ; Soler-Illia, G.; Babonneau, F.; Sanchez, C.; Albouy, P.-A.; Brunet-Bruneau, A.; Balkenende., A. R. *Adv. Mater.* **2001**, 13, 1085;

30. Bojarski, C.; Obermueller, G. *Acta Phys. Pol.* **1976**, A50, 389;

31. Blonski, S. *Chem. Phys. Lett.* **1991**, 184, 229;

32. Del Monte, F.; Levy, D. *J. Phys. Chem. B* **1998**, 102, 8036;

33. Fischer, M.; Georges, J. *Spectrochim. Acta A* **1997**, 53, 1419.

CONCLUSIONS

Mesoporous materials, both as powders and thin films, have been successfully prepared and opportunely functionalized with chemical species interesting for future applications.

Functional silica mesoporous materials have been prepared as powders using different synthetic procedures with aminopropyl groups as functionalizing agents and benzoic acid, phenylphosphonic acid and Schiff-base zinc(II) complex as guest molecules. The structural and surface properties of these host-guest complexation systems were studied using XRD, N_2 adsorption/desorption, TGA, elemental analysis, FTIR and UV-Vis spectroscopies.

The covalent incorporation of a luminescent zinc complex using grafting post-synthesis and one-pot synthesis methods onto different types of mesoporous silica hosts has been successfully carried out. The luminescent behavior of these solids was investigated by direct measurements of emission quantum yield which allows a correlation between luminescent intensity and structure of mesoporous materials.

The changes of the surface parameters and the best luminescent properties of the samples synthesized by one-pot method, compared to grafted samples, indicate a major anchorage and highly homogeneous distribution of zinc complex into the mesoporous wall and within the channels.

Hybrid mesoporous powders have been also prepared by post-synthesis grafting with triethoxysilane functions and/or by a simply impregnation with phenylphosphonic acid. Its incorporation onto two different silica hosts was confirmed by nitrogen sorption analysis and XRD diffraction which show a reduction of the structural parameters and a slight decrease in long-range ordering of the solids. Elemental analysis confirms the efficiency of the grafting process, showing a large amount of the guest molecules in the samples with amino groups.

Mesoporous powders with and without aminopropyl groups, loaded with benzoic acid as guest molecule, have been synthesized by post-synthesis grafting. The resulting solids show significant changes of structural parameters due to the presence of guest molecules on the internal and external surface with a partial pore blocking and reduction of ordered arrangement.

Moreover, mesoporous silica and titania films have been synthesized using supramolecular self-assembly with block copolymer as structuring agents and functionalized with different guest

species to prepare luminescent solids for future applications. Mesostructured thin films fabricated via evaporation induced self-assembly method have been designed with orthorhombic symmetry useful for impregnation process. The luminescent properties of these host-guest materials with reference to the photophysical properties, including the behavior and the stability of the functional species into the channels of mesoporous thin films have been studied.

Mesostructured silica and titania films grafted with luminescent zinc complex are highly fluorescent with a good stability of the emitting properties, preserving at the same time the ordered porosity and high surface area. Leaching experiments show that the complexes incorporated in the matrices are stable because strongly anchored to the mesoporous walls.

Mesoporous silica film have been successfully doped "one-pot" with a fluorescent dye, Rhodamine 6G, studying its aggregations states after incorporation into the film. Despite the presence of dimers, the emission is still observed even at high dye concentrations.

In conclusion, mesoporous powders and thin film have interesting chemical-physical properties useful to fabricate several types of luminescent materials and for the development of controlled solid state devices.

SCIENTIFIC WORK

PUBBLICATIONS:

INTERNATIONAL JOURNALS:

1) D. Aiello, L. Malfatti, T. Kidchob, R. Aiello, F. Testa, I. Aiello, M. Ghedini, M. La Deda, T. Martino, M. Casula, P. Innocenzi: "Blue-emitting mesoporous films prepared via incorporation of a luminescent Schiff base zinc(II) complex", *Journal of Sol-gel Science and Technology*, 47, 2008, 238-289;

2) D. Aiello, L. Malfatti, T. Kidchob, R. Aiello, F. Testa, I. Aiello, M. Ghedini, M. La Deda, T. Martino, M. Casula, P. Innocenzi: "Absolute emission quantum yield determination of self-assembled mesoporous titania films grafted with a luminescent zinc complex", *Inorganic Chimica Acta*, 2008, xxx, xxx;

3) D. Aiello, R. Aiello, F. Testa, I. Aiello, M. Ghedini, M. La Deda, T. Martino: " Incorporation of zinc complex in mesoporous materials via one-pot synthesis and grafting post-synthesis methods ", *Journal of Photochemistry and Photobiology A: Chemistry*, DOI: 10.1016/j.jphotochem2008.10.001;

4) L. Malfatti, T. Kidchob, D. Aiello, F. Testa, R. Aiello, P. Innocenzi: "Aggregation states of rhodamine G6 in mesostructered silica films"; *The Journal of Physical Chemistry C*, 2008,112, 16225-16230.

PROCEEDINGS:

1) D. Aiello, L. Malfatti, T. Kidchob, R. Aiello, F. Testa, I. Aiello, M. Ghedini, M. La Deda, T. Martino, M. Casula and P. Innocenzi: "Titania and silica film grafted with a luminescent zinc(II) complex", *Atti di Convegno*, VIII Convegno Nazionale AIMAT, ISBN 978-88-900948-6-6, pag 9, Ed. Ziino, Piano di Sorrento (NA), 29 giugno-01 luglio 2008;

2) D. Aiello, L. Malfatti, T. Kidchob, R. Aiello, F. Testa, I. Aiello, M. Ghedini, M. La Deda, T. Martino, M. Casula and P. Innocenzi: "Preparazione di film me soporosi ibridi di

silice e titania mediante un complesso luminescente di zinco(II); *Atti di convegno*, Convegno GRICU 2008, pag. 937-940, Le Castella (Kr), 14-17 Settembre.

3) <u>D. Aiello</u>, F. Testa, R. Aiello, T. Martino, I. Aiello, M. La Deda, M. Ghedini: "Incorporation of Zinc Complex in mesoporous materials via direct co-condensation and post-synthesis grafting methods", *Atti di Convegno*, VIII Aiz Congress, 113, 2P12, Torino (Italy), 1st-4nd luglio 2007;

4) I. Aiello, M. Ghedini, T. Martino, M. La Deda, <u>D. Aiello</u>, R. Aiello, F.Testa, A. Torchia, L. Pasqua: "Luminescent molecules grafted on mesoporous materials: preparation and characterization", *Atti di Convegno*, XXII Congresso Nazionale della Società Chimica Italiana, Firenze, 10- 15 settembre 2006;

5) I. Aiello, M. Ghedini, T. Martino, M. La Deda, <u>D. Aiello</u>, R. Aiello, F.Testa: "Studio di materiali mesoporosi funzionalizzati con molecole luminescenti, mediante grafting post-sintesi", *Atti di Convegno*, IX Scuola Nazionale per Dottorandi della Divisione di Chimica Inorganica "Chimica dei Materiali Inorganici", P27, Università della Calabria, Arcavacata di Rende (CS), 26-30 Novembre; 2006.

6) D. Aiello, L. Malfatti, T. Kidchob, R. Aiello, F. Testa, I. Aiello, M. Ghedini, M. La Deda, T. Martino, M. Casula and P. Innocenzi. "Mesoporous hybrid titania and silica films prepared via post-synthesis grafting of luminescent zinc(ii) complex", *Atti di Convegno*, Convegno Internazionale SAMIC 2008, Bressanone, 29 novembre-4 dicembre 2008.

ORAL PRESENTATIONS:

1) D. Aiello, R. Aiello, D. Caputo, C. Colella, P. Frontera, F. Iucolano and L. Pasqua: "Preparation and characterization of Ag+-bearing MCM-41", Presentazione Orale, *Atti di convegno, VIII Convegno Nazionale AIMAT*, Palermo, 27 giugno-1 luglio 2006;

2) D. Aiello, L. Malfatti, T. Kidchob, R. Aiello, F. Testa, I. Aiello, M. Ghedini, M. La Deda, T. Martino, M. Casula and P. Innocenzi: "Blue-emitting titania and silica films prepared via incorporation of a luminescent zinc complex*",* Presentazione Orale, *Atti di Convegno, VI Convegno Nazionale sulla Scienza e Tecnologia dei Materiali,* CO3, Università degli Studi di Perugia, 12-15 Giugno 2007.

PARTICIPATION AT PhD SCHOOL:

1) XII Scuola Nazionale di Scienza dei Materiali, 11-16 settembre 2006, Bressanone, Sede estiva dell'Università di Padova.

WORKS ABROAD:

1) 10 ottobre-20 dicembre 2006: Laboratorio di Scienza dei Materiali e Nanotecnologie, D.A.P., Università di Sassari;

2) 14 ottobre-21 dicembre 2007: Laboratorio di Scienza dei Materiali e Nanotecnologie, D.A.P., Università di Sassari;

3) 10 gennaio-12 maggio: Laboratoire Chimie de la Matière Condensée de Paris, Universitè Pierre et Marie Curie VI, Paris (France).

DIDACTIC WORK:

1) 8 settembre-30 settembre 2008: UNIVERSITA' della CALABRIA, Via Pietro Bucci, 87036, Rende (CS), Dipartimento di Ingegneria Chimica e dei Materiali: Esercitatrice corsi di potenziamento nell'ambito del progetto: "POR CALABRIA 2000-2006, MISURA 3.7 AZIONE 3.7.a POR FSE CALABRIA 2007-2013 - ASSE IV, OB. OPERATIVO L.1 E L.2 AZIONE 3.2.5 PERCORSI AZZERAMENTO DEFICIT COMPETENZE DEL PIANO REGIONALE PER LE RISORSE UMANE - PIANO D'AZIONE 2008";

2) Da ottobre 2008 a novembre 2008: UNIVERSITA' della CALABRIA, Via Pietro Bucci, 87036, Rende (CS), Dipartimento di Ingegneria Chimica e dei Materiali,Tutor del corso "Laboratorio di Ingegneria Chimica 1" per gli iscritti al 2° anno del Corso di Laurea Triennale in Ingegneria Chimica.

ACKNOWLEDGMENTS